Modeling and flexible predictive control of buildings space-heating demand in district heating systems

Nadine Aoun

université PARIS-SACLAY

NNT : 2019SACLC104

CentraleSupélec

Modelling and flexible predictive control of buildings space-heating demand in district heating systems

Thèse de doctorat de l'Université Paris-Saclay
préparée à CentraleSupélec

École doctorale n°580 Sciences et Technologies de l'Information et de la Communication (STIC)
Spécialité de doctorat: Automatique

Thèse présentée et soutenue publiquement à Gif-sur-Yvette, le 2 Décembre 2019, par

Nadine Aoun

Composition du Jury :

Monsieur **Bruno Lacarrière** Professeur, IMT Atlantique	Rapporteur
Monsieur **Stéphane Ploix** Professeur, Université Grenoble-Alpes	Rapporteur
Monsieur **Khalil El Khoury** Professeur, Université Libanaise	Président du jury
Monsieur **Etienne Wurtz** Directeur de recherche, CNRS CEA-INES	Examinateur
Monsieur **Marc Petit** Professeur, CentraleSupélec	Examinateur
Madame **Sihem Guernouti** Chargée de recherche, Cerema	Examinatrice
Monsieur **Vittorio Verda** Professeur, Politecnico di Torino	Examinateur
Monsieur **Guillaume Sandou** Professeur, CentraleSupélec	Directeur de thèse
Monsieur **David Canal** Ingénieur de recherche, ADEME	Invité
Monsieur **Roland Bavière** Ingénieur de recherche, CEA	Co-Directeur de thèse
Monsieur **Mathieu Vallée** Ingénieur de recherche, CEA	Co-Directeur de thèse

Thèse de doctorat

I suffered,
I learned,
I changed.

Kahlil Gibran

Acknowledgments

It is often said that the journey matters more than the destination. If this PhD's destination is a degree with my name on it, its journey is graved with names of people to whom I shall forever be grateful.

First and foremost, my sincere thanks must go to those who guided me along the path, 3 people that I am indebted to: my advisors, **Roland BAVIÈRE** and **Mathieu VALLÉE**, for their great ideas and all the tools that they have put at my disposal to achieve this work, and my PhD director, **Guillaume SANDOU**, for his insightful supervision and *rational* motivation.

I gratefully acknowledge the funding received towards my PhD from ADEME and CEA. I extend my thanks to ADEME referent engineer **David CANAL** for his engagement and followship. I am thankful for the hospitality and invaluable advices of **Nathalie DUPASSIEUX**, **Stéphane COLASSON** and **Cédric PAULUS** who received me in their CEA labs (LSED and L2ST). Thanks are also due to my CEA *bonus* host lab (LADIS) whose members welcomed me for short stays at Saclay.

I sincerely thank all members of the Jury for showing their interest in evaluating my thesis. I would like to express my special appreciation to **Prof. Bruno LACARRIÈRE** and **Prof. Stéphane PLOIX** for reviewing my manuscript.

I am grateful for the technical support of **Aurélie FOUCQUIER**, **Adrien BRUN** and **Nicolas LAMAISON**, for the much-needed mother-like affection of **Angela DISDIER** and for the companionship of **Mathilde WIRTZ**. I thank my fellow labmates. It has been a great delight being among you, if you find your name down below then you have left a beautiful memory in my mind.

I deeply thank my family for being my driving force to pursue doctoral studies. I dedicate this work to my mother **Mélanie**, to my father **Camille**, to my brother **Michel**, to my grand-mother **Nadia**, and in the loving memory of my grand-parents.

Finally, there are no proper words to convey my gratitude to my fiancé **Roland**, but here's a try. Throughout these years, you have been my best-friend, my joy, my mentor, my part-time advisor and the love of my life. Thank you.

Résumé substantiel en langue française

Modélisation et commande prédictive flexible de la demande en chauffage des bâtiments raccordés à des réseaux de chaleur

Introduction

Le chauffage occupe actuellement le premier poste de consommation énergétique dans le secteur résidentiel, responsable à lui seul d'un tiers de l'énergie finale consommée en France. Les réseaux de chaleur sont des systèmes énergétiques à l'échelle urbaine qui permettent d'assurer ce besoin de chauffage de manière collective entre les bâtiments.

Dans un réseau de chaleur, on distingue trois éléments fondamentaux : tout d'abord, une ou plusieurs unités de production de chaleur centralisées pour chauffer de l'eau ; ensuite, un réseau de distribution pressurisé pour acheminer l'eau ; et finalement, des points de livraison, également connus sous le nom de sous-stations, pour transférer la chaleur portée par l'eau du réseau aux systèmes de chauffage internes aux bâtiments.

Dans les zones urbaines denses, ce système de chauffage collectif s'annonce plus efficace qu'un mode de chauffage employant plusieurs chaudières décentralisées. D'autre part, une caractéristique importante d'un réseau de chaleur réside dans sa capacité à intégrer et à mobiliser les énergies renouvelables et de récupération qui assurent plus de 50% de l'énergie fournie par les réseaux de chaleur en France, en 2016 [FEDENE, 2017], et pourront potentiellement assurer, en 2060, 100% de l'énergie circulée dans les réseaux de chaleur les plus développés au Danemark [Lund *et al.*, 2018a].

Toutefois, des activités de recherche seront nécessaires pour aboutir à de tels objectifs. Nous nous positionnons autour de l'axe de recherche et développement des outils de pilotage qui visent à optimiser l'opération des réseaux de chaleur. L'optimisation opérationnelle peut intervenir au niveau de la production, la distribution et la demande. Dans cette thèse, nous nous focalisons sur la gestion optimale de la demande en chauffage du bâtiment qui prend place au niveau de sa sous-station.

La demande en chauffage des bâtiments est influencée par plusieurs facteurs ; la température extérieure étant le facteur le plus impactant. A partir de ce constat, le mode de gestion classique de la demande dans les réseaux de chaleur, couramment appelé régulation par loi d'eau, se base sur des courbes de chauffe statiques qui déterminent la température de l'eau alimentant le circuit de chauffage interne au bâtiment en fonction des variations de la température extérieure : quand cette dernière chute, la température de chauffage est élevée, permettant ainsi au bâtiment de puiser plus de puissance du réseau. La régulation par loi d'eau présente des atouts en termes de simplicité et de robustesse dans la satisfaction de la demande [Ionesi et al., 2015]. Pourtant, ce mode de gestion manque de flexibilité.

La flexibilité de la demande est un élément-clef valorisé par les stratégies de gestion optimale. Elle émerge dès lors qu'on prend en compte d'autres facteurs qui agissent sur la demande en chauffage. L'inertie thermique du bâtiment décale sa demande par rapport aux variations de la température extérieure ; plusieurs études ont démontré l'intérêt de l'exploitation de cette inertie pour le stockage et le déstockage de l'énergie dans l'objectif de réduire les coûts de chauffage [Reynders, 2015a; Le Dréau et Heiselberg, 2016a]. Les sources de chaleur passive, c.-à-d. l'ensoleillement et les apports internes dus au comportement des occupants, peuvent couvrir jusqu'à 20% de la demande des bâtiments basse consommation [Foteinaki *et al.*, 2018a; Touria *et al.*, 2015], donc leur anticipation présente un potentiel de réduction de la consommation en chauffage. Le prix variable de l'énergie, initialement apparu dans les réseaux intelligents électriques pour inciter les consommateurs à adapter leurs habitudes de consommation afin de réaliser des économies énergétiques, entre en jeu dans les stratégies de gestion avancées des réseaux de chaleur envisageant la modulation de la demande en chauffage. La modulation automatisée de la demande est l'action de contrôle permettant à l'opérateur du réseau d'adapter les courbes de charge des bâtiments, dans le cadre d'une optimisation opérationnelle, à condition de bien veiller sur le confort thermique des usagers [Robillart, 2015a; Hu *et al.*, 2019a].

Une stratégie de gestion optimale de la demande des bâtiments raccordés à des réseaux de chaleur valorise la flexibilité de la demande par des actions de modulation en tenant compte de certains ou tous les facteurs suivants : la température extérieure, l'inertie thermique du bâtiment, l'ensoleillement, le comportement des occupants et le prix de l'énergie. Ses apports économiques et environnementaux à l'échelle d'un réseau de chaleur sont prometteurs selon plusieurs études théoriques [Kärkkäinen et al., 2003; Wernstedt et al., 2007]. Cependant, son implémentation n'est pas aussi simple qu'une loi d'eau ; elle requiert tout d'abord un modèle thermique du bâtiment qui permet la prédiction des éventuelles conséquences de la modulation sur les conditions de confort thermique dans le bâtiment, et ensuite, en se basant sur ce modèle, une loi de commande prédictive doit être conçue pour calculer la trajectoire optimale de la température de chauffage en fonction des prévisions relatives aux facteurs impactant la demande.

En pratique, les méthodologies proposées dans la littérature pour les deux étapes de modélisation et de conception du contrôleur prédictif sont difficilement applicables à grande échelle pour la gestion de la demande dans les réseaux de chaleur. Pour ce qui est de la modélisation du bâtiment, les modèles proposés dans la littérature ne sont souvent pas identifiables avec le peu de données disponibles à grande échelle pour l'opérateur du réseau de chaleur, et quand ils le sont, ils ne représentent pas proprement l'inertie du système. Par conséquent, le contrôle basé sur de tels modèles ne sera pas pertinent.

L'objectif de cette thèse est de proposer une méthodologie de modélisation de bâtiment et une stratégie de commande optimale prédictive de la demande en chauffage basée sur le modèle obtenu en ne s'appuyant que sur des données et moyens de contrôle disponibles et facilement accessibles en sous-station, tout en exploitant l'inertie thermique du système composé du bâtiment avec son circuit de chauffage. L'avantage principal de ce travail par rapport à la littérature sera la possibilité d'implémenter la gestion optimale de la demande à grande échelle dans les réseaux de chaleur.

Ces travaux sont menés et démontrés par simulation numérique. De ce fait, nous commençons par développer des simulateurs thermiques dynamiques de bâtiments résidentiels représentatifs du parc immobilier français qui constitueront notre environnement de recherche virtuel. Ensuite, une méthodologie de développement d'un modèle d'ordre réduit de bâtiment est proposée. Elle commence par la définition d'une structure convenable à notre application de contrôle et se poursuit par une approche d'identification paramétrique qui se sert strictement des données disponibles en sous-station. Enfin, un contrôleur flexible et prédictif est conçu pour calculer la trajectoire optimale de la température de chauffage en permettant un compromis entre coûts de chauffage et confort thermique des usagers. Les grandes lignes des méthodologies employées à chaque étape ainsi que les importants résultats obtenus sont présentés dans la suite de ce résumé.

Modélisation thermique et simulation dynamique de bâtiments résidentiels multizones

Choix de l'outil de simulation

Parmi les plusieurs outils de simulation numérique dédié à la thermique du bâtiment, nous avons choisi un outil qui remplit les conditions suivantes :

- Une modélisation par approche nodale, où les volumes de contrôle sont de la taille d'une zone thermique supposée à température uniforme, sans rentrer dans la modélisation détaillée du flux d'air ou des champs de température à l'intérieur de la zone. Cette condition élimine les outils de simulation CFD.

- Une modélisation dynamique où un système d'équations différentielles est résolu à des pas de temps variables ou fixes, et multi-physique où des phénomènes appartenant à divers domaines peuvent être modélisés ; notamment des phénomènes thermiques, hydrauliques et d'asservissement.
- La possibilité de traiter les échelles de temps suivantes :
    - Observation des dynamiques à l'échelle d'une minute ;
    - Actions de contrôle au niveau de la sous-station à des pas de temps de 15 minutes ;
    - Horizon de prédiction relatif à la commande prédictive de l'ordre de 24 heures ;
    - Simulations sur 2 semaines ;
    - Temps de simulation sur 2 semaines entre 5 à 10 minutes.
- Une bonne documentation des modèles trouvés pour les outils commerciaux ou développés au sein des laboratoires de recherche externes ce qui facilitera leur utilisation, ainsi que la possibilité d'accéder aux codes pour modifier ou compléter les modèles selon notre besoin.
- La compatibilité avec d'autres outils qui feront partie de la chaine d'exécution dans la commande prédictive via le standard FMI.

Parmi plusieurs outils candidats comme SIMBAD – Matlab, COMFIE – PLEAIDES, EnergyPlus, TRNSYS, nous avons choisi de travailler en langage Modelica dans l'environnement Dymola qui satisfait toutes les conditions requises. Notre simulateur sera basé sur des modèles validés des librairies *Buildings* développée au laboratoire LBNL de l'Université de Californie [Wetter *et al.*, 2011a] et *DistrictHeating* développée au sein de notre laboratoire LSED du CEA [Giraud *et al.*, 2015a].

Composition du simulateur

Comme mentionné précédemment, nous employons la modélisation par approche nodale. De ce fait, le composant de base dans le simulateur du bâtiment est un modèle de zone thermique équivalente à une ou plusieurs pièces. Il s'agit d'un volume de contrôle rempli d'air homogène, à température uniforme, qui échange avec son environnement via des connections appelés ports thermiques en langage Modelica.

Une zone thermique est connectée à, et échange avec, une enveloppe de bâtiment, composée de parois opaques et vitrées multicouches. Les phénomènes de transfert thermique modélisés dans ces parois sont la conduction thermique monodirectionnelle dans les couches discrétisées, la convection naturelle des deux côtés intérieur et extérieur de la paroi, et la transmittance du flux radiatif solaire à travers les vitres.

Un modèle de distribution et de réflexion du flux solaire suppose que la totalité du flux transmis par les vitres est reçu par le sol où une partie sera absorbée et le reste sera reflété vers les autres surfaces. Ensuite un échange radiatif infrarouge prend place entre toutes les surfaces internes.

Nous avons constaté d'après l'étude bibliographique que la masse interne dans les bâtiments, constituée principalement par le mobilier et les partitions internes, a un impact non négligeable sur la ralentissement des dynamiques de la température interne [Johra et Heiselberg, 2017a; Antonopoulos et Koronaki, 2000a; Al-Sanea *et al.*, 2012a]. Afin d'intégrer cet effet au simulateur, nous représentons la masse interne par des parois supplémentaires en bois, métal, céramique et matériau léger avec des proportions suggérées dans la littérature.

La ventilation est modélisée en tant que pertes thermiques vers l'extérieur à un taux constant représentatif du taux de renouvellement d'air dans les bâtiments.

Un modèle détaillé d'un système de chauffage hydraulique est connecté à la zone thermique. Il est composé d'un robinet thermostatique dont la fonction est de réguler la température de la zone à une température de consigne donnée par contrôle du débit de l'eau de chauffage traversant un émetteur de chaleur de type radiateur et acheminée dans un circuit de tuyauterie avec une ligne d'aller et une ligne de retour. Ce circuit de chauffage est alimenté par une sous-station de réseau de chaleur où la gestion de la demande par contrôle de la température de chauffage prend place.

Une deuxième source de chaleur qui vient s'injecter dans la zone thermique provient d'un modèle stochastique des apports internes. Ce modèle est basé sur des données statistiques de l'occupation de différentes pièces dans un bâtiment, à partir desquelles des profils d'usage des appareils électriques et de l'eau chaude sanitaire sont générés. Ses profils sont ensuite convertis en chaleur dissipée dans les zones équivalentes. Cette modélisation est issue des travaux de la littérature [Richardson *et al.*, 2008a, 2010a; Jordan et Vajen, 2005].

Enfin, les conditions aux limites de la zone thermique telle la température extérieure, l'ensoleillement, la vitesse de l'air, etc., sont transmises à travers un lecteur de fichier météo.

Nous avons choisi d'assembler quatre zones thermiques, équivalentes d'une zone de jour, une zone de nuit, une cuisine et une salle de bain, pour composer un étage. Plusieurs étages pourront ensuite être empilés pour simuler un bâtiment multizone et multiétage.

Introduction des cas d'étude

Une fois le simulateur de bâtiment générique développé, trois cas d'étude spécifiques sont introduits de manière à représenter trois classes énergétiques différentes :

- *Bâtiment 1915* représentant des bâtiments anciens haute consommation énergétique ;
- *Bâtiment 1975* représentant des bâtiments moyenne consommation ;
- *Bâtiment 2012* représentant des bâtiments basse consommation, de type RT2012.

Ces trois cas d'étude partagent les mêmes caractéristiques géométriques – celles d'un bâtiment résidentiel nommé *Le Salammbô* – en termes d'orientation, surface au sol, surfaces des façades, surfaces vitrées, fractions des surfaces équivalentes, etc. *Le Salammbô* est situé à Grenoble et raccordé à une boucle basse pression du réseau de chaleur du quartier *Zac Flaubert*. Il pourra potentiellement jouer le rôle de démonstrateur expérimental des stratégies de gestion avancées de la demande.

Ce qui différencie les cas d'étude et les répartit sur des classes énergétiques différentes, ce sont leurs matériaux de construction et les caractéristiques relatives à leurs systèmes de chauffage et de ventilation. Pour les matériaux de construction, nous nous sommes référés à une étude statistique appelée *TABULA* [FR_TABULA, 2015a] effectuée sur le parc immobilier français qui fournit un exemple-type de la construction des bâtiments par année de construction. *Bâtiment 1915* est construit en pierre massive, sans isolation thermique avec des fenêtres simple vitrage. *Bâtiment 1975* est construit en parpaing avec 4 cm d'isolation par l'extérieur et des fenêtres double vitrage à air. *Bâtiment 2012* est construit en béton avec 16 cm d'isolation par l'extérieur et des fenêtres double vitrage à argon. En ce qui concerne le modèle du système de ventilation, nous avons fixé des taux de renouvellement d'air constants distincts par bâtiment, de 0.5 Vol/h, 0.4 Vol/h et 0.3 Vol/h pour les *Bâtiments 1915, 1975* et *2012,* respectivement. Par conséquence des matériaux de construction et des taux de renouvellement d'air, les besoins en chauffage des cas d'étude sont différents et ainsi la puissance de dimensionnement de leurs sous-stations. Donc nous avons calculé ces puissances et nous avons trouvé 114 W/m^2, 60 W/m^2 et 28 W/m^2 pour les *Bâtiments 1915, 1975* et *2012,* respectivement. Finalement, nous avons défini des courbes de chauffe statiques pour chacun des cas d'étude qui seront utilisées ultérieurement pour comparaison entre une loi de commande prédictive optimale et une gestion classique par loi d'eau.

Modélisation d'ordre réduit du bâtiment

Définition du modèle recherché

Une fois l'environnement de simulation développé, nous rentrons dans l'étape la plus cruciale pour la mise en place de la stratégie de commande prédictive : la modélisation du bâtiment. Nous commençons par définir le modèle recherché. Il s'agit d'un ensemble d'équations différentielles et algébriques paramétrisées qui, par résolution dynamique dans le temps, permettront de calculer à tout instant les sorties observables et les états cachés du système en fonction de ses entrées contrôlables et non contrôlables. Dans le cas d'un bâtiment équipé d'un système de chauffage hydraulique, raccordé à un réseau de chaleur et contrôlé au niveau de sa sous-station, les entrées non contrôlables du point de vue de l'opérateur du réseau sont la température extérieure et le flux d'ensoleillement, ainsi que la température de consigne de l'air interne, qui est contrôlée par les occupants. La seule entrée contrôlable en sous-station est la température de départ du circuit de chauffage. Les observations récupérées en sous-

station sont la température de retour du circuit de chauffage, le débit d'eau y circulant et la puissance puisée du réseau. Le principal état caché qui doit être prédit par le modèle est la température moyenne d'air interne.

Le processus de développement du modèle commence par la définition de sa structure, c.-à-d. le nombre et la forme de ses équations ; ceci peut être accompli en se basant sur des connaissances physiques dans une approche appelée modélisation de type boite grise. Ensuite, le processus se poursuit par l'identification des paramètres ; ceci peut être traité en tant que problème d'optimisation dont l'objectif est de trouver l'ensemble de paramètres qui minimise l'erreur entre un historique de sorties du système et les sorties du modèle soumis à un même jeu d'entrées.

Le modèle ainsi développé doit satisfaire trois critères essentiels. Tout d'abord, il doit être précis en termes de prédiction de la température interne moyenne du bâtiment. Cette précision est atteinte, à la fois, grâce à une structure qui tient compte des éléments les plus influençant sur les dynamiques thermiques du bâtiment, et grâce à un algorithme d'identification paramétrique robuste. Ensuite, afin d'assurer son intégration dans un problème d'optimisation en ligne lors de la commande prédictive optimale, il est crucial que le modèle soit numériquement efficace. A cet effet, les modèles d'ordre-réduit à structure linéaire sont privilégiés. Finalement, le modèle doit être identifié en ne se servant que des sorties observables au niveau de la sous-station, notamment en s'abstenant d'utiliser des mesures de température interne qui est considérée comme un état caché dans cette thèse, contrairement aux travaux de modélisation similaires trouvés dans la littérature.

Méthodologie de modélisation

Structure

La famille de modèles qui nous intéresse est à structure interprétable physiquement (boite grise), souvent représentée graphiquement par analogie thermique-électrique sous forme de circuit électrique.

La structure la plus simple correspond à un modèle de 1er ordre où tous les éléments du bâtiment sont agrégés dans un seul nœud de température en échange avec l'extérieur. Or, cette structure ne permet pas de distinguer les dynamiques lentes des éléments à forte capacité thermique des dynamiques rapides de l'air. De ce fait, elle est déconseillée pour des applications de contrôle qui visent à exploiter la capacité de stockage thermique dans la masse du bâtiment [Reynders *et al.*, 2013a; Vivian *et al.*, 2017a]. Pour de telles applications, il est souvent recommandé d'employer un modèle du 2nd ordre avec un nœud de température qui représente l'air interne et un autre pour l'enveloppe extérieure. Des échanges thermiques entre ces nœuds, et avec l'extérieur, sont modélisés par des coefficients d'échange constants [Berthou *et al.*, 2014a; Reynders *et al.*, 2014a]. Nous adoptons cette structure de base et nous l'enrichissons d'un 3ème nœud de température pour représenter la masse interne dont les dynamiques sont plus lentes que

celles de l'air et qui, d'après une étude préliminaire effectuée sur le simulateur, influe considérablement sur la capacité de stockage thermique court-terme dans le bâtiment et augmente la flexibilité de sa demande. Pour prendre en compte l'effet de l'ensoleillement, nous modélisons les apports solaires par un modèle linéaire qui multiplie le flux d'irradiation solaire par un coefficient constant et l'injecte dans chacun des trois nœuds.

Jusqu'à présent la structure ressemble à certains modèles trouvés dans la littérature [Leśko *et al.*, 2018]. Mais pour notre application dans le cadre des réseaux de chaleur, il est nécessaire de faire apparaitre la température de chauffage dans le modèle comme étant la variable de contrôle de la demande. Nous complétons alors le modèle du bâtiment par un modèle du système de chauffage. Ceci est rarement présenté dans la littérature. Dans une première tentative, nous commençons par ajouter un nœud de température qui représente le système de chauffage et qui échange de la chaleur par un coefficient constant avec l'air. Ce nœud est alimenté d'un flux de chaleur de la sous-station dont la valeur est proportionnelle à l'écart entre la température au nœud de chauffage et la température de consigne contrôlée en sous-station ; bien sûr ce flux sera borné entre zéro et la valeur maximale de dimensionnement. L'avantage de cette structure est qu'elle soit linéaire et donc numériquement efficace pour le contrôle. Cependant, en essayant de faire des identifications paramétriques, nous obtenons des modèles qui prédisent bien la sortie, la puissance demandée en sous-station, mais qui entrainent de larges erreurs sur la prédiction de la température de l'air. Pour remédier, nous introduisons deux nœuds de température dans le modèle du système de chauffage. Un premier nœud qui reçoit le flux de la sous-station comme précédemment décrit, et un deuxième qui représente les émetteurs à l'intérieur du bâtiment et qui échange avec l'air. Ensuite nous faisons apparaitre une nouvelle variable mesurable en sous-station qui est le débit d'eau circulant dans le circuit de chauffage. Ce débit est proportionnel à l'écart entre la température de l'air et la température de consigne contrôlée par les occupants. Il régit le flux de chaleur entre le nœud du circuit de chauffage en sous-station et les émetteurs. De cette manière, la structure intègre un modèle représentatif de l'opération des robinets thermostatiques et fournit une information directe en sous-station sur l'écart entre la température de l'air et sa température de consigne à travers la sortie débit. Elle devrait être plus précise dans la prédiction de la température de l'air, mais elle est non-linéaire puisque le flux entre les deux nœuds du système de chauffage est un produit de deux variables, le débit et l'écart de température entre les émetteurs et la sous-station. Cette non-linéarité sera traitée ultérieurement dans ls formulation du problème d'optimisation.

La structure finale ainsi obtenue est exprimée par 7 équations (Eq. 2.39 à Eq. 2.45) dans lesquelles figurent 3 entrées non-contrôlables : la température extérieure, le flux d'irradiation solaire et la température de consigne de l'air. On récupère 2 sorties observables en sous-station : la puissance et le débit de chauffage. Il y a 5 états cachés étant les températures au niveau des nœuds, et 16 paramètres à identifier.

$$C_{air} \cdot \frac{dT_{air}}{dt} = U_{[air-ext]} \cdot (T_{ext} - T_{air}) + U_{[air-env]} \cdot (T_{env} - T_{air}) + U_{[air-mass]} \cdot (T_{mass} - T_{air}) + U_{[air-em]} \cdot (T_{em} - T_{air}) + k^{s}_{air} \cdot \phi_{sol} \quad \text{Eq. (1)}$$

$$C_{env} \cdot \frac{dT_{env}}{dt} = U_{[env-ext]} \cdot (T_{ext} - T_{env}) + U_{[air-env]} \cdot (T_{air} - T_{env}) + k^{s}_{env} \cdot \phi_{sol} \quad \text{Eq. (2)}$$

$$C_{mass} \cdot \frac{dT_{mass}}{dt} = U_{[air-mass]} \cdot (T_{air} - T_{mass}) + k^{s}_{mass} \cdot \phi_{sol} \quad \text{Eq. (3)}$$

$$C_{em} \cdot \frac{dT_{em}}{dt} = U_{[air-em]} \cdot (T_{air} - T_{em}) + \dot{m}_{SST} \cdot c_p \cdot (T_{cir} - T_{em}) \quad \text{Eq. (4)}$$

$$C_{cir} \cdot \frac{dT_{cir}}{dt} = \eta_l \cdot \Phi_{SST} + \dot{m}_{SST} \cdot c_p \cdot (T_{em} - T_{cir}) \quad \text{Eq. (5)}$$

$$\Phi_{SST} = \Phi^{max}_{SST} \cdot \left[\!\left[G^{p}_{cir} \cdot \left(T^{set}_{cir} - T_{cir}\right) \right]\!\right]^{1}_{0} \quad \text{Eq. (6)}$$

$$\dot{m}_{SST} = \dot{m}^{max}_{SST} \cdot \left[\!\left[G^{p}_{air} \cdot \left(T^{set}_{air} - T_{air}\right) \right]\!\right]^{1}_{0} \quad \text{Eq. (7)}$$

Identification paramétrique

L'identification paramétrique revient à résoudre un problème d'optimisation dont l'objectif est de trouver l'ensemble des 16 paramètres du modèle qui minimisent une fonction d'erreur sur les sorties entre le modèle d'ordre réduit et un historique de données généré par le simulateur. Nous formulons la fonction objectif (Eq. (8)) sous la somme des erreurs quadratiques normalisées sur les deux sorties du modèle, la puissance et le débit en sous-station, cumulées sur une période d'identification de deux semaines avec un pas de discrétisation de cinq minutes. Afin de garantir une minimisation cohérente des erreurs sur les deux sorties à la fois, nous introduisons des poids sur les deux termes de la fonction objectif. Les paramètres sont contraints dans une plage physiquement plausible.

$$f_{obj} = \frac{1}{\Delta_{tr}} \cdot \int_{0}^{\Delta_{tr}} \left[\frac{1}{3} \cdot \left(\frac{Q^{HOM}_{SST} - Q^{ROM}_{SST}}{Q^{max}_{SST}} \right)^2 + \frac{2}{3} \cdot \left(\frac{\dot{m}^{HOM}_{SST} - \dot{m}^{ROM}_{SST}}{\dot{m}^{max}_{SST}} \right)^2 \right] dt \quad \text{Eq. (8)}$$

Afin de mener cette approche d'identification, nous considérons tout d'abord un jeu de données d'entrée sur deux semaines pendant lesquelles le simulateur est contrôlé par une loi d'eau avec un réduit de nuit qui sert à stimuler les dynamiques du circuit de chauffage et améliorer l'identifiabilité de ses paramètres. Le modèle d'ordre réduit sera soumis à ces mêmes entrées afin de calculer ses sorties qui seront comparées aux sorties du simulateur pour évaluer la fonction objectif. Les paramètres du modèle sont dictés par un algorithme d'optimisation métaheuristique hybride PSO-HJ convenable à ce type de fonction objectif non-linéaire, présentant plusieurs minima locaux et relativement rapide à calculer. Après plusieurs itérations, l'algorithme converge vers un ensemble de paramètres qui minimise l'erreur.

Nous définissons trois critères de performance du modèle ainsi identifié. Tout d'abord nous évaluons un indicateur de correspondance sur les sorties (Eq. (9)) pendant la phase d'identification et pendant une deuxième phase, également de deux semaines, de validation. Ensuite, nous étudions l'erreur sur la température de l'air interne (Eq. (10)) en terme de moyenne et écarts maximaux, sur les deux phases d'identification et de validation. Toutefois, comme nous le montrons dans les applications suivantes, de

bons indicateurs de correspondance sur les sorties et une faible erreur sur la température de l'air pourront être assurés par plusieurs ensembles de paramètres. Donc, pour obtenir l'ensemble le plus pertinent, il est nécessaire d'effectuer le processus d'identification plusieurs fois et retenir les résultats qui montreront une meilleure pertinence physique du coefficient de pertes global du bâtiment, jugée par un indice de correspondance (Eq. (13)) entre une valeur estimée à partir des données de dimensionnement (Eq. (11)) et une valeur calculée à partir des paramètres identifiés (Eq. (12)).

$$\varphi_x = \left(1 - \sqrt{\overline{\left(\frac{x^{HOM} - x^{ROM}}{x^{max} - \bar{x}}\right)^2}}\right) \times 100 \quad \text{Eq. (9)}$$

$$\varepsilon_{T_{air}} = T_{air}^{ROM} - T_{air}^{HOM} \quad \text{Eq. (10)}$$

$$U_{build}^{sizing} = \frac{Q_{SST}^{max}}{T_{air}^{sizing} - T_{ext}^{sizing,Grenoble}} \quad \text{Eq. (11)}$$

$$U_{build}^{ident} = \frac{U_{[air-env]} \cdot U_{[env-ext]} + U_{[env-ext]} \cdot U_{[air-ext]} + U_{[air-ext]} \cdot U_{[air-env]}}{U_{[air-env]} + U_{[env-ext]}} \quad \text{Eq. (12)}$$

$$\epsilon_{U_{build}} = \frac{U_{build}^{ident} - U_{build}^{sizing}}{U_{build}^{sizing}} \times 100 \quad \text{Eq. (13)}$$

Applications

Tests analytiques

Dans un premier temps, nous appliquons la stratégie d'identification sur un historique de données synthétiques généré à partir d'un modèle d'ordre réduit, l'objectif étant de vérifier si l'approche d'identification est capable de retrouver l'ensemble de paramètres connus à priori.

Deux tests sont menés. Dans le premier test, nous identifions les paramètres 1 par 1. Le processus d'identification est alors lancé 16 fois ; à chaque fois, 15 paramètres sont fixés à leurs bonnes valeurs et l'algorithme recherche la valeur optimale du 16ème paramètre. Les résultats montrent que certains paramètres sont precisement identifiés, alors que d'autres sont difficilement identifiables parce qu'ils impactent très légèrement la fonction objective.

Dans le deuxième test, nous identifions les 16 paramètres simultanément et nous lançons le processus d'identification 9 fois avec une initialisation de recherche différente à chaque essai. Les résultats rejoignent ceux du premier test. Certains paramètres sont bien identifiés indépendamment de l'initialisation, et d'autres prennent des valeurs différentes à chaque essai.

Nous concluons alors que le problème d'identification paramétrique est mal-posé, c.-à-d. que plusieurs solutions au problème d'optimisation peuvent coexister (fonction objectif à plusieurs minima locaux) et l'algorithme d'identification ne pourrait pas discerner le meilleur ensemble de paramètres à retenir. Ceci peut être dû à plusieurs causes :

- La structure du modèle est trop complexe ;
- Le scenario de génération de données d'identification ne capte pas toutes les dynamiques du système ;
- L'algorithme d'optimisation n'explore pas l'espace de recherche rigoureusement.

Pour s'affranchir de ce problème, nous proposons de lancer l'algorithme d'identification plusieurs fois et de retenir l'ensemble de paramètres le plus pertinent d'après le critère de pertinence physique présenté précédemment.

Application sur les cas d'étude

Nous appliquons maintenant l'approche d'identification sur des données générées par les simulateurs.

Les résultats concernant les critères de performance montrent tout d'abord une correspondance à plus de 90% entre le simulateur détaillé et le modèle d'ordre réduit pour les deux sorties, cela étant valable pour les trois cas d'étude pendant la phase d'identification. Cette correspondance se dégrade peu et reste au-delà de 85% en phase de validation (Figure 1).

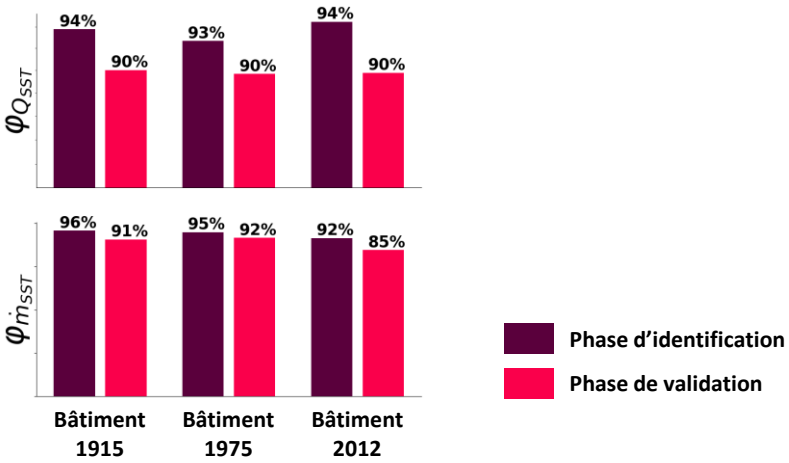

Figure 1 Résultats des indices de correspondance sur les sorties (Eq. (9)) suite à l'identification paramétrique des modèles des 3 cas d'étude

En ce qui concerne l'erreur sur la température interne, les valeurs moyennes trouvées pendant les phases d'identification et de validation sont de moins de 0.1°C, avec des erreurs maximales autour de 0.5°C, en valeurs absolues (Figure 2).

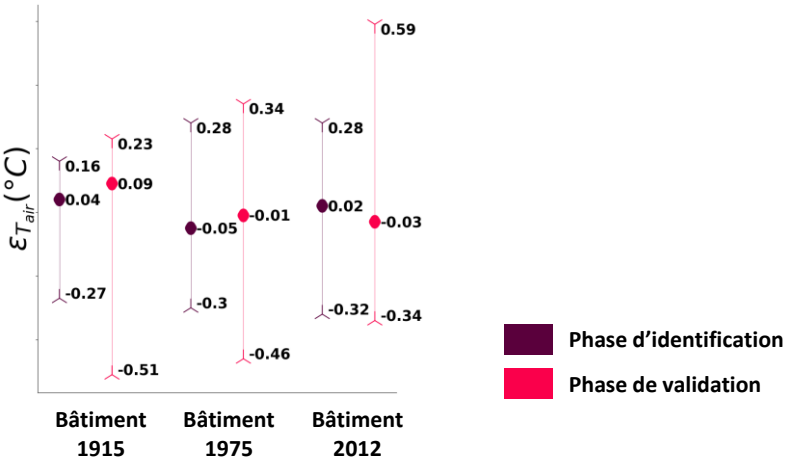

Figure 2 Résultats des moyennes et des écart maximaux de l'erreur sur la température de l'air interne moyenne (Eq. (10)) suite à l'identification paramétrique des modèles des 3 cas d'étude

En examinant les réponses temporelles (Figure 3), nous vérifions la bonne ressemblance sur les sorties des trois cas d'étude et nous remarquons que les erreurs les plus importants sur la température interne se produisent dans le *Bâtiment 2012* pendant les périodes de nuit. Nous interprétons alors que pour ce type de bâtiments fortement sensibles aux apports internes, qui d'ailleurs ne sont pas pris en compte dans le modèle d'ordre réduit, les paramètres identifiés pourront être biaisés de manière à compenser l'effet des apports internes pendant le jour, ce qui engendre plus d'erreur en absence de ces apports.

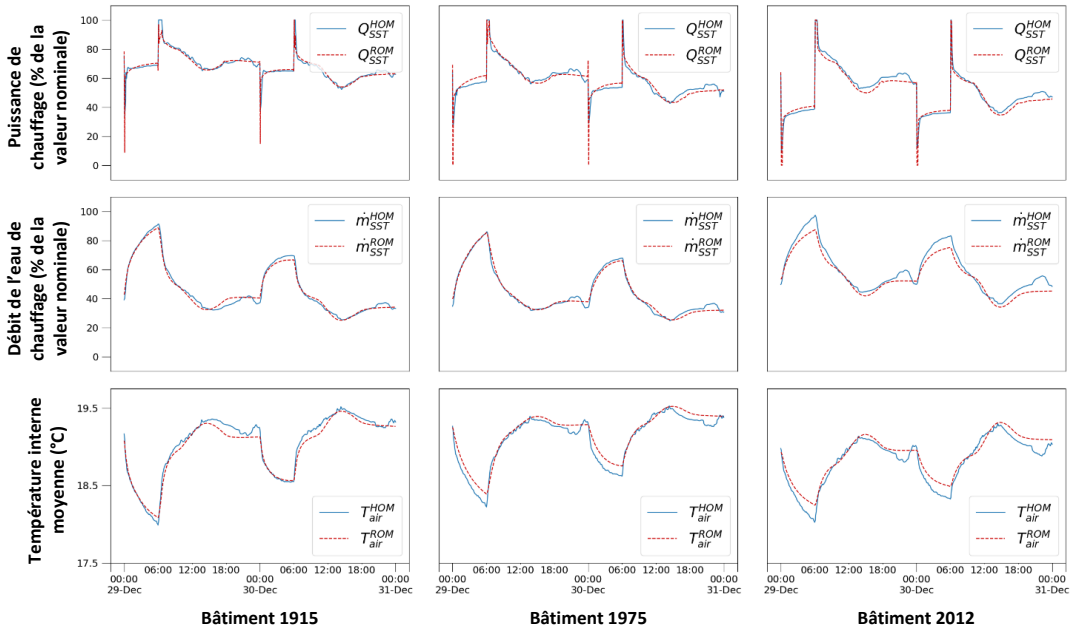

Figure 3 Comparaisons entre les données du simulateur (courbes en bleu) et les prédictions du modèle réduit (courbes en rouge) suite à l'identification paramétrique des modèles des 3 cas d'étude

Finalement, le critère de pertinence physique est évalué. Les ensembles de paramètres retenus assurent des erreurs minimes entre la valeur du coefficient de pertes global estimée U_{build}^{sizing} (Eq. (11)) et la valeur obtenue par identification paramétrique U_{build}^{ident} (Eq. (12)), pour les 3 cas d'étude (Figure 4). L'erreur la plus importante qui atteint 10% a été obtenue pour le *Bâtiment 2012*. Ceci est aussi interprété en lien avec la sensibilité de ce bâtiment aux apports internes.

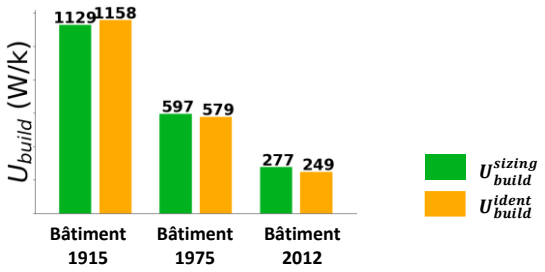

Figure 4 Vérification de la pertinence physique des coefficients de pertes globales suite à l'identification paramétrique des modèles des 3 cas d'étude

Nous concluons finalement que les modèles ainsi obtenus sont de précision suffisante pour notre application de commande prédictive.

Commande prédictive flexible de la demande en chauffage des bâtiments

Schéma de la commande prédictive

Rappelons tout d'abord que l'avantage essentiel de la commande prédictive par rapport à la régulation classique par loi d'eau est la possibilité de moduler la température de l'air interne dans le bâtiment, tout en veillant à ce qu'elle reste comprise dans la zone du confort thermique.

Afin d'effectuer cette modulation de manière optimale, la commande prédictive anticipe les facteurs impactant la demande en chauffage sur un horizon de prédiction, et emploie un contrôleur optimal qui, en se basant sur le modèle d'ordre réduit, prédit l'évolution de ses états et calcule la trajectoire optimale de la variable de contrôle (température de chauffage). L'optimalité est définie au sens d'un compromis entre coûts de l'énergie et confort thermique. Le contrôleur applique la consigne optimale au simulateur et remet à jour ses états par un observateur d'états. L'horizon de prédiction sera alors décalé d'un pas selon le principe de l'horizon fuyant. Ces étapes sont représentées dans Figure 5.

Nous avons implémenté la commande prédictive dans une plateforme appelée PEGASE qui permet la cosimulation des différents modules compatibles. La brique principale étant le contrôleur, nous allons détailler sa conception dans le paragraphe suivant.

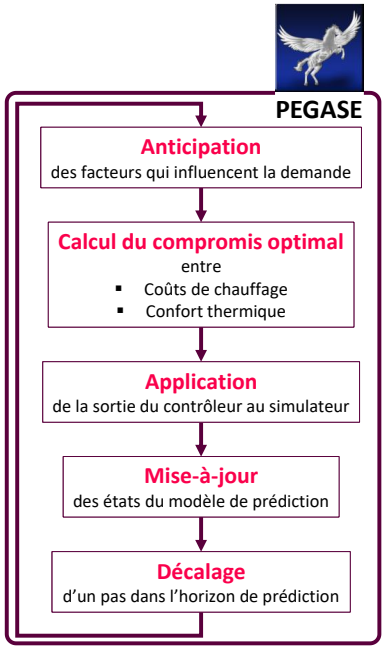

Figure 5 Schéma de la commande prédictive montrant les principales briques implémentées dans l'outil de cosimulation PEGASE

Conception du contrôleur flexible

La conception du contrôleur revient à formuler un problème d'optimisation dont la fonction objectif (Eq. (14)) comprend plusieurs termes à minimiser de façon à ce que la résolution du problème mène au compromis optimal entre eux.

Le premier terme de la fonction objectif représente la consommation énergétique pour le chauffage du bâtiment dont le coût est calculé par intégration du produit de l'énergie consommée par le prix de l'énergie sur l'horizon de prédiction.

Le deuxième et le troisième terme pénalisent l'inconfort thermique qui se produit lorsque la température de l'air s'écarte de la température de consigne à laquelle on soustrait un seuil de flexibilité contrôlable en sous-station par l'opérateur du réseau. Lorsque cet écart est d'une valeur positive, une sur-chauffe sera pénalisée et dans le cas contraire, une sous-chauffe sera pénalisée. Pour chacun de ces deux cas un coefficient de pénalisation distinct est affecté.

Le quatrième terme de la fonction objectif pénalise les pertes dans le circuit de chauffage. Physiquement, ces pertes augmentent avec l'augmentation de l'écart entre la température de chauffage et la température ambiante. Toutefois, du fait que cette physique n'a pas été représentée dans la structure du modèle réduit, le contrôleur ne discriminera pas un chauffage à haute température sans l'ajout de ce dernier terme.

$$f_{obj}^{MPC} = \sum_{n=1}^{N_{MPC}} \begin{pmatrix} p^{energy}[n] \cdot Q_{SST}[n] \cdot \Delta t_{MPC} \\ +p^{overheat}[n] \cdot \Delta T_{air}^{overheat}[n] \cdot \Delta t_{MPC} \\ +p^{underheat}[n] \cdot \Delta T_{air}^{underheat}[n] \cdot \Delta t_{MPC} \\ +p^{losses}[n] \cdot \Delta T_{cir}^{losses}[n] \cdot \Delta t_{MPC} \end{pmatrix} \quad \text{Eq. (14)}$$

L'ensemble des contraintes est constitué principalement des équations discrétisées du modèle d'ordre réduit (Eq. (15) à Eq. (21)). Les trois premières équations sont linéaires. Un terme bilinéaire apparait dans Eq. (18) et Eq. (19), et requiert une linéarisation que nous avons réalisée en utilisant la méthode de relaxation par enveloppes de McCormick [McCormick, 1976]. Des saturations apparaissent dans les deux dernières équations. Nous les avons traitées par une méthode de linéarisation par morceaux. Ces linéarisations introduisent des variables binaires au problème d'optimisation. Par conséquent, la formulation obtenue est linéaire-mixte. Le problème est résolu par le solveur adéquat de l'outil commercial CPLEX.

$$\boldsymbol{C_{air} \cdot \frac{T_{air}[n]-T_{air}[n-1]}{\Delta t} = U_{[air-ext]} \cdot (T_{ext}[n] - T_{air}[n]) + U_{[air-env]} \cdot (T_{env}[n] - T_{air}[n]) + U_{[air-mass]} \cdot (T_{mass}[n] - T_{air}[n]) + U_{[air-em]} \cdot (T_{em}[n] - T_{air}[n]) + k_{air}^{s} \cdot I_{sol}[n]} \quad \text{Eq. (15)}$$

$$\boldsymbol{C_{env} \cdot \frac{T_{env}[n]-T_{env}[n-1]}{\Delta t} = U_{[env-ext]} \cdot (T_{ext}[n] - T_{env}[n]) + U_{[air-env]} \cdot (T_{air}[n] - T_{env}[n]) + k_{env}^{s} \cdot I_{sol}[n]} \quad \text{Eq. (16)}$$

$$\boldsymbol{C_{mass} \cdot \frac{T_{mass}[n]-T_{mass}[n-1]}{\Delta t} = U_{[air-mass]} \cdot (T_{air}[n] - T_{mass}[n]) + k_{mass}^{s} \cdot I_{sol}[n]} \quad \text{Eq. (17)}$$

$$\boldsymbol{C_{em} \cdot \frac{T_{em}[n]-T_{em}[n-1]}{\Delta t} = U_{[air-em]} \cdot (T_{air}[n] - T_{em}[n]) + \dot{m}_{SST}[n] \cdot c_{wat} \cdot (T_{cir}[n] - T_{em}[n])} \quad \text{Eq. (18)}$$

$$\boldsymbol{C_{cir} \cdot \frac{T_{cir}[n]-T_{cir}[n-1]}{\Delta t} = \eta_l \cdot Q_{SST}[n] - \dot{m}_{SST}[n] \cdot c_{wat} \cdot (T_{cir}[n] - T_{em}[n])} \quad \text{Eq. (19)}$$

$$\boldsymbol{Q_{SST}[n] = Q_{SST}^{max} \cdot [\![G_{cir}^{p} \cdot (T_{cir}^{set}[n] - T_{cir}[n])]\!]_0^1} \quad \text{Eq. (20)}$$

$$\boldsymbol{\dot{m}_{SST}[n] = \dot{m}_{SST}^{max} \cdot [\![G_{air}^{p} \cdot (T_{air}^{set}[n] - T_{air}[n])]\!]_0^1} \quad \text{Eq. (21)}$$

Application

Nous appliquons la commande prédictive sur les 3 cas d'étude en considérant 3 scenarios :

- Un 1er scenario avec un prix d'achat de l'énergie fixe et un niveau de modulation de la température interne fixe et limitée à 0.5°C ;
- Un 2ème scenario avec un prix d'achat de l'énergie fixe et un niveau de modulation de la température interne limitée égal à 0.5°C pendant la journée et 2°C pendant les heures de nuit ;
- Un 3ème scenario avec un prix d'achat de l'énergie 10 fois plus élevée en début de matinée que le reste du jour et un niveau de modulation de la température interne limitée égal à 0.5°C pendant la journée et 2°C pendant les heures de nuit.

Le but de ces essais est de vérifier la réactivité du contrôleur vis-à-vis des sollicitations, de comparer la commande prédictive à la régulation classique par loi d'eau en observant l'exploitation de l'inertie thermique du bâtiment traduite dans les actions de contrôle prédictif en sous-station et de s'assurer du respect des conditions de confort thermique aux usagers.

L'essentiel des observations peut être déduit des graphes de la Figure 6 :

- Nous observons l'anticipation du gain solaire par le contrôleur prédictif, ce qui réduit la température de chauffage avant le pic d'irradiation solaire. Lorsque la température de chauffage est réduite, l'air interne se refroidit, ce qui déclenche l'ouverture du robinet thermostatique, augmentant ainsi le débit massique de l'eau de chauffage à travers la sous-station. Avec la commande prédictive, nous avons donc pu manipuler la température intérieure tout en veillant au confort thermique. Cela n'est pas possible dans le cas d'une régulation par loi d'eau en se basant uniquement sur une courbe de chauffe standard.
- Pendant le délestage de nuit, la commande prédictive prend compte de l'inertie thermique du bâtiment. On distingue 3 phases de cette prise en compte dans le graphique de la température de chauffage du *Bâtiment 2012* ci-dessous. Dans une 1ère phase, le contrôleur diminue la température de chauffage pour arrêter complètement la puissance injectée en sous-station avant le début du délestage. La 2ème phase démarre immédiatement après avoir atteint un débit de chauffage maximal. Ainsi, le système de chauffage fonctionne à débit maximal constant en re-augmentant lentement la température de chauffage au fil du temps. La 3ème phase débute avant la fin du délestage nocturne. Encore une fois, le moment de retour au mode de fonctionnement normal est décidé en fonction de l'inertie du bâtiment. Cependant, la régulation par loi d'eau suit strictement l'impulsion préprogrammée du délestage sans tenir compte des retards dus à l'inertie thermique.

- En examinant les résultats du 3ème scenario appliqué au *Bâtiment 1915*, on constate que le contrôleur prédictif diminue la consommation du bâtiment pendant les périodes à prix d'énergie élevé en réglant la température de chauffage à sa limite inférieure. Afin de limiter l'inconfort qui en résulte, le contrôleur prédictif stocke de la chaleur dans la masse thermique du bâtiment juste avant ces périodes. La chaleur stockée sera ensuite évacuée pendant les périodes à prix d'énergie élevé.

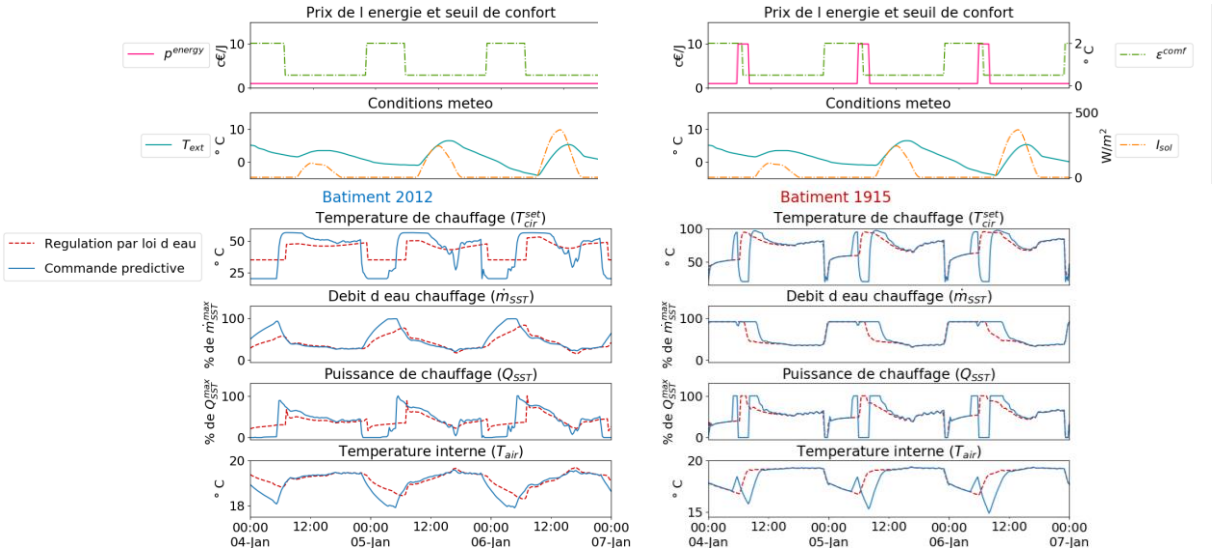

Figure 6 Exemple des résultats du contrôle : comparaison entre la commande par loi d'eau et la commande prédictive sous le 2ème scenario pour le *Bâtiment 2012* et sous le 3ème scenario pour le *Bâtiment 1915*

Nous concluons finalement que la commande prédictive présente un potentiel de modulation de la demande qui pourra être exploité pour déplacer les pics de consommation et effacer les charges dans le but de minimiser le recours aux générateurs d'appoint à grande échelle.

Conclusion

Dans le cadre de l'optimisation opérationnelle des réseaux de chaleur, les recherches menées dans cette thèse visent à développer et à démontrer numériquement une stratégie de contrôle avancé de la demande en chauffage des bâtiments, réalisable pratiquement à l'échelle d'un réseau de chaleur.

L'une des principales motivations de cette recherche est le fait que l'inertie thermique des bâtiments rend leur demande en chauffage intrinsèquement flexible. Toutefois cette flexibilité n'est pas pleinement (ou du tout) exploitée dans les pratiques de contrôle actuelles. Actuellement dans les réseaux de chaleur, la demande en chauffage est partiellement contrôlée en sous-station par une loi d'eau : un réglage statique de la température de l'eau d'alimentation du système de chauffage interne du bâtiment (souvent des radiateurs ou des dalles chauffantes) en fonction de la température extérieure. Cette stratégie de contrôle

conventionnelle néglige l'inertie thermique du bâtiment et vise à répondre à tout prix à la demande de manière plutôt stricte. Son remplacement par une stratégie de contrôle intelligente et flexible est essentiel pour l'optimisation opérationnelle des réseaux de chaleur car il permet une gestion efficace des sources de chaleur, l'intégration de l'énergie renouvelable intermittente et la réduction des coûts globaux économiques et environnementaux.

Dans cette thèse, nous proposons la commande prédictive comme une alternative à la régulation par loi d'eau. La principale contribution est le développement d'une stratégie de contrôle de la demande en chauffage complète et cohérente. Elle commence par l'étape la plus cruciale de modélisation d'ordre réduit du bâtiment suivie par la conception et la mise en œuvre de la loi de commande, le tout en respectant les défis pratiques de la disponibilité des données et de la contrôlabilité du système depuis la sous-station.

L'étude est réalisée par simulation numérique. Nous avons donc commencé par développer un simulateur thermique dynamique d'un bâtiment résidentiel connecté à une sous-station d'un réseau de chaleur dans l'environnement Modelica / Dymola. Le simulateur permet la représentation de bâtiments multi-zones et multi-étages basée sur une approche nodale. Il sera paramétré pour représenter 3 cas d'étude de bâtiments résidentiels appartenant à des classes énergétiques variées : basse, moyenne et haute consommation, qui constitueront l'environnement de recherche virtuel de ces travaux.

La commande prédictive nécessite un modèle d'ordre réduit du bâtiment, capable de prédire les dynamiques thermiques du système à court terme. Le développement de ce modèle s'effectue en deux étapes. Premièrement, nous définissons la structure du modèle en se basant sur des connaissances physiques, ensuite nous mettrons en place une stratégie d'identification paramétrique en se servant d'un historique de données généré par le simulateur. Des études préliminaires nous ont conduit à opter pour un modèle de bâtiment linéaire du 3ème ordre couplé à un modèle non linéaire du système de chauffage. L'identification des paramètres s'appuie sur des mesures couramment trouvées en sous-station : la puissance et le débit massique de l'eau de chauffage. La recherche de l'ensemble optimal de paramètres qui minimise l'erreur entre les prédictions du modèle et l'historique du simulateur est effectuée par un algorithme hybride d'optimisation méta-heuristique (PSO-HJ). Des limitations de cette approche ont été identifiées à partir de tests analytiques. Elles se résument par une faible identifiabilité de certains paramètres, ce qui nécessite l'engagement de l'interprétation physique dans l'approche d'identification. Pour les applications sur les 3 cas d'étude, des résultats satisfaisants basés sur l'évaluation des critères de performance ont finalement été obtenus.

Une fois le modèle de bâtiment développé, la commande prédictive est mise en œuvre par la conception d'un contrôleur optimal. Dans cette thèse, le contrôleur est élaboré par programmation linéaire mixte. Il s'agit d'un problème d'optimisation dont la fonction objectif (à minimiser) est principalement composée

d'un terme qui pénalise les coûts de chauffage dépendant du prix d'achat de l'énergie, et des termes affectés par des paramètres de réglage qui pénalisent l'inconfort thermique, caractérisé par une déviation de la température intérieure par rapport à un point cible défini au sous-station. Ainsi, le contrôleur permet de calculer un compromis optimal entre les coûts de chauffage et l'inconfort thermique. La relation physique entre les variables du système est fournie par les équations linéarisées du modèle d'ordre réduit constituant les principales contraintes du problème. Contrairement à la régulation par loi d'eau qui détermine la température de l'eau de chauffage uniquement en fonction de la température extérieure, la commande optimale prédictive trouve des trajectoires optimales de cette variable de contrôle sur un horizon fuyant et tenant compte de l'inertie thermique du système. Ainsi, la commande prédictive proposée permet une exploitation responsable de la flexibilité de la demande. La mise en œuvre de la stratégie de contrôle est réalisée à l'aide de la plate-forme de cosimulation PEGASE. La démonstration sur les 3 cas d'étude basée sur leurs modèles identifiés a montré une exploitation correcte de leur inertie thermique lors des essais de délestage et de sensibilité aux variations des coûts de l'énergie.

Les travaux de recherche présentés dans cette thèse ont été réalisés par simulation numérique et à l'échelle du bâtiment. Nous distinguons 3 axes de recherche en perspectives. Tout d'abord, une application expérimentale s'avère nécessaire pour la validation des résultats. De nouveaux défis pourront être rencontrés à ce stade, en termes de quantification des incertitudes que ce soit au niveau des données utilisées dans l'identification paramétrique ou au niveau de la prédiction météorologique lors de la commande. Dans une deuxième perspective, il sera intéressant de passer à l'échelle ; tout d'abords par la commande distribuée d'un parc de bâtiment et ensuite par la commande optimale couplée de la production, la distribution et la demande à l'échelle d'un réseau de chaleur. Finalement, une étude techno-économique sera sans-doute intéressante pour évaluer les apports et les conséquences économiques et environnementales de la commande prédictive à grande échelle.

Acronyms and notations

Acronym	Definition
BL	Bi-Linear
BTS	Building Thermal Simulator
DH	District Heating
DHS	District Heating System
DHW	Domestic Hot Water
DMPC	Distributed Model Predictive Control
DSM	Demand-Side Management
ED	Electric Device
HJ	Hooke-Jeeves
HOM	Higher-Order Model
HVAC	Heating, Ventilation and Air Conditioning
IG	Internal Gain
LP	Linear Programming
MILP	Mixed-Integer Linear Programming
MIP	Mixed-Integer Programming
MPC	Model Predictive Control
MSE	Mean-Square Error
NLP	Non-Linear Programming
PSO	Particle Swarm Optimization
PWL	Piece-Wise Linear
RC	Resistance-Capacitance
RMSE	Root Mean-Square Error
ROM	Reduced-Order Model
SG	Smart Grid
SH	Space-Heating
SMPC	Stochastic Model Predictive Control
SSE	Sum-Squared Error
TRV	Thermostatic Radiator Valve
WCC	Weather Compensation Control

Notations introduced in Chapter 1

Latin letter	Unit	Definition
$c_{...}$	$[J/kg \cdot K]$	Specific thermal capacity
e_{lay}	$[m]$	Thickness of a construction element layer
f_r	$[-]$	Fraction of the radiative to the total heat emitted by a radiator
h_{conv}^{ext}	$[W/m^2 \cdot K]$	Surface heat convection coefficient between the external surfaces and the outdoor environment
h_{conv}^{int}	$[W/m^2 \cdot K]$	Surface heat convection coefficient between the thermal zone air and the internal surfaces
h_{flo}	$[m]$	Storey height
$k_{...}$	$[W/m \cdot K]$	Thermal conductivity
$m_{...}$	$[kg/m^2]$	Mass per unit floor area
$\dot{m}_{...}$	$[kg/s]$	SH water mass flowrate
n_{rad}	$[-]$	Radiator exponent of heat transfer
n_{vent}	$[1/hr]$	Number of air changes per hour for a thermal zone
v_{mix}	$[m/s]$	Mixing air velocity through the door opening
C_{TRV}	$[-]$	TRV flow coefficient
D_{bulb}	$[m]$	Diameter of the cylindrical TRV bulb
I_{sol}^{dir}	$[W/m^2]$	Direct normal solar irradiation
I_{sol}^{glo}	$[W/m^2]$	Global horizontal solar irradiation
I_{sol}^{dif}	$[W/m^2]$	Diffuse horizontal solar irradiation
J_{in}	$[W]$	Incoming solar radiosiy through a window
N_{dir}	$[-]$	Number of direct heat flows injected into a thermal zone
N_{flo}	$[-]$	Number of floors in the BTS
$N_{int\ surf}$	$[-]$	Number of internal surfaces in contact with the thermal zone air
N_{neigh}	$[-]$	Number of neighbouring nodes to a thermal zone
N_{rad}	$[-]$	Number of discretised volumes in the radiator model
$N_{rad\ sour}$	$[-]$	Number of radiant sources in a thermal zone
N_{sta}	$[-]$	Number of discretized states for a construction element layer
N_{sta}^{ref}	$[-]$	Normalizing number of discretization states
N_{win}	$[-]$	Number of windows for a thermal zone
N_{zones}	$[-]$	Number of thermal zones in the BTS
Q_{conv}^{ext}	$[W]$	Convective heat exchange between an envelope element and the outdoor environment
Q_{conv}^{int}	$[W]$	Convective heat exchange between an envelope element and the thermal zone
Q_{dir}	$[W]$	Direct heat flows injected into a thermal zone
Q_{env}^{gla}	$[W]$	Total heat loss through the building envelope glazing systems

Q_{env}^{opa}	$[W]$	Total heat loss through the building envelope opaque constructions
$Q_{door\ open}$	$[W]$	Heat exchange due to door opening
$Q_{rad\ sour}$	$[W]$	Radiative heat emitted by a radiant source
$Q_{rad\ sour}^{int\ surf}$	$[W]$	Radiative heat received by an internal surface from a radiant source
Q_{rad}^{lw}	$[W]$	Long wave radiant heat emitted by a surface
Q_{rad}^{conv}	$[W]$	Convective heat emitted by a radiator
Q_{rad}^{rad}	$[W]$	Radiative heat emitted by a radiator
Q_{rad}^{tot}	$[W]$	Total heat emitted by a radiator
Q_{sol}	$[W]$	Total solar irradiation received by a thermal zone
$Q_{sol}^{all\ non-flo}$	$[W]$	Diffused irradiation reflected by the floor surface to all non-floor surfaces in a thermal zone
Q_{sol}^{flo}	$[W]$	Solar irradiation absorbed and transmitted by the floor surface in a thermal zone
Q_{therm}^{DHW}	$[W]$	Internal heat gain due to DHW usage
Q_{therm}^{ED}	$[W]$	Internal heat gain due to ED
Q_{elec}^{ED}	$[W]$	ED electric power
Q_{therm}^{occ}	$[W]$	Internal heat gain due to occupancy
Q_{vent}	$[W]$	Heat exchange due to ventilation
Q_{IG}	$[W]$	Total internal heat gain
Q_{SST}	$[W]$	SH power at the substation
S_{bulb}	$[m^2]$	Surface area of the cylindrical TRV bulb
$S_{ext\ surf}$	$[m^2]$	Surface area of an external surface
S_{door}	$[m^2]$	Surface area of an open door between two thermal zones
$S_{int\ surf}$	$[m^2]$	Surface area of an internal surface
$S_{int\ slab}$	$[m^2]$	Surface area (per side) of an internal mass equivalent slab
S_{flo}	$[m^2]$	Floor surface area
$S_{non-flo}$	$[m^2]$	Surface area of a non-floor internal facing surface
S_{surf}	$[m^2]$	Surface area in the long wave irradiation balance
S_{zone}	$[m^2]$	Floor surface area of a thermal zone
SG_{water}	$[-]$	Specific gravity of water
T_{air}^{zone}	$[K]$	Homogeneous temperature of the thermal zone air
T_{amb}	$[K]$	Ambient temperature surrounding the heating circuit
$T_{ext\ surf}$	$[K]$	Temperature of an external surface
$T_{int\ surf}$	$[K]$	Temperature of an internal surface
T_{neigh}	$[K]$	Temperature at a thermal zone neighbouring node
$T_{neigh\ zone}^{air}$	$[K]$	Temperature of a neighbouring thermal zone separated by a door
T_{oper}^{zone}	$[K]$	Thermal zone operative temperature
T_{rad}	$[K]$	Temperature at a volume in the radiator model
T_{rad}^{zone}	$[K]$	Thermal zone radiative temperature
T_{surf}	$[K]$	Surface temperature in the long wave irradiation balance
T_{DHW}	$[K]$	DHW temperature

T_{SST}^{ret}	$[K]$	Secondary return water temperature measured at the substation
T_{SST}^{sup}	$[K]$	Secondary supply water temperature delivered at the substation
$T_{SST}^{HC\,max}$	$[K]$	Maximum temperature of a heating curve
$T_{SST}^{HC\,min}$	$[K]$	Minimum temperature of a heating curve
T_{SST}^{nom}	$[K]$	Nominal supply water temperature at the substation
$T_{air}^{set\,nom}$	$[K]$	Nominal air set point temperature
U_{neigh}	$[W/K]$	Heat transfer coefficient between a thermal zone and a neighbouring node
UA_{rad}	$[W/K]$	Radiator coefficient of heat exchange
V_{DHW}	$[m^3]$	DHW volume during one usage
V_{zone}	$[m^3]$	Internal volume of a thermal zone

Greek letter	Unit	Definition
$\alpha_{...}$	$[-]$	Solar absorptivity
α_{zone}^{surf}	$[-]$	Fraction surface area of a thermal zone to the total floor area
α_{TRV}	$[\%]$	Opening percentage of the TRV bulb
$\varepsilon_{int\,slab}$	$[m]$	Thickness of an internal mass equivalent slab
ε_{surf}	$[-]$	Surface emissivity in the long wave irradiation balance
$\varepsilon_{SST}^{losses}$	$[-]$	Thermal losses coefficient in the substation
η_{IG}	$[-]$	Efficiency conversion into internal gain
θ_{build}	$[rad]$	Building orientation angle from the North
κ_{IG}	$[-]$	Internal gain staggering coefficient
$\rho_{...}$	$[kg/m^3]$	Density
σ	$[W/m^2 \cdot K^4]$	Stephan-Boltzmann constant
τ_{flo}	$[-]$	Solar transmissivity of the floor surface
Δt_{DHW}	$[s]$	Duration of a DHW usage
ΔP_{TRV}	$[Pa]$	Differential pressure between the TRV inlet and outlet
ΔT_{TRV}^{max}	$[K]$	Maximum temperature difference from the set point temperature before the TRV fully opens

Notations introduced in Chapter 2

Latin letter	Unit	Definition
f_{obj}	$[-]$	Objective function for the ROM parameters identification
$k_{...}^{s}$	$[m^2]$	Solar aperture surface area
l_{cog}^{PSO}	$[-]$	Cognitive learning factor
l_{soc}^{PSO}	$[-]$	Social learning factor
$q_{T_{air}}$	$[-]$	Normalized quadratic error integral on the indoor air temperature
r^{HJ}	$[-]$	Mesh size divider in the HJ algorithm
s^{HJ}	$[-]$	Step size in the HJ algorithm

s_p^{PSO}	$[-]$	Particle step size in the PSO algorithm
t^{HJ}	$[-]$	Mesh size exponent increment in the HJ algorithm
w^{PSO}	$[-]$	Step-size weight in the PSO algorithm
$C_{...}$	$[J/K]$	Thermal capacitance
$G_{...}^{p}$	$[K]$	Proportional gain for temperature regulation
I_{sol}	$[W/m^2]$	Global horizontal solar irradiation in the ROM
N_{red}^{HJ}	$[-]$	Maximum number of mesh size reductions in the HJ algorithm
N_{gen}^{PSO}	$[-]$	Number of generations
N_{par}^{PSO}	$[-]$	Number of particles
$T_{...}$	$[K]$	Temperature in the ROM
T_{air}^{HOM}	$[K]$	HOM mean indoor air temperature
T_{oper}^{HOM}	$[K]$	HOM mean operative temperature
T_{rad}^{HOM}	$[K]$	HOM mean radiative temperature
$U_{[a-b]}$	$[W/K]$	Heat transfer coefficient between temperature nodes a and b in the ROM
U_{build}^{ident}	$[W/K]$	Building equivalent heat loss coefficient computed from its ROM identified parameters
U_{build}^{sizing}	$[W/K]$	Building equivalent heat loss coefficient estimated from its sizing conditions

Greek letter | Unit | Definition

$\varepsilon_{T_{air}}$	$[°C]$	Arithmetic mean error on the indoor air temperature
η_{cir}	$[-]$	Heat transfer efficiency in the SH circuit
φ_x	$[\%]$	Fit on an output x
θ	$[-]$	Set of normalized parameters for the ROM
θ_{opt}	$[-]$	Optimal set of normalized parameters for the ROM
θ_{opt}^{theo}	$[-]$	Theoretical set of normalized optimal parameters for the ROM
θ_b^{HJ}	$[-]$	Base search point
θ_p^{HJ}	$[-]$	Pattern search point
θ_p^{PSO}	$[-]$	Particle position defined by its set of normalized parameters
$\theta_{p,opt}^{PSO}$	$[-]$	Optimal set of normalized parameters found by a particle p
$\theta_{n,opt}^{PSO}$	$[-]$	Optimal set of normalized parameters in a neighbourhood n
θ_{opt}^{PSO}	$[-]$	Optimal set of normalized parameter found by the PSO algorithm
ρ_{cog}^{PSO}	$[-]$	Cognitive random variable
ρ_{soc}^{PSO}	$[-]$	Social random variable
τ_{-1}	$[s]$	Building SH demand flexibility index
τ_{build}	$[s]$	Building time constant
$\epsilon_{U_{build}}$	$[\%]$	Relative error between U_{eq}^{sizing} and U_{eq}^{ident}
Δ_b^{HJ}	$[-]$	Mesh size in the HJ algorithm

Δ_{tr}	$[s]$	Training interval for parameters identification
μ	$[-]$	Arithmetic mean
σ	$[-]$	Standard deviation

Notations introduced in Chapter 3

Latin letter	Unit	Definition
$c^{\cdots}$	$[€]$	Cost term in the MILP objective function
f_{obj}^{MPC}	$[€]$	Objective function for the MPC problem
$p^{discomfort}$	$[€/(K \cdot s)]$	Discomfort price
p^{energy}	$[€/J]$	Energy price
p^{losses}	$[€/(K \cdot s)]$	Thermal losses price
$p^{overheat}$	$[€/(K \cdot s)]$	Over-heat price
$p^{underheat}$	$[€/(K \cdot s)]$	Under-heat price
H_{MPC}	$[s]$	MPC prediction horizon
N_{MPC}	$[-]$	Number of sampling instances in H_{MPC}

Greek letter	Unit	Definition
$\alpha, \delta, \omega, \varphi, \rho$	$[-]$	Intermediate variables introduced in the MILP problem
ε^{comf}	$[K]$	Comfort threshold
$\lambda^{\cdots}$	$[1/K]$	Price correlation coefficient
Δt_{MPC}	$[s]$	MPC sampling time
$\Delta T_{\cdots}^{\cdots}$	$[K]$	Temperature difference

Superscript Definition

$\dots^{ana}$	Relative to the analytical testing
$\dots^{discomfort}$	Relative to thermal discomfort
$\dots^{ini}$	Initial value
$\dots^{losses}$	Relative to thermal losses in the SH circuit
$\dots^{max}$	Maximum threshold
$\dots^{min}$	Minimum threshold
$\dots^{nom}$	Nominal value
$\dots^{set}$	Set-point
$\dots^{target}$	Relative to the MPC controller target indoor temperature
$\dots^{overheat}$	Relative to over-heating
$\dots^{underheat}$	Relative to under-heating
$\dots^{HJ}$	Relative to the HJ algorithm
$\dots^{HOM}$	Computed by the higher-order model
$\dots^{PSO}$	Relative to the PSO algorithm
$\dots^{ROM}$	Computed by the reduced-order model
$\dots^{SH}$	Relative to SH

Subscript Definition

$\cdots_{air}$	Relative to the building internal air
$\cdots_{build}$	Relative to the building as a whole
$\cdots_{cir}$	Relative to the SH circuit
$\cdots_{em}$	Relative to the SH emitters
$\cdots_{env}$	Relative to the building envelope
$\cdots_{ext}$	Relative to the building external environment
$\cdots_{flo}$	Relative to a floor surface in the BTS
$\cdots_{heater}$	Relative to the heater
$\cdots_{int\ slab}$	Relative to the material of an internal mass equivalent slab
$\cdots_{int\ surf}$	Relative to an internal facing surface in the BTS
$\cdots_{mass}$	Relative to the building internal mass
$\cdots_{mat}$	Relative to the material of a construction element
$\cdots_{non\ flo}$	Relative to a non-floor surface in the BTS
$\cdots_{wat}$	Relative to the SH water
$\cdots_{zone}$	Relative to an equivalent thermal zone in the BTS
$\cdots_{bulb}$	Relative to the TRV bulb
$\cdots_{BL}$	Relative to the bilinear term in the MILP problem
$\cdots_{PWL}$	Relative to the piecewise linear terms in the MILP problem
$\cdots_{TRV}$	Relative to the TRV

Dimensionless number	Expression
Nusselt Number	$Nu = \frac{l \cdot h}{k}$ l: Characteristic length $[m]$ h: Convective heat transfer coefficient $[W/m^2 \cdot K]$ k: Thermal conductivity $[W/m \cdot K]$
Rayleigh Number	$Ra = \frac{g \cdot \beta \cdot \Delta T \cdot l^3}{\alpha \cdot \nu}$ g: Gravitational acceleration $[m/s^2]$ β: Coefficient of linear thermal expansion $[1/K]$ ΔT: Temperature difference $[K]$ l: Characteristic length $[m]$ α: Thermal diffusivity $[m^2/s]$ ν: Kinematic viscosity $[m^2/s]$

Contents

Introduction

Background of district heating systems

In dense urban areas, thermal energy demand for Space-Heating (SH), Domestic Hot Water (DHW) preparation and some industrial processes may be supplied to consumers collectively through a closed network of centrally-produced heat carrier. This heating mode is known as District Heating (DH). The centralized heat generation sources of various types, the distribution network and the heat delivery points, also called substations, constitute the main elements of a District Heating System (DHS), beautifully illustrated in Figure 1.1.

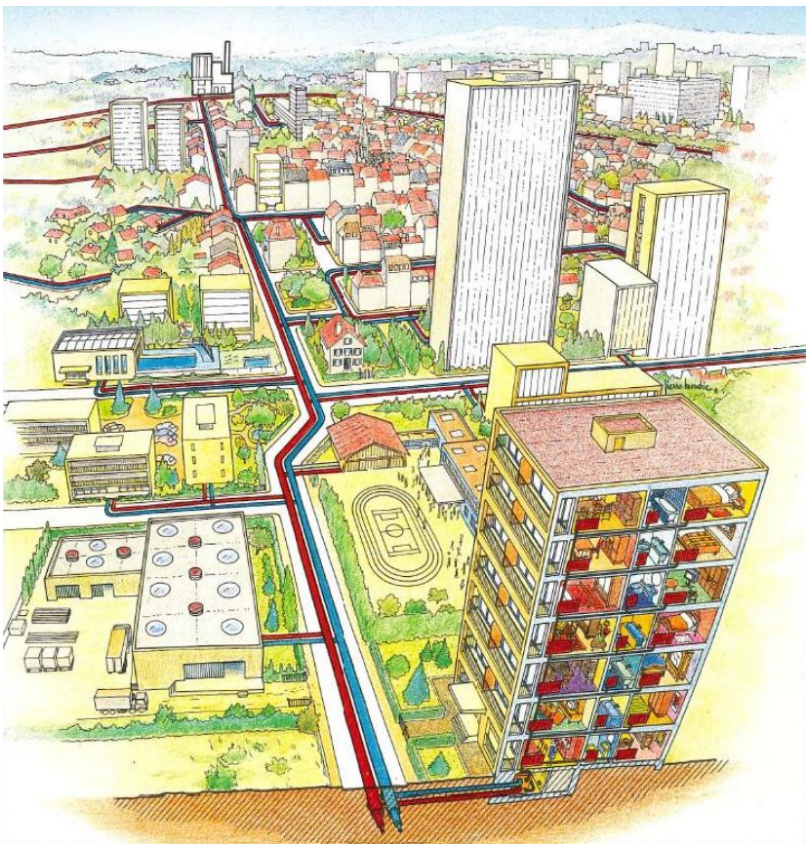

Figure 1.1 Drawing of a DHS by Pierre Merchie form the reference book *District Heating and Cooling* by Swend Frederiksen and Sven Werner [Frederiksen et Werner, 2013]

DH has its roots way back in the 14th century; the first known DHS was established in the French village of Chaudes-Aigues, where 80°C water produced by geothermal heat is circulated in wooden pipes to serve about 30 houses [Mazhar *et al.*, 2018]. Nowadays, 5 generations of DHSs are formally identified.

1st generation DHSs were installed from the 1880s to the 1930s. They were first introduced in the USA, and their technology was then brought to Europe. They operate on steam as the heat carrier, distributed in concrete ducts. They are the least efficient among all generations, since steam entails substantial heat losses and maintenance costs, and the most dangerous with a record of severe steam pipes explosions. Paris and New York have ones of only few left 1st generation DHSs [Lund *et al.*, 2014; Werner, 2017b].

2nd generation DHSs, installed between the 1930s and the 1970s, began using pressurized hot water as the heat carrier circulated in pipes embedded inside concrete ducts, with supply temperatures over 100°C. This generation introduced co-generation in combined heat and power plants as a heat source to the network, and consequently allowed considerable primary energy savings. Most DHSs in Eastern Europe are based on this technology [Paiho et Reda, 2016; Lund *et al.*, 2014].

3rd generation DHSs appeared in the 1970s and dominated most extensions made on existing networks in the 1980s and beyond. They are characterized by temperature levels lower than 100°C circulated in pre-insulated pipes directly buried in the ground. They favour local heat sources such as coal, biomass and waste heat, and integrate renewable solar and geothermal power. Their technology originates from Scandinavian countries and used in many countries in replacement of the 2nd generation [Werner, 2017a; Lund *et al.*, 2014].

4th generation is a new concept that portrays DHSs as major elements in the future of sustainable and increasingly efficient energy systems. Improvements with respect to its antecedents encompass:

- Reforming metering and pricing policies;
- Enhancing the layout so as to reduce losses in the network;
- Lowering supply temperatures below 70°C;
- Reinforcing intermittent renewable energy (solar and geothermal) and low-temperature waste heat penetration;
- Installing seasonal thermal energy storage;
- Introducing large-scale heat pumps in combined heat and power plants;
- Establishing synergies between various energy systems typically electrical, thermal and gas;
- Developing advanced control strategies to optimally manage all the components in the system.

4th generation DHSs have been initiated at small scales as demonstrators in pilot projects. Denmark is the leading country promoting their role in achieving 100% renewable energy systems [Münster *et al.*, 2012; Werner *et al.*, 2014; Lund *et al.*, 2010, 2018b, 2014].

5th generation DHS is an emerging technology suggesting distributing the heat carrier at near ground temperatures, and equipping buildings with heat pumps to extract/reject heat from/into the network. Thus, we rather talk about district heating and cooling systems, where heat wasted by consumers requiring cooling is recovered by those demanding heating within the same loop. Advantages include minimal losses in the network, light and less expensive pipelines, exploitation of very low temperature heat sources and potential decarbonisation of both heating and cooling sectors. Conceptual studies have investigated the use of CO_2, with special pressure control, as the heat carrier for more compactness. In real applications, Switzerland, the Netherlands and Germany are dominating this technology [Buffa *et al.*, 2019; Von Rhein *et al.*, 2019; Henchoz *et al.*, 2015; Verhoeven *et al.*, 2014].

Buildings space-heating demand control

The previous section introduced DHSs and gave insights into their role and their evolution. In this section, we focus on the operation of a particular component, the DH substation (Figure 1.2).

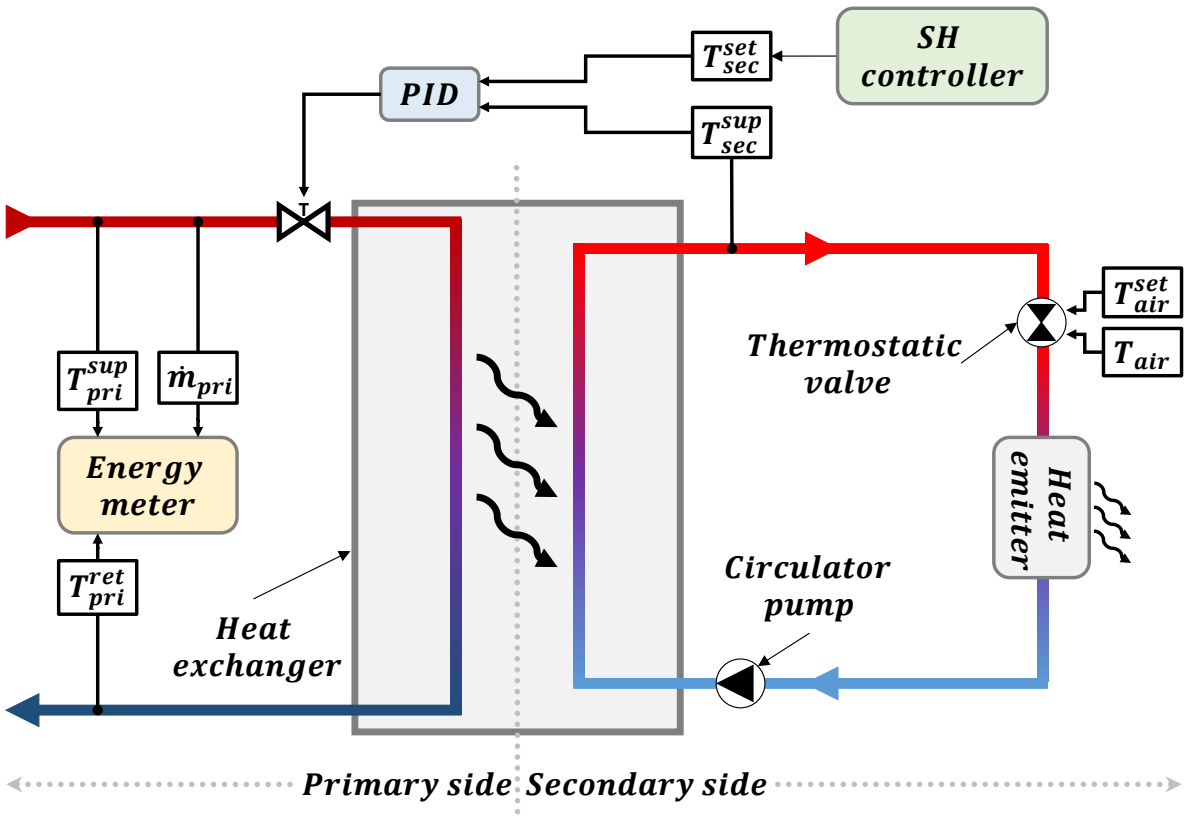

Figure 1.2 Schematic diagram of a DHS substation and an internal SH system

T_{sec}^{set}: secondary supply water set-point temperature and only control variable at the substation level
T_{sec}^{sup}, T_{pri}^{sup} and T_{pri}^{ret}: respectively, secondary supply, primary supply and return water temperatures
$\dot{m}_{pri}$: primary water mass flowrate controlled by the PID function of difference between T_{sec}^{set} and T_{sec}^{sup}
T_{air}^{set}: indoor air set-point temperature controlled by the consumers inside the building
T_{air}: indoor air temperature

The substation is the interface between the DH network and the building internal heating systems, e.g. radiators, floor heating, DHW taps. Inside the substation, there are heat exchangers that ensure heat transfer from the network (primary side) to the building (secondary side), control valves to control the amount of heat being transferred and metering devices to take measurements mainly for billing purposes.

In this thesis, we consider heat supply, control and measurements at the substation for SH usage only.

SH supply to a building equipped with a properly sized heating system of constant efficiency depends on two quantities: the heating water mass flowrate in the secondary circuit and its supply temperature.

Usually, secondary mass flowrate results from the mechanical action of thermostatic valves installed inside the building at the heat emitters level. This regulation is directly linked to the temperature difference between the indoor air and its set-point defined by the consumer; for instance, when the temperature difference to the set-point decreases, the thermostatic valves gradually close and the secondary water flowrate automatically reduces. At the substation, there is no direct control over the secondary SH water flowrate.

On the other hand, the secondary supply water temperature can be controlled from the substation to a specific set-point value by means of a PID controller that regulates the primary water flowrate. To define the set-point value, a SH controller is installed at the substation and a conventional control technique is widely used. It fundamentally presumes that SH demand is majorly influenced by the outdoor temperature; as the outdoor temperature drops, SH demand increases, whereof secondary supply water temperature should be raised. Hence, the technique uses outdoor temperature measurements from a sensor installed outside the building, and relies on a so-called heating curve that determines the secondary supply water temperature inversely-proportional to the outdoor temperature variations. This control scheme is known as the Weather Compensation Control (WCC) [Frederiksen et Werner, 2013].

Main problematic

WCC has been broadly implemented in DHSs. Nowadays, DH substation manufacturers have mastered the heating curve tuning approaches depending on the building environment, energy class and consumer preferences. Thus, WCC is considered as a robust SH control strategy, reliable in fulfilling the demand.

However, buildings have intrinsic, and often non-negligible, thermal inertia: a property that describes the degree of *slowness* of a system's thermal dynamics. Therefore, SH is not instantly dependent on the outdoor temperature, and indoor temperature is not immediately impacted by the SH water temperature. Thanks to their thermal inertia, buildings allow some flexibility margin in regard to their SH demand. In this context, flexibility is the *permission* to adjust SH demand in benefit of the DHS as a whole, without threatening consumers' thermal comfort. Flexibility is particularity valuable in above 3rd

generation DHSs because it allows better management of heat sources by avoiding peak-load generation and conveniently shifting demand to periods when cheap and sustainable intermittent power is available.

WCC does not consider buildings thermal inertia, consequently it does not allow proper exploitation of SH demand flexibility, hence the need for an advanced alternative control strategy to comply with the global evolution of DHSs.

Thesis objectives

The aim of this thesis is to propose an intelligent control strategy that allows exploitation of SH demand flexibility in DHSs by optimal modulation of buildings indoor temperature, with the same control actuators available in conventional DH substations.

Model Predictive Control (MPC) is a promising approach to complete this task, as demonstrated in the context of electric heating [Halvgaard, 2014]. MPC consists of anticipating future conditions acting on the system, planning an optimal sequence of control actions over a future horizon in view of the anticipations whilst respecting a set of constraints on the system's states. MPC is based on a model of the system that predicts its dynamics under future conditions and control actions. At regular time steps, the controller applies the first solution of the sequence, shifts the horizon and restarts the process of anticipation and optimal planning [Rossiter, 2003].

The basic step towards implementation of MPC for SH demand management consists of deriving a simplified model of the building. This constitutes a challenging objective of this thesis, because we intend to develop an accurate model taking good account of the system thermal inertia while restricting available information to strictly non-intrusive data easily accessible at a DHS scale. Besides technical difficulties and additional expenses of installing data loggers inside dwellings, this restriction is made to avoid possible infringement of consumers' privacy, according to the European regulations *Règlement Général sur la Protection des Données* (RGPD), currently applicable in France [Lerouge, 2019].

Once the model is developed, the following objective is to design an optimal controller for the SH water supply temperature and implement MPC. The controller should be able to track variations of the indoor temperature by integrating the simplified building model, and most importantly, it should allow flexible control by reasonably trading consumer's thermal comfort for energy savings at a higher level.

Demonstration and assessment of building simplified modelling and MPC implementation are performed on three buildings of different energy classes by numerical simulation means. Hence, the starting-point objective consists of developing a generic thermal dynamic simulator of a building connected to a DH substation, well-representative of thermal phenomena with considerable impact on SH demand.

Structure of the dissertation

The core of the dissertation is presented in 3 chapters. Chapter 1 covers the development of the building simulator which constitutes the virtual experimental environment used to carry out the rest of the work. Chapter 2 addresses the thesis crucial problematic of developing a simplified yet representative building thermal model, suitable for the intended control strategy, using only data available at substation level. Chapter 3 proceeds with the design of a flexible control approach that allows DHS operators to optimally modulate buildings SH demand, without jeopardizing consumers comfort.

Each chapter starts with a short synopsis giving the reader a general idea of the central research question of the chapter and the main findings. The first paragraph introduces the chapter followed by a literature review. The third paragraph describes the work methodology followed by applications and assessments of the outcomes. The fifth paragraph concludes the chapter.

At the end, a general conclusion summarizes the work methodology and contributions of this thesis and gives outlooks for future research.

Thesis framework

This work is accomplished in collaboration with 3 parties:

- *Commissariat à l'Énergie Atomique et aux Énergies Alternatives* (**CEA**),
- *Agence de l'Environnement et de la Maîtrise de l'Énergie* (**ADEME**),
- *Laboratoire des Signaux et Systèmes* (**L2S**) – a joint research unit of the *Centre National de la Recherche Scientifique* (CNRS), *CentraleSupélec* and *Université Paris-Sud*.

This PhD thesis is jointly funded by CEA and ADEME within its program *Thèses*[1].

The host laboratory is *Laboratoire des Systèmes Énergétiques et Démonstrateurs territoriaux* (LSED) of CEA, partly located at *Institut National de l'Énergie Solaire* (INES).

Publications

- Nadine Aoun, Roland Bavière, Mathieu Vallée, Antoine Aurousseau, Guillaume Sandou
  Modelling and flexible predictive control of buildings space-heating demand in district heating systems
  In *Energy, 2019, Volume 188*

[1] https://www.ademe.fr/recherche-innovation/financer-theses-recherche-linnovation/faire-these-lademe/programme-theses

https://doi.org/10.1016/j.energy.2019.116042

- Nadine Aoun, Roland Bavière, Mathieu Vallée, Guillaume Sandou

  Development and assessment of a reduced-order building model designed for model predictive control of space-heating demand in district heating systems

  In *32nd International Conference on Efficiency, Cost, Optimization, Simulation and Environmental Impact of Energy Systems*, Wroclaw, Poland, June 23-28, 2019

  http://www.s-conferences.eu/FTP/ECOS-files/ECOS2019_proceedings_v2.pdf

- Nadine Aoun, Roland Bavière, Mathieu Vallée, Adrien Brun, Guillaume Sandou

  Dynamic simulation of residential buildings supporting the development of flexible control in district heating systems

  In *13th International Modelica Conference*, Regensburg, Germany, March 4-6, 2019

  https://hal-centralesupelec.archives-ouvertes.fr/hal-02068479/file/Paper_Modelica.pdf

Chapter 1

Thermal modelling and dynamic simulation of multi-zones residential buildings

Synopsis

This chapter sets-up the research experimental environment for buildings reduced-order modelling and SH control presented in the following chapters. First, we clarify the requirements on the multi-zones building thermal model. These requirements lead us to adopt Modelica/Dymola as simulation framework. Nevertheless, other potential tools frequently encountered in the literature are reviewed here. Detailed description of the modelled phenomena in the building thermal dynamic simulation is presented. At last, 3 case study building simulators obtained after parametrization of the generic model are introduced to be used throughout the applications in this thesis.

1.1 Definition of and requirements on the building simulator

In this work, we call Building Thermal Simulator (BTS) the detailed thermal model representative of a typical (not specific) residential building with its SH system supplied by a DHS substation that can be dynamically simulated over time and serves as digital experimental environment for the entire study.

The role of the BTS is to replace a real building for the study of model-based SH control strategies: it generates data to tune the model parameters and it is later used to demonstrate the SH control strategy. Moreover, the BTS computes signals that are not measurable in real-life, for instance the indoor air temperature, which is assumed to be unavailable throughout this thesis. Access to such signals is essential during preliminary studies to earn a better understanding of the building system thermal

behaviour and during control applications to assess its impact on the consumers' thermal comfort. Additionally, the BTS offers the possibility of easily changing parameters, conducting sensitivity analyses and validating the research outcome on not only one, but multiple case-studies.

The requirements on the BTS are mainly:

- Good representability of the buildings short-term thermal dynamics;
- Multi-physics system simulation, i.e. coupled simulation of simultaneously occurring phenomena from different fields, specifically thermal, hydraulics and control;
- Resolution at a time step in the order of minutes or less;
- Practical parametrization to generate multiple case-studies from a generic model;
- Compatibility with other software used in the rest of the work.

There exist several building thermal dynamic simulation tools. The next section reviews 5 propitious options and reveals the selected one in this work.

1.2 Literature review

1.2.1 Buildings dynamic energy simulation tools

1.2.1.1 SIMBAD

SIMBAD (SIMulator of Building And Devices) is a Matlab/Simulink toolbox developed by CSTB[2] and dedicated for buildings thermal dynamic simulation.

The first form of building simulator provided by SIMBAD was a mono-zone model under the Resistance-Capacitance analogy [Husaunndee *et al.*, 1997]. The model is fully described by 3 resistances and 2 capacitors. Developing a simulator requires the user to specify the type of lodging (individual housing, flat), the size category and the period of construction. The toolbox then assigns typical parameters to the model. These typical parameters have been pre-processed through a typological study carried-out on 120 residential lodgings representative of the building stock in France.

The following version of SIMBAD allowed multi-zones building thermal simulation with detailed description of the envelope and Heating, Ventilation and Air Conditioning (HVAC) systems [El Khoury *et al.*, 2005]. The simulator is structured into Simulink blocks where the physical modelling of the thermal phenomena is coded in Matlab and remains inaccessible to the end-user. The blocks are then interconnected. The main blocks are: homogenous air zone, multilayer wall, window, infrared heat exchange and solar irradiation models. In that version, SIMBDI (Simbad Building Description Interface)

[2] CSTB : Centre Scientifique et Technologique du Bâtiment

is introduced as user interface. It allows users to draw buildings, floor-by-floor in 2D, providing envelope characteristics. The interface then automatically generates a thermal zone per floor.

The latest version of SIMBAD has been re-written in C++ language for faster simulations and lighter memory load [Ansanay-Alex, 2010]. Some models have been added as well, e.g. the air quality model.

SIMBAD is particularly convenient for applications involving implementation of control strategies applied to HVAC, shading or lighting systems through the Simulink graphical interface. Newer version of Matlab/Simulink support the Functional Mock-up Interface (FMI) standard[3]. FMI allows exporting models as Functional Mock-up Units (FMUs) which can exchange inputs and outputs during the simulation run with other software modules in a co-simulation framework.

SIMBAD has been adopted as the simulation environment to assess MPC strategies implemented in the PhD theses of [Morosan, 2011] and [Lamoudi, 2012].

1.2.1.2 TRNSYS

TRNSYS (TRaNsient SYStem simulation tool) is a commercial simulation software internationally developed by collaborations between the TESS[4] and the University of Wisconsin – Solar Energy Laboratory (United States), CSTB (France) and TRANSSOLAR Energietechnik (Germany).

TRNSYS has a modular structure, i.e. complex models are implemented in a component-based approach. An extensive library of components currently exists. Most of these components (also known as Types) are written in Fortran. Users may extend existing models or develop ones of their own. Once models are assembled in the Simulation Studio visual interface, an executable file may be called to run the simulation engine (or Kernel). The simulation engine reads and processes input files, iteratively solves the system of algebraic and differential equations and delivers output files. Upon the executable call, an online plotter allows visualization of variables evolution. Fixed integration time step is set by the user, it may be less than a minute, however it should be 1/n of an hour where n is an integer.

TRNSYS has a detailed multi-zones building thermal simulator (called Type 56). TRNSYS3D, a plugin for SketchUp, allows users to draw the building geometry in 3D. Drawings include internal surfaces view factors, over-hangs and side fins whose shading effects are taken into account in the radiation distribution and exchange model. Geometry parameters are then imported into the TRNSYS Building environment – TRNBuild where all non-geometry data is to be set, such as construction material properties, HVAC systems control settings or internal heat gain profiles.

[3] https://fmi-standard.org/docs/3.0-dev/
[4] TESS : Thermal Energy System Specialists

Here are some noteworthy features of building modelling in TRNSYS. Solar irradiation balance is carefully modelled: view factors for long wave radiant exchange between internal surfaces are precisely calculated given detailed geometric information. Stratification is taken into account by addition of multiple air nodes. Convective heat transfer between zones is modelled. Effect of thermal bridges is considered in an external wall type. A radiator model with a thermostatic valve may be connected to each zone in the simulator. An integrated model for thermo-active walls can be used for heating/cooling floors/ceiling. Particular attention is given to the ground-coupled heat transfer via a slab model with 3D finite difference soil field. Moisture balance is computed for every zone and may be used in some HVAC humidity control units. A thermal comfort model includes clothing factor, metabolic rate, external work and relative air velocity. No influence of humidity, direct or diffuse solar irradiation are considered. Furnishing elements are not represented in separate nodes from the air zone, albeit their heat capacity should be taken into account by the user to correct the heat capacity of the zone air volume [Duffy *et al.*, 2009; Energietechnik GmbH, 2010].

As for interoperability, TRNSYS models can be exported as FMUs via the TRNSYS FMU Export Utility. It can therefore co-simulate with models developed in other software. Furthermore, TRNSYS and Matlab/Simulink are mutually compatible: a TRNSYS component can be exported into a Simulink project and a Simulink subsystem can be transformed into a TRNSYS component.

TRNSYS is used in the work of [Braun, 1990] to simulate a building with its HVAC system. Inverse modelling using this simulator is then applied to infer a simplified model of the system, which is later used in operational optimization to control the building set-point temperature using its thermal inertia to reduce operating costs. Also, TRNSYS detailed building thermal simulation was coupled to Matlab strong HVAC control mechanisms for load shifting MPC applications in [Alibabaei *et al.*, 2016].

1.2.1.3 EnergyPlus

EnergyPlus is a modular simulation engine developed by the US Department of Energy upon an initiative to combine 2 hourly building energy simulation programs: BLAST and DOE-2.

EnergyPlus is written in Fortran. It is only a simulation engine; several Graphical User Interface (GUI) have been developed to wrap around EnergyPlus, the most popular of which are DesignBuilder and OpenStudio. Through these GUIs, users sketch-up the 3D building geometry of multi-zones buildings (similarly to TRNSYS) and add HVAC systems. The simulation engine then employs a zone heat balance method that includes surface heat balance and air heat balance to compute building thermal load. EnergyPlus allows variable time step between 1 minute and 1 hour.

Some particular features of EnergyPlus thermal modelling include the option to choose from different solution algorithms; for instance, for heat conduction a transfer function and a finite difference

algorithms exist and are user-specified. Internal mass may be modelled as multi-layer internal walls, with separate thermal capacitance from the zone air volume. They interact with the zone heat balance on one side and are adiabatic on the other. They do not receive direct solar irradiation but participate in the long wave radiative exchange with all other internal surfaces. EnergyPlus has an anisotropic sky model, so sky radiance is calculated as a function of the sun position for accurate diffuse of solar irradiation on tilted surfaces. Simulators may have controllable blinds glazing systems. A model computes interior daylight illuminance from windows, which allows dimming control actions. EnergyPlus also has a thermal comfort model based on the inside dry bulb temperature, occupants activity, air humidity and radiation [Crawley *et al.*, 2001]. Besides its user friendly interface, these features made EnergyPlus quite popular among engineers for buildings thermal load calculations.

Co-simulation with EnergyPlus is possible. Simulators may be exported as FMUs via the EnergyPlusToFMU Python package. Alternatively, EnergyPlus may be linked and exchange data during the time integration with software which particularly do not support the FMI standard, via the Building Controls Virtual Test Bed (BCVTB) [Wetter, 2012].

EnergyPlus was used in a MPC application that investigates latent heat storage in buildings equipped with heat exchangers containing phase-change material in [Gholamibozanjani *et al.*, 2018]. It was also used to apply MPC in [Bianchini *et al.*, 2016], relying on a linear reduced-order model identified from data generated by a radiant floor heated simulators. EnergyPlus served as well in a study of the effect of internal mass on buildings peak loads in [Raftery *et al.*, 2014].

1.2.1.4 COMFIE – Pleiades

COMFIE (Calcul d'Ouvrages Multizones Fixé à une Interface Experte), is a thermal dynamic simulation engine developed at CES[5] – Mines ParisTech. Pleiades is a software developed by IZUBA Energies that uses COMFIE.

Pleaides has an interface (Alcyone in earlier versions) that allows users to sketch a building in 3D, split it into several zones, define its envelope properties by choosing construction materials from component libraries, expose it to boundary conditions through a weather file and specify heating and cooling set-point temperatures per zone as well as infiltration rates and mechanical ventilation scenarios, optionally with bypass. Given these data, objects are created and inter-connected via pointers.

The simulation engine is written in Pascal programming language under the Delphi environment. It performs spatial discretization of partial derivative equations using the finite difference method. COMFIE has the particularity of using modal analysis for the linear part of the system and adopts a

[5] CES: Centre Efficacité énergétique des Systèmes

model order reduction technique to eliminate fast modes [Peuportier et Blanc, 1991]. This feature yields relatively fast simulations without greatly compromising accuracy when used for hourly or annual heating load calculations. However, COMFIE – Pleaides is not recommended for finer time steps [Salomon *et al.*, 2005]

Thermal phenomena modelled in COMFIE – Pleaides include natural convection and mono-directional heat conduction. Solar irradiation penetrating through windows is assumed only diffused, without a direct component since the simulator does not consider internal geometric details to properly distribute direct radiation. Diffuse radiation is distributed among internal surfaces weighted by their surface area. No long-wave radiant exchange between surfaces is mentioned. No mass or enthalpy balance is computed. A stochastic occupant behaviour model is developed in a bottom-up approach based on French statistical data. This model generates scenarios of occupants presence in the simulator zones, internal heat gain due to electric appliances and lighting, and windows opening [Vorger *et al.*, 2014]. This particular model allows design optimization through uncertainty quantification and sensitivity analysis in the Pleaides AMAPOLA module. Furthermore, dedicated modules for life-cycle analysis at building and neighbourhood scales, namely ACV Equer and Énergie-Carbone, are available in Pleaides.

COMFIE models are delivered as black-boxes, therefore accessibility to the core of the software is not possible which consequently prevents any user extension or module development. Since heating systems are modelled in a rather simplistic way as predefined scenarios of maximum power and set-point temperatures, COMFIE – Pleiades is rarely used on its own for operational control applications. In [Gaaloul *et al.*, 2011], a COMFIE – Pleiades simulator was coupled to a convective heating system model in Matlab/Simulink. It was also coupled to Matlab/Simulink in [PAPAS *et al.*, 2016] within a project called ADREAM for buildings energy consumption optimization. In the thesis of [Robillart, 2015b] COMFIE – Pleiades was adopted as the simulation environment in the development of advanced control for peak shaving in energy efficient buildings.

1.2.1.5 Modelica libraries

Modelica is a programming language, not specifically made for building thermal dynamic simulation as other tools reviewed so far, and there exists a number of Modelica libraries dedicated for building systems simulation. This section introduces the language and the main libraries of this field.

Modelica is an essentially acausal equation-based, object-oriented programming language which supports class inheritance, hierarchical structuring and model reuse. Modelica suggests breaking down the global system into smaller components (or objects). Each component is individually modelled and may have some or all of the following:

- A system of differential algebraic equations (algebraic relations and differential equations with time derivatives);
- Parameters used in the equations. By definition, parameters are constants, i.e. their values set at initialization, cannot be changed in the course of a simulation run;
- States which are unknown variables calculated by solving the system of equations;
- Inputs to the system of equations which may be variable during a simulation run;
- Outputs from the component (states or inputs) that might serve as inputs to other components.

Components may then be connected in a script or a graphical editor via ports – which themselves are Modelica components for signal transmission or conservation – so as to assemble the global system. This assembly may be viewed as gathering all the sub-equation-systems into a larger one. A compiler translates the Modelica code into a causal C code to be solved by a proper solver. Variable time steps in the order of seconds may be specified depending on the chosen solver. A concise presentation of the Modelica language principles and semantics is given in [Fritzson et Engelson, 1998].

Modelica is quite appealing for several reasons. Non-causality is a major advantage. For a particular component, if the user does not specify a variable as input or output at the model development stage, the compiler will automatically determine its nature on the basis of computationally efficient solution sequence. Not only does this simplify programming efforts, it also increases reusability of developed components. Furthermore, Modelica is a multi-physics modelling language. Modelica is a non-proprietary language developed and promoted by the Modelica Association[6] and several commercial and open source compilers are available on the market like SimulationX, OpenModelica, JModelica, LMS Imagine.Lab AMEsim, MapleSim, MathModelica, and Dymola. As for components libraries, the Modelica Association maintains standard conforming libraries, some users share versions of their own libraries and there are also commercial libraries.

A number of open-source libraries dedicated for building systems simulation have been developed by research teams, validated and shared to be readily used by others:

- *BuildSysPro* developed by EDF for buildings, districts and energy systems modelling [Plessis *et al.*, 2014];
- *IDEAS* (Integrated District Energy Assessment Simulations) developed at KU Leuven simulation of thermal, hydronic and electrical processes at urban scale [Jorissen *et al.*, 2018];
- *BuildingSystems* developed at UdK Berlin for building and plan energy simulation [Nytsch-Geusen, 2019];
- *AixLib* developed at RWTH Aachen University for building performance simulations [Müller *et al.*, 2016];

[6] https://www.modelica.org

- *Buildings* developed at the Lawrence Berkeley National Laboratory (LBNL) of the University of California for building energy and control systems simulation [Wetter *et al.*, 2014].

These libraries include models of thermal zones, walls, windows, heating systems, control systems and weather file readers. We do not intend to investigate each library individually since this would be an overwhelming task. However, our interest is on one particular library, *Buildings*, renowned for being comprehensive, very well documented and for the excellent reactivity and assistance from its developers. However, a multi-zones simulator is not readily delivered in *Buildings*, as opposed to TRNSYS or EnergyPlus where simple sketch-ups allow automatic generation and connection of several zones. Nevertheless, homogeneous thermal zones of *Buildings* can be inter-connected using appropriate ports to assemble a multi-zones building model. In order to achieve the desired BTS, the building model should integrate a SH system with a heating circuit connected to a DHS substation. Our laboratory has pre-developed and validated its in-house Modelica Library called *DistrictHeating* with the necessary components (dual-pipes, heat exchangers, substations) [Giraud *et al.*, 2015b].

All Modelica models can be encapsulated in FMUs for co-simulation. Furthermore, a Python package – *buildingspy*[7] – by *Buildings* library developers is available for pre and post-processing. It is useful in parametric studies to automatically edit parameters and run a series of Modelica simulations. Moreover, *Buildings* includes a package with blocks and functions that embed Python in Modelica. So for instance a Modelica model can exchange data with Python, call a Python function or be part of a hardware-in-the-loop simulation in which Python communicates with the hardware.

With all the available libraries and associated tools, Modelica is earning greater attention in the literature of building energy simulation. *BuildSysPro* was used in the thesis of [Blervaque, 2014] to simulate a low-consumption building with floor heating coupled to a heat pump with the aim of comparing different modelling aspects, e.g. time steps, heat emitters and control regulations. *IDEAS* was used in [Reynders, 2015b] to investigate short-term heat storage in residential buildings for active demand-response.

1.2.2 Selected simulation tool

All the above presented simulation tools can be potentially used in our application. Indeed, their building models are validated under the BESTEST validation standard. BESTEST is developed by the National Renewable Energy Laboratory on behalf of the International Energy Agency and consists of a series of benchmark comparative analytical and empirical tests to validate individual components and the overall building energy model accuracy [Judkoff et Neymark, 1995]. Most of these tools allow multi-physics simulation, with different degrees of difficulty. However, not all of them are well-documented for

[7] https://simulationresearch.lbl.gov/modelica/buildingspy

external uses, particularly those developed in academic laboratories. On the other hand, commercial tools do not allow direct accessibility to the codes for eventual modifications.

The selected tool for this work is Modelica language. This choice is justified by the open-source availability of the necessary components for the building structure and heat emitters models in *Buildings* library, and components for the heating circuit and DHS substation models in our in-house *DistrictHeating* library. The used compiler is Dymola and the selected solver is Radau IIa for its advantageous simulation speed and accuracy [Liu *et al.*, 2010]. Conveniently, the Modelica/Dymola environment allows multi-physics simulations, time step resolutions in the order of seconds, possibility to access, modify and add components to the libraries and it supports co-simulation by encapsulating models into FMUs. Therefore, it is adopted throughout this thesis.

1.3 Detailed description of the modelled elements

This section presents the main component models and their assembly into a BTS.

1.3.1 Homogeneous thermal zones

The fundamental elements of the BTS are thermal zones. A thermal zone is a volume of perfectly mixed air – therefore having a uniform temperature. This control volume is surrounded by construction elements, such as internal or external walls, and exchanges heat with their internal surfaces through thermal convection. It can also exchange heat with neighbouring environments or directly with a heat source or sink. An energy balance may then be established for this control volume as in Eq. 1.1.

$$C_{zone} \cdot \frac{dT_{air}^{zone}}{dt} = \sum_{i=1}^{N_{int\ surf}} h_{conv}^{int} \cdot S_{int\ surf}^{i} \cdot \left(T_{int\ surf}^{i} - T_{air}^{zone}\right) + \sum_{j=1}^{N_{neigh}} U_{neigh}^{j} \cdot \left(T_{neigh}^{j} - T_{air}^{zone}\right) + \sum_{k=1}^{N_{dir}} Q_{dir}^{k} \qquad \text{Eq. 1.1}$$

C_{zone} is the thermal capacitance of the air volume in the thermal zone and T_{air}^{zone} is its temperature assumed to be uniform. The zone has $N_{int\ surf}$ interior-facing surfaces that could be elements of the envelope of internal partition walls and furniture. $T_{int\ surf}$ is the temperature of an interior-facing surface and $S_{int\ surf}$ its surface area, h_{conv}^{int} is a constant internal heat convection coefficient between the zone and the surrounding interior surfaces. A typical value is 3 W/m^2.K. The zone might have N_{neigh} neighbouring environments (e.g. adjacent thermal zones). The second summation in the right hand side of Eq. 1.1 is used to represent simplified heat exchange between the zone and a neighbouring

environment at temperature T_{neigh} using an equivalent heat transfer coefficient U_{neigh}; ventilation and door opening are modelled using this formula (§ 1.3.4). The last term in the right hand side of Eq. 1.1, $\sum Q_{dir}$ is the algebraic summation of N_{dir} direct heat flows from heat sources and sinks independent form T_{air}^{zone}, e.g. internal heat gains (§ 1.3.7).

Besides the T_{air}^{zone}, a zone thermal state is described by 2 other temperatures:

- $T_{zone}^{rad.}$ is the zone radiative temperature; it is the mean temperature of a surface facing the internal of the zone calculated according to Eq. 1.2:

$$T_{rad}^{zone} = \frac{\sum_{i=1}^{N_{int\ surf}} \left(T_{int\ surf}^{i} \cdot S_{int\ surf}^{i}\right)}{\sum_{i=1}^{N_{int\ surf}} S_{int\ surf}^{i}} \qquad \text{Eq. 1.2}$$

- $T_{zone}^{oper.}$ is the zone operative temperature; it is the mean temperature perceived by a human being inside the zone. According to [Auliciems *et al.*, 1997], when air flow velocity is less than 0.2 m/s, the operative temperature can be approximated by the average of the air and radiative temperature (Eq. 1.3):

$$T_{oper}^{zone} = \frac{T_{air}^{zone} + T_{rad}^{zone}}{2} \qquad \text{Eq. 1.3}$$

The component that models a homogenous thermal zone and computes its heat balance is called *MixedAir* from *Buildings Library*. In fact *MixedAir* also models mass exchange with a ventilation system or from water condensation due to latent internal gain. A mass balance can then be established for the control volume. However, in our BTS ventilation is modelled in a rather simplified way (§ 1.3.4) and no latent heat is added, therefore the mass balance is invariant.

1.3.2 Envelope elements

The building envelope is made up of opaque constructions (walls, floor, ceiling) and glazing systems. An opaque construction is a multi-layers wall. A glazing system is a succession of glass panes and gas-filled gaps with a frame embedded inside an opaque construction.

1.3.2.1 Thermal convection

Opaque constructions and glass panes of the glazing systems are subject to thermal convection on their extreme layers. Their innermost layer exchanges heat of intensity Q_{conv}^{int} with *MixedAir* (Eq. 1.4). Similarly, their outer-most layer exchanges heat of intensity Q_{conv}^{ext} with the outdoor environment of temperature T_{ext} assuming the constant external heat convection coefficient h_{conv}^{ext} (Eq. 1.5). A typical value is 10 W/m^2.K. $S_{ext\ surf}$ is the external surface of the construction, equal to $S_{int\ surf}$.

$$Q_{conv}^{int} = h_{conv}^{int} \cdot S_{int\ surf} \cdot \left(T_{air}^{zone} - T_{int\ surf}\right) \quad \text{Eq. 1.4}$$

$$Q_{conv}^{ext} = h_{conv}^{ext} \cdot S_{ext\ surf} \cdot \left(T_{ext} - T_{ext\ surf}\right) \quad \text{Eq. 1.5}$$

Inside a gas layer of the glazing system, convective heat exchange is modelled. A correlation for convection inside cavities is used, therefore the intensity of the heat exchange depends on the Nusselt and Rayleigh numbers calculated as a function of the tilt of the window, the thickness of the gas gap and its thermal properties. No heat storage is considered inside the gas layers.

1.3.2.2 Thermal conduction

One-directional (1-D) heat conduction is assumed through layers of the opaque constructions and glass layers of the glazing systems. In each layer, the 1-D version of the Fourier equation (Eq. 1.6) is solved using the finite volume method, where ρ_{mat}, c_{mat} and k_{mat} are respectively the density, thermal capacity and thermal conductivity of the layer material, x is the surface normal axis along which heat conduction is assumed, t designates time and T temperature.

$$\rho_{mat} \cdot c_{mat} \cdot \frac{\partial T(x,t)}{\partial t} = k_{mat} \cdot \frac{\partial^2 T(x,t)}{\partial x^2} \quad \text{Eq. 1.6}$$

Each material layer is discretized into N_{sta} volumes given by Eq. 1.7. N_{sta} is proportional to the layer thickness e_{lay} and inversely proportional to the square root of the material thermal diffusivity $\sqrt{\frac{k_{mat}}{\rho_{mat} \cdot c_{mat}}}$. N_{sta}^{ref} is a normalizing number of states that corresponds to discretizing a 20 cm layer of concrete into 3 finite volumes:

$$N_{sta} = N_{sta}^{ref} \cdot \frac{e_{lay}}{\sqrt{\frac{k_{mat}}{\rho_{mat} \cdot c_{mat}}}} \quad \text{Eq. 1.7}$$

Details of the finite volume method applied to 1-D heat conduction are not given here for succinctness.

A rather simplified thermal conduction is modelled through the glazing system frame. This heat transfer can be seen as thermal conductance between the thermal zone and the outdoors and it is one of the terms in the second summation in Eq. 1.1, where the neighbour is the external environment at temperature $T_{neigh} = T_{ext}$ and the heat conductance coefficient is a property of the frame $U_{neigh} = U_{fra}$.

1.3.2.3 Thermal radiation

A thermal zone receives direct and diffuse solar irradiation (direct normal I_{sol}^{dir}, global horizontal I_{sol}^{glo} and diffuse horizontal I_{sol}^{dif}) through its windows and elements of its envelope exchange heat in between each other through infrared radiation. In *MixedAir*. Direct solar irradiation is transmitted through the glass panes of the glazing systems; its total intensity Q_{sol} is given by Eq. 1.8 with N_{win} the number of windows in a thermal zone and J_{in} the incoming solar radiosity through each window depending on its surface area, tilt and orientation.

$$Q_{sol} = \sum_{i=1}^{N_{win}} J_{in}^{i} \qquad \text{Eq. 1.8}$$

Q_{sol} is assumed to first strike the floor where part of it is absorbed and transmitted (Q_{sol}^{flo} in Eq. 1.9); the rest is diffusely reflected ($Q_{sol}^{all\ non-flo}$ in Eq. 1.10) to all $N_{non-flo}$ non-floor interior-facing surfaces, including those of the building envelope (walls, ceiling, windows) and those representing internal mass (§ 1.3.3). α_{flo} and τ_{flo} are absorptivity and transmissivity of the floor inner surface, respectively.

$$Q_{sol}^{flo} = Q_{sol} \cdot (\alpha_{flo} + \tau_{flo}) \qquad \text{Eq. 1.9}$$

$$Q_{sol}^{all\ non-flo} = 1 - Q_{sol}^{flo} \qquad \text{Eq. 1.10}$$

So diffuse solar irradiation is distributed among all non-floor surfaces weighted by their surface areas (Eq. 1.11, $Q_{sol}^{non-flo}$ is the fraction received by an individual surface, $S_{non-flo}$ its surface area, $\alpha_{non-flo}$ its absorptivity and $\tau_{non-flo}$ its transmissivity).

$$Q_{sol}^{non-flo} = Q_{sol}^{all\ non-flo} \cdot \frac{S_{non-flo} \cdot \left(\alpha_{non-flo} + \tau_{non-flo}\right)}{\sum_{k=1}^{N_{non-flo}} S_{non-flo}^{k} \cdot \left(\alpha_{non-flo}^{k} + \tau_{non-flo}^{k}\right)} \quad \text{Eq. 1.11}$$

If additionally the thermal zone receives radiative heat from a radiator or radiating internal gain sources, then the sum of this radiative heat is distributed among all interior-facing surfaces weighted by the surface areas and absorptivity. In Eq. 1.12, $Q_{rad\ sour}^{int\ surf}$ is the fraction received by an internal surface, $N_{rad\ sour}$ is the number of internal radiative sources and $Q_{rad\ sour}$ is the radiative heat injected by each.

$$Q_{rad\ sour}^{int\ surf} = \sum_{i=1}^{N_{rad\ sour}} Q_{rad\ sour}^{i} \cdot \frac{S_{int\ surf} \cdot \alpha_{int\ surf}}{\sum_{k=1}^{N_{int\ surf}} S_{int\ surf}^{k} \cdot \alpha_{int\ surf}^{k}} \quad \text{Eq. 1.12}$$

Long wave infrared radiant exchange takes place between the sky and all exterior facing opaque surfaces and in-between interior-facing opaque surfaces. The Stephan-Boltzmann law (Eq. 1.13) is used to calculate the power Q_{rad}^{lw} radiated from a surface of area S_{surf}, emissivity ε_{surf}, and at temperature T_{surf} using the Stephan-Boltzmann constant σ. This equation may optionally be linearized in *MixedAir*. The incoming radiation from a surface to another is calculated using a view factor that is approximated to the surface fraction area, not considering any coordinate system. Q_{rad}^{lw} calculation involves writing all equations for all internal surfaces and establishing a heat balance such that the total exchanged radiation sums to zero. Details of these calculations are well explained in [Wetter *et al.*, 2011b].

$$Q_{rad}^{lw} = \sigma \cdot S_{surf} \cdot \varepsilon_{surf} \cdot T_{surf}^{4} \quad \text{Eq. 1.13}$$

1.3.3 Internal mass

Furnishing elements and light partition walls are modelled as mono-layer vertical slabs. Just as for opaque construction envelope elements, 1-D heat conduction is modelled through the internal mass layer. Unlike the envelope walls, both surfaces of a furniture-equivalent slab exchange heat with the thermal zone air via thermal convection. They also receive diffuse radiation and participate in the infrared heat exchange with the other internal surfaces.

The properties of the internal mass material figure in Table 1.1. We referred to [Johra et Heiselberg, 2017b], a survey on the internal mass and its equivalent heat capacity found in residential and single office buildings in Denmark, to set material properties, mass and dimensions of furniture equivalent slabs. The amount of internal mass added inside a zone is defined in mass per zone floor area using the

parameter $m_{int\ slab}$ of Table 1.1. The thickness of the equivalent slab stays invariant, its surface area $S_{int\ slab}$ is calculated using Eq. 1.14 where S_{zone} is the surface area of the thermal zone. Therefore, by increasing $m_{int\ slab}$, we increase the thermal capacity and consequently the short-term heat storage inside the zones, and also we increase heat exchange with the zone air and envelope elements.

$$S_{int\ slab} = S_{zone} \cdot \frac{m_{int\ slab}}{\rho_{int\ slab} \cdot \varepsilon_{int\ slab}} \qquad \text{Eq. 1.14}$$

Table 1.1 Properties of the internal mass equivalent slabs: thermal conductivity ($k_{int\ slab}$), specific thermal capacity ($c_{int\ slab}$), density ($\rho_{int\ slab}$), thickness ($\varepsilon_{int\ slab}$) and mass per floor area ($m_{int\ slab}$)

Material	$\mathbf{k_{int\ slab}}$ $(\mathbf{W/m \cdot K})$	$\mathbf{c_{int\ slab}}$ $(\mathbf{J/kg \cdot K})$	$\boldsymbol{\rho}_{\mathbf{int\ slab}}$ $(\mathbf{kg/m^3})$	$\boldsymbol{\varepsilon_{int\ slab}}$ $(\mathbf{mm})$	$\mathbf{m_{int\ slab}}$ $(\mathbf{kg/m^2})$
Metal	60	450	8000	3	25
Wood / Plastic	0.2	1400	800	18	25
Ceramic / Glass	1.25	950	2000	10	5
Light material	0.03	1400	80	120	15
Light partition walls	0.015	1150	384	100	25

1.3.4 Ventilation and door opening

Heat loss due to ventilation is one of those terms represented by the second summation in Eq. 1.1, with $T_{neigh} = T_{ext}$ and $U_{neigh} = \rho_{air} \cdot c_{air} \cdot V_{zone} \cdot n_{vent}$, ρ_{air} being the air density, c_{air} its thermal capacity, V_{zone} the volume of the thermal zone and n_{vent} the number of volume changes per hour. Thus, heat loss due to ventilation is as given by Eq. 1.15. In reality n_{vent} is often variable and should be stochastically modelled depending on tenant's behaviour. However in our work we assume a constant value recommended under European standards. Typical values for n_{vent} range between 0.2 and 0.6 volume changes per hour [ASHRAE Standard: Ventilation for Acceptable Indoor Air Quality, 1989].

$$Q_{vent} = \rho_{air} \cdot c_{air} \cdot V_{zone} \cdot \frac{n_{vent}}{3600} \cdot (T_{ext} - T_{air}^{zone}) \qquad \text{Eq. 1.15}$$

Similarity, heat exchange due to door opening between neighbour zones is modelled using Eq. 1.16, where S_{door} is the open area separating the two adjacent zones, v_{mix} is an equivalent mixing air velocity through the door opening. The default value for v_{mix} is $0.13\ m/s$ [Van Schijndel *et al.*, 2003]. This model has been introduced into the BTS as a means to homogenize temperatures of the zones if needed.

$$Q_{door\ open} = \rho_{air} \cdot c_{air} \cdot S_{door} \cdot v_{mix} \cdot \left(T^{air}_{neigh\ zone} - T^{zone}_{air}\right) \quad \text{Eq. 1.16}$$

1.3.5 Assembly into a multi-zones, multi-storeys building simulator

The BTS is assumed to have a rectangular footprint. Its length and width are parameters set by the user, along with the height of a storey and the building orientation. Note that the orientation angle (θ_{build} in Figure 1.3) is a parameter used in the solar irradiation model. A floor in the BTS is discretized into 4 equivalent thermal zones: a *Night zone*, a *Kitchen*, a *Day zone* and a *Bathroom* as shown in Figure 1.3. Accordingly, if the real building has a floor with multiple apartments, rooms of the apartments are aggregated into the 4 equivalent thermal zones in the BTS. The user only needs to define the fraction surface area of each zone with respect to the total footprint surface area; this quantity is denoted α^{surf}_{zone}. User should also specify the construction materials and the fraction of glazed surface per facade (to the North, West, South and East). The Modelica code will automatically instantiate 4 *MixedAir* components with the corresponding volumes, as well as all the envelope elements surrounding each of them and the interior walls separating them from each other. The zones will then be connected in between each other through the appropriate connection code.

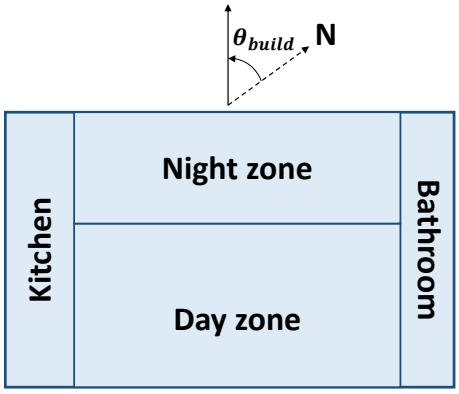

Figure 1.3 Schematic of the floor discretization into 4 thermal zones

To build-up a multi-storey building, the user should specify the number of floors N_{flo} and the code automatically generates 1 floor with particular material for the ground (this is the ground floor), $N_{flo} - 2$ floors with particular material for the floor and ceiling (these are the intermediate floors) and 1 floor with particular material for the roof (this is the top floor) as depicted in Figure 1.4. Hence the floors have slight differences in the envelope construction material, however they are identical in terms of geometry and internal composition and discretization. Yet another distinction is that each floor receives a different internal gain signal because the internal gain model (of § 1.3.7) generates data specifically tailored to a building called *Le Salammbô* (will be introduced in § 1.4) and this later has different types of apartments per floor, yielding different internal heat gains. The instantiated floors are then connected

in between each other and conductive heat exchange takes place through the common intermediate ceiling between two consecutive floors.

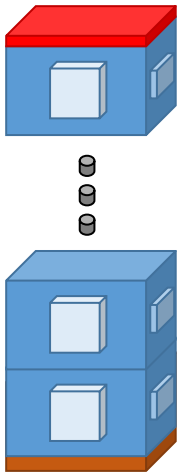

Figure 1.4 Schematic of the floors assembly into a multi-storeys BTS

1.3.6 Space-heating system

A SH system in the BTS is a component connected to each zone and fulfils its demand by maintaining its air temperature as close as possible to its set-point temperature. We consider 2 SH system models presented in this section. Either one can be connected to the assembled building model, given a dynamic set point temperature per zone.

1.3.6.1 Space-heating system with zero thermal inertia

The simplest SH system model assumes that the air temperature in a thermal zone – T_{air}^{zone} of Eq. 1.1 – should equal the given set-point temperature at all times. Therefore, it provides the deficit heat if the air temperature is below the set-point or takes away the excess heat in case the air temperature is above the set-point. The model also features a thermal switch, which is a variable thermal resistance between the heat source and the thermal zone. During a simulation run, the variable resistance may be set to epsilon to switch on the heating or it may be set to infinity to switch off the heating.

We refer to such a model as a SH system with zero thermal inertia. Neither the SH system thermal inertia, nor the regulation time delays are considered. Yet, this model is useful to size SH power under steady-state conditions (§ 1.4.3), and to assess the influence of the SH system thermal inertia (§ 2.3.1).

1.3.6.2 Hydronic space-heating system served by a DHS substation

The second SH model is meant to account for the thermal inertia of the heating circuit, and to feature realistic control variables involved in SH demand in DHSs. Components-wise, this system is composed of hydronic radiators injecting convective and radiant heat into the thermal zones, equipped with a

thermostatic valve, fed by an insulated dual-pipe distribution network and powered by a DHS substation. Models of the detailed SH system are described hereafter.

1.3.6.2.1 Substation

In DHSs, heat delivery from the primary network to the building heating circuit takes place at the substation usually placed in the building basement. Referring to Figure 1.5, the main components concerning SH demand supply typically found in a substation are:

- A heat exchanger;
- A control valve to regulate the heating water mass flowrate at the primary side;
- A PID controller acting on the control valve to regulate the secondary supply water temperature to a specific set point temperature provided by a heating curve or other advanced strategy;
- A circulator pump to balance the heating circuit at the secondary side;
- Some metering devices such as the supply water temperature sensor, return water temperature sensor, flowmeter and heat meter to measure energy consumption and allocate costs.

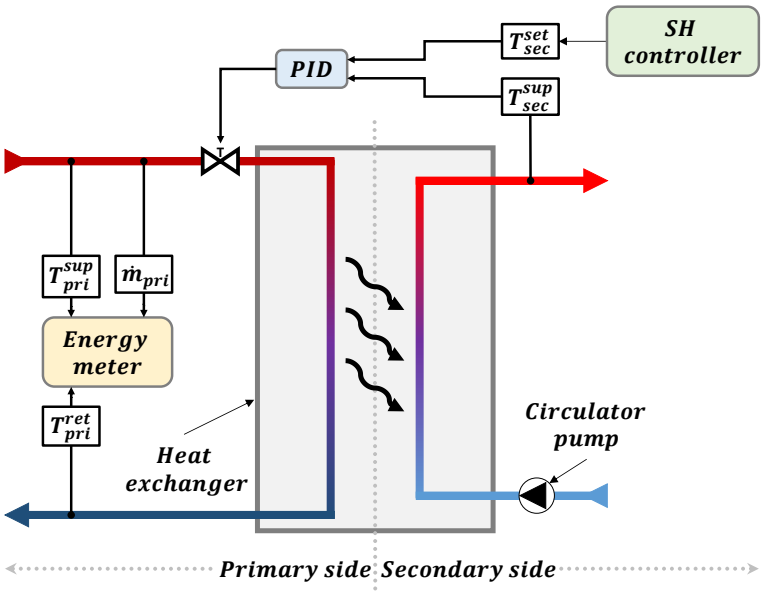

Figure 1.5 Simplified schematic of the main components found in a DHS substation

Since this thesis particularly focuses on the demand side management, modelling of the heat exchange between the primary and the secondary sides is beyond our scope. Our modelling (and later control) simply assumes that a certain amount of heat Q_{SST} needs to be delivered at the substation to the building, regardless of its origin. Thus, the only variables in the substation model are the secondary supply (T_{SST}^{sup}) and return (T_{SST}^{ret}) water temperatures, the secondary water mass flowrate ($\dot{m}_{SST}$) and the SH power (Q_{SST}); while variables related to the primary side are omitted.

The substation model used in this work is found in the *DistrictHeating* library and described in [Giraud *et al.*, 2015b]. We recall the main assumptions:

- $T_{SST}^{sup} = T_{SST}^{set}$; in fact, the PID dynamics can be ignored with respect to other slower dynamics in the system, thus during regimes where the substation fulfils the SH demand, the secondary supply water temperature is assumed to perfectly match its set-point;
- T_{SST}^{ret} and $\dot{m}_{SST}$ are inputs to the substation model from the dual-pipe and the thermostatic radiator valve models presented hereafter;
- Heat losses in the substation are proportional to the temperature difference between T_{SST}^{sup} and the ambient temperature T_{amb}, assumed constant and equal to 20°C. $\varepsilon_{SST}^{losses}$ is the corresponding heat loss coefficient.

The remaining variable Q_{SST} is computed by establishing a heat balance for the SH water control volume and it is constrained by the substation sizing power Q_{SST}^{max}. It expression is given in Eq. 1.17:

$$Q_{SST} = min\left(\dot{m}_{SST} \cdot c_{wat} \cdot \left(T_{SST}^{sup} - T_{SST}^{ret}\right) + \varepsilon_{SST}^{losses} \cdot \left(T_{SST}^{sup} - T_{amb}\right), Q_{SST}^{max}\right) \qquad \text{Eq. 1.17}$$

1.3.6.2.2 Dual-piping network

A pipe model is also taken from the *DistrictHeating library*. The modelling approach, thoroughly described and experimentally validated in [Giraud *et al.*, 2015b] relies on the node method. The model considers a metal pipe surrounded by an insulation layer. It computes the heat propagation along the pipeline and accounts for the hydraulic head losses, heat losses to the surroundings and transportation time delays.

By associating a pair of pre-insulated pipes, one for supply (hot) and one for return (cold), a model of a dual-pipe is obtained. Note that heat exchange between the supply and return lines is neglected.

To model a heating system circuit, copper dual-pipes are used considering the configuration of Figure 1.6. Large dual-pipes are 26 cm in nominal diameter and their length is equal to the height of a storey. Small ones are 16 cm in diameter and their length is equal to half the diagonal of the rectangular floor footprint. The first large diameter dual-pipe model is connected to the substation at its inlet and to 4 small diameter dual-pipes which will then be connected to the radiators inside the thermal zones at the first floor. Its outlet is also connected to the inlet of the second large diameter dual-pipe model, which will feed the second floor, and so on. At both ends of a connection (dashed line in Figure 1.6), pressure is conserved and mass flowrate algebraically sums to zero.

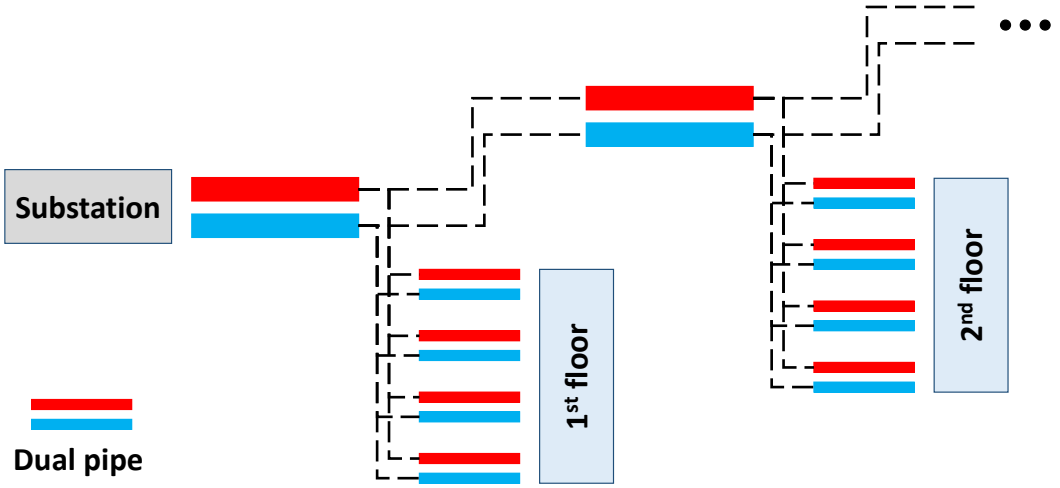

Figure 1.6 Configuration of the SH network

1.3.6.2.3 Radiators

The *RadiatorEN442_2* model from *Buildings library* is used to model a radiator inside each zone. It is connected at one end to the supply pipe outlet of a dual-pipe model, and at the other end to the return pipe inlet. Given water temperature, pressure and mass flow rate, the model injects heat inside the zone.

The model implements the finite volume method, therefore a radiator is discretised into a series of N_{rad} volumes of fluid. For each, thermal capacity of the metallic part is lumped to that of the water volume to take into account the thermal inertia of the emitter. About each volume, a heat balance is evaluated to compute radiative heat (Q_{rad}^{rad}) and convective heat (Q_{rad}^{conv}) delivered to the thermal zone according to Eq. 1.18 and Eq. 1.19 respectively. Q_{rad}^{conv} is added to the heat balance of the thermal zone as a direct heat (Eq. 1.1) whereas Q_{rad}^{rad} is distributed as diffuse radiation (Eq. 1.12). To favour numerical efficiency, we limit the discretization level to 3 fluid control volumes (N_{rad} = 3).

$$Q_{rad}^{rad} = f_r \cdot \frac{UA_{rad}}{N_{rad}} \cdot |T_{rad} - T_{rad}^{zone}|^{n_{rad}} \quad \text{Eq. 1.18}$$

$$Q_{rad}^{conv} = (1 - f_r) \cdot \frac{UA_{rad}}{N_{rad}} \cdot |T_{rad} - T_{air}^{zone}|^{n_{rad}} \quad \text{Eq. 1.19}$$

f_r is the fraction of radiative heat from the total heat delivered by the radiator and n_{rad} is an exponent of heat transfer. We stick to default values in *Buildings*: $f_r = 0.35$ and $n_{rad} = 1.24$. UA_{rad} is the coefficient of heat exchange calculated from the radiator sizing values according to Eq. 1.20.

$$UA_{rad} = \frac{Q_{SST}^{max} / N_{flo} / \alpha_{zone}^{surf} / N_{rad}}{T_{SST}^{nom} - T_{air}^{set\,nom}} \quad \text{Eq. 1.20}$$

Q_{SST}^{max} is the sizing (maximum) power of the building substation. This sizing power is equally divided into the N_{flo} floors, then divided among the 4 zones weighted by the fraction surface area α_{zone}^{surf} and again equally divided between the finite volumes. Hence, the numerator of Eq. 1.20 gives the sizing power for each element in a radiator. It is divided by the difference between the nominal supply water temperature at the substation T_{SST}^{nom} (set to the maximum supply temperature given a heating curve $T_{SST}^{nom} = T_{SST}^{HC\,max}$) and the air set point temperature $T_{air}^{set\,nom}$ to compute UA_{rad}.

Similarly to 1-D heat conduction, details of the finite volume method applied to heat transfer between the mixing volumes are not expanded in this manuscript. The total heat Q_{rad}^{tot} emitted by a radiator is given in Eq. 1.21.

$$Q_{rad}^{tot} = \sum_{i=1}^{N_{rad}} Q_{rad}^{conv\,i} + Q_{rad}^{rad\,i} \quad \text{Eq. 1.21}$$

1.3.6.2.4 Thermostatic radiator valves

The mass flowrate input to the radiator is controlled by a Thermostatic Radiator Valve (TRV) model.

We developed a model of this component to fulfil requirements of the European standard NF EN 215 in terms of the TRV time-response. Therefore, a careful modelling of the sensing bulb is carried out. It is represented by a thermal mass of heat capacity C_{bulb} and temperature T_{bulb}. As formulated in Eq. 1.22, the bulb exchanges heat with the zone air by natural convection. The heat exchange coefficient is calculated using the variable Nusselt number Nu_{bulb} of Eq. 1.23, which itself depends on the Rayleigh number of Eq. 1.24 according to a standard correlation valid for natural convection flows around a vertical cylinder [Kang *et al.*, 2014].

$$C_{bulb} \cdot \frac{dT_{bulb}}{dt} = \frac{Nu_{bulb} \cdot k_{bulb}}{D_{bulb}} \cdot S_{bulb} \cdot (T_{air}^{zone} - T_{bulb}) \quad \text{Eq. 1.22}$$

$$Nu_{bulb} = 0.67 \cdot {Ra_{bulb}}^{1/4} \quad \text{Eq. 1.23}$$

$$Ra_{bulb} = \frac{g \cdot \beta_{air} \cdot (T_{bulb} - T_{air}^{zone}) \cdot {D_{bulb}}^3}{\alpha_{air} \cdot \nu_{air}} \quad \text{Eq. 1.24}$$

k_{bulb} is the thermal conductivity of the bulb material, D_{bulb} is its diameter and S_{bulb} its surface area assuming a cylindrical shape (1.5 cm in diameter and 1 cm in length). In most practical situations, this leads to an equivalent thermal time constant of approximately 10 minutes.

$g = 9.8\,m/s^2$ is the gravitational acceleration, $\beta_{air} = 3.43 \times 10^{-3}\,1/K$ is the coefficient of linear thermal expansion of air, $\alpha_{air} = 2.12 \times 10^{-5}\,m^2/s$ is the thermal diffusivity of air and $\nu_{air} = 15.11 \times 10^{-6}\,m^2/s$ is the kinematic viscosity of air.

T_{bulb} is then compared with the air set-point temperature (T_{air}^{set}) to regulate the valve opening $\alpha_{TRV} = \frac{open\ TRV\ cross\ section}{total\ TRV\ cross\ section} \times 100$, assuming the linear opening law given in Eq. 1.25[8] and plotted in Figure 1.7. ΔT_{TRV}^{max} is the maximum temperature difference between T_{bulb} and T_{air}^{set} above which the valve is fully open. Typically, $\Delta T_{TRV}^{max} = 2$°C.

$$\alpha_{TRV} = \left[\frac{100}{\Delta T_{TRV}^{max}} \cdot \left(T_{air}^{set} - T_{bulb}\right)\right]_0^{100} \quad \text{Eq. 1.25}$$

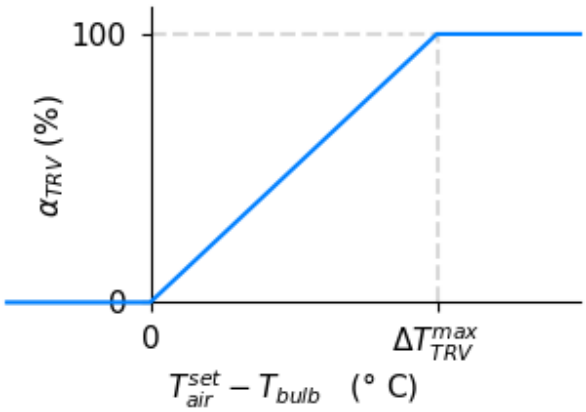

Figure 1.7 TRV opening law: The valve is fully closed when T_{bulb} is greater than T_{air}^{set} (dead zone), fully open when T_{bulb} drops ΔT_{TRV}^{max} below T_{air}^{set} (saturation), and opens proportionally to the temperature difference between the two extreme positions.

[8] The notation $y = [x]_a^b$ means: $y = \begin{cases} x\ if\ a < x < b \\ a\ if\ x \le a \\ b\ if\ x \ge b \end{cases}$

The valve flow coefficient (or flow-capacity) C_{TRV} given in Eq. 1.26 is a measure of the valve efficiency at allowing fluid flow. It relates the mass flowrate across the valve ($\dot{m}$) to the pressure drop between its inlet and outlet (ΔP_{TRV}) (SG_{water} is the specific gravity of water in a TRV and equals 1).

$$C_{TRV} = \dot{m}_{TRV} \cdot \sqrt{\frac{SG_{water}}{\Delta P_{TRV}}} \qquad \text{Eq. 1.26}$$

Our model relies on the assumption of linear valve characteristic. This means that C_{TRV} varies linearly with the valve opening position α_{TRV} as depicted in Figure 1.8.

At full opening, $C_{TRV} = C_{TRV}^{nom} = \dot{m}_{TRV}^{nom} \cdot \sqrt{\frac{SG_{water}}{\Delta P_{TRV}^{nom}}}$ where $\dot{m}^{nom}$ is the nominal mass flowrate across the fully open valve under the nominal differential pressure ΔP_{TRV}^{nom}. Hence, $\dot{m}_{TRV} \cdot \sqrt{\frac{SG_{water}}{\Delta P_{TRV}}} = \dot{m}_{TRV}^{nom} \cdot \sqrt{\frac{SG_{water}}{\Delta P_{TRV}^{nom}}} \cdot \alpha_{TRV}$ which allows us to derive $\dot{m}$ according to Eq. 1.27. The nominal values are parameters set by the user, whereas ΔP_{TRV} is an input to the TRV model obtained from the pressure drop in the dual-pipe model. Note that this pressure drop itself is affected by the mass flowrate inside the pipes.

$$\dot{m}_{TRV} = \dot{m}_{TRV}^{nom} \cdot \sqrt{\frac{\Delta P_{TRV}}{\Delta P_{TRV}^{nom}}} \cdot \alpha_{TRV} \qquad \text{Eq. 1.27}$$

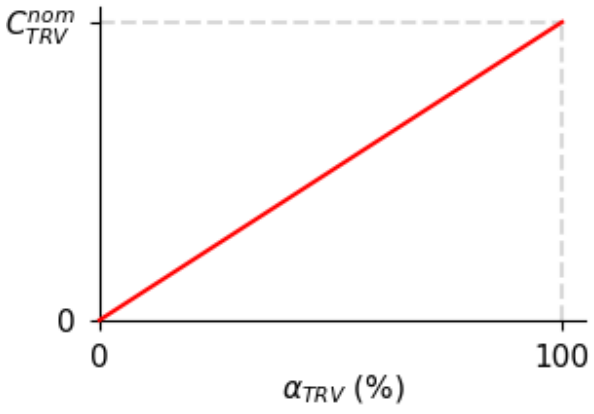

Figure 1.8 Linear valve characteristic: C_{TRV} is directly proportional to α_{TRV} and its maximal value is reached under nominal conditions when the valve is fully open.

1.3.7 Internal heat gain

Besides the heating system, a building receives passive heat (other than solar irradiation) from internal heat gain sources. Internal heat gain is particularly influential on well-insulated, low energy

consumption buildings as it may provide up to 20% of the SH load [Firląg et Zawada, 2013]. We developed a stochastic model to take into account such effects.

The internal gain (IG) model is prepared separately under csv file format, in a floor-by-floor approach. The signal is then injected into the thermal zones of the assembled BTS. The modelling approach considers that a floor represents a certain number of apartments having a specific number of residents. These numbers are set by the modeller. A building having different types of apartments per floor will eventually have different IG per floor as mentioned in 1.3.7.

The modelling technique starts by stochastically generating an occupancy profile for each equivalent thermal zone in the floor with time steps of 10 minutes. Based on this occupancy profile, signals of IG dissipated by 3 sources are modelled:

- Internal heat gain due to occupants' activity;
- Internal heat gain due to domestic hot water usage;
- Internal heat gain due to electric devices.

Here is a brief description of the stochastic modelling of signals contributing to the internal heat gain.

Occupancy profile generation

In order to generate this profile, surveyed time-use data describing the activity of residents in the UK during weekdays and weekends over the year of 2000 is used (with the lack of similar data in France). Then a first-order Markov chain technique is applied to generate synthetic data that has the same overall statistics as the original surveyed data. This technique, presented in [Richardson *et al.*, 2008b], considers that a resident living in an apartment can either be present or not at different times during the day, and furthermore, if he is present, he might be active or not (e.g. sleeping). The transition from one state to another is described in transaction probability matrices derived from the survey, as the one illustrated in Figure 1.9. It results at generating an occupancy profile in terms of presence and activity status of the residents discerning weekdays from weekends at a 10 minutes resolution.

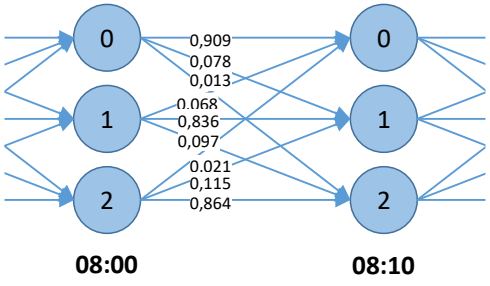

Figure 1.9 Example of a transaction probability matrix: Let an apartment have 2 residents; if only one resident is present at 8:00, the probability of him being still present alone at 8:10 is 0.836, the probability of him leaving the apartment is 0.068 and that of the other resident joining him is 0.097.

Internal heat gain due to occupants' activity

Given the occupancy profile for a floor, occupants are distributed over the 4 zones. We assume:

- All inactive occupants are systematically present in the night zone;
- All active occupants are present in the day zone except during the periods between 12:00 and 14:00 (lunch time) or between 18:00 and 20:00 (dinner time);
- All active occupants are present in the kitchen during lunch time and dinner time;
- No IG due to occupant's activity is dissipated in the bathroom.

Referring to [Arrêté du 30 avril 2013 relatif à des méthodes de calcul des caractéristiques thermiques et exigences de performance énergétique des bâtiments nouveaux, 2013], we assign 90 W of internal heat gain dissipated by an active occupant and 63 W by an inactive occupant. Simple multiplication yields the IG profile due to occupants' activity inside each zone denoted Q_{therm}^{occ}.

Internal heat gain due to domestic hot water usage

IG due to Domestic Hot Water (DHW) requires first generating a stochastic profile of DHW usage. This profile is indeed related to the occupant's activities profile modelled beforehand. DHW usage may then be converted in terms of dissipated thermal heat.

Again we based our model on works found in the literature [Jordan et Vajen, 2001], where the following four types of DHW loads are defined:

- Short load (e.g. hand washing);
- Medium load (e.g. dish washing);
- Shower;
- Bath.

For each type, statistical data is given in Table 1.2. It covers the daily number of usage per resident, its time duration (Δt) and the volume (V) of DHW used during 1 usage. For a given number of residents, we perform a first sampling to generate a profile for the number of daily DHW usages per floor for each type. For the sampling we assume normal probability distributions for all types except for *Bath* to which we assign a Bernoulli distribution. We set means μ calculated from the values of Table 1.2 and standard variation $\sigma = 0.25 \cdot \mu$.

Having the number of daily DHW usages for each type, we proceed to a second sampling to distribute these usages over the periods of the day. Again, probabilistic distribution are assigned to each type as indicated in [Jordan et Vajen, 2001]. A uniform distribution is assigned for short and medium loads in the kitchen between 5:00 and 23:00. In the bathroom, showers have 2 probability peaks per day, one at

7:00 and another at 19:00 whereas baths have 1 probability peak at 20:00. We combine these probabilities with the occupancy probability. This gives us the cumulative frequencies. An example of the cumulative frequency for the event is plotted in Figure 1.10. To generate the final DHW usage profile, we apply the inverse transform method as described in [Jordan et Vajen, 2001]

A numeric example might help understanding this model. Suppose a floor has 5 occupants. We already know for every 10 minutes the number of active and inactive occupants. Suppose we are interested in determining the instants when a *Shower* usage happened. The daily average number of showers according to Table 1.2 is 5. We perform the first sampling and get the actual number of showers taken on that day equal to 3 (rounded to the closest integer). We perform the second sampling to determine the 3 time periods when a usage occurred. We randomly get 0.25, 0.5 and 0.75. Using the cumulative frequency graph of Figure 1.10, we spot the sampled time instants 6:50, 7:50 and 17:50. We make sure that the obtained values are realistically coherent with other usages, for instance a *Shower* and a *Bath* do not coincide. This finally gives the profile of *Shower* taken at a 10 minutes resolution in a day.

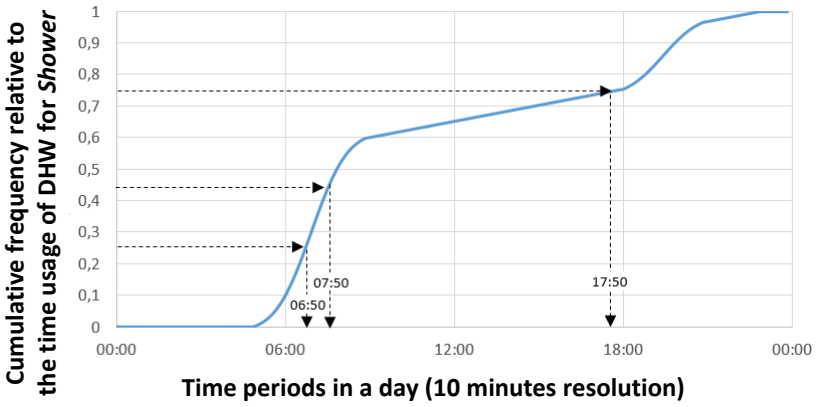

Figure 1.10 Illustration of the inverse transform method used to determine the time instants of DHW usage of type *Shower*

Given the time instants of the day when a usage is turned on p_{ON}^{DHW}, DHW usage may be converted into thermal energy dissipation using Eq. 1.28. In the calculations, we consider the duration and the DHW volume for every usage of Table 1.2 and we assume cold water for short and medium loads at $T_{DHW} =$ 15°C and hot water for showers and baths at $T_{DHW} = 40$°C (ρ_{wat} and c_{wat} being respectively the density and specific thermal capacity of water) and an ambient air temperature at constant value T_{amb} = 20°C. This formula takes into account the thermal inertia of DHW via a staggering coefficient κ_{IG} and the efficiency of the conversion via the coefficient η_{IG} given in Table 1.2. Considering internal heat gain is constant per 10 minutes, we generate the corresponding power profile.

$$\sum_{p=p_{ON}^{DHW}}^{p_{ON}^{DHW}+\kappa_{IG}\cdot\Delta t_{DHW}} Q_{therm}^{DHW}(p) = \eta_{IG} \cdot \sum_{p=p_{ON}^{DHW}}^{p_{ON}^{DHW}+\Delta t_{DHW}} \frac{V_{DHW}}{\Delta t_{DHW}} \cdot \rho_{wat} \cdot c_{wat} \cdot (T_{DHW}(p) - T_{amb}) \quad \text{Eq. 1.28}$$

Table 1.2 Characteristics of DHW usages: μ_{DHW} is the mean number of usages per occupant per day, V_{DHW} is the water volume per usage, Δt_{DHW} is the time duration of one usage, κ_{IG} is the staggering coefficient and η_{IG} is the efficiency of the conversion into internal heat gain.

Thermal zone	**DHW usage type**	μ_{DHW} **(usage/occupant/day)**	V_{DHW} **(l)**	Δt_{DHW} **(s)**	T_{DHW} **(K)**	κ_{IG} **(-)**	η_{IG} **(-)**
Kitchen	Short load	9	1	10	288.15	1	0.2
	Medium load	4	6	60	288.15	1	0.5
Bathroom	Shower	1	40	300	313.15	1	0.5
	Bath	0.047	140	600	313.15	3	0.7

Internal heat gain due to electric devices

IG due to electric devices (EDs) is based on a bottom-up model of ED usage from the literature [Richardson *et al.*, 2010b], obtained from surveyed data in the UK. The model generates electric power consumption profiles based on the presence of active occupants in a zone at a 10 minutes step considering the following aspects for each device:

- Average number of functioning cycle per year;
- Time duration of each functioning cycle;
- Waiting time before starting-up a new cycle;
- Mean power consumption during a functioning cycle;
- Mean power consumption when on stand-by mode.

From the obtained electric power usage profile, we can generate the profile of thermal IG dissipated from an electrical device while accounting for its thermal inertia, similarly to DHW. Consider Eq. 1.29, a device that has been turned on at instant p_{ON}^{ED} and off at instant p_{OFF}^{ED}, consumes Q_{elec}^{ED} of electric power and dissipates Q_{therm}^{ED} of internal heat gain during the corresponding period p. It is characterized by a staggering coefficient κ_{IG} and a conversion factor between electrical and thermal power η_{IG}. Values for κ_{IG} and η_{IG} for common devices are listed in Table 1.3.

$$\sum_{p=p_{ON}^{ED}}^{p_{ON}^{ED}+\kappa_{IG}\cdot(p_{OFF}^{ED}-p_{ON}^{ED})} Q_{therm}^{ED}(p) = \eta_{IG} \cdot \sum_{p=p_{ON}^{ED}}^{p_{OFF}^{ED}} Q_{elec}^{ED}(p) \quad \text{Eq. 1.29}$$

For the distribution of EDs between the thermal zones of a floor, we assume:

- No EDs are present in the night zone;
- A computer, a TV, a vacuum cleaner and a clothes iron are present in the day zone;
- A refrigerator, a freezer, a cooking plate, an oven, a microwave and water boiler are present in the kitchen;
- Only a clothes dryer is present in the bathroom.

Table 1.3 Characteristics of EDs used in the thermal IG dissipation model

Thermal zone	**ED**	κ_{IG} **(-)**	η_{IG} **(-)**
Day zone	Computer	1	0.7
	TV	1	0.7
	Vacuum cleaner	1	0.7
	Clothes iron	2	0.7
Kitchen	Refrigerator	1	1
	Freezer	1	1
	Cooking plate	2	1
	Over	2	1
	Microwave	2	1
	Water boiler	2	1
Bathroom	Clothes dryer	1.5	0.5

Aggregation and injection of internal heat gain

Once internal heat gains from all 3 sources are generated (Q_{therm}^{occ}, Q_{therm}^{DHW}, Q_{therm}^{ED}), we inject their sum denoted Q_{IG} into the thermal zone. Half of it is assumed to be convective and therefore it is directly added to the heat balance of a thermal zone (Eq. 1.1); the other half is radiative and *MixedAir* integrates it into the radiative exchange between the internal surfaces as described in § 1.3.2. *MixedAir* can also handle latent heat gain and integrate it into a mass balance, yet it is not used in our work for simplification. An example Q_{IG} over one day is shown in Figure 1.11.

Figure 1.11 Example result of an internal heat gain signal over 1 weekday in the 4 zones of a floor

1.3.8 Boundary conditions

The BTS is exposed to boundary conditions (external temperature, solar irradiation, wind speed, etc.…) using a specific component from *Buildings Library* that reads weather data files. The user can either create customized weather data or use data files for a Typical Meteorological Year (TMY).

1.4 Case study BTSs

Throughout the rest of the thesis, we consider 3 case study BTSs. They are chosen to be representative of the French buildings stock, which allows comparative results analysis. The multiple case study is also important to support the robustness of the proposed methodologies.

Instantiation of building case-studies requires setting the envelope parameters: geometry and construction material. It also involves specifying certain characteristics of the SH systems.

1.4.1 Envelope geometry – common to all study case BTSs

As for the footprint, internal decomposition and facades dimensions, we based our BTSs on a building named *Le Salammbô* (Figure 1.12). It is located in the *Zac Flaubert* neighbourhood of Grenoble, composed of 37 residential lodgings on 8 floors and connected to a DHS branch that serves as a demonstrator of advanced control strategies in the *City-zen*[9] project. Potentially, the control strategy designed in this thesis could be applied in real-life on *Le Salammbô*. The actual building, inaugurated in 2018, is certified RT2012 -20%, i.e. it fulfils the requirements of the latest thermal regulation RT2012, and consumes 20% less than the standard maximum threshold of 50 kWh/m²/year in primary energy.

[9] http://www.cityzen-smartcity.eu/fr/grenoble/

Figure 1.12 Photograph of *Le Salammbô* – Grenoble, 2018
Photo credit: http://www.gre-mag.fr

Figure 1.12 shows 8 stories with some balconies and terraced areas. However, the BTSs have only one floor to save on computation times. As described in § 1.3.5, floors have a rectangular footprint with one equivalent square shaped window per façade, without balconies nor terraced areas.

Geometric parameters of the BTS floor are given in Table 1.4. The building orientation θ_{build}, storey height h_{flo} and total floor area S_{flo} are those of *Le Salammbô*. The zones percentage areas to the total floor area α_{zone}^{surf} are average values on the 8 stories. Floor surface area and zone volume may then be simply calculated according to Eq. 1.30 and Eq. 1.31.

$$S_{zone} = S_{flo} \cdot \alpha_{zone}^{surf} \quad \text{Eq. 1.30}$$

$$V_{zone} = S_{zone} \cdot h_{flo} \quad \text{Eq. 1.31}$$

Similarly, average areas of opaque and glazed surfaces of the 4 *Salammbô* facades are given in Table 1.5. Parameters shown in these 2 tables are common to all 3 study-case BTSs.

Table 1.4 Geometric parameters of one floor

N_{flo}	θ_{build} (rad)	h_{flo} (m)	S_{flo} (m²)	α_{zone}^{surf} (-)			
				Night zone	Kitchen	Day zone	Bathroom
1	π/2	2.5	306 (10.85m x 28.21m)	0.35	0.15	0.4	0.1

Table 1.5 Geometric parameters of the facades

	East facade	South facade	West facade	North facade
Opaque areas (m²)	54.30	17.09	45.84	23.60
Glazed areas (m²)	16.22	10.04	24.68	3.53

Important remark

Note that unless otherwise indicated, all BTSs have the default amount of internal mass given in Table 1.1. They all receive the same IG signal described in § 1.3.7.

Also note that since *Le Salammbô* is located in Grenoble, throughout the dynamic simulation runs, the BTSs are exposed to the TMY weather file of the city of Grenoble. Whenever a steady-state condition is required, the default value of the external temperature is fixed to $T_{ext}^{sizing,Grenoble}$ = -11°C which is the extreme temperature used for sizing of heating systems in Grenoble.

1.4.2 Envelope construction materials – specific per case study BTS

The 3 case study BTSs belong to 3 different energy consumption classes. The properties of their envelope construction materials are the main factor contributing to this distinction. We referred to TABULA [FR_TABULA, 2015b] in the choice and parameterization of these case study buildings.

TABULA is a European project to create a harmonized structure for residential buildings typologies. One main use of TABULA's outcome is recommending strategic refurbishment of the building stock per building type, climatic zone and economic policies for the European Union member countries. Meanwhile, TABULA has been used in other works as a reference for typical buildings characteristic [Reynders, 2015b].

TABULA classifies the residential buildings into 4 categories (see column headings in Table 1.6) and encompasses 10 construction periods (see row headings in Table 1.6). It gives typical data for an example building from each category per construction period. Table 1.6 shows the distribution of living space in the French residential stock.

Table 1.6 Percentage of living space for each group of buildings in the total French residential stock, post-processed from [FR_TABULA, 2015b]

	Single-family house	Terraced house	Multi-family house	Apartment building
Before 1915	9.23%	2.76%	2.49%	1.42%
1915 - 1944	4.79%	1.35%	1.19%	0.90%
1945 - 1967	4.99%	1.33%	2.20%	4.36%
1968 - 1974	4.58%	1.15%	1.11%	4.03%
1975 - 1981	5.99%	1.40%	0.55%	2.51%
1982 - 1989	6.06%	1.33%	0.63%	1.43%
1990 - 2000	7.45%	1.39%	0.99%	2.82%
2001 - 2005	4.65%	0.88%	0.55%	1.40%
2006 - 2012	5.64%	1.21%	0.93%	2.27%
After 2012	1.01%	0.24%	0.23%	0.55%

From the *Multi-family house* category, we selected the two extremes and one intermediate case listed below. Despite the fact that *Single-family houses* occupy the highest portions of residential living space, buildings connected to DHSs mostly fall in the *Multi-family house* category. The choice of the *1975 – 1981* construction period as intermediate case study was motivated by the event taking place in 1974 following the oil crisis, when the first thermal regulation (RT 1974) was introduced in France. The standard aimed at reducing the energy consumption in buildings by 25%. In order to achieve this objective, the RT 1974 imposed all building envelopes to have insulation layers and heating emitters to have temperature regulators. A transition has consequently been made in the 1974 – 1981 period. Therefore we consider the following case study buildings, whose envelop compositions are described layer-by-layer in Table 1.7:

- A *Multi-family house* from the *Before 1915* construction period, called the *1915 Building*;
- A *Multi-family house* from the *1975 – 1981* construction period, called the *1975 Building*;
- A *Multi-family house* from the *After 2012* construction period, called the *2012 Building*.

Table 1.7 Envelop composition (form outer to inner layer) of the case study BTSs

	1915 Building	***1975 Building***	***2012 Building***
Roof	1 cm tiles	10 cm mineral wool	16 cm polyurethane
	2 cm wood	20 cm roofing concrete	20 cm roofing concrete
	2 cm glass wool		
	13 cm plaster		
Ground	20 reinforced concrete	2 cm expanded polystyrene	16 cm extruded polystyrene
	6 cm concrete	15 cm reinforced concrete	20 cm reinforced concrete
Opaque facade	40 cm stone	1.3 cm plaster	1.5 cm cement mortar
	2 cm lime plaster	4 cm expanded polystyrene	16 cm expanded polystyrene
		20 cm cinderblock	18 cm concrete
Glazing system	0.4 cm glass	0.4 cm glass	0.4 cm glass
		0.6 cm air	1.6 cm argon
		0.4 cm glass	0.4 cm glass
Ceiling between intermediate floors	20 cm reinforced concrete	20 cm reinforced concrete	20 cm reinforced concrete
	16 cm glass wool	16 cm glass wool	16 cm glass wool
	5 cm concrete	5 cm concrete	5 cm concrete

1.4.3 Ventilation and SH characteristics – specific per case study BTS

For ventilation, we need to set the number of air volume changes per hour, n of Eq. 1.15. Theoretically, the air renewal rate should depend on the type of the zone, the number of its occupants and their activities [Arrêté du 24 Mars 1982 modifié le 28 Octobre 1983 relatif à l'aération des logements, 1983]. However, for the sake of simplicity, we assume a constant and equal n_{vent} in all zones in a BTS, and different number for each case study. This distinction is made because, according to the standards, newer buildings should have lower air renewal rates so as to reduce their energy consumption (the RT2012 recommends rates as low as 0.2 Vol/hr). Additionally, we consider that this model also accounts for infiltrations, thus old buildings are less airtight and should have higher losses due to infiltration, hence higher n_{vent}. The assigned average values shown in Table 1.8 are from the literature [Holøs *et al.*, 2018].

The distinctive envelope properties and air renewal rates cause the BTSs to have different energy needs. Naturally, they have different SH sizing powers. The SH system with zero thermal inertia of § 1.3.6.1 is used to find the sizing power (Q_{SST}^{max} in Eq. 1.20) under the following steady-state conditions:

- Indoor air set-point temperature is set to its nominal value T_{air}^{set} = 20°C;
- External temperature is set to $T_{ext}^{sizing,Grenoble}$ = -11°C;
- Direct and diffuse solar irradiations are set to 0 W/m²;
- Internal heat gain is deactivated.

Results of Q_{SST}^{max} are given in Table 1.8.

Besides the sizing power, the SH system operates using different heating curves shown in Figure 1.13, under the same differential pressure of 1.5 bar. Older buildings usually require high heating temperatures, as opposed to newer buildings. The maximum and minimum heating temperature reported in Table 1.8 are set based on common practices and in such a way to ensure stable mass flow rates in the heating systems for each case. The maximum temperature $T_{SST}^{HC\,max}$ is reached when the external temperature drops below -11°C, whereas the minimum temperature $T_{SST}^{HC\,min}$ is used when the external temperature exceeds 15°C and during night-time set-backs.

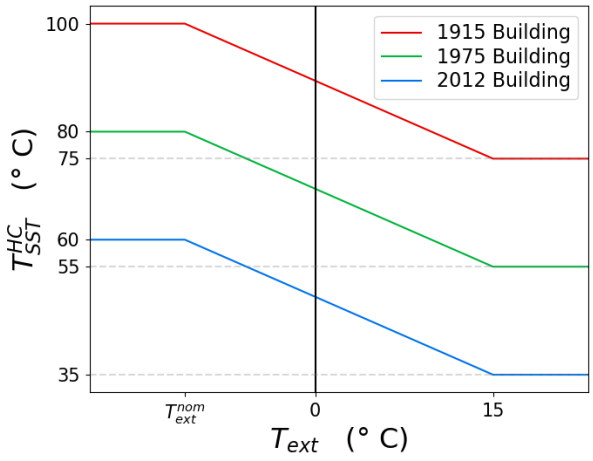

Figure 1.13 Heating curves defining secondary water supply temperature at the substation T_{SST}^{sup} function of the external temperature T_{ext}, used in conventional SH WCC of the 3 case study BTSs

Table 1.8 Heating and ventilation characteristics of the case study BTSs

	1915 Building	***1975 Building***	***2012 Building***
n_{vent} (1/hr)	0.5	0.4	0.3
Q_{SST}^{max} (kW)	35	18.5	8.6
$T_{SST}^{HC\,max}$ (°C)	100	80	60
$T_{SST}^{HC\,min}$ (°C)	75	55	35

1.4.4 Typical simulation scenario

We present typical simulation runs of the BTSs to verify the energy balance conservation in the model and to point the main energetic differences between the 3 case studies. During these simulations, the SH controller sets the secondary supply water temperature T_{SST}^{sup}:

- Using the heating curves of Figure 1.13 during the day;
- To the lower bound of the heating curves from mid-night until 6:00 am, as night-time set-back.

In Table 1.9, energy losses and gains that can be easily calculated by time integration of heat flows are reported. Note that energy loss through the opaque envelope encompasses losses through all opaque facades, the roof and the floor. Energy loss through glazing systems accounts for infiltrations through the frame as well as losses through the glass layers. The values show the difference in terms of energy consumption between the 3 case study BTSs. However, they all receive the same internal heat gain signal; therefore, the contributions of internal gain are not equivalent. Over the simulated day, internal heat gain covered about 40% of the *2012 Building* SH demand, whereas it only contributed to roughly 10% of the *1915 Building* SH demand.

Table 1.9 shows that the sum of energy losses is slightly greater than energy supply. Assuming that the energy balance of the system should be conserved during the one-day cycle (indoor air temperature at the beginning and at the end of the day should be almost the same), we interpret the difference between losses and supply to be due to the contribution of solar heat gain which is not straightforward to compute.

Time series simulation results are shown in Figure 1.14, Figure 1.15 and Figure 1.16. They graphically depict the particular sensitivity of the *2012 Building* toward internal and solar heat gain.

In the figures, Q_{env}^{opa} denotes heat loss through the opaque envelope and Q_{env}^{gla} denotes heat loss through the glazing systems. I_{sol}^{dir}, I_{sol}^{glo} and I_{sol}^{dif} are respectively the solar direct normal, global horizontal and diffuse horizontal irradiations used the BTS radiation model. Q_{rad}^{tot} is the total heat emitted from all 4 radiators in the BTS and Q_{SST} is the power supplied from the DHS substation.

Table 1.9 Energetic assessment of thermal losses, internal gain and SH, unit $(kWh/m^2/day)$

BTS	Energy loss through the opaque envelope	Energy loss through the glazing systems	Energy loss through ventilation	Energy supply through internal heat gain	Energy supply through the radiators	Energy supply – Energy losses
1915 Building	1.18	0.34	0.17	0.15	1.52	-0.03
1975 Building	0.53	0.20	0.14	0.15	0.70	-0.02
2012 Building	0.13	0.16	0.10	0.15	0.22	-0.03

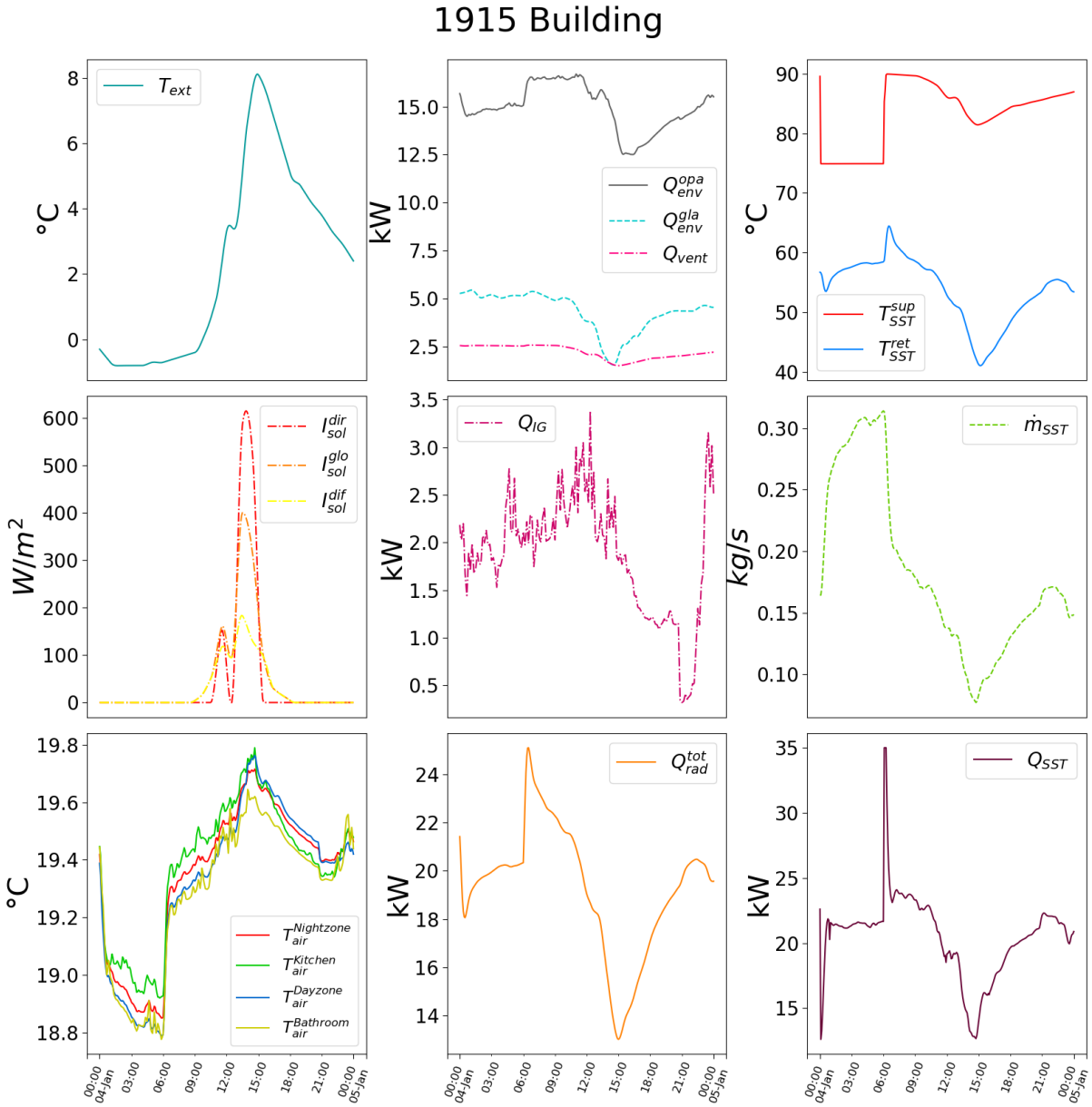

Figure 1.14 Simulation results from the 1915 Building

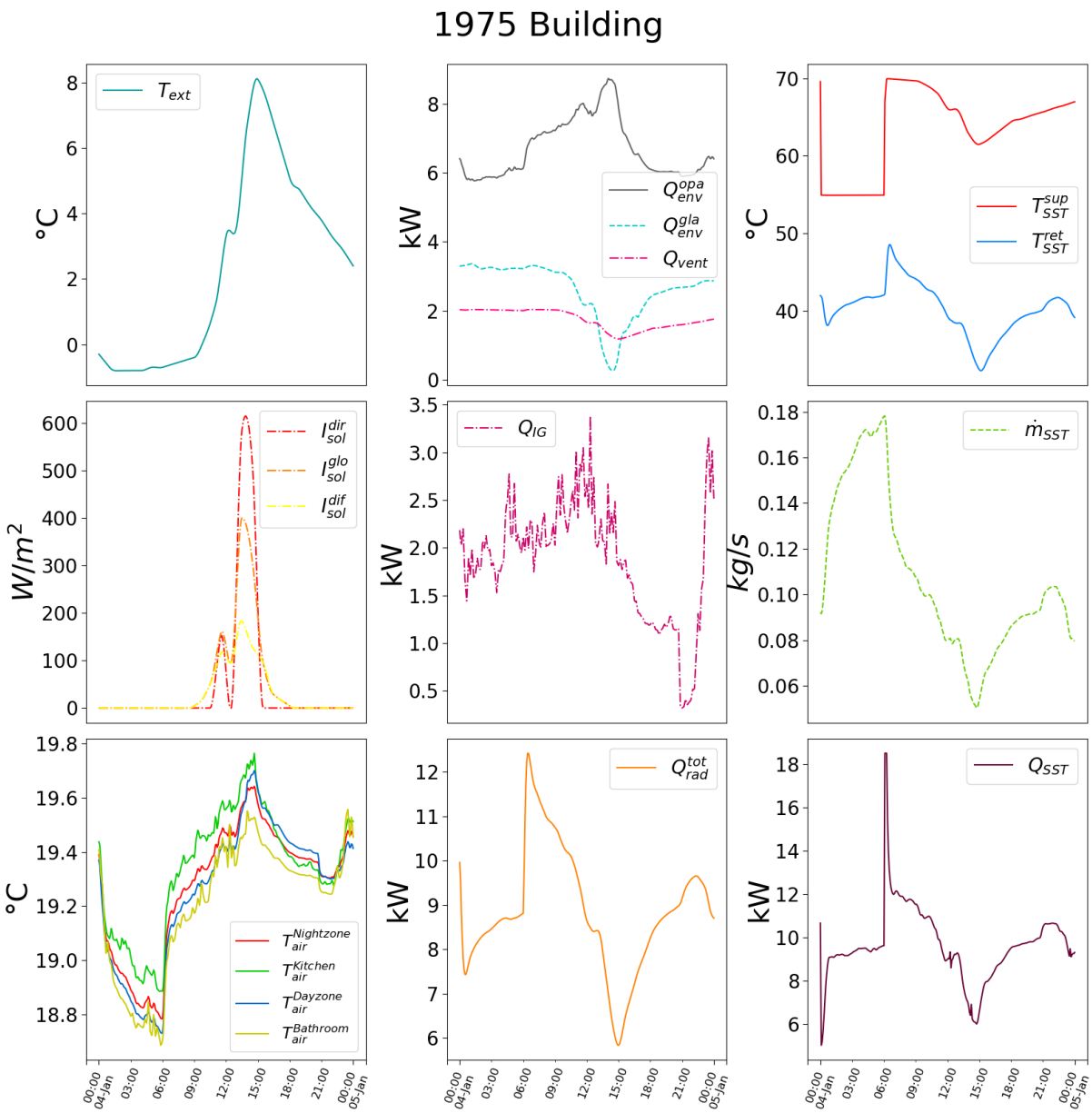

Figure 1.15 Simulation results from the 1975 Building

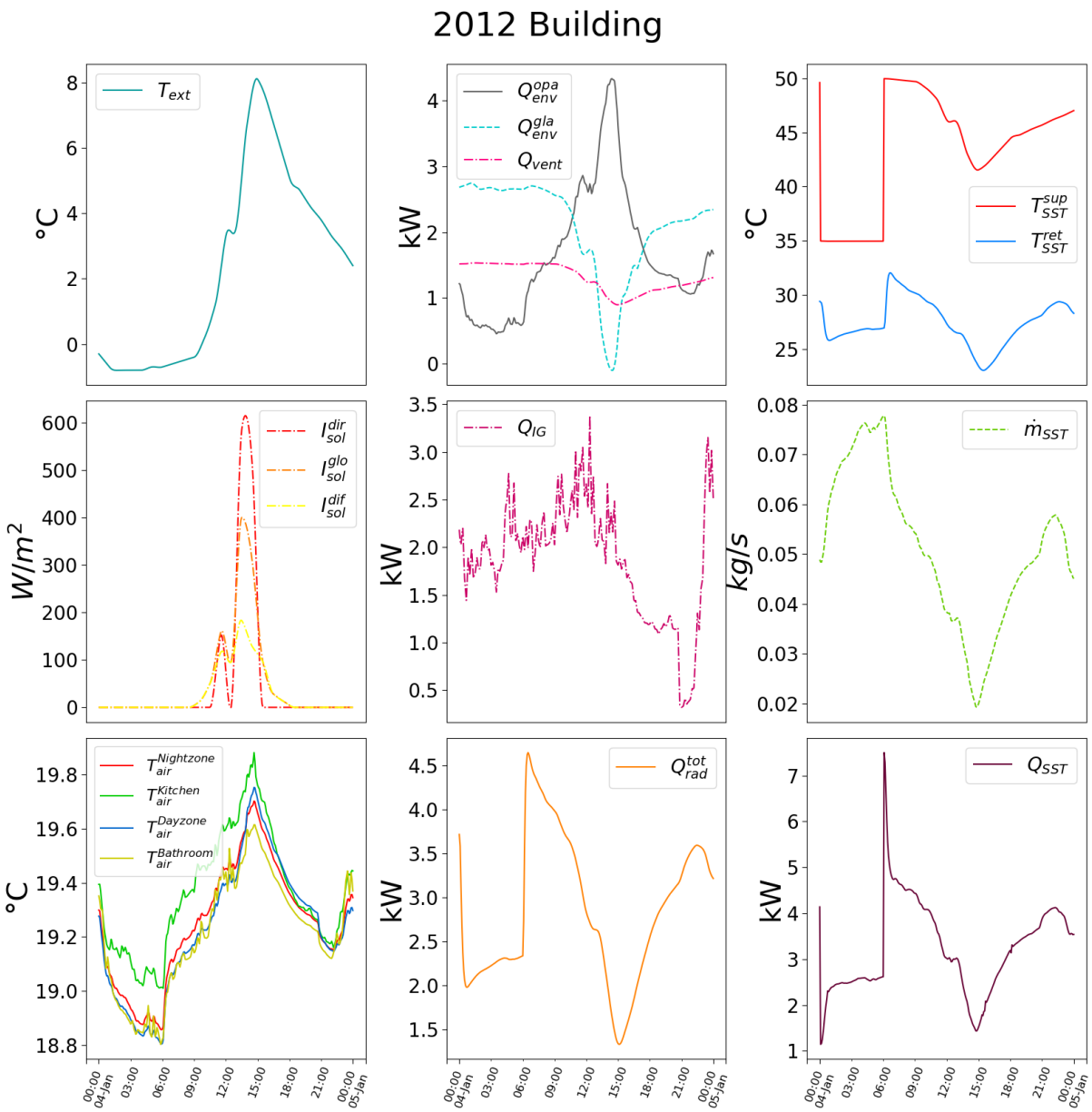

Figure 1.16 Simulation results from the *2012 Building*

Note the peak in losses through opaque envelope elements (top row, second column) which counterintuitively coincides with the solar radiation peak. We explain this peak is due to the increase in floor temperature, being directly struck by the solar rays, in thermal exchange with a surface at a fixed temperature (10°C). This is remarkably visible in the *2012 Building* since this low-consumption building has particularly low losses through other envelope elements.

1.5 Conclusion

This chapter described the development of BTSs. We followed the object-oriented principle of Modelica in the description of the BTS components and we detailed the physical thermal phenomena and mathematical models considered in each. Three case study BTSs have been introduced to represent different energy classes found in the French building stock and parameterized based on thermal regulations applied in France. A typical simulation scenario is presented to illustrate the differences between the case studies and to assess the heat balance conservation in the model. These BTSs will constitute our virtual experimental environment for the rest of the thesis.

Chapter 2

Reduced-order building modelling

Synopsis

After setting up the simulation environment, the objective of this chapter is to infer a simplified reduced-order thermal building model from data generated by the BTS, to be later used in the MPC application. The model should fulfil several requirements: it should be accurate, identifiable from a limited set of available data at a DHS scale and computationally efficient for the intended optimization problem. A literature review concludes that such a model is yet to be proposed and it would constitute a contribution of this thesis. We develop a suitable modelling approach, then apply and assess its outcome on analytical cases. Some limitations are identified; we propose some adjustments and carry-on application on the three case study BTSs introduced in the previous chapter. Final results show that the obtained models are accurate enough to be used in MPC.

2.1 Definition and requirements on the reduced-order model

A Reduced-Order Model (ROM) is a simplification of a complex Higher-Order Model (HOM) that preserves dominant dynamics of the system with a relatively small number of equations for the purpose of reducing computational times and data storage capacity [Antoulas *et al.*, 2000].

In this thesis, we call ROM (of a building system) the set of mathematical equations describing the system thermal dynamics. As any model, the ROM is driven by input signals, some of them are controllable by the DHS operator while others are disturbances. It has state variables: some of them are measurable at the DHS substation and therefore constitute the outputs or observations; others are hidden states. It has time-invariant parameters that require identification based on historical observations generated by the BTS regarded as the corresponding HOM. In our case, we consider ROMs that keep some physical interpretation. Hence, the process of developing a ROM starts by defining its structure, i.e. the underlying equations, inputs, outputs and hidden states, followed by a parametric identification.

The role of the ROM is to predict the thermal behaviour of the building so that its controllable input may be optimized over a prediction horizon in a MPC framework to achieve some control objectives that will be given in the following chapter. It shall fulfil certain requirements explained hereafter.

2.1.1 Accuracy

In MPC, an inaccurate model causes the controller to drive the system on sub-optimal trajectories. For instance, in our application, a sub-optimal trajectory implies thermal discomfort and/or extra energy costs for SH which defeats the purpose of MPC. Whereof, it is patently crucial to carefully derive an accurate ROM [Prívara *et al.*, 2013a]. This requires a ROM structure well-representative of the most influential dynamics in the building system, paired with a robust parametric identification strategy [Blum *et al.*, 2019]. According to [Stigter et Beck, 1994], uncertainty over the model structure is a relevant source of discrepancies, whereas parametric uncertainty often has only marginal contributions.

2.1.2 Identifiability

The ROM structure should be well-designed so that all parameters are identifiable using the available observations during usual operation modes. Over-parametrization given few observation signals results in poorly identifiable parameters, i.e. different sets of parameters can produce almost the same results [Brun *et al.*, 2001]. In this thesis, we assume that available observations are solely measurements found at the substation. Beyond the substation is a black-box from the DHS operator perspective. Thus, geometric description of the building, construction material, year of construction and internal measurements are all to be considered as unavailable in this study. Moreover, the identification should be processed from real-life scenarios, non-intrusive to the inhabitants. In this regard, admissible scenarios to gather observations shall not entail immoderately prolonged power cut-offs.

2.1.3 Computational efficiency

In MPC, the controller solves an optimization problem over a prediction horizon, i.e. it shall compute optimal values for all decision variables (controllable inputs) at all sampling times of the horizon. This needs to be executed within few minutes. Usually linear models are well handled and efficient solvers promote their incorporation in MPC. However, since most real-life systems feature nonlinear dynamics at some point, one may intuitively attempt to model these non-linearities so as to obtain a rather accurate model. Non-linear ROM can be linearized for control implementation; nevertheless, when their linearization entails insertion of additional variables, they quickly become prohibitive in computational efficiency. The solver will then fail at finding the optimal solution within the given time step. Therefore, it is recommended for MPC to avoid strongly nonlinear models and find alternative linear, or at most bilinear, representations of the system dynamics [Lehmann *et al.*, 2013a].

2.2 Literature review

Building modelling is an extensively researched topic. Based on the model requirements specific to our application, a narrowed-down literature review is presented hereafter.

2.2.1 ROM structures

Often in the literature, building energy models are classified into 3 categories [Foucquier *et al.*, 2013; Harish et Kumar, 2016; Li et Wen, 2014; Kramer *et al.*, 2012]:

- White-box models;
- Black-box models;
- Grey-box models.

White-box models are developed in a forward approach which essentially involves modelling the building components using physical equations and setting all parameters from given physical characteristics. White-box models are rather HOMs. The BTS presented in Chapter 1 is such an example. Therefore, no further expatiation on white-box models is given in this section.

Black-box models may developed by machine learning approaches which inspect historical data to learn relationships between inputs and outputs. Popular approaches for black-box modelling include Box-Jenkins derivatives for linear models [Ríos-Moreno *et al.*, 2007; Rabl, 1988] and artificial neural networks for non-linear models [Huang *et al.*, 2015]. Black-box models are fast and parsimonious ROMs; however they only link outputs to inputs; hidden states of the system cannot be reconstructed because the obtained model parameters are not physically interpretable. In our problem, the indoor temperature is a hidden state that needs to be reconstructed through the ROM in order to assess and modulate thermal comfort during MPC. Therefore black-box models cannot be used for our application.

Grey-box models are semi-physical: equations of the model are formulated based on physical laws, thus its parameters have physical significance, however they are virtual (or equivalent). In grey-box building modelling, several elements of the building model are lumped (or aggregated) into a single node and therefore have a uniform temperature and equivalent physical properties. A thermal capacitance is associated to a temperature node, whereof the grey-box model is sometimes called lumped-capacitance model. Thermal/electrical analogy arises when establishing the heat balance for each node, whereof a lumped-capacitance model is commonly represented with an electric circuit schema and called RC / RxCy (Resistance-Capacitance) model. Similarities in the thermal/analogy are stated in Table 2.10.

Table 2.10 Analogy chart between thermal RC building models and electric circuits

RC building model	Electric circuit
Node of lumped elements	Electric potential terminal
Temperature	Electric potential
Heat flow	Current
Imposed temperature	Voltage source
Imposed heat flow	Current source
Thermal resistance	Resistor
Thermal capacitance	Capacitor

Moreover, a linear RC model has thermal resistances and capacitances that do not vary with the imposed temperatures or heat flows. A time-invariant RC model has resistances and capacitances that do not vary with time.

RC models have a limited number of equations. Imposed heat flows and temperatures constitute their inputs. Depending on the available observations, temperatures at the nodes and heat flows between nodes constitute their outputs. Thus, they are ROMs whose parameters can be identified from HOMs. Furthermore, their physical parameters can be used to reconstruct hidden states. Therefore they seem convenient for our application.

The number of thermal capacitances in an RC model determines the ROM order. The order, the layout of the nodes and connections between them, together with the specification of inputs / outputs determine the ROM structure. Numerous structures can be found in the literature.

Important remark

Note that in the sequel, thermal resistance (R) will only appear in its inverse form ($1/R$), hence we introduce the global heat transfer coefficient $U = 1/R$ (expressed in W/K), for sake of simplicity.

2.2.1.1 First order models

First order models have 1 thermal capacitance C_{build}. All building elements are lumped into one node and have uniform temperature T_{build}. Establishing the heat balance for the single node yields Eq. 2.32.

$$C_{build} \cdot \frac{dT_{build}}{dt} = U_{build} \cdot (T_{ext} - T_{build}) + Q_{heater} + \{extra\ terms\} \quad \text{Eq. 2.32}$$

The building mainly loses heat to the external environment at temperature T_{ext} and receives heat from a heating system Q_{heater}. Sophisticated models include extra terms to account for solar gain, internal heat gain or other factors. First order models may also have massless nodes that exchange heat with the node to which C_{build} is associated, however temperatures of massless nodes must be inputs to the model.

2.2.1.1.1 Static energy signature models

Static energy signature models are 1st order models that assume a constant value over time for T_{build}. This is formulated in Eq. 2.33:

$$C_{build} \cdot \underbrace{\frac{dT_{build}}{dt}}_{=0} = U_{build} \cdot (T_{ext} - T_{build}) + Q_{heater} + \{extra\ terms\} = 0 \qquad \text{Eq. 2.33}$$

These models are valid on relatively long time steps of at least a day where the actual mean temperature of the building is quasi constant and equal to the assumed T_{build}. They are mainly used to linearly correlate the average heating load Q_{heater} to the average external temperature T_{ext} (and other factors in case of extra terms). The result is a linear plot ($Q_{heater}\ vs\ T_{ext}$) called the energy signature of the building, hence the name.

Static energy signature models are the simplest models to develop at a city scale since they do not require measurements of internal temperature [Rabl et Rialhe, 1992; Mutani *et al.*, 2017; Fels, 1986].

However, since the effect of the building thermal capacitance C_{build} is cancelled out, these models do not reflect any thermal inertia of the system. For optimal control strategies which principally aim at exploiting thermal inertia to reduce heating costs by modulating T_{build} over short time steps, static energy signature models would not be suitable.

2.2.1.1.2 Dynamic first order models

Dynamic 1st order models have the structure formulated in Eq. 2.32 with variable T_{build}.

They are often used at city-scale for their computational efficiency and because identification of their few parameters requires only little data. They were investigated and used in [Elci *et al.*, 2018; Lin *et al.*, 2012; Guelpa et Verda, 2016; Muthalib et Nwankpa, 2014; Park *et al.*, 2011].

When assimilating a building to a 1st order system, it is assumed to have a single time constant τ_{build} calculated as in Eq. 2.34.

$$\tau_{build} = \frac{C_{build}}{U_{build}} \qquad \text{Eq. 2.34}$$

This is only valid for buildings with light and poorly insulated envelopes. In fact, buildings are complex systems with multiple time constants of different magnitudes. In case of a heavy and well-insulated building, envelope elements such as external walls have a large time constant, while indoor air has low thermal capacity thus a much shorter time constant. Therefore, 2 dynamics are present. When aggregating indoor air and envelope elements into one node, they are both allocated the same dynamics expressed by the variations of T_{build}. T_{build} is then a fictive in-between temperature that cannot be used to modulate indoor temperature, neither does it reflect the slow dynamics due to the thermal inertia of structure elements. Hence, a 1st order ROM structure is not recommended for optimal control applications [Reynders *et al.*, 2013b; Vivian *et al.*, 2017b].

2.2.1.2 Second order models

Second order models have 2 thermal capacitances, usually one representing the external envelope and another for the internal environment: internal mass and indoor air aggregated at a common temperature node (Figure 2.17 (a)) or internal mass and massless indoor air at separate nodes (Figure 2.17 (b)).

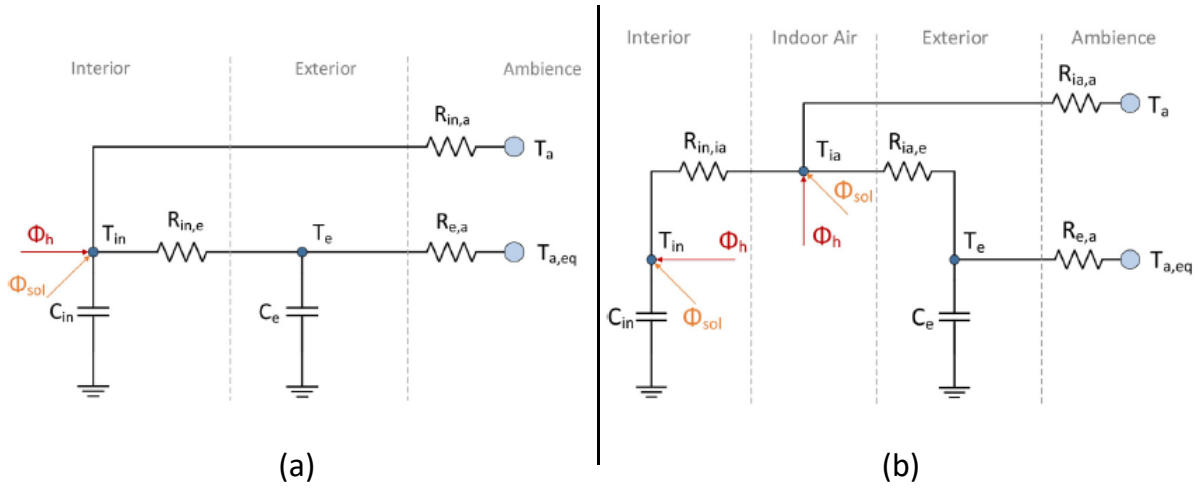

Figure 2.17 Example of 2nd order ROM structure in [Harb *et al.*, 2016]
(a) 1 indoor temperature node representing both indoor air and internal mass
(b) 2 indoor temperature nodes, one for the massless indoor air and another for internal mass
Structure in (b) was found more accurate than that in (a).

The model then consists of 2 heat balance differential equations for each node exchanging heat in between each other and with the external environment.

The 2nd order ROM structure is often found to be more accurate than the 1st order in comparative studies, especially short time steps predictions, while retaining the main advantages of simplicity, identifiability and computational efficiency [Berthou *et al.*, 2014b; Reynders *et al.*, 2014b; Ferracuti *et al.*, 2017].

However, for buildings with heavy internal mass (furniture and partition walls), when aggregating the indoor air with internal mass as in Figure 2.17 (a) the model falls into the same limitations of the 1st order. Hence, a structure with separate node for indoor air, whether with a thermal capacitance or not, seems more persuasive.

2.2.1.3 Third order models

Third order models have 3 thermal capacitances: one for the external envelope, another for internal mass and a third for indoor air. Examples of equivalent RC networks are the one similar to Figure 2.17 (b) with an additional capacitance to the air node and the one in Figure 2.18.

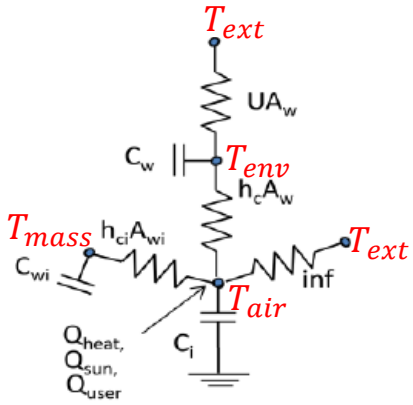

Figure 2.18 Example of 3rd order ROM structure with T_{air} the temperature at the air node, T_{env} at the envelope node and T_{mass} at the internal mass node, studied in [Reynders *et al.*, 2013b] and found to outperform a 1st and a 2nd order models

The model consists of 3 differential equations establishing heat balances for the nodes.

Within the same order, different structures are possible depending on how solar heat gain, internal gain and connections between nodes are modelled. For instance in Figure 2.17 (b), solar heat gain is modelled as direct heat flux injected into the air and the internal mass nodes and its effect on the envelope is account for by correcting the external temperature ($T_{ext} = T_a$ in Figure 2.17 (b) is substituted with $T_{a,eq} = T_{ext} + \alpha \cdot I_{sol}$ with I_{sol} the solar irradiation and α a constant parameter). Whereas in Figure 2.18, solar gain is simply injected as direct flux into the air node. On the other hand, internal heat gain is represented in Figure 2.18 but not in Figure 2.17 (b), and heating power is injected into the air and the internal mass node in Figure 2.17 (b) but only in the air node in Figure 2.18. A variety of other 3rd order ROM structures are found in the literature [Berthou *et al.*, 2014b; Lauster *et al.*, 2014].

2.2.1.4 Structures with combinations of 1st and 2nd order ROMs

Some structures are of intermediate elaboration between a 3rd order ROM and a white-box HOM. Typically in these models, the centre node represents indoor air. Other constructions such as ceiling, floor, external walls, windows and internal partition walls are each modelled with an equivalent 1st or 2nd order RC network. An example is shown in Figure 2.19.

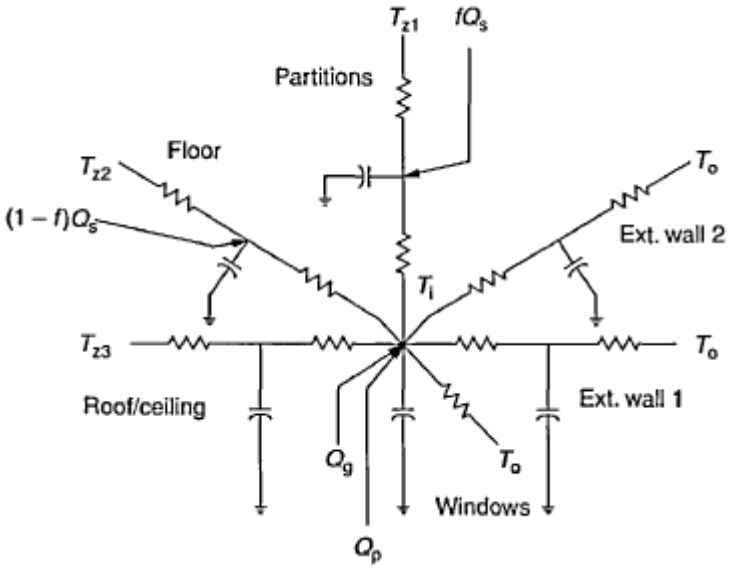

Figure 2.19 Example of a structure combining RC networks for constructions elements with a 1st order ROM in [Gouda *et al.*, 2000]

Accuracy of models in this category is allegedly high, if all parameters are precisely identified [Lehmann *et al.*, 2013b; Xu et Wang, 2008; Hudson et Underwood, 1999; Gouda *et al.*, 2000]. Since the number of parameters escalates, identification requires more observations such as surface temperature measurements at various nodes. With observations limited to few signals at the DHS substation, these models are not identifiable and therefore are not feasible in our work.

2.2.1.5 Structures with a heating system model

Some works intend to represent the thermal inertia and control settings of the heating system within the ROM structure instead of simply injecting a direct heat flux into the nodes. The model than features a temperature node for the heat emitter, an associated thermal capacitance and heat transfer coefficient. Depending on the considered heating system and level of complexity, its model might be linear [Harb *et al.*, 2016; Bacher et Madsen, 2011] or non-linear [Gouda *et al.*, 2000; Saurav et Chandan, 2017]. Figure 2.20 depicts an example of a structure featuring a thermal capacitance C_{pp} for pipes plan embedded in a floor which itself is represented with a 1st order model with thermal capacitance C_{fl}.

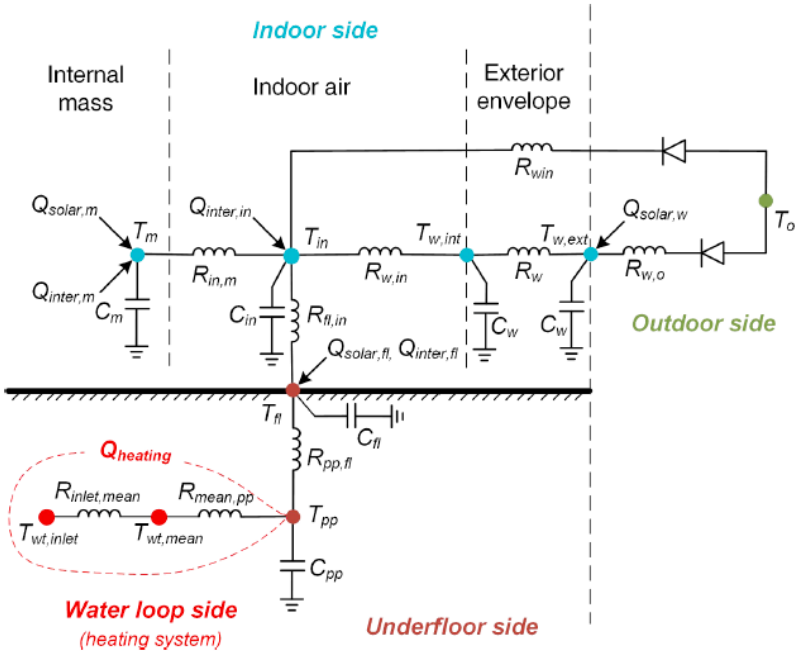

Figure 2.20 Example of a ROM structure with a heating system in [Hu *et al.*, 2019b]

Exploiting the thermal inertia of heating systems is beneficial in control strategies and MPC for instance, particularly in case of floor-heating or long heating circuits operating at high temperatures in DHS. Therefore we ought to consider integrating the heating system within our proposed structure.

2.2.2 Parametric identification

Once the ROM structure is defined, the remaining task is to identify values for its parameters from historical data. In this thesis, we only consider time-invariant RC models, i.e. with constant parameters that need to be identified once and for all.

In the literature, parameters identification approaches are classified under 3 categories: estimation based on physical interpretations, deterministic optimization and probabilistic inference [Fabrizio et Monetti, 2015; Fernández *et al.*, 2018; Kim et Park, 2016; Reddy, 2006].

2.2.2.1 Estimation based on physical interpretations

This approach does not require any automated algorithm. It simply relies on the modellers' own experience, knowledge about the system and some physical interpretations of the observations.

For instance in [Guelpa et Verda, 2016], the authors identified the 2 parameters (C_{build} and U_{build}) of the 1st order ROM (Eq. 2.32 with no extra terms) by interpreting the SH power and return temperature measurements at the substation of a building connected to a DHS. The parameters are identified separately: first, the authors observed that the building indoor temperature T_{build} undergoes very little variations in the afternoons, therefore it may be considered constant. By collecting time-series data of

the external temperature T_{ext} and the heating power Q_{heater} during these periods, they estimated U_{build} by least-squares fitting. Then, they assumed that after shutting-down Q_{heater}, T_{build} undergoes transient dynamics similar to those of the heating water return temperature. By analysing the water temperature dynamics, they estimated the building time constant τ_{build} (Eq. 2.34) and compute C_{build}.

Estimation approaches can be used for models with a small number of parameters, therefore they are limited to 1st order ROMs.

2.2.2.2 Deterministic optimization

Parameters identification can be expressed as an optimization problem where the objective is to maximize the resemblance between the ROM and the HOM outputs. Mathematically, this is equivalent to a minimization problem of the error between the ROM and the HOM outputs.

Depending on the model states that are considered as outputs (observations), an objective function is formulated. In the vast majority of works, the objective function is the Root Mean-Square Error (RMSE[10]), or the Mean-Square Error (MSE[11]) or the Sum-Squared Error (SSE[12]) of the indoor air temperature [Penman, 1990; Dewson *et al.*, 1993; Harb *et al.*, 2016; Andrade-Cabrera *et al.*, 2017; Hu *et al.*, 2016; Viot *et al.*, 2015; Le Mounier *et al.*, 2014]. [Berthou *et al.*, 2014b] formulated the objective function as the summation of the SSE of the heating power and the indoor air temperature. [Prívara *et al.*, 2013b] used the summation of the MSE on the heating water return temperature and the indoor air temperature. [Kramer *et al.*, 2013b] used RMSE on indoor air temperature and relative humidity to identify parameters of a hydrothermal ROM. [Wang et Xu, 2006] relied solely on the RMSE of the cooling/heating load to identify a 2nd order model.

There exist various methods to solve the optimization problem, i.e. to find the set of ROM parameters that minimizes the objective function. When the ROM structure is linear, gradient-based algorithms are often employed, such as the interior point algorithm usually implemented with inequality constraints to limit the search space within physically plausible range [Harb *et al.*, 2016; Berthou *et al.*, 2014b; Viot *et al.*, 2015; Le Mounier *et al.*, 2014; McKinley et Alleyne, 2008]. For non-linear problems, an algorithm based on the solution of the Kuhn–Tucker equations is used in [Gouda *et al.*, 2002] and other gradient-free algorithms are more commonly employed. For instance, genetic algorithms [Wang et Xu, 2006; Kramer *et al.*, 2013a] and evolutionary particle swarm optimization [Andrade-Cabrera *et al.*, 2017].

[10] $RMSE(x) = \sqrt{\sum_{N_{obs}} (x - \hat{x})^2 / N_{obs}}$

[11] $MSE(x) = \sum_{N_{obs}} (x - \hat{x})^2 / N_{obs}$

[12] $SSE(x) = \sum_{N_{obs}} (x - \hat{x})^2$

N_{obs} is the number of observation points, x is the HOM output and $\hat{x}$ is the ROM output

2.2.2.3 Probabilistic inference

Another approach for parametric identification is the probabilistic Bayesian inference based on Bayes' theorem stated in Eq. 2.35 where θ denotes the unknown set of parameters and Y is the set of historical observations. Given prior believes about the probability density functions of θ (denoted $P(\theta)$) and the likelihood of the observations $P(Y|\theta)$, Bayes' theorem yields posterior distributions of θ (denoted $P(\theta|Y)$), read the probability of θ given Y.

$$P(\theta|Y) \propto P(Y|\theta) \cdot P(\theta) \qquad \text{Eq. 2.35}$$

The identification process requires sampling of values for θ such that the probabilistic properties of the prior probability density functions are preserved. This can be achieved via stochastic Markov chain Monte Carlo simulations. The sampling number grows exponentially with the number of parameters to be identified and can quickly become computationally intensive. This constitute the main drawback of the technique. On the other hand, probabilistic Bayesian inference offers several advantages over deterministic optimization. It systematically incorporates prior physical knowledge about the system ($P(\theta)$) in the calculation of $P(\theta|Y)$. Then, uncertainties on the observations due to measurement errors or unmeasured disturbances such as internal heat gain may be accounted for. And finally, instead of punctual identification of a parameter, it provides richer information about its probability distribution. Identifiability at DHS depends on the available observations, therefore both deterministic and probabilistic identification approaches are equally feasible.

Bayesian inference for a 2nd order building ROM identification was demonstrated in the works of [Zayane, 2011] and it was found better suited for this particular problem compared to a classical optimization approach.

2.2.3 Conclusion

We conclude that a grey-box model of at least 2nd order with a representation of the heating system is the most propitious candidate as ROM structure for our application. While such structure does not form a novelty to the research field by itself, a non-intrusive parametric identification approach of such structure relying solely on measurements available at a DHS substation, to our knowledge, has not been investigated yet. Therefore, we aim at filling-in this gap by proposing and assessing a model structure and parametric identification strategy intending to fulfil all requirements discussed in § 2.1.

2.3 Methodology

This section presents our ROM development. First, a preliminary study is carried-out for a better understanding of the building thermal dynamics. In light of this study, a ROM structure is proposed, then a parametric identification strategy. The methodology is applied on analytical case studies, then on the 3 case study BTSs introduced in the previous chapter of this manuscript. As a result, 3 ROMs are identified and assessed, the limitations of the approach being highlighted.

2.3.1 Preliminary study

2.3.1.1 Space-heating demand flexibility and purpose of the study

SH demand flexibility is the *"ability to adapt the [building] energy profile without jeopardizing technical and comfort constraints"*, as defined in [Reynders *et al.*, 2018]. This ability is key for SH demand side management and it is inherently offered by buildings thermal inertia.

Thermal inertia is the *"degree of slowness with which the temperature of a body approaches that of its surroundings and which is dependent upon its absorptivity, its specific heat, its thermal conductivity, its dimensions, and other factors"*[13].

Buildings are composed of many elements, each having its own thermal inertia. The purpose of this preliminary study is to quantify the impact of thermal inertia of selected elements in a building on its SH demand flexibility.

Here we investigate elements that have been pointed-out in the literature for being impactful on heat demand flexibility:

- Buildings envelope insulation level and air-tightness: These factors seem to have the greatest impact on demand flexibility [Le Dréau et Heiselberg, 2016b; Foteinaki *et al.*, 2018b; Johra *et al.*, 2019]. Well-insulated buildings with low infiltration and air renewal rates preserve their indoor climate longer than those on the other end of the spectrum; therefore they have higher thermal inertia and provide more heat demand flexibility.
  In this study we consider the 3 BTSs described in § 1.4 as different classes of insulation level and air-tightness:
  - *1915 Building*, uninsulated with a high infiltration and air renewal rate;
  - *1975 Building*, poorly insulated with moderate infiltration and air renewal rate;
  - *2012 Building*, well-insulated with low infiltration and air renewal rate.

[13] https://www.merriam-webster.com/dictionary/thermal%20inertia

- Thermal mass: Buildings thermal mass or equivalent thermal capacitance is a property that measures the thermal energy storage capacity within the building envelope, internal partitions and furniture. Thermal mass is the second most influential factor on demand flexibility [Johra *et al.*, 2019; Johra et Heiselberg, 2017b; Antonopoulos et Koronaki, 2000b; Arteconi *et al.*, 2019].

  In this study we consider 3 levels of building thermal mass by changing the parameter for internal mass density in the BTS ($m_{int\ slab}$ in Eq. 1.14):

  - Empty thermal zones with no internal mass, $\sum m_{int\ slab} = 0\ \ kg/m^2$;
  - Light thermal mass, $m_{int\ slab} = 1/2$ values listed in Table 1.1, $\sum m_{int\ slab} = 47.5\ kg/m^2$;
  - Heavy thermal mass, $m_{int\ slab} =$ values listed in Table 1.1, $\sum m_{int\ slab} = 95\ kg/m^2$.
- Heating system: Fewer studies assessed the effect of heating systems on heat demand flexibility [Le Dréau et Heiselberg, 2016b; Arteconi *et al.*, 2019]. Hydronic heating systems and, even more so, those embedded in concrete slabs (floor heating) have high thermal inertia, and their control is thus more flexible.

  In this study we consider 3 heating systems of different thermal inertia:

  - *0 Inertia* heating system is the SH system with ideal temperature regulation described in § 2.3.6;
  - *50°C Radiators* is the hydronic SH system served by a DHS substation described in § 2.3.7 and operating with a constant supply temperature of 50°C at the sizing external temperature;
  - *70°C Radiators* is the same system as *50°C Radiators* but operating with a constant supply temperature of 70°C at the sizing external temperature.

There is no universal measure of SH demand flexibility, but numerous quantification methods have been suggested in the literature and reviewed in [Reynders *et al.*, 2018]. In our study, we suggest an experimental protocol together with a flexibility indicator to allow quantitative comparison between different cases.

2.3.1.2 Experimental simulation protocol and flexibility index

First, we define 3 mean temperatures in the BTS, referred to as the HOM, where N_{zones} the number of equivalent thermal zones:

- The HOM mean air temperature T_{air}^{HOM}:

$$T_{air}^{HOM} = \frac{\sum_{i=1}^{N_{zones}} \left(S_{zone}^{i} * T_{air}^{zone\,i} \right)}{\sum_{i=1}^{N_{zones}} S_{zone}^{i}} \quad \text{Eq. 2.36}$$

- The HOM mean radiative temperature T_{rad}^{HOM}:

$$T_{rad}^{HOM} = \frac{\sum_{j=1}^{N_{zones}} \sum_{i=1}^{N_{int\ surf}} \left(T_{int\ surf}^{i,j} \cdot S_{int\ surf}^{i} \right)}{\sum_{j=1}^{N_{zones}} \sum_{i=1}^{N_{int\ surf}} S_{int\ surf}^{i,j}} \quad \text{Eq. 2.37}$$

- The HOM mean operative temperature T_{oper}^{HOM}:

$$T_{oper}^{HOM} = \frac{T_{air}^{HOM} + T_{rad}^{HOM}}{2} \quad \text{Eq. 2.38}$$

The experimental protocol consists in maintaining the HOM under constant thermal conditions:

- Constant external temperature, here we set $T_{ext} = T_{ext}^{sizing,Grenoble} = -11°C$;
- Constant internal air temperature, here we aim at maintaining T_{air}^{HOM} close to 19°C. To ensure this condition for different heating systems, we set $T_{air}^{set} = 19°C$ in case of a *0 Inertia* heating system and $T_{air}^{set} = 20°C$ in case of a *Radiators* heating system. In fact a TRV acts like a proportional controller, in steady-state conditions, if $T_{air}^{set} = 20°C$, T_{air}^{HOM} will be less than $20°C$, somewhere around $19°C$, to allow a constant and stable water mass flow rate through the TRV;
- No solar gain;
- No internal heat gain.

Then the heating power is cut-off from its source and the system free response is observed. For study-cases with *0 Inertia* heating system (Figure 2.21 (a)), the heating power is directly cut-off at the zones air node via the thermal switch, whereas in case of a *Radiators* heating system (Figure 2.21 (b)), it is shut-down at the substation level by limiting the delivered SH power Q_{SST}^{max} to 0 W. Note that the upper plots of Figure 2.21 show the variations of the heat injected into the air zone, not the one delivered at the substation. All three mean temperatures are monitored and the time delays for a $1°C$ drop in each of these temperatures are registered.

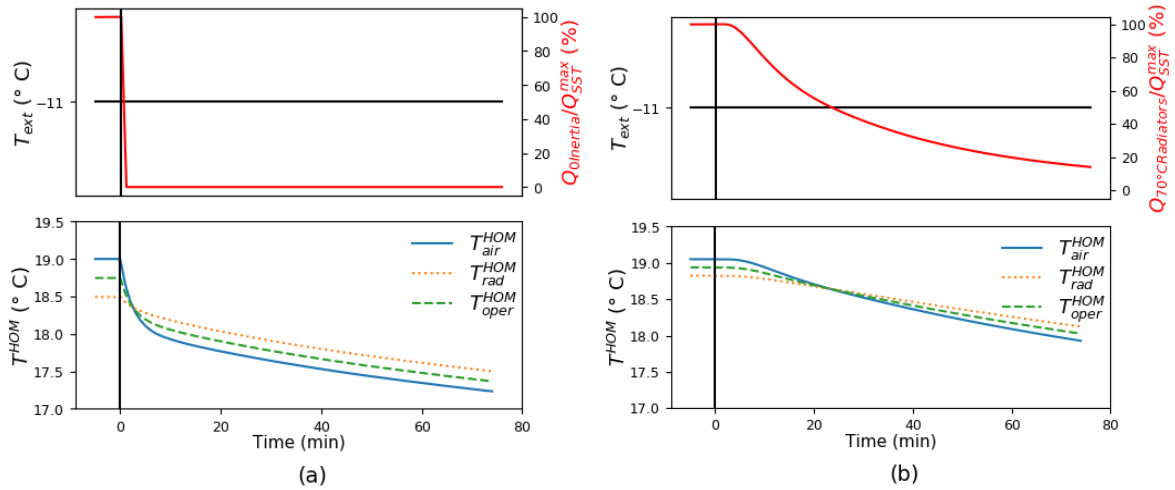

Figure 2.21 *2012 Building* with *Light* internal mass thermal response following the SH power cut-off: (a) case of *0 Inertia* heating system, (b) case of *70°C Radiators* heating system

The time delay for 1°C drop in T_{oper}^{HOM}, denoted τ_{-1}, is the building SH demand flexibility index: a larger τ_{-1} means that the heating power may be shut-down for a longer period before 1°C drop is perceived by the consumers, which implies larger flexibility.

2.3.1.3 Results and conclusions

Before discussing heat demand flexibility, looking at Figure 2.21, three observations can be noted regarding buildings thermal dynamics:

- Within the few minutes following the power cut-off, the air temperature (T_{air}^{HOM}) drop is remarkably sharper than the surface temperature (T_{rad}^{HOM}) drop. This is due to the relatively low thermal inertia of internal air compared to that of the envelope and the internal constructions. Whereof we infer that a ROM of at least second order is required to distinguish these two dissimilar dynamics. This conclusion is coherent with others findings in the literature (e.g. [Vivian *et al.*, 2017b]).
- After a few minutes, the surface temperature crosses over the air temperature. Heat transfer is now reversed, given-off by the walls surfaces to heat-up the internal air. This phenomena is sometimes called activation of building thermal mass short-term heat storage [Wolisz *et al.*, 2015; Le Dréau et Heiselberg, 2016b; Olsthoorn *et al.*, 2017]. Notice how air temperature drop gets smoother from this point forward. The drop velocity of air, surface and their average perceived temperature becomes uniform and only on the long run the building system seems to behave as a first-order system.
- When comparing *0 Inertia* to *Radiators* heating systems, we observe that the heating power from the latter decreases gradually after the cut-time, owing to the thermal inertia of the heating system itself (piping and heating water). This leads to overall slower temperature drops.

Results of τ_{-1} for all 27 studied cases (3 building envelopes x 3 thermal mass levels x 3 heating systems) are displayed in Figure 2.22.

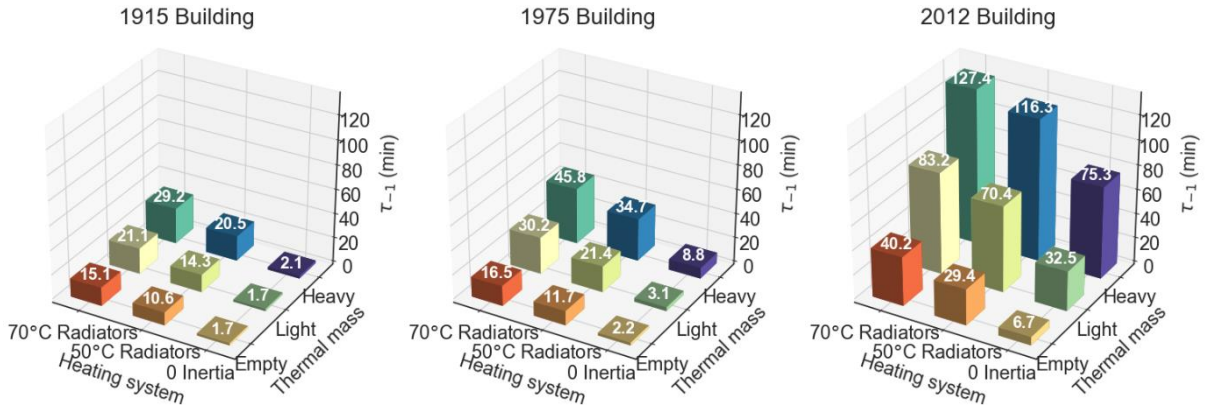

Figure 2.22 SH demand flexibility index τ_{-1}

Conclusions with respect to τ_{-1}:

- In a well-insulated building (2012) with heavy internal mass, a *0 Inertia* heating system yielded longer τ_{-1} than *Radiators* heating systems in equivalent empty building. This conclusion is not valid for the 2 other building classes (1975 and 1915). Therefore, we conclude that internal mass is particularly influential on short-term thermal dynamics in buildings with high thermal insulation and air-tightness. Buildings SH demand estimations ignoring internal mass may induce large discrepancies, as reported in the literature, e.g. in [Al-Sanea *et al.*, 2012b; Johra *et al.*, 2019; Le Dréau et Heiselberg, 2016b; Reynders *et al.*, 2013c; Malisani *et al.*, 2011].
- On average, buildings with $70°C$ *Radiators* had 35% longer τ_{-1} than those with $50°C$ *Radiators*. The lower the insulation level, and the lower the thermal mass level, the higher is the sensitivity towards heating water temperatures.
- Recall that τ_{-1} gives an order of magnitude of how long the heating system could be set-back before the $1°C$ drop is perceived by a consumer from a control point of view, in sizing conditions (i.e. $T_{ext} = T_{ext}^{sizing,Grenoble} = -11°C$). Interestingly, according to our BTS, average values of these τ_{-1} are:
  - More than an hour for the *2012 Building*;
  - 20 minutes for the *1975 Building*;
  - 15 minutes for the *1915 Building*.

τ_{-1} only reveals the flexibility potential from the users thermal comfort point of view. To evaluate flexibility income on the network, all cases are simulated again and the amount of energy that would have been consumed during τ_{-1} but without the power cut-off is computed. This gives the energy savings per floor area (in Wh/m²) made during τ_{-1} shown in Figure 2.23.

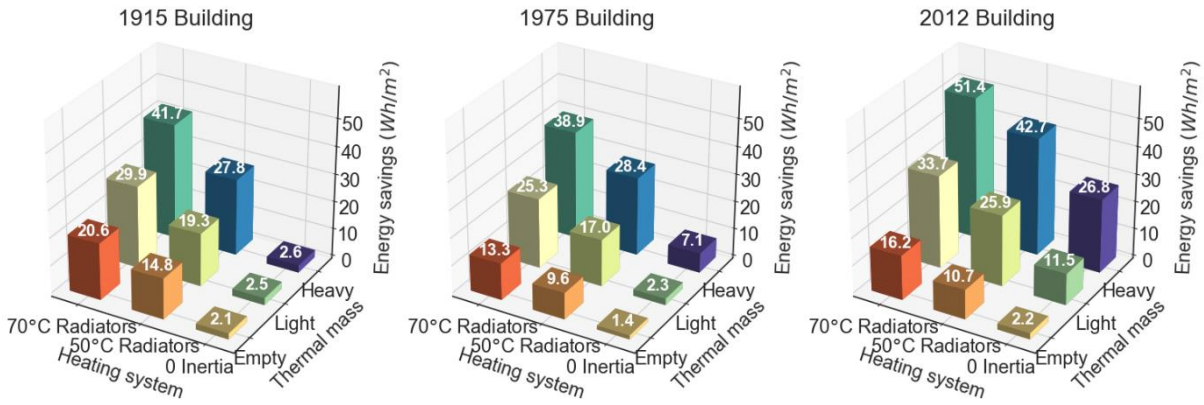

Figure 2.23 Energy savings made during the 1°C drop delays in perceived temperature (Wh/m²)

We may finally conclude that despite the fact that buildings from different energy classes have very different SH demand flexibilities, their energy savings potentials are quite comparable.

2.3.2 ROM structure

Based on the preliminary study and pursuant to the literature review, we conclude that at least a 2nd order model is necessary to capture the thermal dynamics in a building system. Furthermore, thermal inertia of the internal mass and the heating circuit are non-negligible for short-term predictions. We would like to represent these dynamics in the proposed ROM structure and attempt to identify their corresponding parameters. Thus, the resulting ROM is a conjunction of a linear 3rd order building model coupled to a non-linear heating system model. The full modelling differential-algebraic system of equations is shown below (Eq. 2.39 – Eq. 2.45). Its time invariant parameters are marked with an asterisk (*) and correspond to unknown parameters that need to be identified.

$$C_{air}^{*} \cdot \frac{dT_{air}}{dt} = U_{[air-ext]}^{*} \cdot (T_{ext} - T_{air}) + U_{[air-env]}^{*} \cdot (T_{env} - T_{air}) + U_{[air-mass]}^{*} \cdot (T_{mass} - T_{air}) + U_{[air-em]}^{*} \cdot (T_{em} - T_{air}) + k_{air}^{s\,*} \cdot I_{sol} \quad \text{Eq. 2.39}$$

$$C_{env}^{*} \cdot \frac{dT_{env}}{dt} = U_{[env-ext]}^{*} \cdot (T_{ext} - T_{env}) + U_{[air-env]}^{*} \cdot (T_{air} - T_{env}) + k_{env}^{s\,*} \cdot I_{sol} \quad \text{Eq. 2.40}$$

$$C_{mass}^{*} \cdot \frac{dT_{mass}}{dt} = U_{[air-mass]}^{*} \cdot (T_{air} - T_{mass}) + k_{mass}^{s\,*} \cdot I_{sol} \quad \text{Eq. 2.41}$$

$$C_{em}^{*} \cdot \frac{dT_{em}}{dt} = U_{[air-em]}^{*} \cdot (T_{air} - T_{em}) + \dot{m}_{SST} \cdot \mathrm{c_{wat}} \cdot (T_{cir} - T_{em}) \quad \text{Eq. 2.42}$$

$$C_{cir}^{*} \cdot \frac{dT_{cir}}{dt} = \eta_{cir}^{*} \cdot Q_{SST} + \dot{m}_{SST} \cdot \mathrm{c_{wat}} \cdot (T_{em} - T_{cir}) \quad \text{Eq. 2.43}$$

$$Q_{SST} = Q_{SST}^{max} \cdot [\![G_{cir}^{p\,*} \cdot (T_{cir}^{set} - T_{cir})]\!]_0^1 \quad \text{Eq. 2.44}$$

$$\dot{m}_{SST} = \dot{m}_{SST}^{max} \cdot [\![G_{air}^{p\,*} \cdot (T_{air}^{set} - T_{air})]\!]_0^1 \quad \text{Eq. 2.45}$$

With the notation $y = [\![x]\!]_a^b \Rightarrow \begin{cases} y = x \; if \; a \leq x \leq b \\ y = a \; if \; x < a \\ y = b \; if \; x > b \end{cases}$

As can be derived from the equations, the model has 5 lumped nodes each having a homogeneous mean temperature and an associated thermal capacitance. They represent:

- Indoor air of temperature T_{air} and thermal capacitance ${C_{air}}^*$;
- Envelope of temperature T_{env} and thermal capacitance ${C_{env}}^*$;
- Internal mass of temperature T_{mass} and thermal capacitance ${C_{mass}}^*$;
- Heat emitters of temperature T_{em} and thermal capacitance ${C_{em}}^*$;
- Heating circuit of temperature T_{cir} and thermal capacitance ${C_{cir}}^*$.

A power balance is established for each of these 5 nodes (Eq. 2.39 – Eq. 2.43).

The following heat exchange phenomena are modelled through heat transfer coefficients:

- The air node exchanges heat directly with the external environment of temperature T_{ext} due to ventilation through the heat transfer coefficient ${U_{[air-ext]}}^*$;
- The air node and the envelope node exchange heat through ${U_{[air-env]}}^*$;
- The air node and the internal mass node exchange heat through ${U_{[air-mass]}}^*$;
- The air node and the heat emitters exchange heat through ${U_{[air-em]}}^*$;
- The envelope node exchanges heat with the external environment through ${U_{[env-ext]}}^*$.

Solar heat gain is linearly modelled as the product of the global horizontal solar irradiation I_{sol} by a fixed solar aperture surface area. It is injected into the first 3 nodes:

- The air node receives solar heat gain through the solar aperture ${k_{air}^s}^*$;
- The envelope node receives solar heat gain through the solar aperture ${k_{env}^s}^*$;
- The internal mass node receives solar heat gain through the solar aperture ${k_{mass}^s}^*$.

The linear 3rd order building model is represented under the thermal-electrical analogy in Figure 2.24.

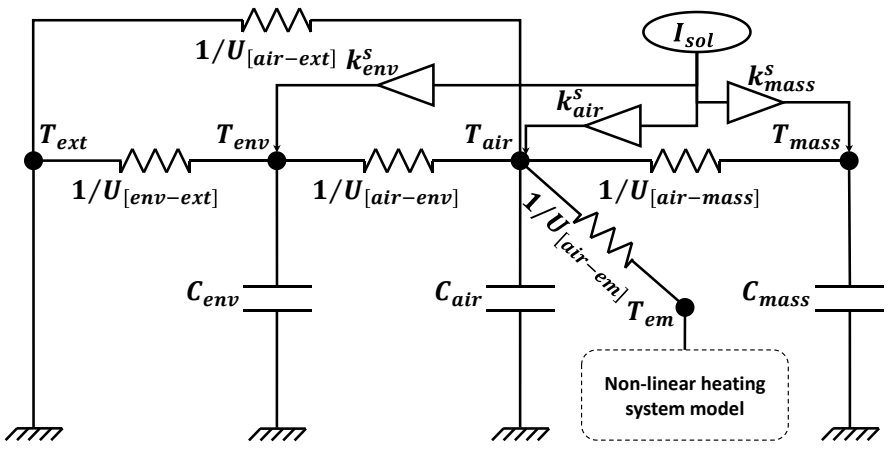

Figure 2.24 RC representation of the building model structure

The first non-linearity appears in the heating system model (Eq. 2.42 and Eq. 2.43) as the bilinear term between the heating water mass flow rate $\dot{m}$ and the temperature difference $(T_{cir} - T_{em})$, c_{wat} being the constant specific thermal capacity of water. This term represents the heat flow from the heating circuit into the emitters. To take into account transmission losses in the heating circuit, we introduced an efficiency coefficient denoted $\eta_{cir}{}^{*}$ in Eq. 2.43.

The system model operates in a closed loop by regulating the heating circuit temperature and internal air temperature. In fact, T_{cir} is regulated to a set point temperature T_{cir}^{set} controlled at the substation level by the DHS operator. The substation heating power Q_{SST} may then be derived by Eq. 2.44 using a proportional gain $G_{cir}^{p}{}^{*}$ and bounded by the maximum sizing power of the substation Q_{SST}^{max}. This double-ended saturation expression is a second non-linearity in the SH system model.

Whereas, T_{air} is regulated to a set point temperature T_{air}^{set} controlled by the building residents acting on their TRVs. Similarly to Eq. 2.44, Eq. 2.45 is a bounded formulation of the heating water mass flow rate at the substation $\dot{m}_{SST}$ which is assumed to vary linearly to T_{air} using a proportional gain $G_{air}^{p}{}^{*}$. When the temperature difference reaches a given threshold, all TRVs are fully open and $\dot{m}_{SST}$ is saturated to its nominal value $\dot{m}_{SST}^{max}$. Note that Q_{SST}^{max} and $\dot{m}_{SST}^{max}$ are parameters known beforehand and need not be identified. Indeed, Q_{SST} and $\dot{m}_{SST}$ are the ROM outputs, both being non-intrusively observable and measurable at the substation. Moreover, when unsaturated, Eq. 2.45 may be used to observe T_{air} and therefore this key equation dispenses with using intrusive indoor temperature.

Overall, the ROM has:

- 3 uncontrollable inputs or disturbances (T_{ext}, I_{sol} and T_{air}^{set});
- 1 controllable input (T_{cir}^{set});
- 2 outputs (Q_{SST} and $\dot{m}_{SST}$);
- 5 hidden states ($T_{air}, T_{env}, T_{mass}\ T_{em}$ and T_{cir});
- 16 parameters to be identified.

2.3.3 Parametric identification

After defining the ROM structure, the remaining unknowns in the ROM development problem are numerical values for its 16 constant parameters. Parametric identification by optimization based on historical input/output data is the approach used in this thesis.

2.3.3.1 Data generation

The proposed parametric identification approach uses input and output signals to calibrate the ROM parameters given its predefined structure. Input and output signals generation, or data generation for

short, is done by simulating the HOM over a training period of 3 weeks at a time step of 5 minutes for parameters identification, and other 3 weeks to assess the model prediction ability.

Generated datasets should be rich in information, i.e. the input signals must cover a large spectrum so as to well excite the system modes. Yet on the other hand, for a methodology to be applicable in real-life, data generation should be done during regular operation days where occupants are present inside the building. Therefore we specified the HOM inputs as follows:

- T_{ext} and I_{sol} are taken from the TMY weather file of the city of Grenoble as mentioned in § 2.5.1. Based on this TMY, we chose a training period with significant temperature variations, which happen to be from December 10th to the 31st.
- T_{air}^{set} in all zones of the building is constant and equal to 20°C.
- T_{cir}^{set} is set using a heating curve during the day and is restrained to a minimum value from midnight until 6:00 pm as a form of power set-back. This operation mode is still acceptable in terms of thermal comfort and it stimulates the thermal dynamics of the heating circuit, therefore it enhances the identifiability of its associated parameters. For the applications of § 2.4, the heating curves of Figure 1.13 are adopted, each for its corresponding case study, and the asymptotic minimum value is set during the night-time set-back.

The assumption of perfectly controlled and fixed indoor set-point temperature T_{air}^{set} is indeed strong; in real-life, it is controlled by the building residents therefore it is unknown or may be variant. However, it is assumed that the stochastic internal gain signal added to the BTS (§ 1.3.7) aggregates all the uncertainties of the system, so there is no need to add noise to T_{air}^{set}.

Another dataset is generated under the same conditions from January 4th to the 25th for a validation test.

2.3.3.2 Parameters optimization

The concrete step of identifying the ROM parameters consists of iteratively trying a combination of parameters and assessing its results until finding the optimal set that minimizes the error between the ROM and the HOM outputs. To achieve this goal, we first define the objective function to be minimized, then we introduce the search algorithm and finally the model performance criteria.

2.3.3.2.1 Objective function

Let $\theta \in \mathbb{R}^{16}$ the set of 16 ROM parameters, normalized with respect to reference values (to keep a homogenous order of magnitude). θ_{opt} is the set of optimal θ: θ_{opt} minimizes the weighted summation of the normalized quadratic outputs errors integral between the ROM and the HOM over the training

interval. This is formulated in Eq. 2.46 and Eq. 2.47 where f_{obj} denotes the objective function and Δ_{tr} the training interval in seconds.

To break down the formula, a quadratic error on an output X is $(X^{HOM} - X^{ROM})^2$ where X^{HOM} is the HOM output and X^{ROM} is the ROM output. Recall there are 2 outputs available at the substation: the SH power Q_{SST} and the heating water mass flow rate $\dot{m}_{SST}$. The quadratic error on each output is normalized by the squared maximum value of that output X^{max2}. This is essential because Q_{SST} is in the orders of $10^3 W$, whereas $\dot{m}_{SST}$ is around $10^{-1}\, kg/s$. Through normalization, we seek consistent minimization of both errors. To further enhance the results quality, we add degrees of freedom to f_{obj} by affecting a weight for each error term. Weight values of $1/3$ for Q_{SST} and $2/3$ for $\dot{m}_{SST}$ were estimated by trial and error.

$$f_{obj} = \frac{1}{\Delta_{tr}} \cdot \int_0^{\Delta_{tr}} \left[\frac{1}{3} \cdot \left(\frac{\mathrm{Q}_{SST}^{HOM} - \mathrm{Q}_{SST}^{ROM}}{\mathrm{Q}_{SST}^{max}} \right)^2 + \frac{2}{3} \cdot \left(\frac{\dot{m}_{SST}^{HOM} - \dot{m}_{SST}^{ROM}}{\dot{m}_{SST}^{max}} \right)^2 \right] dt \qquad \text{Eq. 2.46}$$

$$\theta_{opt} = argmin(f_{obj}) \qquad \text{Eq. 2.47}$$

2.3.3.2.2 Search algorithm

The search algorithm for θ_{opt} starts with a Particle Swarm Optimization (PSO), a stochastic technique known for its efficiency in inspecting large search areas, then the solution is refined with a deterministic Hooke-Jeeves (HJ) pattern search.

PSO was introduced by [Kennedy et Eberhart, 1995] as an optimization concept for non-linear functions. Its algorithm is inspired from observations made on large groups of organisms in synchronous movement such as bird flocks or fish schools. Through these observations, it is assumed that in a group, individuals keep a distance between them and share information for the sake of an evolutionary goal. Take the example of a flock of birds searching an area for a single piece of food. All birds randomly start the search. They do not know the exact location of the food, yet they have instinctive ability to assess how far it is at each search iteration, and they socially communicate this information. Then naturally, the best strategy to find the food is to follow the bird which is closest to the goal.

In PSO, a particle is a searching agent. Its position is spotted by a potential set of parameters θ_p^{PSO} and it moves at a step size s_p^{PSO}. At initialization, the algorithm launches N_{par}^{PSO} particles and randomly places them in the search space. Each particle iteratively evaluates the objective function (Eq. 2.46) using its

affected parameters, and updates its position and step size. The number of iterations, also called generations, is denoted N_{gen}^{PSO}.

The position and step size update follows specific rules. At every generation, each particle keeps in memory its best found position thus far, denoted $\theta_{p,opt}^{PSO}$. Besides, the algorithm identifies the best position found in the particles neighbourhood thus far, denoted $\theta_{n,opt}^{PSO}$. There are several definitions for neighbourhood; it could be the entire group of particles (the swarm), as it may be a small group of particles with indices-dependant relationships. Using $\theta_{p,opt}^{PSO}$ and $\theta_{n,opt}^{PSO}$, the particle's step size and position are updated at every generation of index k according to Eq. 2.48 and Eq. 2.49 respectively:

$$s_p^{PSO}[k+1] = w^{PSO} \cdot s_p^{PSO}[k] + l_{cog}^{PSO} \cdot \rho_{cog}^{PSO}[k] \cdot \left(\theta_{p,opt}^{PSO}[k] - \theta_p^{PSO}[k]\right) + l_{soc}^{PSO} \cdot \rho_{soc}^{PSO}[k] \cdot \left(\theta_{n,opt}^{PSO}[k] - \theta_p^{PSO}[k]\right) \quad \text{Eq. 2.48}$$

$$\theta_p^{PSO}[k+1] = \theta_p^{PSO}[k] + s_p^{PSO}[k+1] \quad \text{Eq. 2.49}$$

w^{PSO} is called inertia weight. It is introduced in [Shi et Eberhart, 1998] to reduce the step size s_p^{PSO} of the particles as they proceed from a generation to another which is proven to enhance the search. Its value is calculated at each generation of index k as given in Eq. 2.50, where $w^{PSO}[0]$ and $w^{PSO}\left[N_{gen}^{PSO}\right]$ predefined typically with $w^{PSO}\left[N_{gen}^{PSO}\right] < w^{PSO}[0]$.

$$w^{PSO}[k] = w^{PSO}[0] - \frac{k}{N_{gen}^{PSO}} * \left(w^{PSO}[0] - w^{PSO}\left[N_{gen}^{PSO}\right]\right) \quad \text{Eq. 2.50}$$

l_{cog}^{PSO} and l_{soc}^{PSO} are called learning factors and are positive real fixed values. l_{cog}^{PSO} takes into account the particle's own experience, thus it is called cognitive learning factor, while l_{soc}^{PSO} is associated with the social interaction between particles, hence it is called social learning factor.

ρ_{cog}^{PSO} and ρ_{soc}^{PSO} are uniformly distributed random variables between 0 and 1. They reveal the stochastic character of the algorithm introduced to enhance the search space exploration.

The iterations stop after reaching the specified number of generations N_{gen}^{PSO}, i.e. the objective function has been evaluated $N_{par}^{PSO} \times N_{gen}^{PSO}$ times and the best found position is reported as θ_{opt}^{PSO}.

HJ is a structured search method introduced by [Hooke et Jeeves, 1961]. Its algorithm consists in 2 parts: a sequence of exploratory moves around a base point and a pattern move.

Given an initial base point of associated parameters set θ_b^{HJ}, exploratory moves consist in incrementing each parameter in turn by a step s_b^{HJ} in the positive direction then – only if the objective function is not reduced – in the negative direction. If any of these 2 moves is successful, i.e. the objective function is reduced, the resulting value of the corresponding parameter is retained. After checking all parameters, a new base point θ_{b+1}^{HJ} is reached. If $\theta_{b+1}^{HJ} \neq \theta_b^{HJ}$, a pattern move from θ_b^{HJ} is made.

A pattern move is an attempt to accelerate the search considering that the direction towards the optimum is likely to be $\theta_{b+1}^{HJ} - \theta_b^{HJ}$. Therefore a new sequence of exploratory moves is performed about the pattern point θ_p^{HJ} given in Eq. 2.51. Δ_b^{HJ} is the mesh size whose value is gradually reduced through the iterations according to Eq. 2.52 where r^{HJ} is a fixed parameter called the mesh size divider. If a better point than θ_{b+1}^{HJ} is found then a new base point θ_{b+2}^{HJ} is reached and another pattern move is made towards θ_{p+1}^{HJ}. Elsewise the guessed direction is adjudicated wrong and the pattern move has failed, so we restart with exploratory moves about θ_{b+1}^{HJ} but this time with an incremented value for s_{b+1}^{HJ} according to Eq. 2.53 where t^{HJ} is a parameter called the mesh size exponent increment. The search stops after a maximum number of mesh size reductions N_{red}^{HJ} is reached.

$$\theta_p^{HJ} = \theta_b^{HJ} + \Delta_b^{HJ} \cdot \left(\theta_{b+1}^{HJ} - \theta_b^{HJ}\right) \quad \text{Eq. 2.51}$$

$$\Delta_b^{HJ} = \frac{1}{r^{HJ^{s_b^{HJ}}}} \quad \text{Eq. 2.52}$$

$$s_{b+1}^{HJ} = s_b^{HJ} + t^{HJ} \quad \text{Eq. 2.53}$$

In the hybrid PSO-HJ search algorithm, HJ search is initialized with θ_{opt}^{PSO} and its final result is reported as the set of optimal identified parameters θ_{opt} (without guarantees of an absolute global optimum).

The choice of this particular search algorithm is justified by the shape and computation times of the objective function (Eq. 2.46). In fact, f_{obj} is non-linear with multiple local minima, hence a stochastic (in all directions) search is necessary; and it has reasonable computation times, thus an intensive (numerous iterations) search is feasible. PSO sweeps-over the search space and it is most likely to converge towards an acceptable minimum with no guarantees of global optimality, not even locally. This is where HJ steps-in to closely inspect the area around the found minimum. HJ, as all pattern-search algorithms, is quite sensitive to initialization. Yet this is not limiting, assuming that its initial point given by PSO is rather a *good* starting point.

The implementation of the search technique is done using the open-source software package GenOpt (**Gen**eric **Opt**imization Program) [Wetter, 2016]. GenOpt is an optimization software conceived to solve optimization problems with computationally expensive objective functions assessed by an external simulation tool such as Dymola. Within GenOpt, several search algorithms are provided, among which the hybrid PSO-HJ algorithm. Fixed parameters for the PSO-HJ algorithm are given in Table 2.11.

Table 2.11 PSO-HJ algorithm parameters

Algorithm parameter	Setting value
N_{par}^{PSO}	150
N_{gen}^{PSO}	150
$w^{PSO}[0]$	1.2
$w^{PSO}[N_{gen}^{PSO}]$	0
l_{cog}^{PSO}	2.8
l_{soc}^{PSO}	1.3
$s_p^{PSO}[0]$	0.01
r^{HJ}	3
t_b	1
N_{red}^{HJ}	4

Practically, historical data generated as described in § 2.3.3.1 are saved to a text file. The ROM is coded in a Dymola model which reads input signals from the text file, computes the ROM outputs and returns the value of the objective function (Eq. 2.46) to GenOpt. GenOpt then updates and returns the parameters to the ROM, and so on until reaching θ_{opt}.

2.3.3.3 Performance criteria

At the end of the parametric identification, some performance criteria are evaluated to decide whether to accept or reject θ_{opt}. These criteria should reflect 3 aspects of the model:

- Ability to forecast the thermal behaviour of the building under the validation dataset (different than the identification dataset), otherwise overfitting has occurred during identification.
- Ability to reproduce hidden states that were not used during the identification (indoor temperature), as well as the outputs.
- Physical plausibility of some identified parameters.

For an output x, we define the fit function φ_x in Eq. 2.54, inspired from [Berthou *et al.*, 2014b], with little modifications, and evaluate its value over the training and the validation periods. A higher and consistent fit between training and validation gives more confidence in θ_{opt}.

$$\varphi_x = \left(1 - \sqrt{\overline{\left(\frac{x^{HOM} - x^{ROM}}{x^{max} - \bar{x}}\right)^2}}\right) \times 100 \quad \text{Eq. 2.54}$$

For hidden states, the main concern is on the indoor air temperature; we inspect the mean and standard deviation of the error $\varepsilon_{T_{air}}$ in Eq. 2.55, and its range $\left[\varepsilon_{T_{air}}^{min}, \varepsilon_{T_{air}}^{max}\right]$ during training and validation phases.

$$\varepsilon_{T_{air}} = T_{air}^{ROM} - T_{air}^{HOM} \quad \text{Eq. 2.55}$$

For physical plausibility, we compare the building equivalent heat loss coefficient U_{build}^{sizing} estimated using sizing conditions by Eq. 2.56 to the equivalent heat loss coefficient U_{build}^{ident} computed using identified parameters by Eq. 2.57. U_{build}^{ident} is derived from the ROM analogical electric circuit (Figure 2.24) as the inverse of the equivalent resistance between nodes T_{ext} and T_{air} assuming steady-state (eliminating C_{env} and C_{air}) and no solar heat gain (eliminating k_{env}^{s}). The smaller the relative error between them $\epsilon_{U_{build}}$ given in Eq. 2.58, the better the physical plausibility of the identified parameters.

$$U_{build}^{sizing} = \frac{Q_{SST}^{max}}{T_{air}^{sizing} - T_{ext}^{sizing,Grenoble}} \quad \text{Eq. 2.56}$$

$$U_{build}^{ident} = \frac{U_{[air-env]} \cdot U_{[env-ext]} + U_{[env-ext]} \cdot U_{[air-ext]} + U_{[air-ext]} \cdot U_{[air-env]}}{U_{[air-env]} + U_{[env-ext]}} \quad \text{Eq. 2.57}$$

$$\epsilon_{U_{build}} = \frac{U_{build}^{ident} - U_{build}^{sizing}}{U_{build}^{sizing}} \times 100 \quad \text{Eq. 2.58}$$

2.4 Application

2.4.1 Analytical testing

Analytical testing aims at assessing the proposed parameters optimization technique in finding a beforehand known set of parameters. For this end, we define an analytical parameters set (Table 2.12), and we generate a noise-free analytical dataset denoted with a superscript $...^{ana}$.

Table 2.12 Parameters used to generate analytical data

ROM parameter	Analytical value ($\cdots^{ana}$)	
C_{air}	2.5E+07	$[J/K]$
C_{env}	2E+08	$[J/K]$
C_{mass}	1.5E+08	$[J/K]$
C_{cir}	1E+05	$[J/K]$
C_{em}	2E+03	$[J/K]$
$U_{[air-ext]}$	252.83	$[W/K]$
$U_{[air-env]}$	25	$[W/K]$
$U_{[env-ext]}$	1500	$[W/K]$
$U_{[air-mass]}$	3000	$[W/K]$
$U_{[air-em]}$	350	$[W/K]$
k_{air}^{s}	15	$[m^2]$
k_{env}^{s}	15	$[m^2]$
k_{mass}^{s}	5	$[m^2]$
η_l	0.95	$[-]$
G_{cir}^{p}	0.3	$[1/K]$
G_{air}^{p}	0.5	$[1/K]$
Q_{SST}^{max}	8600	[W]
$\dot{m}_{SST}^{max}$	0.137	[kg/s]

In this analytical testing, θ is normalized with respect to the known set of parameters. Consequently, the theoretically optimal set of parameters to be found by the search algorithm should be $\theta_{opt}^{theo} = \{1\}$. During the search, the value of the objective function is computed according to Eq. 2.59. For further analyses, we compute the normalized quadratic error integral on the indoor temperature $q_{T_{air}}^{ana}$ according to Eq. 2.60.

$$f_{obj}^{ana}(\theta) = \frac{1}{\Delta_{tr}} \cdot \int_0^{\Delta_{tr}} \left[\frac{1}{3} \cdot \left(\frac{\mathrm{Q}_{SST}^{ana} - \mathrm{Q}_{SST}^{ROM}}{\mathrm{Q}_{SST}^{max}} \right)^2 + \frac{2}{3} \cdot \left(\frac{\dot{m}_{SST}^{ana} - \dot{m}_{SST}^{ROM}}{\dot{m}_{SST}^{max}} \right)^2 \right] dt \qquad \text{Eq. 2.59}$$

$$q_{T_{air}}^{ana}(\theta) = \frac{1}{\Delta_{tr}} \cdot \int_0^{\Delta_{tr}} \left(\frac{T_{air}^{ana} - T_{air}^{ROM}}{T_{air}^{set}} \right)^2 dt \qquad \text{Eq. 2.60}$$

Upon re-simulating the ROM with θ_{opt}^{theo}, we found the values listed in Table 2.13. Note that the objective function is not exactly equal to zero as it should have been, nor are the quadratic errors. The reason for this is small numeric discrepancies produced while interpolating the analytical data from the text file.

Table 2.13 Objective function and error values corresponding to the theoretically optimal set of parameters found using the analytical dataset

$\boldsymbol{\theta_{opt}^{theo}}$	$\boldsymbol{f_{obj}^{ana}(\theta_{opt}^{theo})}$	$\boldsymbol{q_{T_{air}}^{ana}(\theta_{opt}^{theo})}$
{1}	1.06E-04	3.03E-10

The analytical dataset is then used to:

- Identify each parameter separately, given all other parameters (§ 2.4.1.1)
- Identify all 16 parameters at once (§ 2.4.1.2)

2.4.1.1 Individual parameter identification from analytical data

In this test, 16 algorithm runs are launched. At each run, in turn, a parameter $\theta[i]$ is initialized to $\theta[i]^{ini}$ (chosen to 0.75) and the algorithm searches for its optimal value $\theta[i]^{opt}$ that minimizes Eq. 2.59 while all other parameters $\theta[j]\ \forall\ j \neq i$ are fixed to 1. The search space is delimited between 1/3 and 3 for all parameters except for the efficiency parameter η_{cir} which is restrained such that it does not exceed 1.

This test aims at:

- Assessing the algorithm ability in converging towards an optimum at least as good as $\theta[i]^{opt}$. This should be an easy task given than the algorithm only searches in one direction for a single parameter value.
- Finding out whether the found optimum is equal to $\theta[i]^{opt} = 1\ \forall\ i$ (theoretical optimum).
- Understanding the shape of the objective function along each direction. As the algorithm searches for the optimum, the tested points are registered together with their corresponding objective function value. Thus a sensitivity analysis of Eq. 2.59 towards the variations of each parameter separately can be carried out.

Results are plotted in Figure 2.25. The following observations are made:

- The algorithm finds a point with an objective function equal or less than $f_{obj}^{ana}(\theta_{opt}^{theo})$ (Table 2.13) $\forall\ i$.
- The optimum is not always 1; the algorithm did not converge to 1 for $C_{env}, C_{cir}, k_{env}^{s}$, and G_{cir}^{p} (legend in red). We interpret from the corresponding plots that f_{obj}^{ana} is relatively flat around 1. With the small numerical discrepancies due to the interpolation of the data evoked earlier, other

points (different than 1) were found to further minimize f_{obj}^{ana}. This result emphasizes the non-convex shape of f_{obj}^{ana} in the directions of these parameters.

- $C_{env}, C_{em}, U_{env}^{ext}$ and k_{env}^{s} have very little impact on f_{obj}^{ana}. Roughly speaking, any value for these parameters would yield the same value of f_{obj}^{ana}. Therefore they are hardly identifiable with the proposed dataset generation conditions and available measurements. 3 of these parameters are relative to the envelope which is characterized by a slow time constant and 1 of them is relative to the heating system emitters characterized by a fast time constant. On the other hand, $U_{air}^{ext}, U_{air}^{em}, U_{air}^{env}$, k_{air}^{s} and G_{air}^{p} have the highest impact on f_{obj}^{ana}. All of them are relative to the indoor air node. Parameters relative to the internal mass and the heating circuit are fairly impactful on f_{obj}^{ana}.

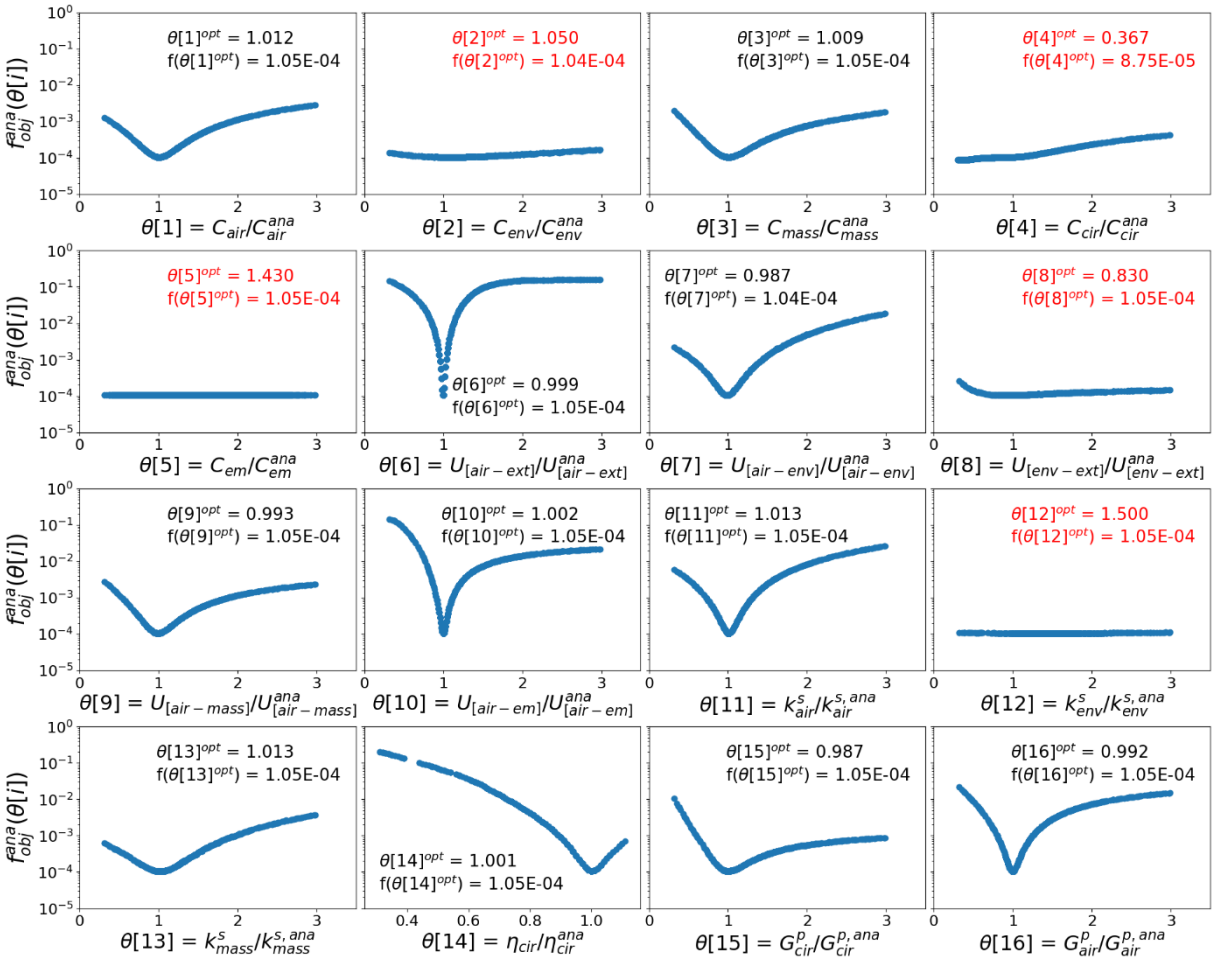

Figure 2.25 Objective function versus individual parameter variations for all 16 ROM parameters using the analytical dataset

2.4.1.2 Full parameters set identification from analytical data

In this test, the algorithm searches for all 16 parameters at each run. 9 runs are lunched, each with a distinct randomly generated set of initial points. Similarly to the previous test, the search space is delimited between 1/3 and 3 for all parameters except for η_{cir}.

This test aims at:

- Examining whether the found optimum θ_{opt} is close to θ_{opt}^{theo}.
- Assessing the algorithm convergence ability from different initial points.
- Inspecting whether a minimization in the objective function f_{obj}^{ana} (errors on observations at the substation) systematically yields minimization in the unobserved indoor temperature error $q_{T_{air}}^{ana}$.

Values of the initial and optimal parameters sets (θ_{ini} and θ_{opt}) are reported in Table 2.14 and results of the optimal value identified for each parameter per run are plotted in Figure 2.26.

Table 2.14 Numerical values of initial (randomly generated) and optimal (found by the PSO-HJ algorithm) in the analytical test

θ	Run 1		Run 2		Run 3		Run 4		Run 5		Run 6		Run 7		Run 8		Run 9	
	θ_{ini}	θ_{opt}	θ_{ini}	θ_{opt}	θ_{ini}	θ_{opt}	θ_{ini}	θ_{opt}	θ_{ini}	θ_{opt}	θ_{ini}	θ_{opt}	θ_{ini}	θ_{opt}	θ_{ini}	θ_{opt}	θ_{ini}	θ_{opt}
C_{air}/C_{air}^{ana}	2.95	1.56	1.40	1.36	1.15	1.21	1.05	1.11	0.40	1.18	2.65	1.42	0.85	1.43	2.25	0.93	1.35	1.36
C_{env}/C_{env}^{ana}	1.50	1.19	1.10	1.38	0.30	0.98	1.35	2.11	1.15	2.48	2.90	0.82	1.80	1.30	1.05	2.42	1.65	1.64
C_{mass}/C_{mass}^{ana}	1.85	1.70	2.60	1.44	0.90	1.27	2.40	1.08	2.10	0.92	2.30	1.39	2.90	1.54	2.50	0.92	0.95	1.24
C_{cir}/C_{cir}^{ana}	2.55	0.34	0.45	0.92	1.15	0.39	1.30	0.35	1.65	0.74	1.60	0.30	1.45	0.39	2.80	0.90	2.30	1.20
C_{em}/C_{em}^{ana}	1.90	2.18	2.50	0.88	0.85	2.13	2.45	1.68	2.60	2.53	0.55	2.73	2.95	0.69	0.45	1.79	1.35	1.25
$U_{[air-ext]}/U_{[air-ext]}^{ana}$	0.35	1.11	1.40	1.05	1.00	1.01	2.90	1.01	1.30	0.98	1.50	1.00	2.45	1.16	2.40	0.99	1.05	1.02
$U_{[air-env]}/U_{[air-env]}^{ana}$	0.80	0.99	0.75	1.15	2.60	1.55	0.65	1.17	2.90	2.26	0.70	1.14	0.45	0.51	0.30	1.19	1.10	1.23
$U_{[env-ext]}/U_{[env-ext]}^{ana}$	1.50	1.53	2.90	2.27	2.60	2.09	2.85	2.64	1.95	2.79	1.80	1.04	2.95	1.17	2.65	2.34	1.85	1.91
$U_{[air-mass]}/U_{[air-mass]}^{ana}$	2.45	1.54	1.75	1.39	1.80	1.11	0.65	1.05	2.30	1.20	1.50	1.40	1.25	1.48	1.45	0.92	1.10	1.27
$U_{[air-em]}/U_{[air-em]}^{ana}$	1.30	1.22	2.30	1.24	2.35	1.15	0.95	1.08	0.90	1.23	1.50	1.07	2.90	1.21	0.45	1.05	0.90	1.21
$k_{air}^{s}/k_{air}^{s,ana}$	2.95	1.06	0.50	1.05	2.10	1.03	2.20	1.03	2.50	1.14	1.50	1.04	1.70	1.14	1.00	0.97	0.75	1.06
$k_{env}^{s}/k_{env}^{s,ana}$	2.45	2.47	2.70	0.88	1.80	2.81	0.40	2.20	2.40	0.68	0.95	2.22	2.05	2.46	0.85	3.00	2.55	1.34
$k_{mass}^{s}/k_{mass}^{s,ana}$	1.85	1.81	2.90	1.48	0.60	1.34	2.95	1.04	0.70	1.04	1.60	0.93	1.30	1.52	0.40	1.14	1.15	0.99
$\eta_{cir}/\eta_{cir}^{ana}$	0.60	1.10	0.80	1.07	0.75	1.06	0.65	1.03	1.00	1.10	0.40	1.03	0.35	1.10	0.45	1.00	0.85	1.06
$G_{cir}^{p}/G_{cir}^{p,ana}$	1.00	1.34	0.75	0.75	0.95	0.93	0.85	0.93	1.05	1.13	1.20	1.26	0.80	1.22	1.10	0.75	0.90	0.75
$G_{air}^{p}/G_{air}^{p,ana}$	0.90	1.43	0.95	1.31	1.05	1.12	1.10	1.05	0.35	1.10	1.35	1.36	1.40	1.26	0.55	0.95	1.20	1.24

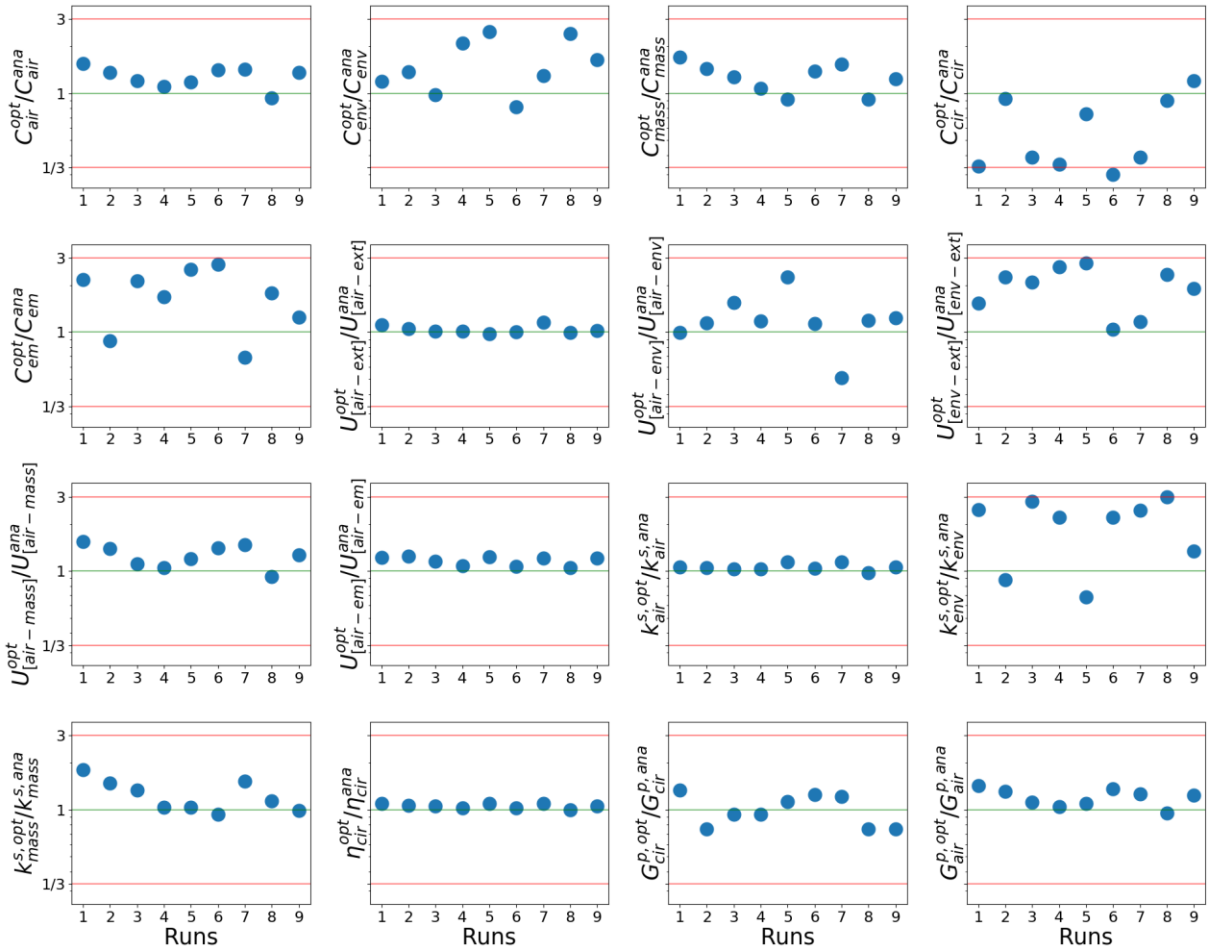

Figure 2.26 Optimal parameter sets identified at the end of 9 test runs from the analytical dataset

Figure 2.26 and Table 2.14 shows that:

- None of the runs has exactly converged to θ_{opt}^{theo}. At each run, a different θ_{opt} is found. However, it is unclear whether the search initialization or the stochastic nature of the PSO is more responsible for that difference.
- Some parameters that were found well identifiable in § 2.4.1.1 are identified within a 15% error range from θ_{opt}^{theo}, namely U_{air}^{ext}, U_{air}^{em}, k_{air}^{s} and η_{cir}.

Results concerning the objective function minimization are plotted in Figure 2.27. Per run, the scatter visualizes, for all tested search points (θ), the value of $f_{obj}^{ana}(\theta)$ (Eq. 2.59) in ordinate and the corresponding value of $q_{T_{air}}^{ana}(\theta)$ (Eq. 2.60) in abscissa. A subplot also spots the coordinates $(f_{obj}^{ana}, q_{T_{air}}^{ana})$ of the initial search point θ_{ini} in a red x, those of the found optimum θ_{opt} in a green arrow head and those of the theoretical optimum θ_{opt}^{theo} in an orange diamond. Bear in mind that these plots do not give information about the tested θ (a part from θ_{ini} and θ_{opt}), i.e. 2 nearby points on the scatter do not necessary correspond to 2 closely related θ.

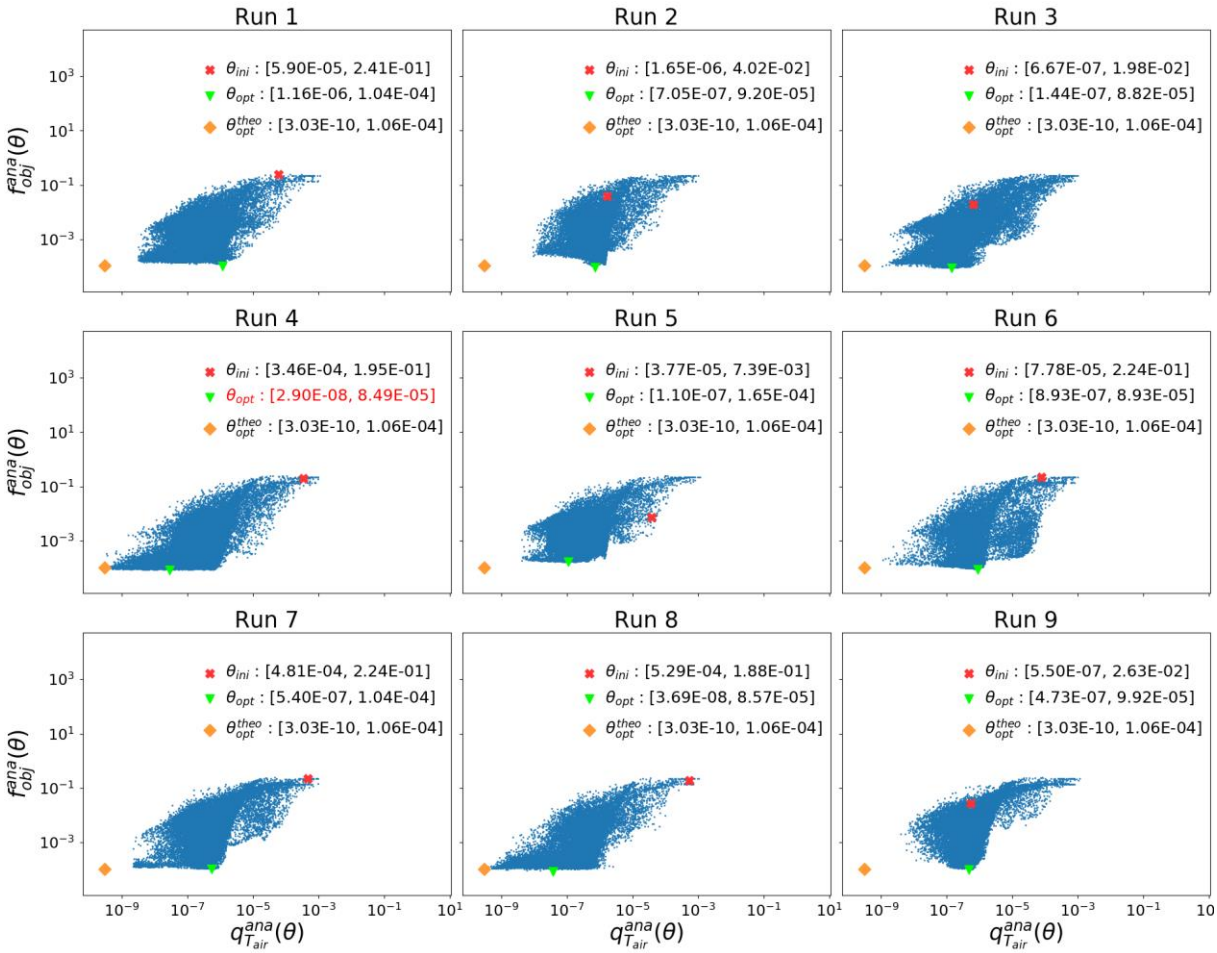

Figure 2.27 f_{obj}^{ana} *vs* $q_{T_{air}}^{ana}$ for all search points θ (≈ 25K θ /run); *Run 4* has the overall best solution

The following observations are made:

- For all runs, the algorithm has substantially reduced f_{obj}^{ana} to a value as low as $f_{obj}^{ana}(\theta_{opt}^{theo})$. This proves that the algorithm has quite good searching ability, regardless of the initial point.
- Nonetheless, the found optima, at different runs, do not all equivalently approach $q_{T_{air}}^{ana}(\theta_{opt}^{theo})$. One may imagine multiple valleys in the objective function surface (local minima) with points at roughly equal levels to $f_{obj}^{ana}(\theta_{opt}^{theo})$ that seem to attract the search particles, yet they do not all allow the ROM to well-predict the hidden state T_{air}.
- Therefore we conclude that, due to the objective function shape at close levels to $f_{obj}^{ana}(\theta_{opt}^{theo})$, a minimization in $f_{obj}^{ana}(\theta)$ does not systematically yield a minimization in $q_{T_{air}}^{ana}(\theta)$.

Figure 2.28 shows the performance of the identified parameters in 3 sample runs. The graphs illustrate how 3 different sets of parameters yield similar predictions of Q_{SST}, quasi-identical predictions of $\dot{m}_{SST}$ and slightly different predictions of T_{air}.

Also, the top graphs show that the largest errors on Q_{SST} occur at the transitions to/from the night-time set-back. At these particular moments, the thermal inertia of the heating system, represented in the ROM by parameters C_{cir} and C_{em} with C_{cir} being dominant in magnitude (Table 2.12), plays its major role. A fault identification of C_{cir} in particular is responsible for the large momentary errors. According to Table 2.14, *Run 9* has the best identified C_{cir}, explaining why it best predicts Q_{SST}.

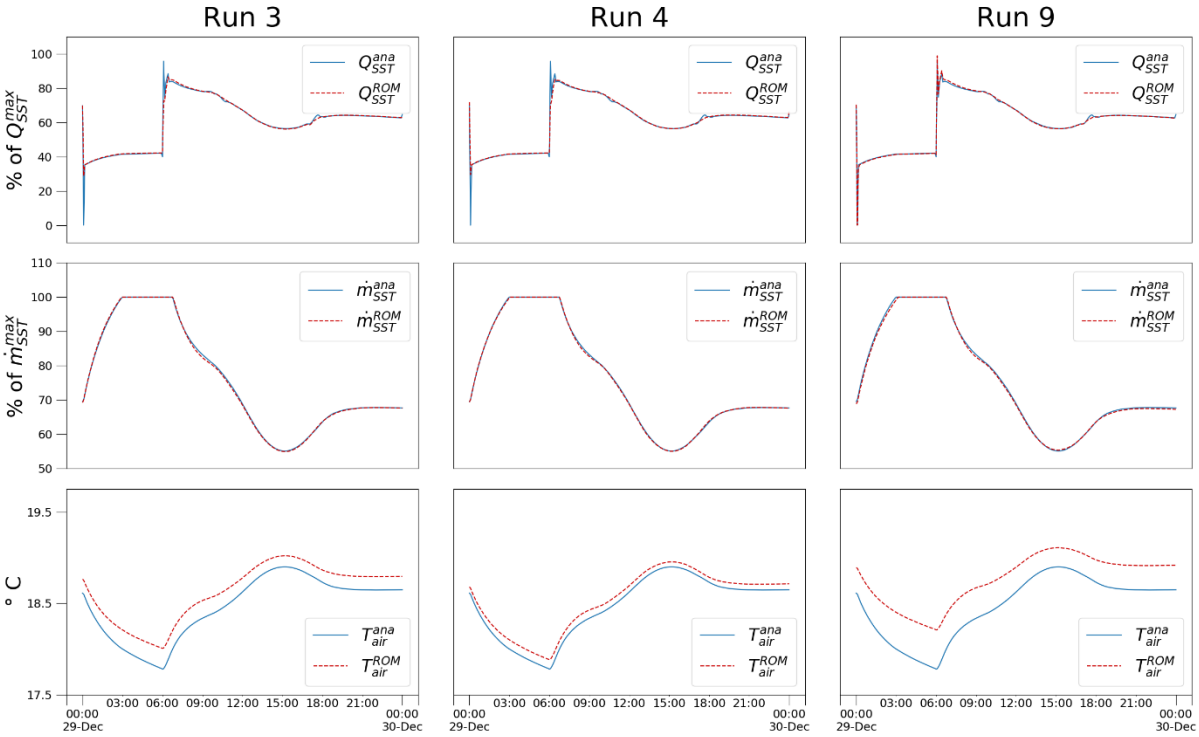

Figure 2.28 Comparison between analytical data and the corresponding ROM predictions for sample runs 3, 4 (best found solution) and 9

2.4.1.3 Limitations and adjustments

Analytical testing has revealed important limitations for the proposed ROM identification approach:

- Some parameters have mediocre influence on the objective function; therefore they are poorly identifiable.
- The problem is ill-posed, i.e. the observations can be fitted by different sets of parameters which do not all guarantee reliable prediction of hidden states, specifically the indoor air temperature.
- Correlation between parameters may exist, however this was not investigated in this study.

Some adjustments ought to be made. One may consider modifying the objective function. The change can be brought at different levels: adjusting the ROM structure, integrating more observations or simply changing the weights in Eq. 2.46. At this point, we do not intend to test another structure and we stick to the assumption that no other measurements are available. We tried different combinations of weighing factors but this did not help overcoming the problem.

On the bright side, since the ROM is semi-physical, prior physical knowledge could be used to assist the search algorithm. Concretely, the search space should be delimited within a tight physically plausible region. Multiple runs with different initializations should be performed. The choice of the retained set of parameters should be made based on the assessment of a physical indicator, such as $\epsilon_{U_{build}}$ proposed in § 2.3.3.3. With no further modifications in the model structure or the identification approach, physical interpretation seems the only guide to discern the *correct* θ_{opt} among several local optima.

2.4.2 ROM identification for the building simulators

In this section, we intend to identify parameters for the 3 case study buildings introduced in § 1.4. Identification datasets are generated using the BTSs as described in § 2.3.3.1. Unlike analytical testing, datasets generated from the BTSs are noisy and theoretically optimal parameters to fit the measurements are not known beforehand.

Following conclusions of § 2.4.1.3, we rely on some physical knowledge to initialize the search algorithm. The search is normalized with respect to the chosen initial values and delimited between 1/3 and 3. Multiple initializations are performed, performance criteria of § 2.3.3.3 are evaluated at the end of each and the overall best point is retained.

2.4.2.1 Identification results

Final identified parameters are shown in Table 2.15, together with the value of the objective function at the optimal point $f_{obj}(\theta_{opt})$ (Eq. 2.46) and the normalized quadratic error integral on the indoor temperature at the optimal point given in Eq. 2.61.

$$q_{T_{air}}(\theta) = \frac{1}{\Delta_{tr}} \cdot \int_0^{\Delta_{tr}} \left(\frac{T_{air}^{HOM} - T_{air}^{ROM}}{T_{air}^{set}} \right)^2 dt \qquad \text{Eq. 2.61}$$

The algorithm converges to the identified parameters after about 25k simulations, taking around 25 minutes on a 2-processors, of 18 cores each, machine. Note that $f_{obj}(\theta_{opt})$ for the *2012 building* is the highest among the others. This is due to the sensitivity of this building class to internal heat gain accounting for about 20% of its SH sizing power (Figure 2.29), which is not modelled in the ROM equations (Eq. 2.39 to Eq. 2.45). To compensate the effect of internal gain, the search algorithm might find biased parameters: over-estimated solar gain coefficients and under-estimated heat loss coefficients. This eventually leads to larger errors.

Table 2.15 Identified parameters, minimal objective function value and corresponding error on the indoor temperature for the 3 case study buildings

Identification results		***1915 Building***	***1975 Building***	***2012 Building***
C_{air}	$[J/K]$	1.76E+07	3.45E+07	2.58E+07
C_{env}	$[J/K]$	2.08E+09	3.50E+08	1.78E+08
C_{mass}	$[J/K]$	1.20E+07	4.62E+05	1.68E+08
C_{cir}	$[J/K]$	2.73E+05	2.52E+05	2.72E+05
C_{em}	$[J/K]$	6.30E+02	1.41E+03	6.90E+03
$U_{[air-ext]}$	$[W/K]$	560.25	372.75	225
$U_{[air-env]}$	$[W/K]$	1114.5	379.73	24.24
$U_{[env-ext]}$	$[W/K]$	1289.63	450	1840
$U_{[air-mass]}$	$[W/K]$	3360	1760	3060
$U_{[air-em]}$	$[W/K]$	460	435	380
k^s_{air}	$[m^2]$	12.75	7.15	13.05
k^s_{env}	$[m^2]$	2.1	1.96	15.3
k^s_{mass}	$[m^2]$	3.15	0.9	5.1
η_l	$[-]$	0.84	0.96	0.95
G^p_{cir}	$[1/K]$	0.34	0.85	0.32
G^p_{air}	$[1/K]$	0.46	0.53	0.5
$f_{obj}(\theta_{opt})$	$[-]$	6.15E-04	1.26E-03	1.55E-03
$q_{T_{air}}(\theta_{opt})$	$[-]$	3.46E-08	7.78E-08	9.94E-08

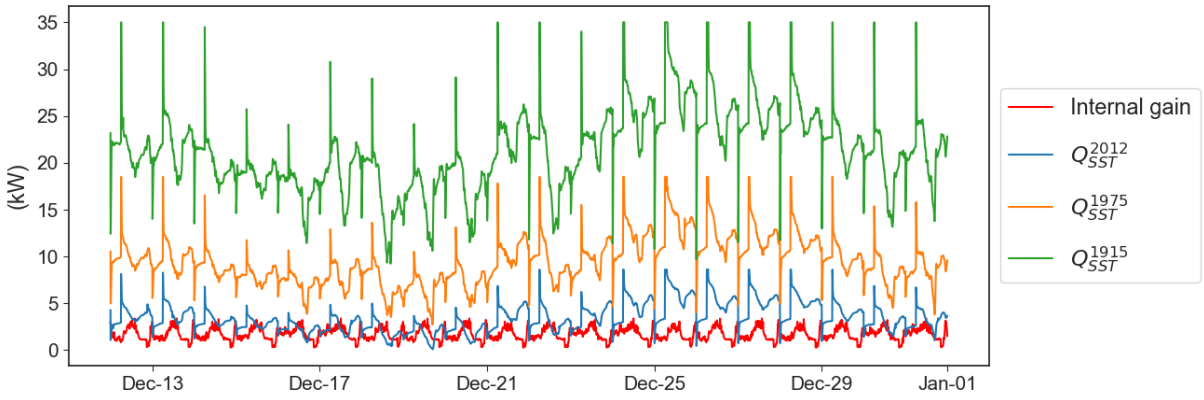

Figure 2.29 Proportions of the internal heat gain (noise) compared to the substation SH power (observation) for the 3 case study buildings showing that the *2012 Building* is the most sensitive to internal gain

2.4.2.2 Performance criteria for the 3 case study buildings

Results of the fit criterion (Eq. 2.54) on the model outputs Q_{SST} and $\dot{m}_{SST}$ are listed in Table 2.16. The deterioration in the fit between identification and validation phases for all buildings is less than 5%.

Table 2.16 Results of the output fit assessment criterion

Fit (%)	Phase	*1915 Building*	*1975 Building*	*2012 Building*
$\varphi_{Q_{SST}}$	Identification	93.78	92.68	94.46
	Validation	90.02	89.69	89.79
$\varphi_{\dot{m}_{SST}}$	Identification	95.80	94.98	91.55
	Validation	90.73	91.62	84.58

Results of the indoor air temperature error (Eq. 2.55) are shown in Table 2.17. The obtained mean μ and standard deviation σ of $\varepsilon_{T_{air}}$ imply very good predictive ability during the identification and validation phases. Furthermore, the errors range between -0.32°C and 0.28°C during identification, and between --0.51 and 0.59 during validation. These tight error ranges are quite satisfactory considering the fact that the identification approach did not rely on any internal temperature measures.

Table 2.17 Results of the indoor air temperature assessment criterion

		Phase	*1915 Building*	*1975 Building*	*2012 Building*
$\mu(\varepsilon_{T_{air}})$	$[°C]$	Identification	0.04	-0.05	0.02
		Validation	0.09	-0.01	-0.03
$\sigma(\varepsilon_{T_{air}})$	$[°C]$	Identification	0.05	0.08	0.09
		Validation	0.1	0.11	0.16
$[\varepsilon_{T_{air}}^{min}, \varepsilon_{T_{air}}^{max}]$	$[°C]$	Identification	[-0.27, 0.16]	[-0.30, 0.28]	[-0.32, 0.28]
		Validation	[-0.51, 0.23]	[-0.46, 0.34]	[-0.34, 0.59]

A close-up on 2 days in Figure 2.30 allows visual comparison between the HOMs reference data and the ROMs predictions. We note that air temperature trajectories of the *2012 Building* (most sensitive to internal heat gain) show that the largest discrepancies between the HOM and the ROM occur during night-time when the internal gain magnitude is very low. This observation supports the doubt that biased parameters might have been identified to compensate the influence of internal gain whenever it is present (day time), eventually leading to larger errors whenever it is not (night time).

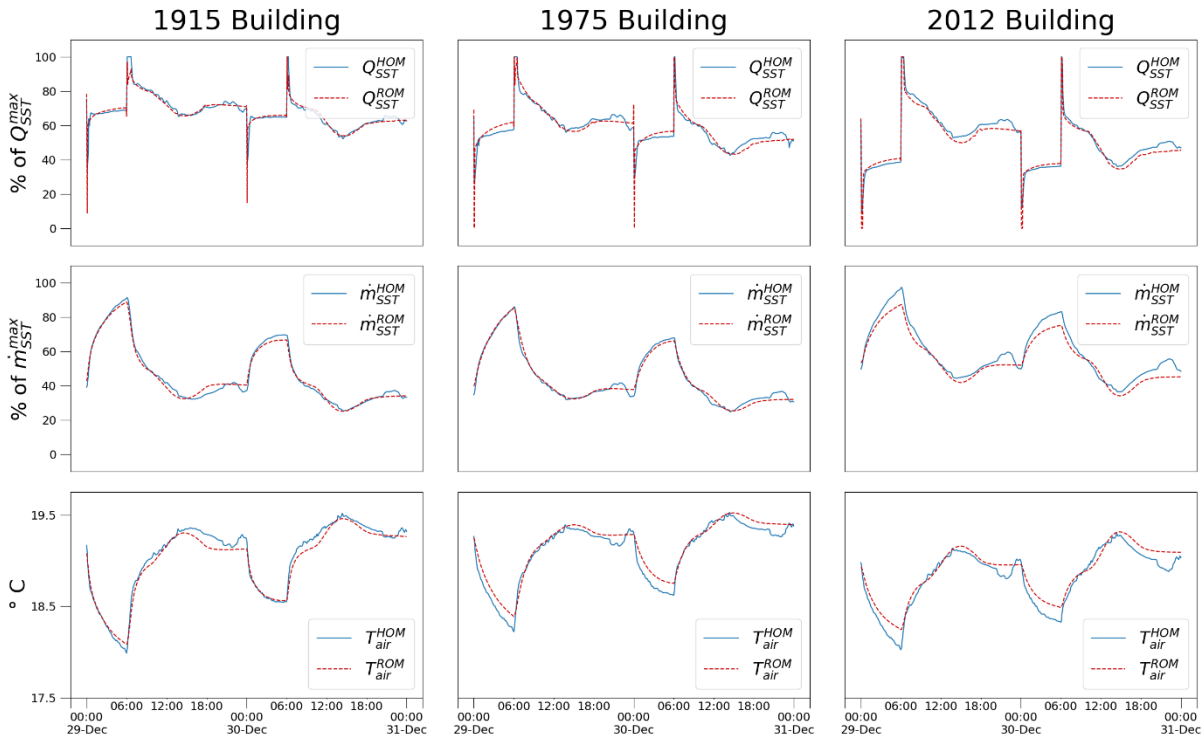

Figure 2.30 Comparison between the HOMs data and the corresponding ROMs predictions for the 3 case study buildings

Finally, results of the building equivalent heat loss coefficient are given in Table 2.18. They show overall good consistency between U_{build}^{estim} (Eq. 2.56) and U_{build}^{ident} (Eq. 2.57). Again, the largest relative error $\epsilon_{U_{build}}$ (Eq. 2.58) was found for the *2012 Building*. It is indeed underestimated in the identification, which compensates the effect of internal gain.

Table 2.18 Results of the building equivalent heat loss coefficient physical plausibility

		1915 Building	***1975 Building***	***2012 Building***
$\boldsymbol{U_{build}^{sizing}}$	$[W/K]$	1129.03	596.77	277.42
$\boldsymbol{U_{build}^{ident}}$	$[W/K]$	1158.09	578.69	248.92
$\boldsymbol{\epsilon_{U_{build}}}$	[%]	2.57	-3.03	-10.27

Performance criteria reassure that all 3 identified ROMs have high prediction ability [Aoun *et al.*, 2019]. Thus they will be used in the MPC application of the next chapter.

2.5 Conclusion

Developing a building model for model-based control is a crucial and time-consuming step. Moreover, limited data availability at a city or a DHS scale further restrict the potential approaches.

In this chapter, the goal is to establish a methodology to infer an accurate, identifiable from measurements available at the DHS substation and computationally efficient reduced-order building model from data generated by the BTSs. To this end, 2 complementary tasks are accomplished: firstly, designing a convenient model structure and secondly, identifying unknown parametric.

A literature review inspected building model structures and identification techniques. It was found that physically interpretable grey-box models of at least 2^{nd} order and preferably considering thermal inertia of the heating system are well-suited for our application. However, development of a ROM of an order greater than 1 and not relying on indoor measurements has not been proposed in the literature.

The BTS comes in handy to perform a parametric study, which seemed necessary for a better understanding of buildings thermal dynamics. SH demand flexibility of buildings from different energy classes, having different levels of internal mass and equipped with different heating systems is assessed. It was found that thermal inertia of internal mass and radiators-heating systems, in particular those operating at high temperatures, considerably increases demand flexibility, especially in well-insulated buildings. Therefore, a model structure accounting for the effect of these elements is designed. The model has 16 parameters to be identified. An identification strategy is proposed. It strictly uses observations found at the substation: SH power and heating circuit mass flow rate non-intrusively generated under quasi normal operation conditions for the consumer. The identification consists in searching for an optimal set of 16 parameters that minimizes the output error between the reduced order model and the data generated by the BTS. A hybrid PSO-HJ search algorithm is employed for this task and performance criteria are defined to assess the search result.

Before applying the proposed strategy on actual data generated by the complex BTSs, synthetic data was used for analytical testing. Through the tests, limitations of the methodology are uncovered: some parameters are poorly-identifiable and the risks for the algorithm to find an incorrect optimal set of parameters are high. In order to discern the correct set, physical knowledge of the system should be engaged. With these conclusions, we carried on parameters identification to infer ROMs for our 3 case study buildings. Performance assessments of the found results turned-out fairly satisfactory and the ROMs are deemed propitious for MPC.

In the next chapter, a control problem for optimal SH management from the DHS substation will be formulated based on the identified ROM.

Chapter 3

Flexible model predictive control of buildings space-heating demand

Synopsis

In this chapter, we design and demonstrate flexible control of buildings SH demand in DHSs by MPC. After introducing MPC, we review relevant works in the literature and conclude that a realistic and practical MPC implementation within a DHS context has not yet been proposed. We design an optimal controller and introduce its flexibility aspect via a mathematical formulation allowing it to modulate building SH demand, within the thermal comfort zone, based on the identified ROM. Finally we demonstrate the proposed MPC on the BTSs and envision its potential contributions at a DHS scale.

3.1 Introduction to model predictive control

Model predictive control is an approach to control design. It does not imply a specific control law or algorithm; it rather describes a strategy primary based on anticipation and calculation of consequences. On another note, optimal control involves mathematical formulation of a problem and its resolution for the *best* solution. One possible framework to implement optimal control is within the MPC approach.

In this section, we intend to clarify key concepts of MPC and introduce optimal control formulation.

3.1.1 Key concepts of MPC

MPC has its origins in human behaviour. An everyday life activity where humans intuitively approach with MPC is when controlling a car, i.e. driving. To ease explanation, key concepts of MPC presented hereafter are illustrated with the car driving example.

3.1.1.1 Predictions

While driving a car, a driver looks ahead to anticipate future obstacles. The horizon over which he should be looking must be sufficiently far, otherwise obstacles may not be avoided.

MPC relies on predictions (or anticipations, forecasts) of signals that act on the system over a future horizon. Based on these predictions, an implemented controller takes control actions. The length of the prediction horizon depends on the system dynamics; it is chosen large enough to allow actions to take effect within the desired time, but not too large, otherwise calculations may become tedious and useless.

3.1.1.2 Receding horizon

As the car moves forward, the driver takes control actions, his anticipations are refreshed and his horizon shifts along.

In MPC, as time flows, the controller makes decisions and is continually provided with updated predictions. The prediction horizon is always relative to the current point in time and of constant length; therefore as time flows, the horizon recedes. The period at which a decision is made and the horizon is shifted is called the sampling time. This is called the receding horizon principle.

3.1.1.3 Model

Approaching an obstacle, a driver estimates the distance and the time needed to avoid a crash. Then, owing to his experience, he decides to push the brake pedal at the instant which he expects to be the most convenient.

Besides predictions, MPC relies on automated estimation of the system behaviour over the prediction horizon. This automation is done though mathematical models. Controllers given good models (*well-experienced drivers*) are more likely to make better decisions.

3.1.1.4 Feedback

When the car hits the rumble strips on the edge of the road, the driver receives a tactile vibration as an alert to correct its position.

When controlling a system, some states might be continually measured. Feedback is introduced to the control loop when these measurements are considered in new decision making and used to update the model estimations. MPC may incorporate feedback.

3.1.1.5 Multi-variables handling

Driving a car requires the driver to control both the steering wheel and the throttle simultaneously; consequently the car moves along a certain direction at a certain speed.

MPC can be used to handle multi-input multi-output systems by automatically taking account of the interactions between all inputs and outputs through the mathematical model.

3.1.1.6 Constraints handling

A driver controlling the speed of his vehicle should respect speed limits.

One major advantage of a MPC controller is that it attempts to make decisions that strictly satisfy a set of constraints. Other control strategies, typically using PID regulators, would allow some violation of the limits (e.g. over-shoot) and correct the decision afterwards.

3.1.1.7 Performance criterion

Multiple itineraries may be suggested to reach a destination. Some drivers prefer short routes, others value light traffic or cheap tolls, and often times trade-offs must be made. Therefore, a driver defines a criterion and accordingly chooses the itinerary that best suits its.

In MPC, it is essential to define a performance criterion, i.e. a numerical indicator of what *best* means. Thus the controller may compute and compare the performance criterion of potential solutions and accordingly identify the best one. Flexibility may be introduced to the control through a performance criterion defined as a trade-off between 2 or more contradictory objectives.

3.1.2 Optimal control

As mentioned, MPC employs a controller that makes decisions over a finite horizon based on predictions, relying on a mathematical model, subject to some constrains and aiming at finding the best solution according to a performance criterion. This describes a constrained optimal controller.

An optimal controller is configured by formulating an optimization problem and selecting an adequate algorithm to solve for its solution.

The general discrete form (implicit 1st order Euler scheme) of a constrained optimization problem over a prediction horizon is given in Eq. 3.62: H_{MPC} denotes the prediction horizon, Δt_{MPC} the sampling time and N_{MPC} the number of instants (Eq. 3.63); x is the model states vector and u is the model inputs vector composed of controllable inputs (constant over Δt_{MPC}) and predicted uncontrollable disturbances.

Eq. 3.62(a) is the objective function (or cost function), where l is a function closely related to the performance criterion. f in Eq. 3.62(b) is a vector of equality constraints dictating the system dynamics according to its mathematical model. g in Eq. 3.62(c) and h in Eq. 3.62(d) are vectors of inequality constraints on the system states and controllable inputs, respectively, which prohibit undesired solutions and violation of technical limitations. G and H are vectors of bounding parameters.

$$minimize:$$

$$f_{obj}^{MPC} = \sum_{n=1}^{N_{MPC}} l(x[n], u[n]) \qquad \text{Eq. 3.62(a)}$$

$$subject\ to\ (at\ every\ n):$$

$$x[n] = f(x[n-1], u[n]) \qquad \text{Eq. 3.62(b)}$$

$$g(x[n]) \leq G \qquad \text{Eq. 3.62(c)}$$

$$h(u[n]) \leq H \qquad \text{Eq. 3.62(d)}$$

$$N_{MPC} = H_{MPC}/\Delta t_{MPC} \qquad \text{Eq. 3.63}$$

Optimal control problems are categorized depending on the nature of l, f, g, h, x and u. Per category, specific methods and algorithms have been developed to solve the problem. Below, we cite the general categories and some of their proposed resolution methods:

- **Linear programming:** If l, f, g and h are all linear and all variables in x and u are continuous, then the problem in discrete time is referred to as Linear Programming (LP). Standard algorithms to solve LP problems are the Simplex algorithm [Kalai, 1997], the Ellipsoid algorithm [Grötschel *et al.*, 1981] and Karmarkar's algorithm [Karmarkar, 1984].
- **Non-linear programming:** If any of l, f, g or h is non-linear, then the problem is a Non-Linear Programming (NLP) problem. One particular problem is when l is quadratic while all others are linear, then the problem is called Linear Quadratic (LQ) and the solution is provided by a Linear Quadratic Regulator (LQR) [Scokaert et Rawlings, 1998]. If g and h are eliminated (system subject to equality constraints only), the method of Lagrange multipliers can be applied [Rosen, 1999]. Other methods to solve general forms of NLP problems trading optimality for speed involve metaheuristics such as genetic algorithms [Rudolf et Bayrleithner, 1999] and particle swarm optimization algorithms [Das *et al.*, 2008].
- **Mixed-integer programming:** If x or u include variables that are restricted to be integers (called discrete variables), then we are dealing with a Mixed-Integer Programming (MIP) problem. The problem may be solved by branch-and-bound [Land et Doig, 1960] or branch-and-cut [Padberg et Rinaldi, 1991] algorithms. They consist of solving the basic (LP or NLP)

problem ignoring the restriction that some variables are discrete. If the solution happens to satisfy the ignored restriction, then the problem is solved. Otherwise, the unsatisfactory solution is excluded and the problem is solved again. Commercial MIP solvers such as CPLEX[14], GUROBI[15] and MOSEK[16] efficiently accelerate the procedure by several means, for instance by parallelism and cutting planes techniques.

The necessity in MPC to solve the optimization problem within the sampling time Δt_{MPC} raises the requirement of computational efficiency on the controller. In fact, NLP problems are very hard to solve efficiently. It is much more convenient to use a model with linear dynamics and formulate a linear objective function. Yet, if some non-linear dynamics are inevitably necessary to include in the model, the obtained NLP problem may be relaxed into a Mixed-Integer Linear Programming (MILP) problem, i.e. a combination of LP and MIP, by appropriate linearization techniques.

In this chapter, we demonstrate the use of the ROM identified in the previous chapter to formulate a MILP problem and elaborate a MPC strategy for buildings SH demand. But first, a concise literature review on MPC applications in this field is presented.

3.2 Literature review

3.2.1 MPC in smart grids

MPC was first introduced to optimally control space-heating (and cooling) in electric Smart Grids (SGs). As defined in [Momoh, 2009], SG is "*the power system that is capable of assessing its health in real-time, predicting its behavior, anticipatory behavior, adaptation to new environments, handling distributed resources, stochastic demand, and optimal response to the smart appliances*."

The use of MPC was motivated by variable electricity retail prices and the possibility of using thermal inertia of the buildings to shift their demand to periods of lower prices, without jeopardizing consumers thermal comfort. Load shifting, load shedding and peak shaving are all Demand-Side Management (DSM) measures applicable through MPC: they involve manipulation (or modulation) of buildings power demand in order to optimize the overall grid performance (operation costs, voltage stability, renewable energy penetration rates, etc.).

Thus, many studies have been conducted to assess the contributions of DSM through MPC in SGs. In [Halvgaard *et al.*, 2012], MPC is implemented to manipulate a heat pump in a building equipped with a floor heating system. The strategy proved its ability to shift the electrical load to periods with low

[14] https://www.ibm.com/analytics/cplex-optimizer
[15] https://www.gurobi.com/
[16] https://www.mosek.com/

electricity price characterized by high levels of wind power availability. In [Killian *et al.*, 2018], MPC is used to optimally manage thermal and non-thermal devices of a smart home; it was demonstrated that buildings thermal inertia can be efficiently used to store heat and therefore reduce the battery size required in such houses. In [Ma *et al.*, 2012], MPC allowed important cost savings by automatically triggering pre-cooling and peak-load shaving based on dynamic electricity prices. Similar conclusions were reported in a number of other studies, e.g. [Kramer *et al.*, 2016; Chen *et al.*, 2013; Hu *et al.*, 2019b]

3.2.2 MPC in DHSs

Promising results in SGs raised interest in investigating MPC for SH demand in buildings served by a DHS. Yet the application in contemporary DHSs is more challenging. First, identifying a suitable model requires historical data. SGs are rather modern systems, often equipped with smart meters and monitoring devices, therefore more data is available resulting in better models. Second, DSM control actions can only be applied at the substation level in DHSs. For instance, modulating the air set-point temperature inside the building at the radiators level is not possible in a DHS whereas actuators may be readily installed in SGs to do so.

Thus, few studies investigated MPC in DHSs. In [Li et Wang, 2015], a predictive control scheme is proposed where building thermal inertia is used to avoid starting up peak heat boilers in a DHS. In the MPC proposed in [Verrilli *et al.*, 2016], heat demand is treated as a flexible load with curtailable and reschedulable parts. The potential benefits of flexible MPC has been well-noted; however, none of these works have used proper building models or applied control as it is feasible in a DHS.

3.2.3 Real-life implementation

All studies cited so far were conducted by numerical simulation means. As we come to grips with real-life implementation of MPC, several practical challenges arise. Beginning with ROM development, in real-life, measurements are limited and datasets require filtering prior to the identification process. Occupant's behaviour is uncontrollable and may sometimes put the ROM predictions off-track if it was not accounted for during the identification. Moreover, weather forecasts and energy price predictions are never perfect.

In [Liao et Dexter, 2009], MPC is designed and tested on a commercial office building heated with radiators equipped with TRVs. It was concluded that the control scheme outperforms conventional control. However, it is arguable whether MPC including the identification of the ROM using internal temperature measurements would be lucrative on smaller residential buildings. In [Chen, 2002], MPC is applied to a test room with floor heating. Results showed that MPC is more beneficial than standard on-off and PI controllers. [Prívara *et al.*, 2011] presents a real-life implementation of MPC on a university building and concludes on its superiority in reducing peak loads with respect to conventional

WCC. Yet again, the authors stressed that the ROM development is the most crucial part of the problem and estimated the return time of the investment in MPC to 2 years. [Oldewurtel *et al.*, 2012] presents stochastic MPC by simulating uncertain weather forecasts to mimic real-life scenarios. [Zhang *et al.*, 2013] presents randomized MPC that handles uncertainties due to occupancy and weather forecasts. Studies presented in [Liu *et al.*, 2018; Li *et al.*, 2015; Namerikawa et Igari, 2016] investigate the impact of solar irradiation uncertainty on MPC applied to buildings with photovoltaic systems.

So as a conclusion, MPC is deemed promising to tackle buildings SH optimal control. Few studies were conducted in a DHS context. Real-life implementation requires consideration of many aspects including ROM identification conditions (discussed in § 2.1), control actions feasible at the substation level and uncertainty quantification of the predictions.

3.3 Flexible control problem formulation

This section describes our MILP formulation of the optimization problem used to design a flexible controller based on the identified ROM to be solved within a MPC scheme, assuming perfect weather and energy prices predictions. Recall that SH demand flexibility is the ability to modulate the building energy profile within its thermal comfort zone.

3.3.1 Objective function

The optimization problem has one objective function expressed as the sum of multiple terms to be minimized. These terms are measures of SH energy cost, thermal discomfort and thermal losses.

3.3.1.1 Space-heating cost

SH naturally has a cost based on the energy purchase price, denoted p^{energy}. The DHS energy supplier may charge the consumer with variable tariffs that depend on various factors such as heat sources availability or demand intensity. Consequently, the cost of SH over H_{MPC}, c^{SH}, is given in Eq. 3.64.

$$c^{SH} = \sum_{n=1}^{N_{MPC}} p^{energy}[n] \cdot Q_{SST}[n] \qquad \text{Eq. 3.64}$$

3.3.1.2 Thermal discomfort

Thermal discomfort is triggered by a deviation of the indoor air temperature T_{air} from its set-point T_{air}^{set}. A penalty for discomfort $p^{discomfort}$ may be associated to the absolute difference between T_{air} and T_{air}^{set}, and discomfort cost would be formulated as in Eq. 3.65:

$$c^{discomfort} = \sum_{n=1}^{N_{MPC}} p^{discomfort}[n] \cdot \left| T_{air}[n] - T_{air}^{set}[n] \right| \quad \text{Eq. 3.65}$$

We tried a first formulation of the objective function as the sum of the costs in Eq. 3.64 and Eq. 3.65. To minimize it, the controller would either drive T_{air} close to T_{air}^{set} if $p^{discomfort}$ is much more weighing than p^{energy}, or shut-off Q_{SST} otherwise. Finding a well-tuned $p^{discomfort}$ is complicated.

Instead, we introduce a temperature denoted T_{air}^{target} which is a linear translation of T_{air}^{set} by a thermal comfort threshold ε^{comf} as in Eq. 3.66.

$$T_{air}^{target}[n] = T_{air}^{set}[n] - \varepsilon^{comf}[n] \quad \text{Eq. 3.66}$$

Now, T_{air}^{target} replaces T_{air}^{set} in Eq. 3.65. For a reasonable $p^{discomfort}$ with respect to an average p^{energy}, the controller would drive T_{air} close to T_{air}^{target}, unless p^{energy} reaches peak values in which case Q_{SST} is shut-off. Hence, T_{air}^{target} allows the DHS operator to modulate T_{air} around specific values ruled by ε^{comf}. The modulation itself was not possible before introducing T_{air}^{target} because the operator does not have control over T_{air}^{set} (only consumers inside the building can regulate T_{air}^{set}).

ε^{comf} takes positive values because in case of a building with radiators heating system equipped with TRVs, we may not regulate T_{air} above T_{air}^{set}: the TRVs automatically close to prevent over-heating. ε^{comf} defines the thermal comfort zone which may be variable over time, typically ε^{comf} can be increased during night-time.

Furthermore, we distinguish between discomfort due to over-heating and that due to under-heating. Temperature deviation in the former is denoted $\Delta T_{air}^{overheat}$ and takes a positive value (Eq. 3.67), whereas in the latter it is denoted $\Delta T_{air}^{underheat}$ and takes a negative value (Eq. 3.68).

$$\Delta T_{air}^{overheat}[n] = \left[\!\left[T_{air}[n] - T_{air}^{target}[n] \right]\!\right]_{0}^{\infty} \quad \text{Eq. 3.67}$$

$$\Delta T_{air}^{underheat}[n] = \left[\!\left[T_{air}[n] - T_{air}^{target}[n] \right]\!\right]_{-\infty}^{0} \quad \text{Eq. 3.68}$$

A penalty is associate with each temperature deviation. These penalties are correlated with c^{energy} as shown in Eq. 3.69 and Eq. 3.70 through coefficients $\lambda^{overheat}$ and $\lambda^{underheat}$ (both of positive values).

$$p^{overheat}[n] = \lambda^{overheat} \cdot \frac{1}{N_{MPC}} \cdot \sum_{i=0}^{N_{MPC}-1} p^{energy}[n+i] \cdot Q_{SST}^{max} \quad \text{Eq. 3.69}$$

$$p^{underheat}[n] = -\lambda^{underheat} \cdot \frac{1}{N_{MPC}} \cdot \sum_{i=0}^{N_{MPC}-1} p^{energy}[n+i] \cdot Q_{SST}^{max} \quad \text{Eq. 3.70}$$

Finally the cost of discomfort over H_{MPC}, $c^{discomfort}$, is given in Eq. 3.71.

$$c^{discomfort} = \sum_{n=1}^{N_{MPC}} \left(p^{overheat}[n] \cdot \Delta T_{air}^{overheat}[n] + p^{underheat}[n] \cdot \Delta T_{air}^{underheat}[n] \right) \quad \text{Eq. 3.71}$$

3.3.1.3 Thermal losses in the heating circuit

In the ROM structure, thermal losses in the heating circuit are simply modelled proportional to the substation heating power (Eq. 2.43). This simplification uncouples the thermal losses from the temperature of heating circuit water; thus it allows faster resolution of the optimization problem. However, it does not reflect the true physics since heating at higher temperatures results in greater thermal losses, to be avoided by the controller. Moreover, this formulation leads to control decisions with chattering heating temperatures, thus instabilities to be avoided as well.

To ensure that the controller choses low and stable heating temperatures, we append to the objective function a regularization term in the form of a cost for thermal losses in the heating circuit. This is formulated by introducing a temperature difference between the heating circuit and its ambient environment, assumed at constant temperature $T_{amb} = 20°C$ in Eq. 3.72. A penalty price p^{losses} is assigned to these losses in Eq. 3.73 similarly to the discomfort penalties.

$$\Delta T_{cir}^{losses}[n] = T_{cir}[n] - T_{amb} \quad \text{Eq. 3.72}$$

$$p^{losses}[n] = \lambda^{losses} \cdot \frac{1}{N_{MPC}} \cdot \sum_{i=0}^{N_{MPC}-1} p^{energy}[n+i] \cdot Q_{SST}^{max} \quad \text{Eq. 3.73}$$

Hence, the cost of thermal losses in the heating circuit over H_{MPC}, c^{losses}, is given in Eq. 3.74.

$$c^{losses} = \sum_{n=1}^{N_{MPC}} p^{losses}[n] \cdot \Delta T_{cir}^{losses}[n] \quad \text{Eq. 3.74}$$

3.3.1.4 Final form

The MPC objective function to be minimized over H_{MPC} is the sum of all costs (Eq. 3.64, Eq. 3.71 and Eq. 3.74). It is expressed in Eq. 3.75.

$$f_{obj}^{MPC} = \sum_{n=1}^{N_{MPC}} \begin{pmatrix} p^{energy}[n] \cdot Q_{SST}[n] \cdot \Delta t_{MPC} \\ +p^{overheat}[n] \cdot \Delta T_{air}^{overheat}[n] \cdot \Delta t_{MPC} \\ +p^{underheat}[n] \cdot \Delta T_{air}^{underheat}[n] \cdot \Delta t_{MPC} \\ +p^{losses}[n] \cdot \Delta T_{cir}^{losses}[n] \cdot \Delta t_{MPC} \end{pmatrix} \quad \text{Eq. 3.75}$$

The controller is tuned by means of the costs weights: $\lambda^{overheat}$, $\lambda^{underheat}$ and λ^{losses}. The system is subject to a set of constraints mainly constituted of the ROM equations which determine its physical evolution over H_{MPC}. MILP formulation of these constraints is expanded in the following section.

3.3.2 Constraints

Constraints of the MILP problem consist of the discretized and linearized ROM equations, expressions of the new terms introduced in the objective function ($\Delta T_{air}^{overheat}$, $\Delta T_{air}^{underheat}$ and ΔT_{air}^{losses}) and some bounding constraints of the model states and inputs.

3.3.2.1 ROM equations

3.3.2.1.1 Discretization of the differential equations

The ROM differential equations are discretized using the backward (implicit) 1st order Euler scheme at a fixed time step equal to Δt_{MPC} (Eq. 3.76 to Eq. 3.80). These equations are linear equality constraints.

$$C_{air} \cdot \frac{T_{air}[n] - T_{air}[n-1]}{\Delta t_{MPC}} = U_{[air-ext]} \cdot (T_{ext}[n] - T_{air}[n]) + U_{[air-env]} \cdot (T_{env}[n] - T_{air}[n]) + U_{[air-mass]} \cdot (T_{mass}[n] - T_{air}[n]) + U_{[air-em]} \cdot (T_{em}[n] - T_{air}[n]) + k_{air}^{s} \cdot I_{sol}[n] \quad \text{Eq. 3.76}$$

$$C_{env} \cdot \frac{T_{env}[n]-T_{env}[n-1]}{\Delta t_{MPC}} = U_{[env-ext]} \cdot (T_{ext}[n] - T_{env}[n]) + U_{[air-env]} \cdot (T_{air}[n] - T_{env}[n]) + k^{S}_{env} \cdot I_{sol}[n] \quad \text{Eq. 3.77}$$

$$C_{mass} \cdot \frac{T_{mass}[n]-T_{mass}[n-1]}{\Delta t_{MPC}} = U_{[air-mass]} \cdot (T_{air}[n] - T_{mass}[n]) + k^{S}_{mass} \cdot I_{sol}[n] \quad \text{Eq. 3.78}$$

$$C_{em} \cdot \frac{T_{em}[n]-T_{em}[n-1]}{\Delta t_{MPC}} = U_{[air-em]} \cdot (T_{air}[n] - T_{em}[n]) + Q_{BL}[n] \quad \text{Eq. 3.79}$$

$$C_{cir} \cdot \frac{T_{cir}[n]-T_{cir}[n-1]}{\Delta t_{MPC}} = \eta_l \cdot Q_{SST}[n] - Q_{BL}[n] \quad \text{Eq. 3.80}$$

Notice that $\dot{m}_{SST} \cdot \mathrm{c_{wat}} \cdot (T_{cir} - T_{em})$ of Eq. 2.42 and Eq. 2.43 is replaced by a new variable Q_{BL} denoting a bilinear term that is separately treated.

3.3.2.1.2 Linearization of the bilinear term

For simplicity, we first introduce a new variable ΔT_{BL} given by Eq. 3.81, where *BL* denotes Bi-Linear:

$$\Delta T_{BL}[n] = T_{cir}[n] - T_{em}[n] \quad \text{Eq. 3.81}$$

$Q_{BL}[n] = \dot{m}_{SST}[n] \cdot \mathrm{c_{wat}} \cdot \Delta T_{BL}[n]$ is a bilinear term, i.e. it features a product of 2 variables $\dot{m}_{SST}[n]$ and $\Delta T_{BL}[n]$, both being continuous, and as such, requires linearization.

Several linearization approaches are suggested in the literature including the classical linearization around an operating point thoroughly explained in [Roubal *et al.*, 2009] and the piecewise linear formulations reviewed in [Lin *et al.*, 2013].

Linearization around an operating point transforms the non-linear problem into a linear one. The approach approximates the bilinear term to its gradient at a known (not to be optimized) point. The complete formulation is not given here for concision, refer to [Roubal *et al.*, 2009] for details. For a linearization throughout H_{MPC}, the operating point is best chosen to be the previous point to the beginning of H_{MPC}. The linearization is usually acceptable close to that operating point; however, it may entail large errors between the exact non-linear system and the thus linearized version as we move away from the operating point. Thus, linearization around an operating point was quickly abandoned.

Piecewise linear formulations transform the non-linear problem into a mixed-integer linear one. The general approach starts by discretizing one of the variables involved in the bilinear term into pieces (or intervals) by introducing breakpoints. Binary (0-1) variables are associated to these intervals, such that only one of them is equal to 1 (activated) while all others equal 0. Between 2 consecutive breakpoints, the exact bilinear term is said to be relaxed. Several relaxation techniques are derived in the literature with the aim of formulating the tighter relaxation for better accuracy. The one that worked best for our problem is the McCormick relaxation, first introduced in [McCormick, 1976] and used in many works, e.g. [Wicaksono et Karimi, 2008]. A brief demonstration of the McCormick relaxation is given in Appendix A. The complete formulation is expanded hereafter.

$\Delta T_{BL}[n]$ is discretized into a vector of $(N_{disc}+1)$ uniformly spaced positive values $\Delta T_{BL}^{disc}[k]$, creating N_{disc} equal intervals; $\Delta T_{BL}^{disc}[k]$ is the discretized value of ΔT_{BL} at the beginning of interval k.

At every time instance of index n, N_{disc} binary variables $\alpha_{BL}[n][k]$ are introduced such as in Eq. 3.82:

$$\sum_{k=1}^{N_{disc}} \alpha_{BL}[n][k] = 1 \qquad \text{Eq. 3.82}$$

And, we introduce N_{disc} continuous variables defined over finite sets:

- $\delta_{BL}[n][k] \in \left[\Delta T_{BL}^{disc}[k], \Delta T_{BL}^{disc}[k+1]\right]$ if $\alpha_{BL}[n][k]$ =1, else $\delta_{BL}[n][k] = 0$ (Eq. 3.83 and Eq. 3.84)
- $\omega_{BL}[n][k] \in \left[\dot{m}_{SST}^{min}, \dot{m}_{SST}^{max}\right]$ if $\alpha_{BL}[n][k]$ =1, else $\omega_{BL}[n][k] = 0$ (Eq. 3.85 and Eq. 3.86):

$$\delta_{BL}[n][k] \geq \Delta T_{BL}^{disc}[k] \cdot \alpha_{BL}[n][k] \qquad \text{Eq. 3.83}$$

$$\delta_{BL}[n][k] \leq \Delta T_{BL}^{disc}[k+1] \cdot \alpha_{BL}[n][k] \qquad \text{Eq. 3.84}$$

$$\omega_{BL}[n][k] \geq \dot{m}_{SST}^{min} \cdot \alpha_{BL}[n][k] \qquad \text{Eq. 3.85}$$

$$\omega_{BL}[n][k] \leq \dot{m}_{SST}^{max} \cdot \alpha_{BL}[n][k] \qquad \text{Eq. 3.86}$$

Hence, $\delta_{BL}[n][k]$ and $\omega_{BL}[n][k]$ are the *local* variables inside the discretized interval respectively analogue to x and y in the McCormick formulation of Appendix A. The binary term inside each interval

is $\varphi_{BL}[n][k]/\mathrm{c_{wat}} = \delta_{BL}[n][k] \cdot \omega_{BL}[n][k]$, analogue to z. The corresponding graphical representation of the McCormick envelope is shown in Figure 3.31.

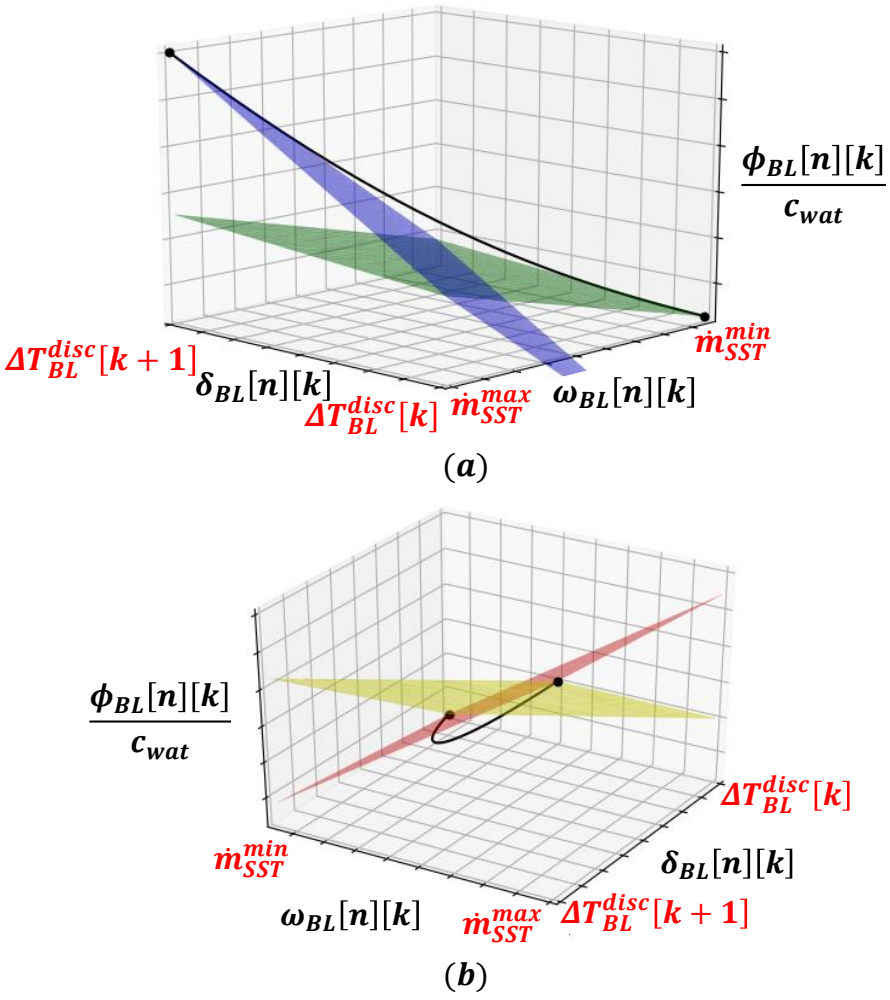

Figure 3.31 McCormick under-estimators (a) and over-estimators (b) for interval of index *k*

The McCormick relaxation is applied through Eq. 3.87 to Eq. 3.90 derived from the general equations Eq. App. 3.1 to Eq. App. 3.4 with one difference: the last terms are multiplied by $\alpha_{BL}[n][k]$ to ensure that $\varphi_{BL}[n][k] = 0$ if $\alpha_{BL}[n][k] = 0$.

$$\frac{\varphi_{BL}[n][k]}{\mathrm{c_{wat}}} \geq \dot{m}_{SST}^{min} \cdot \delta_{BL}[n][k] + \Delta T_{BL}^{disc}[k] \cdot \omega_{BL}[n][k] - \dot{m}_{SST}^{min} \cdot \Delta T_{BL}^{disc}[k] \cdot \alpha_{BL}[n][k] \qquad \text{Eq. 3.87}$$

$$\frac{\varphi_{BL}[n][k]}{\mathrm{c_{wat}}} \geq \dot{m}_{SST}^{max} \cdot \delta_{BL}[n][k] + \Delta T_{BL}^{disc}[k+1] \cdot \omega_{BL}[n][k] - \dot{m}_{SST}^{max} \cdot \Delta T_{BL}^{disc}[k+1] \cdot \alpha_{BL}[n][k] \qquad \text{Eq. 3.88}$$

$$\frac{\varphi_{BL}[n][k]}{c_{wat}} \leq \dot{m}_{SST}^{min} \cdot \delta_{BL}[n][k] + \Delta T_{BL}^{disc}[k+1] \cdot \omega_{BL}[n][k] - \dot{m}_{SST}^{min} \cdot \Delta T_{BL}^{disc}[k+1] \cdot \alpha_{BL}[n][k] \quad \text{Eq. 3.89}$$

$$\frac{\varphi_{BL}[n][k]}{c_{wat}} \leq \dot{m}_{SST}^{max} \cdot \delta_{BL}[n][k] + \Delta T_{BL}^{disc}[k] \cdot \omega_{BL}[n][k] - \dot{m}_{SST}^{max} \cdot \Delta T_{BL}^{disc}[k] \cdot \alpha_{BL}[n][k] \quad \text{Eq. 3.90}$$

Finally, values of $\Delta T_{BL}[n]$, $\dot{m}_{SST}[n]$ and $Q_{BL}[n]$ are respectively equal to $\delta_{BL}[n][k]$, $\omega_{NL}[n][k]$ and $\varphi_{NL}[n][k]$ in the activated interval k (Eq. 3.91, Eq. 3.92 and Eq. 3.93).

$$\Delta T_{BL}[n] = \sum_{k=1}^{N_{disc}} \delta_{BL}[n][k] \quad \text{Eq. 3.91}$$

$$\dot{m}_{SST}[n] = \sum_{k=1}^{N_{disc}} \omega_{NL}[n][k] \quad \text{Eq. 3.92}$$

$$Q_{BL}[n] = \sum_{k=1}^{N_{disc}} \varphi_{NL}[n][k] \quad \text{Eq. 3.93}$$

3.3.2.1.3 Linearization of the saturated terms

Besides the bilinear term, Eq. 2.44 and Eq. 2.45 feature saturations. A saturation is another form of non-linearity characterized by a discontinuity in the function at specific breakpoints. In our case, all saturations are piecewise linear, i.e. the function between 2 consecutive breakpoints is readily linear. A general method to formulate MILP for discontinuous piecewise linear functions is given in Appendix B and applied hereafter.

Linearization of Eq. 2.44

First we introduce variables ΔT_{cir} and ρQ_{SST} respectively analogue to x and y in the general form of Appendix B (Eq. 3.94 and Eq. 3.95).

$$\Delta T_{cir}[n] = T_{cir}^{set}[n] - T_{cir}[n] \quad \text{Eq. 3.94}$$

$$\rho Q_{SST}\,[n] = \frac{\mathrm{Q}_{SST}[n]}{\mathrm{Q}_{SST}^{max}} \qquad \text{Eq. 3.95}$$

Consequently, the saturation function, defined over 3 intervals with 4 breakpoints as depicted in Figure 3.32[17] is linearized by introducing 3 binary variables $\alpha_{PWL,cir}[n][k]$ and 3 continuous variables $\beta_{PWL,cir}[n][k]$ where *PWL* denotes Piece-Wise Linear (n is the index of the time instance and k the index of the interval).

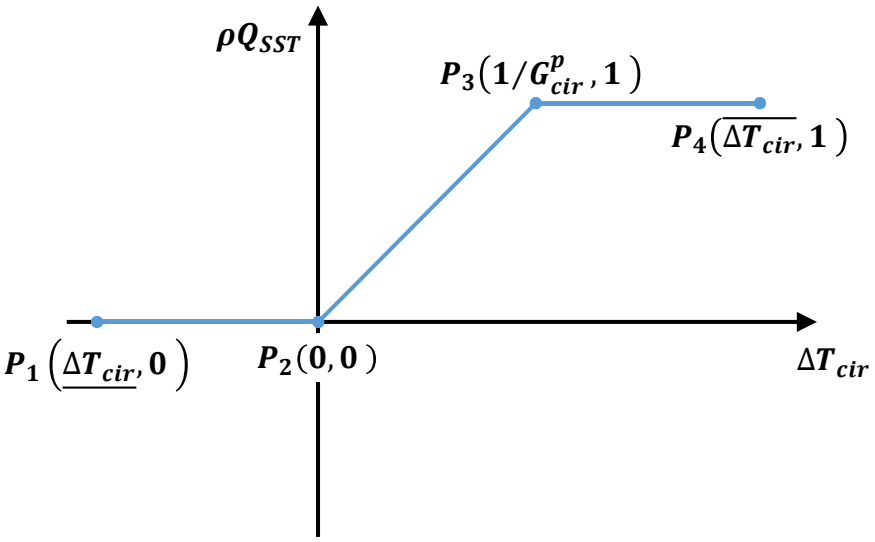

Figure 3.32 Plot of Eq. 3.13 showing the breakpoints used in the linearization

Straightforward application of Eq. App. 3.12 through Eq. App. 3.15 yields Eq. 3.96 through Eq. 3.99:

$$\sum_{k=1}^{3} \alpha_{PWL,cir}[n][k] = 1 \qquad \text{Eq. 3.96}$$

$$0 \le \beta_{PWL,cir}[n][k] \le \alpha_{PWL,cir}[n][k] \qquad \text{Eq. 3.97}$$

$$\Delta T_{cir}[n] = \alpha_{PWL,cir}[n][1] \cdot \underline{\Delta T_{cir}} - \beta_{PWL,cir}[n][1] \cdot \underline{\Delta T_{cir}} + \beta_{PWL,cir}[i][2] \cdot \frac{1}{G_p^{cir}} + \alpha_{PWL,cir}[n][3] \cdot \frac{1}{G_{cir}^{p}} + \beta_{PWL,cir}[i][3] \cdot \left(\overline{\Delta T_{cir}} - \frac{1}{G_p^{cir}}\right) \qquad \text{Eq. 3.98}$$

$$\rho Q_{SST}[n] = \beta_{PWL,cir}[n][2] + \alpha_{PWL,cir1}[n][3] \qquad \text{Eq. 3.99}$$

[17] $\overline{x}$ and $\underline{x}$ respectively denote the upper and lower bounds of variable x.

Linearization of Eq. 2.45

Very similarly, we linearize Eq. 3.14 by Eq. 3.100 to Eq. 3.105:

$$\Delta T_{air}[n] = T_{air}^{set}[n] - T_{air}[n] \quad \text{Eq. 3.100}$$

$$\rho\dot{m}_{SST}\,[n] = \frac{\dot{m}_{SST}[n]}{\dot{m}_{SST}^{max}} \quad \text{Eq. 3.101}$$

$$\sum_{k=1}^{3} \alpha_{PWL,air}[n][k] = 1 \quad \text{Eq. 3.102}$$

$$0 \leq \beta_{PWL,air}[n][k] \leq \alpha_{PWL,air}[n][k] \quad \text{Eq. 3.103}$$

$$\Delta T_{air}[n] = \alpha_{PWL,air}[n][1] \cdot \underline{\Delta T_{air}} - \beta_{PWL,air1}[n][1] \cdot \underline{\Delta T_{air}} + \beta_{PWL,air1}[i][2] \cdot \frac{1}{G_p^{air}} + \alpha_{PWL,air}[n][3] \cdot \frac{1}{G_{air}^{p}} + \beta_{PWL,air}[i][3] \cdot \left(\overline{\Delta T_{air}} - \frac{1}{G_p^{air}}\right) \quad \text{Eq. 3.104}$$

$$\rho\dot{m}_{SST}[n] = \beta_{PWL,air}[n][2] + \alpha_{PWL,air}[n][3] \quad \text{Eq. 3.105}$$

3.3.2.2 Terms in the objective function

$\Delta T_{air}^{overheat}[n]$, $\Delta T_{air}^{underheat}[n]$ and $\Delta T_{air}^{losses}[n]$ of the objective function Eq. 3.75 remain to be modelled in the MILP.

$\Delta T_{air}^{losses}[n]$ is a linear function of $T_{cir}[n]$ (T_{amb} is constant); it is quite simply modelled via Eq. 3.106.

$$\Delta T_{cir}^{losses}[n] = T_{cir}[n] - T_{amb} \quad \text{Eq. 3.106}$$

To model $\Delta T_{air}^{overheat}[n]$ and $\Delta T_{air}^{underheat}[n]$ of Eq. 3.67 and Eq. 3.68 we first express T_{air}^{target} of Eq. 3.66 in the MILP under Eq. 3.107. $\Delta T_{air}^{overheat}[n]$ and $\Delta T_{air}^{underheat}[n]$ are discontinuous functions of the variable ΔT_{air}^{target} introduced in Eq. 3.71, defined over 2 intervals. Their plots are shown in Figure 3.33. Their linearization requires introducing for every time instance 2 additional binary variables denoted $\alpha_{\text{PWL,target}}[n][k]$ and 2 continuous variables denoted $\beta_{\text{PWL,target}}[n][k]$. Applying the linearization method of Appendix B yields Eq. 3.109 to Eq. 3.113.

$$T_{air}^{target}[n] = T_{air}^{set}[n] - \varepsilon^{comf}[n] \quad \text{Eq. 3.107}$$

$$\Delta T_{air}^{target}[n] = T_{air}[n] - T_{air}^{target}[n] \quad \text{Eq. 3.108}$$

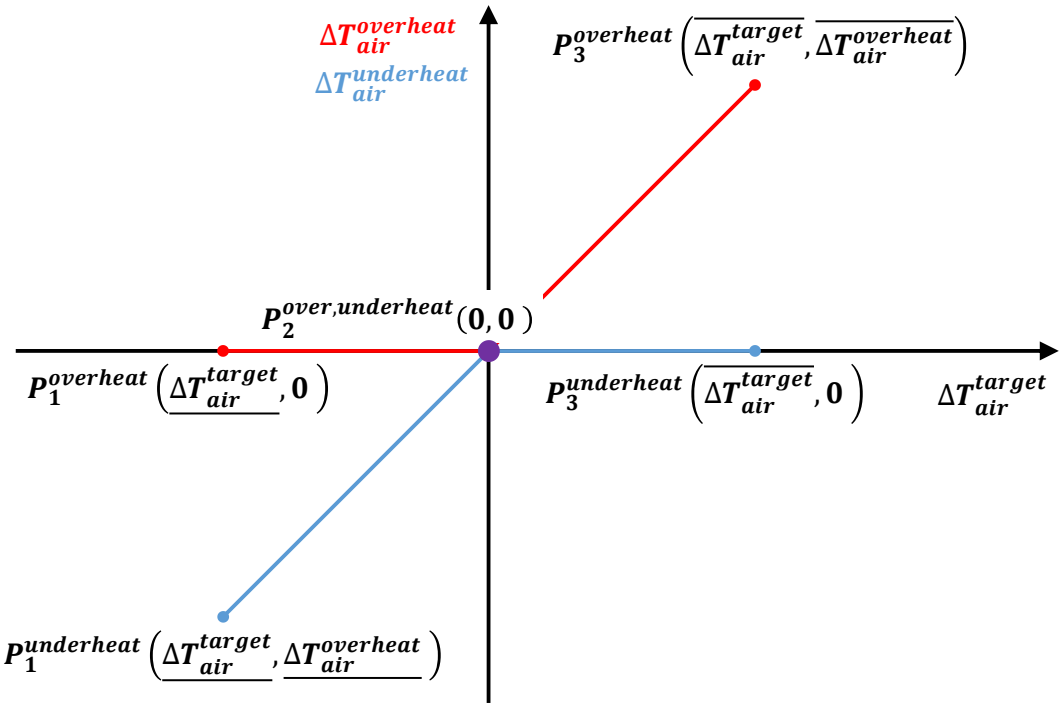

Figure 3.33 Plots of Eq. 3.67 and Eq. 3.68 showing their breakpoints

$$\sum_{k=1}^{2} \alpha_{\text{PWL,target}}[n][k] = 1 \quad \text{Eq. 3.109}$$

$$0 \leq \beta_{\text{PWL,target}}[n][k] \leq \alpha_{\text{PWL,target}}[n][k] \quad \text{Eq. 3.110}$$

$$\Delta T_{air}^{target} = \alpha_{\text{PWL,target}}[n][1] \cdot \underline{\Delta T_{air}^{target}} - \beta_{\text{PWL,target}}[i][1] \cdot \underline{\Delta T_{air}^{target}} + \beta_{\text{PWL,target}}[i][2] \cdot \overline{\Delta T_{air}^{target}} \quad \text{Eq. 3.111}$$

$$\Delta T_{air}^{overheat} = \beta_{\text{PWL,target}}[n][2] \cdot \overline{\Delta T_{air}^{target}} \quad \text{Eq. 3.112}$$

$$\Delta T_{air}^{underheat} = \alpha_{\text{PWL,target}}[n][1] \cdot \underline{\Delta T_{air}^{target}} - \beta_{\text{PWL,target}}[n][1] \cdot \underline{\Delta T_{air}^{target}} \quad \text{Eq. 3.113}$$

3.3.2.3 Bounding constraints

At last, we bound the ROM states: $T_{air}[n]$, $T_{env}[n]$, $T_{mass}[n]$, $T_{em}[n]$ and $T_{cir}[n]$ between physically acceptable values, and the ROM controllable input $T_{cir}^{set}[n]$ within a feasible range. The general form is given in Eq. 3.114:

$$\underline{T_x} \leq T_x[n] \leq \overline{T_x} \qquad \text{Eq. 3.114}$$

3.3.3 MPC implementation

The MILP problem, under the form of Eq. 3.62, is given in Eq. 3.115:

$$\begin{matrix} minimize: \\ \quad \text{Eq. 3.75} \\ subject\ to: \\ \quad \text{Eq. 3.76 to Eq. 3.114} \end{matrix} \qquad \text{Eq. 3.115}$$

MPC is implemented by resolution of the MILP problem and application of the controller output on the BTS (by numerical simulation means), following the receding horizon principle. This section describes the resolution and implementation tool.

3.3.3.1 MILP problem initialization

The problem resolution requires initialization of the states, i.e. values of $T_x[n-1]$ at $n = 1$. Feedback may be integrated at this stage by setting $T_x[0]$ as a function of the system inputs and measured outputs.

Thus a state observer is developed. Classic techniques used for state feedback are the pole placement method described in [Savran, 2013] and the extended Kalman filter [Lee et Ricker, 1994]. Nevertheless, the observability matrix of the linear state-space system obtained after linearizing the ROM around an operation point turned out to be ill-conditioned. Therefore, these common techniques did not work.

Instead, we rely on the following calculations:

- When $\dot{m}_{SST}$ and Q_{SST} are not saturated, $T_{air}[0]$ and $T_{cir}[0]$ are obtained by inversing Eq. 2.44 and Eq. 2.45, respectively using Eq. 3.116 and Eq. 3.117. $T_{cir}^{set}[0]$ is the optimal control decision found by the controller at the previous iteration and $T_{air}^{set}[0]$ is assumed equal to 20°C.

$$T_{air}[0] = T_{air}^{set}[0] - \frac{\dot{m}_{SST}[0]}{\dot{m}_{SST}^{max} \cdot G_{air}^{p}} \qquad \text{Eq. 3.116}$$

$$T_{cir}[0] = T_{cir}^{set}[0] - \frac{Q_{SST}[0]}{Q_{SST}^{max} \cdot G_{cir}^{p}} \quad \text{Eq. 3.117}$$

- The observer simulates the non-linear ROM in parallel to the controller to provide $T_{env}[0]$, $T_{mass}[0]$ and $T_{em}[0]$ at all times, and $T_{air}[0]$ and $T_{cir}[0]$ when $\dot{m}_{SST}$ and Q_{SST} are saturated.

Thus, the control loop is closed.

Important remark

As previously mentioned, T_{air}^{set} is the indoor air set-point temperature, controlled by the consumers, unknown and uncontrollable to the DHS operator. Assuming a constant value of 20°C for T_{air}^{set} throughout the MPC might be questionable; notwithstanding, it is of common practice in DHSs to assume that the building SH demand is not fulfilled when the mass flowrate at the substation is at its maximal level, and that the building is over-heated when the mass flowrate decreases to zero, no matter the real value of T_{air}^{set}. Accordingly, conventional control actions may be taken. This feedback logic is well translated by Eq. 3.118 for the MPC controller.

3.3.3.2 MILP problem resolution

The MILP problem variables are listed in Table 3.19. The number of continuous variables is $26 + 3 \cdot N_{disc}$ and that of discrete binary variables is $8 + N_{disc}$, for every sampling time. Hence, these numbers are multiplied by N_{MPC} to solve one MILP problem over the prediction horizon H_{MPC}.

Table 3.19 List of the MILP variables and their number per sampling time

MILP continuous variable	Number per sampling time	MILP binary variable	Number per sampling time
T_{air}	1	α_{BL}	N_{disc}
T_{env}	1	$\alpha_{PWL,cir}$	3
T_{mass}	1	$\alpha_{PWL,air}$	3
T_{em}	1	$\alpha_{PWL,target}$	2
T_{cir}	1		
Q_{SST}	1		
Q_{BL}	1		
ΔT_{BL}	1		
$\dot{m}_{SST}$	1		
δ_{BL}	N_{disc}		
ω_{BL}	N_{disc}		
φ_{BL}	N_{disc}		
ΔT_{cir}	1		
ρQ_{SST}	1		
$\beta_{PWL,cir}$	3		
ΔT_{air}	1		
$\rho \dot{m}_{SST}$	1		
$\beta_{PWL,air}$	3		
ΔT_{cir}^{losses}	1		
T_{air}^{target}	1		
ΔT_{air}^{target}	1		
$\Delta T_{air}^{overheat}$	1		
$\Delta T_{air}^{underheat}$	1		
$\beta_{PWL,target}$	2		
$\boldsymbol{Total}$	$\boldsymbol{26 + 3 \cdot N_{disc}}$	$\boldsymbol{Total}$	$\boldsymbol{8 + N_{disc}}$

For the resolution, the MILP problem is coded in an IBM ILOG CPLEX project[18].

3.3.3.3 MPC implementation tool

MPC is implemented in PEGASE, a software package developed by our research team at CEA to design and deploy advanced control strategies of complex and multi-domain energy systems [Vallée *et al.*, 2019]. PEGASE features a co-simulation engine that allows explicit coupling (input – output connection) of modules from different languages and running parallel simulations.

[18] https://www.ibm.com/analytics/cplex-optimizer

For our MPC implementation, PEGASE is used as depicted in Figure 3.34: over H_{MPC}, a pre-defined scenario for p^{energy} and ε^{comf} in an Excel file and weather data from an FMU[19] are transferred as inputs to the MILP problem of the CPLEX project. CPLEX solves the optimization problem over H_{MPC} and passes the optimal command (T_{cir}^{set}) to the BTS encapsulated in an FMU. The BTS then runs under T_{cir}^{set} and the same weather conditions used in the optimization (perfect predictions) for the next time step Δt_{MPC}. A state observer collects the observations at the BTS substation (Q_{SST} and $\dot{m}_{SST}$) and the corresponding input signals (T_{ext}, I_{sol}, T_{air}^{set} and T_{cir}^{set}), and returns an estimation of the states (T_{air}, T_{env}, T_{mass}, T_{em} and T_{cir}) to initialize the MILP problem. As the first instance of the optimal control is being applied to the BTS, the horizon is shifted by one step, predictions are updated and resolution of the new optimization problem begins. And so on, the sequence of steps repeats. Other PEGASE modules (not shown in Figure 3.34) manage time lags between modules and allow accelerated visualization of results.

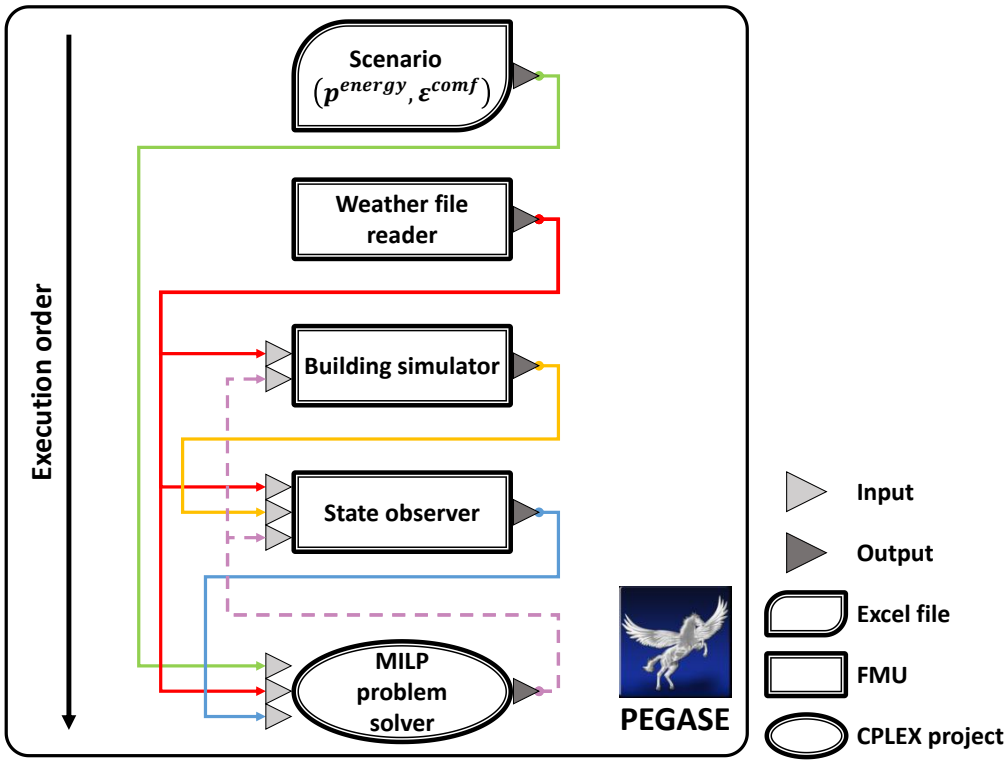

Figure 3.34 Schematic of the main modules co-simulated in PEGASE for the MPC implementation. Output of the MILP problem solver is in dashed-line to mark the time lag with respect to other signals.

3.4 Application

In this section, we apply, assess and compare the proposed MILP-based MPC with conventional WCC strategies. We define particular scenarios of p^{energy} and ε^{comf}, and carry out the applications on the BTSs based on their identified ROMs.

[19] https://fmi-standard.org/docs/3.0-dev/

3.4.1 Settings

Table 3.20 summarizes common parameters set for all applications presented hereafter. Note that these parameters are maintained constant throughout the applications.

Table 3.20 Common settings for all applications

T_{air}^{set}	$\lambda^{underheat}$	$\lambda^{overheat}$	λ^{losses}	H_{MPC}	Δt_{MPC}	N_{disc}
$20\,°C$	$0.5\ 1/K$	$0.025\ 1/K$	$0.01\ 1/K$	$24\ hr$	$15\ min$	1

T_{air}^{set}

For all WCC and MPC applications, the indoor air set-point temperature T_{air}^{set} in all zones of the BTSs is set to the default value of 20°C, at all times, and the same value is given to the controller in MPC applications.

$\lambda^{underheat}$

The MPC controller tuning parameter $\lambda^{underheat}$ is set based on the following:

Suppose a period of time Δt with constant energy price $p^{energy,cst}$;

- The maximum cost of SH that could be paid during this Δt is $c^{SH,max} = p^{energy,cst} \cdot Q_{SST}^{max} \cdot \Delta t$ (when the heating system is operating at full capacity during Δt).
- The maximum cost of discomfort due to under-heating that could be paid during the same Δt is $c^{underheat,max} = \lambda^{underheat} \cdot p^{energy,cst} \cdot Q_{SST}^{max} \cdot \Delta T_{air}^{underheat,max} \cdot \Delta t$; $\Delta T_{air}^{underheat,max}$ being the threshold of temperature deviation from comfort.

$c^{SH,max}$ and $c^{underheat,max}$ must be tantamount. Mathematically, we set $c^{SH,max} = c^{underheat,max}$; thus $\lambda^{underheat} = 1/\Delta T_{air}^{underheat,max}$. Therefore, a practical manner to set $\lambda^{underheat}$ is by defining $\Delta T_{air}^{underheat,max}$ which makes the controller dependent on the consumer preferences between saving on SH costs and trading-off thermal comfort. In our applications, we realistically assumed $\Delta T_{air}^{underheat,max} = 2°C$, hence the value of $\lambda^{underheat}$ in Table 3.20.

$\lambda^{overheat}$

$\lambda^{overheat}$ may be thought of following the same logic of $\lambda^{underheat}$. However, over-heating is indirectly penalized by the MPC controller since it automatically generates SH costs. Nonetheless, it is important to give a non-zero value to $\lambda^{overheat}$ to avoid excessive energy storage plans made by the controller in case the ROM inaccurately predicts the consequences on T_{air}. On the other extreme, a large $\lambda^{overheat}$ will lead the controller to avoid any energy storage. Thus by trial and error, we adopt a ratio of 20 between $\lambda^{overheat}$ and $\lambda^{underheat}$. Hence the value of $\lambda^{overheat}$ in Table 3.20.

λ^{losses}

λ^{losses} is set similarly to $\lambda^{underheat}$ by assuming $\Delta T_{cir}^{losses,max} = 100°C$.

H_{MPC}

In theory, MPC prediction horizon should be slightly larger than the system open-loop settling time, i.e. the time needed to reach a set-point and remain within a narrow error range following a step input [Ydstie, 1987]. Indeed, a too short H_{MPC} may lead to 2 undesirable consequences; first, higher overall costs since some predictions that might substantially affect the system are not considered ahead enough, and second, oscillatory command in open-loop because the controller keeps changing its decision after every step. The *2012 Building* has the longest time constant among all case-studies, with a settling time of 19 hours to drop its indoor temperature by 2°C from 20°C to 18°C at an average external temperature of 10°C. Thus $H_{MPC} = 24\ hrs$ is deemed sufficient for all applications.

Δt_{MPC}

MPC sampling time Δt_{MPC} is also set relatively to the system dynamics. A long Δt_{MPC} might lead to large discrepancies in the controller states predictions. A short Δt_{MPC} leads to instabilities in the closed-loop behaviour and has higher computational costs. We conveniently chose $\Delta t_{MPC} = 15\ min$.

N_{disc}

The number of discretized segments in the bilinear term McCormick relaxation has a major impact on resolution times. In fact, for decided H_{MPC} and Δt_{MPC}, N_{disc} determines the number of binary variables in the MILP problem; binary variables are the most expensive in terms of computation time. On a 2-processors, of 18 cores each, machine and using CPLEX Optimizer version 12.9, for $N_{disc} > 1$ some problems – *depending on the initial conditions and inputs over* H_{MPC} – fail to converge to a feasible solution within Δt_{MPC}. Therefore we set $N_{disc} = 1$. On average, the obtained resolution time for the

MILP problem is 10 seconds. An in-depth analysis of the effect H_{MPC}, Δt_{MPC} and N_{disc} on computational times and accuracy is intriguing but was not performed here.

3.4.2 Space-heating control without night-time setback

The aim of this first application is to demonstrate how the proposed MPC can shift the indoor air temperature regulation from T_{air}^{set} (set at the TRV level by the consumer) to T_{air}^{target} (controlled at the substation level by the DHS operator) and reduce T_{cir}^{set}.

We consider the following scenarios:

WCC scenario (1) WCC control using a static heating curve (Figure 1.13) to set the water heating temperature at the substation T_{cir}^{set}, function of the external temperature T_{ext}.

MPC Scenario (1) MILP-based MPC to optimally plan T_{cir}^{set}, given fixed energy purchase price p^{energy} and fixed thermal comfort flexibility threshold $\varepsilon^{comf} = 0.5°C$, thus the target indoor temperature for the controller is $19.5°C$.

Main results of the control applications during 3 days on the 3 case-study BTSs are shown in Figure 3.35. The top subplot concerns only MPC, since standard WCC is not influenced by energy prices or thermal flexibility. Under constant p^{energy} and ε^{comf}, the only variable predictions in the MPC horizon H_{MPC} are weather conditions (2nd subplot).

From the *1915 Building* plots, the following observations are made:

- We observe anticipation of solar heat gain by the MPC controller, which reduces T_{cir}^{set} prior to the solar irradiation peak (3rd subplot) and subsequently avoids overheating the building during the solar peak (6th subplot).
- In MPC, as T_{cir}^{set} is reduced, the indoor temperature T_{air} cools-down which triggers the TRVs opening position to increase, consequently increasing the heating water mass flow rate across the substation. This explains why MPC $\dot{m}_{SST}$ is higher than WCC $\dot{m}_{SST}$.
- MPC T_{cir}^{set} is lower than WCC T_{cir}^{set}, yet MPC $\dot{m}_{SST}$ is higher than WCC $\dot{m}_{SST}$; ultimately the SH power Q_{SST} is almost the same between the 2 control strategies for a modulation in the indoor temperature of only 0.5°C.
- Through MPC, we were able to manipulate the indoor temperature while watching over thermal comfort. This is not possible in WCC control only relying on a standard heating curve. Furthermore, implementation of the state observer detects the small increases in T_{air} in the early

mornings due to internal heat gain, and feeds-back these observations to the MPC controller to reduce T_{cir}^{set}.

Plots of the *1975 Building* and *2012 Building* confirm the aforesaid observations. A slight difference in the *2012 Building* shows that for the pre-defined heating curve, MPC T_{cir}^{set} is above WCC T_{cir}^{set} during the night, consequently MPC T_{air} variations are closer to the set-point.

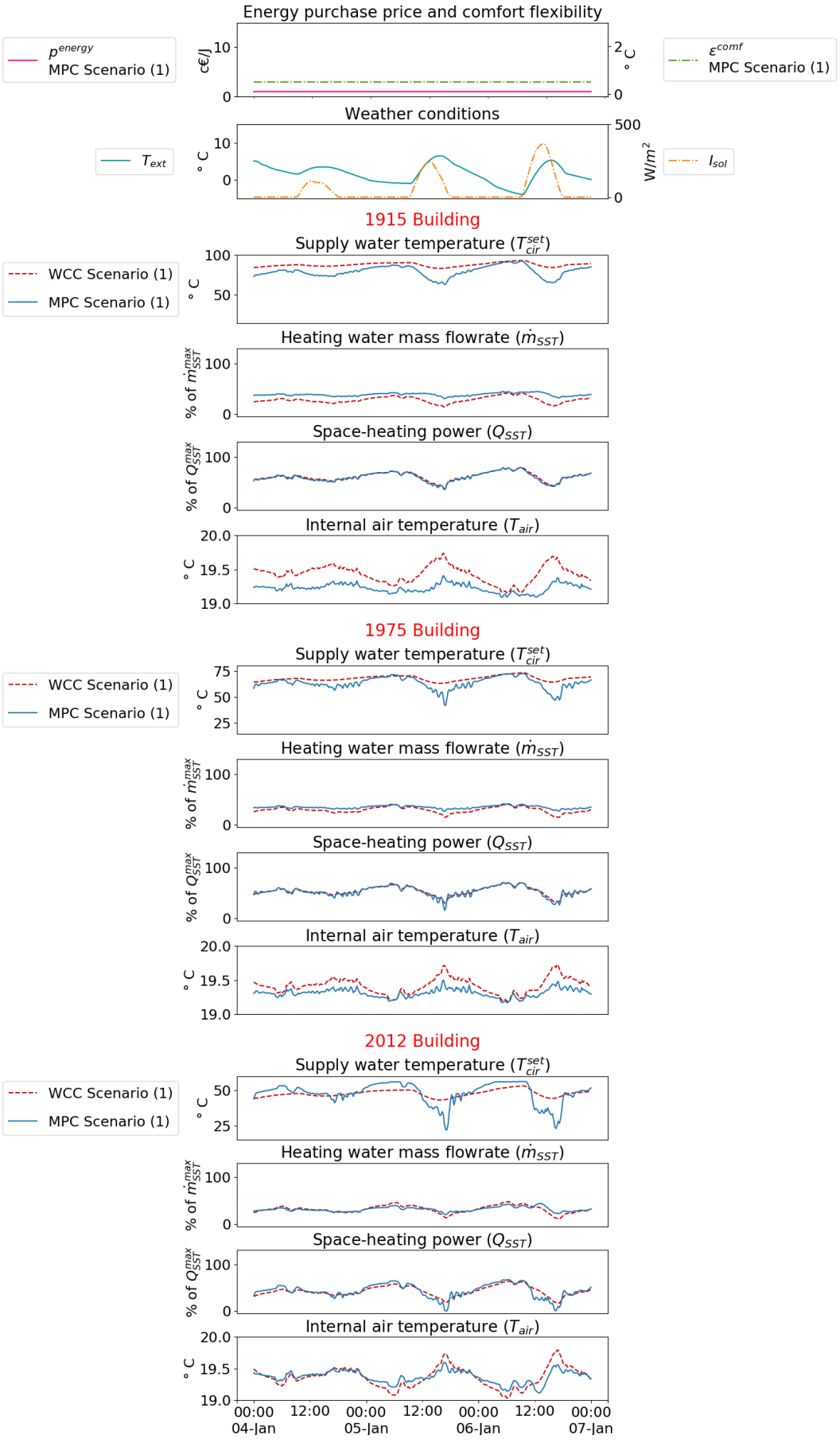

Figure 3.35 **WCC scenario (1) and MPC Scenario (1)** applied to the 3 case study BTSs

3.4.3 Space-heating control with night-time set-back

The aim of this application is to demonstrate how MPC exploits building thermal inertia during a standard DSM measure.

We consider the following scenarios:

WCC scenario (2) WCC control relying on a static heating curve to set T_{cir}^{set} during the day (similar to **WCC scenario (1)**) and systematically sets T_{cir}^{set} to its minimum value on the curve (Figure 1.13) from 11:00 pm to 6:45 am.

MPC scenario (2) MILP-based MPC to optimally plan T_{cir}^{set}, given fixed energy purchase price p^{energy} and variable ε^{comf}: 0.5°C during the day and 2°C from 11:00 pm to 6:45 am, so as to allow greater T_{air} modulation during the night.

Results over 3 application days are shown in Figure 3.36. The top subplot depicts the described ε^{comf} variations of **MPC scenario (2)**.

The following observations are made:

- MPC set-back happens in 3 phases. In a 1st phase, the MPC controller decreases T_{cir}^{set} to completely shut-off Q_{SST}. Note that T_{cir}^{set} reduction debuts *before* the beginning of the set-back. The time lag depends on the building thermal inertia, the largest being that of the *2012 Building*. Consequently, T_{air} drops while $\dot{m}_{SST}$ increases to reach its maximum.
- The 2nd phase starts immediately after reaching $\dot{m}_{SST}^{max}$, when heating is resumed by re-rising T_{cir}^{set}. Thus, the heating system is operated at constant maximal flow by slowly increasing the heating temperature over time. We note that the *2012 Building*, characterized by its high flexibility, has a great ratio of 1st to 2nd phase, i.e. it can endure prolonged power shut-offs while maintaining decent indoor climate.
- The 3rd phase begins *before* the end of the night-time set-back. Again, the moment of reverting to regular operation mode is decided based on the building dynamics. In the plots, *2012 Building* has the longest 3rd phase and, for all buildings, the 3rd phase is slightly longer than the 1st.
- Meanwhile, WCC controllers strictly follow the set-back pulse, i.e. there is no consideration of time delays due to thermal inertia. The pre-programmed set-back laws seem quite conservative; the indoor temperature is barely lowered by 1.5°C in all buildings by the end of the set-back. Indeed, the control strategy is not relying on a physical model or monitored dynamics of the

building and using off-the-shelf heating curves. Thus, it does not allow the DHS operator to make full use of the building demand flexibility.

- After the set-back, peak-loads occur. Since WCC controllers only lowered T_{air} to small extents, they cause lower morning peaks compared to MPC controllers. The duration of the peak depends of the building heating needs, not its inertia; the *1915 Building* peak-load is the longest and reaches 100% of its sizing power, whereas that of the *2012 Building* took place in the 3rd phase of the set-back and briefly reached Q_{SST}^{max}.

On a DHS scale, when night-time set-back is implemented within the demand management strategy, simultaneous peak-loads from all connected buildings accumulate resulting in very high power demands that often require starting-up expensive and pollutant heat generation units. In an attempt to shift individual buildings peak-loads, we test a 5th scenario with variable energy prices.

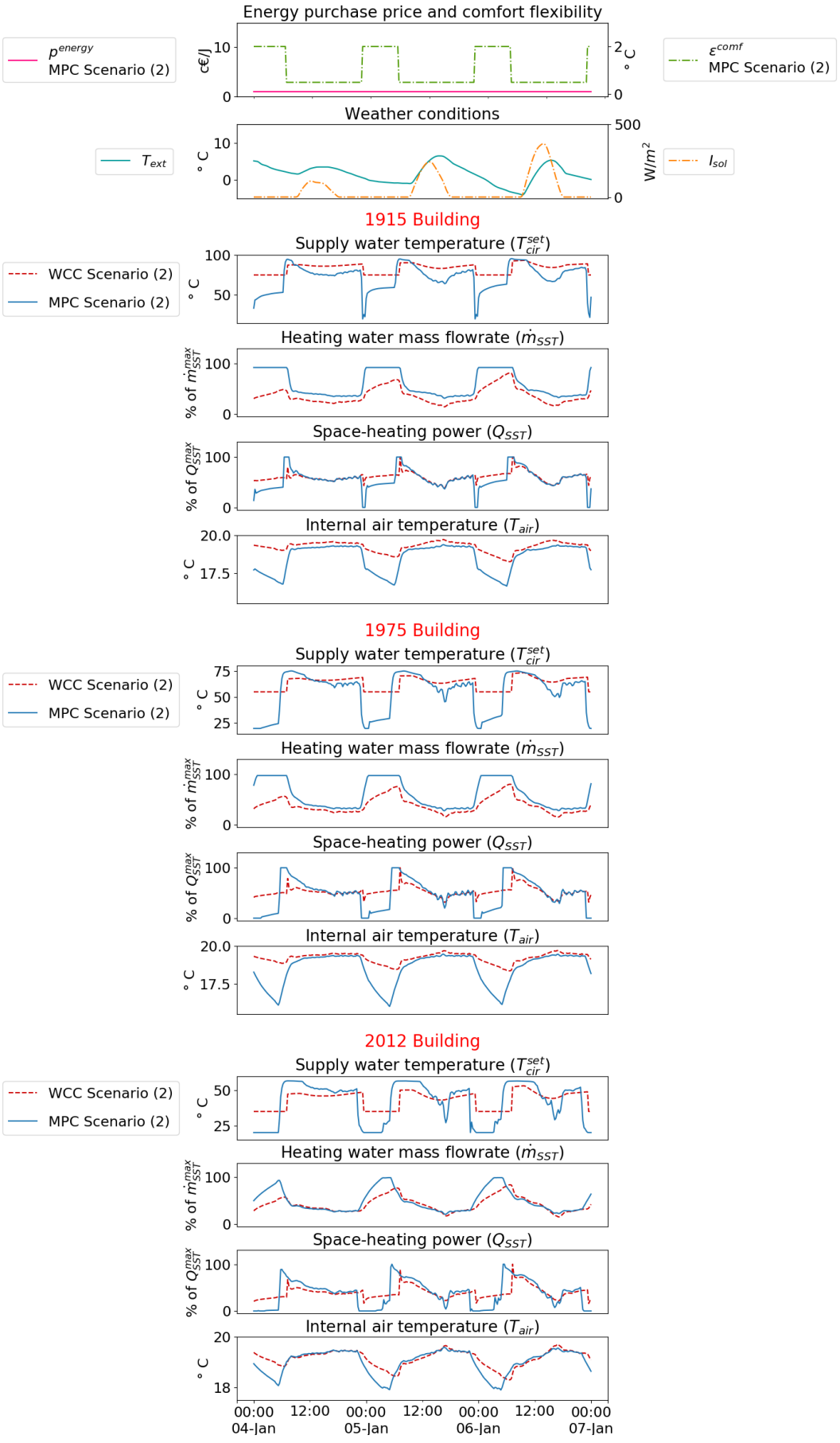

Figure 3.36 **WCC scenario (2)** and **MPC scenario (2)** applied to the 3 case study BTSs

3.4.4 Space-heating control with peak-load shifting

The aim of this last application is to automate MPC peak-load shifting by raising the penalty over energy consumption during specific hours of the day.

We consider the following scenario:

MPC scenario (3)	MILP-based MPC to optimally plan T_{cir}^{set} with variable energy purchase price p^{energy} : 10 times higher from 6:00 to 8:00 am, and variable ε^{comf}, similar to **MPC scenario (2)**.

Results of **MPC scenario (3)** are plotted in Figure 3.37, together with those of **MPC scenario (2)** for the reference, with the top subplot showing variations of p^{energy} and ε^{comf} of **MPC scenario (3)**.

The following observations are made:

- MPC controller diminishes SH consumption during periods of high p^{energy} by setting T_{cir}^{set} to its lower bound.
- In order to contain consequent under-heating, the controller stores heat within the building thermal mass prior to the high p^{energy} period; in the plots we observe maximal Q_{SST} and increasing T_{air}. The stored heat is later discharged during the high p^{energy} period.
- Compared to **MPC scenario (2)**, the *2012* and *1975 Buildings* underwent equivalent under-heating; whereas the *1915 Building* experienced harsher under-heating during high p^{energy} periods. This is mainly due to its low short-term thermal storage capacity and high losses.

Overall, peak-load shifting at building scale may be integrated into the proposed MPC control strategy. At a DHS scale, aggregate peak-load shaving may be feasible by assigning different p^{energy} profiles per building, thus spreading individual peaks over a larger period of time. Here, we adopted common tuning parameters to control 3 buildings of different flexibility levels. Tailored tuning may be necessary to avoid severe under-heating of buildings with low demand flexibility.

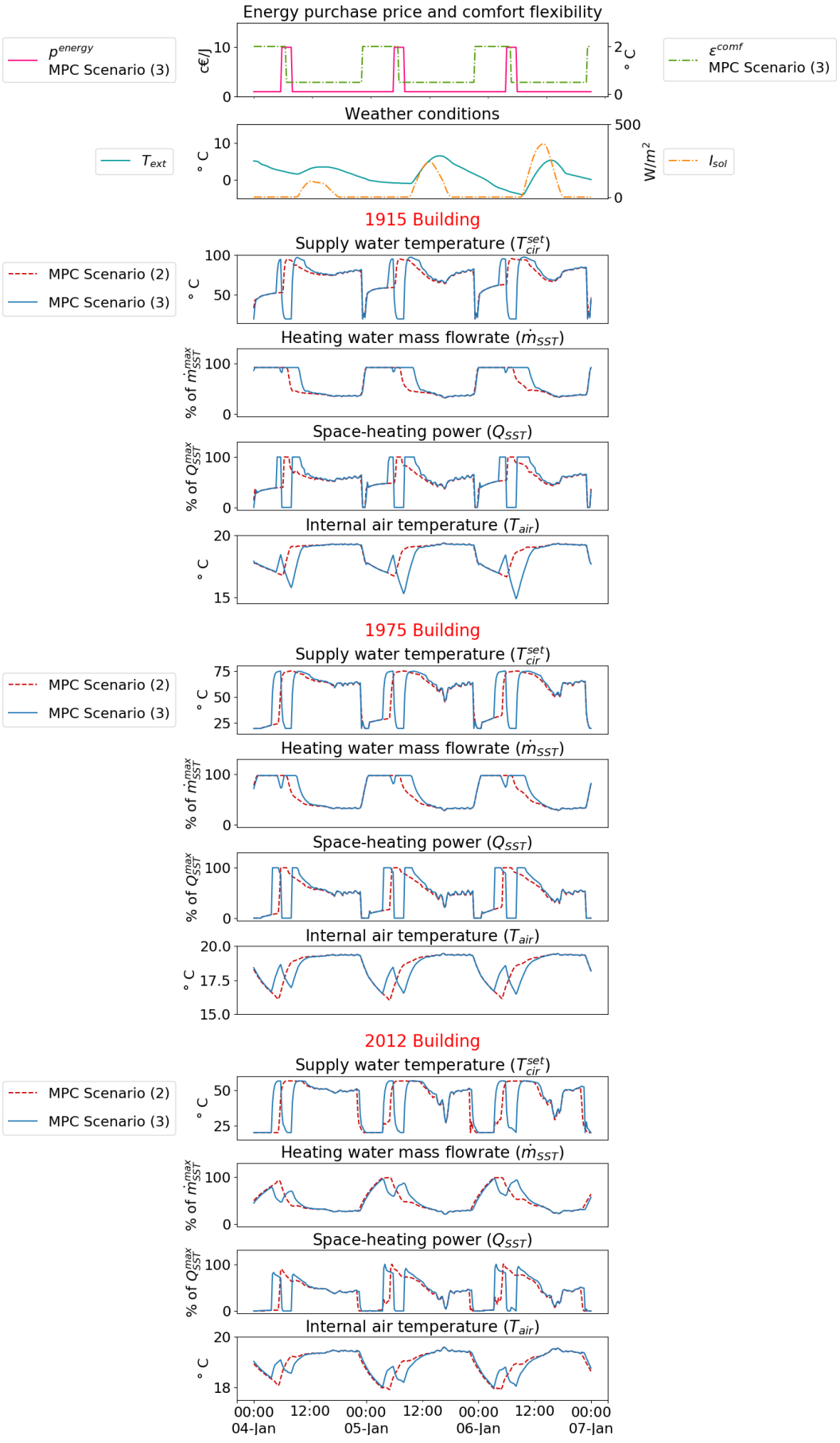

Figure 3.37 **MPC scenario (2) and MPC scenario (3)** applied to the 3 case study BTSs

3.5 Conclusion

Flexible control of SH demand involves modulating buildings thermal comfort within acceptable limits – sometimes not even perceptible by the consumers – with the aim of reducing energy costs and enhancing the overall performance of the DHS. Since buildings thermal dynamics are rather slow, anticipations of the modulation consequences are necessary in order to avoid undesirable response and to allow full exploitation of the system flexibility.

Model predictive control is a suitable approach to address flexible SH control. MPC relies on input predictions acting on the system and embeds an optimal controller hosting a physical model of the system to anticipate its dynamics. Mainly, buildings SH consumption costs are influenced by weather conditions and energy purchase price, both of which may be forecasted ahead of time. As discussed in the previous chapter, building thermal modelling is a mature topic in the scientific community and computationally efficient reduced-order building models may be easily integrated in an optimization problem to manage SH over a prediction horizon. For these favourable factors, several studies have been conducted in the literature to implement and assess MPC within electrical smart-grids. Very few works investigated buildings SH demand MPC in DHSs. None of the studies, for our knowledge, have implemented MPC based on a ROM identifiable at a DHS scale or have considered control variables that are possibly controllable by the DHS operator.

In this thesis, MPC is carried out on a building served by a DHS by solving MILP optimization problems. The objective function is designed to allow trade-off between thermal comfort and energy consumption costs. The problem is constrained by the building ROM equations which require linearization of a bilinear term and piecewise discontinuous functions. An optimization problem is launched at every time instance of the prediction horizon to schedule the heating water supply temperature over the entire horizon; only the solution at the first upcoming step is applied to the system before shifting the horizon and solving an updated problem. At every step, a state observer updates the initial conditions of the MILP problem using observations made at the substation.

Application of the proposed MPC is carried out on the BTSs, using the dedicated co-simulation platform PEGASE. Different control scenarios are presented to test MPC abilities in modulating the building indoor temperature from the DHS substation, taking account of the building thermal inertia when performing night-time set-back and automatically shifting the morning peak demand naturally resulting from the set-back. MPC is compared to conventional WCC strategies and proved to be efficient in terms of exploiting buildings thermal demand flexibility. At a broader scale, we believe that the proposed strategy can play an important role in integrating demand-side management to DHSs operational optimization.

Conclusion

Contributions

In the context of DHSs operational optimization, the research led in this dissertation aimed at the development and numerical demonstration of an advanced control strategy for buildings SH demand, practically implementable at a DHS scale.

One main motivation for this research is the fact that buildings thermal inertia makes their SH demand innately flexible, yet demand flexibility is not fully (or at all) exploited within current control practices in DHSs. Currently in DHSs, SH demand is partly controlled at the substation by setting the supply water temperature of the building's internal heating system (often radiators or floor-heating systems). This temperature is set by a conventional Weather Compensation Control (WCC) strategy, which ignores building thermal inertia and aims at fulfilling SH demand in a rather strict mode at all costs. Replacement of WCC by an intelligent and flexible control strategy is key for operational optimization of DHSs because it allows efficient management of heat sources, integration of intermittent renewable power and reduction in overall economical and environment costs.

In this thesis, we propose Model Predictive Control (MPC) as an advanced alternative to WCC for SH demand control in DHSs. Investigations on MPC in this field have originally started in the context of electric Smart Grids (SGs) and revealed a promising potential. For hydronic heating systems, MPC has been studied at building scale, assuming generous amounts of information are available and control actions at room level are possible. The main contribution of this thesis is the development of a complete and coherent MPC strategy, starting from the basic and most crucial step of model derivation followed by control law design and implementation, by careful consideration of practical challenges of data availability and controllability at DH substation level.

The study is carried out by numerical simulation means, thus it started by developing a generic thermal dynamic simulator of a residential building connected to a DHS in the Modelica/Dymola environment. The simulator enables rapid prototyping of multi-zones, multi-stories buildings based on a zonal approach. Main components are homogeneous air volumes, envelope elements (opaque constructions and glazing systems), internal partition and furniture-equivalent walls, radiators with their thermostatic valves, dual-pipe heating circuit and a DH substation. Modelled thermal phenomena include internal and external heat convection, mono-directional heat conduction, radiant heat exchange, direct heat loss to the outdoor environment due to ventilation and between zones due to door opening, and finally

stochastic internal heat gain dissipated due to occupants' presence, electric appliances and DHW usage. The building simulator is parameterized to represent 3 case-study French residential buildings belonging to a low, a medium and a high energy consumption class. While most components were found pre-developed and validated in the Modelica open-source *Buildings* Library and in-house *DistrictHeating* Library, modelling of the rest of components, assembly into a generic multi-zones multi-stories simulator and definition of case-studies constituted the first accomplishment in this thesis.

MPC starts by deriving a control-oriented Reduced-Order Model (ROM) of the building system. Once integrated in the predictive controller, the role of the ROM is to predict short-term thermal dynamics. Hence, it is crucial to procure an accurate and computationally efficiently ROM. But foremost, development of the ROM should avoid use of hardly-accessible or intrusive data. Under these requirements, inverse grey-box modelling is adopted. It is a two-steps process that starts by defining a ROM structure based on physical knowledge of the system, followed by parameters identification. Preliminary studies lead us to opt for a linear 3rd order building model coupled to a non-linear heating system model with close-loop regulation. The ROM accounts for solar heat gain, whereas internal heat gain is left-out. Parameters identification relied on measurements commonly found at the substation: SH power and water mass flowrate. Search for the optimal set of parameters that minimizes the error between ROM predictions and observations made on the simulator is carried-out by a hybrid Particle Swarm Optimization (PSO) and Hooke-Jeeves (HJ) algorithm. Critical limitations of this approach were identified from analytical tests. For MPC applications, satisfactory results based on assessment of performance criteria were finally obtained for the 3 case-study buildings. Indeed, the proposed ROM stands-out in a plethora of building models developed in the literature with its structure integrating the heating system model, and its parametric identification methodology, which dispenses the need for intrusive indoor temperature measurements.

MPC then requires designing an optimal controller. In this thesis, the controller is elaborated by formulation and resolution of a Mixed-Integer Linear Programming (MILP) optimization problem. Its objective function (to be minimized) is mainly composed of a term that penalizes SH costs which depend upon energy purchase price, and terms affected by tuning parameters that penalize thermal discomfort detected by a deviation of the indoor temperature from a target point defined at the substation. Thus, the MPC controller allows trading savings on SH costs with thermal comfort. The physical relationship between variables of the system is provided via the linearized equations of the ROM constituting the main constraints of the MILP problem. In contrast with WCC which determines the SH supply water temperature as a function of outdoor temperature solely, MILP-based MPC finds optimal trajectories of this control variable over an anticipated receding horizon by involving several factors: energy prices, discomfort tuning parameters, target temperature defined at the substation and dynamic response of the ROM indoor temperature which reflects the building thermal inertia. Whereof, the proposed MPC

allows responsible exploitation of SH demand flexibility. Implementation of MPC is realised using the in-house PEGASE platform. Demonstration of MPC on the 3 case-study building simulators based on their identified ROMs showed correct capitalizing on their thermal inertia during Demand-Side Management (DSM) measures at building scale. Undoubtedly, demand flexibility is much more interesting at larger scale, hence further research is needed to effectively take MPC to the DHS level.

Outlooks

Identified outlooks for this research include the following:

1. Real-life application of the proposed ROM identification and implementation of the MPC scenario with night-time set-back is to be considered for validation purposes on the dedicated demonstrator connected to the DHS of Grenoble, *Le Salammbô*.
2. With real-life implementations, new challenges arise: processing data is often required prior to model identification and uncertainty quantification in regards to weather predictions is necessary. Stochastic Model Predictive Control (SMPC) approaches are potential solutions to handle such issues as demonstrated in [Oldewurtel *et al.*, 2010; Zhang *et al.*, 2013].
3. Back to numerical simulation, scaling-up to neighbourhood level can be studied via Distributed Model Predictive Control (DMPC): each building is operated with a distinct energy purchase price signal, such as done in the MPC scenario with night-time set-back and peak-load shifting, and a controller at higher level coordinates these signals to evenly distribute the global morning load over time. Coordinated price-driven demand response control of this type is presented in [Ferrarini *et al.*, 2014; Costanzo *et al.*, 2013].
4. Expending the study to encompass other heat-emitters and buildings types. Typically, it would be interesting to investigate floor-heating systems characterized by their substantial thermal inertia, and non-residential buildings, e.g. schools, office buildings and hospitals, since these consumers have different occupancy profiles, hence distinct comfort flexibility schedules when controlled at neighbourhood scale.
5. Furthermore, operational optimization of heat sources in a DHS integrating flexible loads and thermal storage capacities in the network would be first of its kind in the scientific community. This is possible by coupling SH demand optimization with the optimal control strategy of heat production and distribution developed in the course of the PhD thesis of Loïc Giraud [Giraud, 2016]. Initially given non-flexible SH demand profiles, these works demonstrated the exploitation of the DH distribution network thermal inertia and proposed optimal commitment of heat sources with different operation and start-up costs.

Appendix A

McCormick relaxation for MILP of bilinear terms

In [McCormick, 1976], McCormick stated that the tightest envelope for a non-convex bilinear term, defined over a finite set, are 2 convex under-estimators and 2 concave over-estimators.

Formulation

Let $\mathcal{B}(x, y) = z = x \cdot y$ a bilinear term where $x \in [x_l, x_u]$ and $y \in [y_l, y_u]$.

Then, the McCormick envelope of $\mathcal{B}(x, y)$ is defined by Eq. App. 3.1 to Eq. App. 3.4:

$$z \geq y_l \cdot x + x_l \cdot y - x_l \cdot y_l \qquad \text{Eq. App. 3.1}$$

$$z \geq y_u \cdot x + x_u \cdot y - x_u \cdot y_u \qquad \text{Eq. App. 3.2}$$

$$z \leq y_l \cdot x + x_u \cdot y - x_u \cdot y_l \qquad \text{Eq. App. 3.3}$$

$$z \leq y_u x + x_l \cdot y - x_l \cdot y_u \qquad \text{Eq. App. 3.4}$$

Similar statement was later independently proven in [Al-Khayyal et Falk, 1983].

Numerical example

Let $\in [1,3]; y = e^x \Longrightarrow y \in [e^1, e^3]; \mathcal{B}(x, y) = z = x \cdot y$.

The tightest under-estimators of z are plans $\left(\mathcal{P}_1^{under}\right)$ and $\left(\mathcal{P}_2^{under}\right)$ defined by Eq. App. 3.5 and Eq. App. 3.6 respectively:

$$\left(\mathcal{P}_1^{under}\right): e^1 \cdot x + 1 \cdot y - 1 \cdot e^1 = 0 \qquad \text{Eq. App. 3.5}$$

$$\left(\mathcal{P}_2^{under}\right): e^3 \cdot x + 3 \cdot y - 3 \cdot e^3 = 0 \qquad \text{Eq. App. 3.6}$$

The tightest over-estimators of z are plans $(\mathcal{P}_1^{over})$ and $(\mathcal{P}_2^{over})$ defined by Eq. App. 3.7 and Eq. App. 3.8 respectively:

$$(\mathcal{P}_1^{over}): e^1 \cdot x + 3 \cdot y - 3 \cdot e^1 = 0 \qquad \text{Eq. App. 3.7}$$

$$(\mathcal{P}_2^{over}): e^3 \cdot x + 1 \cdot y - 3 \cdot e^3 = 0 \qquad \text{Eq. App. 3.8}$$

A graphical representation of the $\mathcal{B}(x, y)$ and its McCormick envelope is shown in Figure App. 3.1:

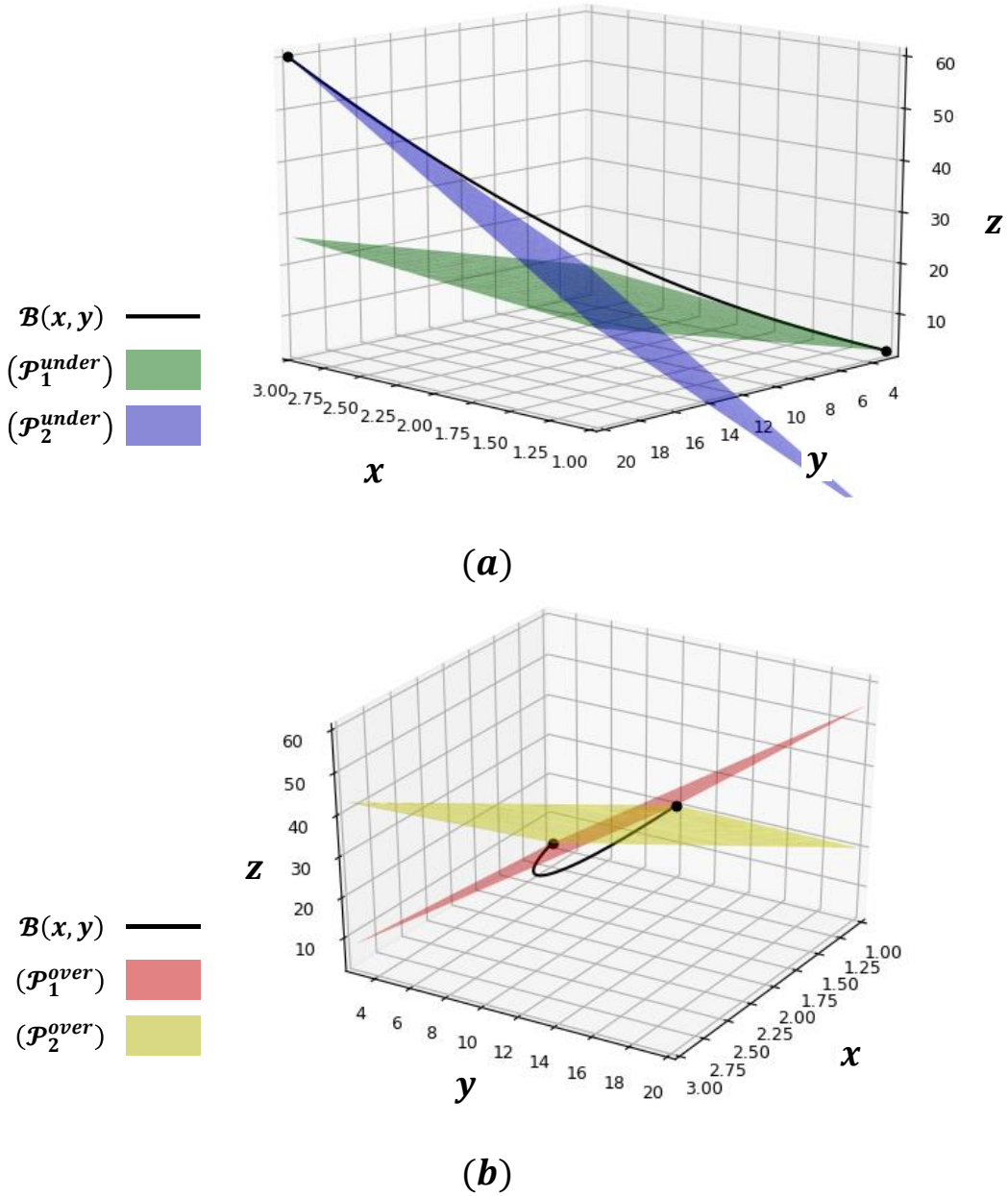

Figure App. 3.1 Graphical representation of the example bilinear term $\mathcal{B}(x, y)$ with its McCormick under-estimators (a) and over-estimators (b)

Use in linear programming

For LP, the McCormick relaxation suggests that any occurrence of a bilinear term $\mathcal{B}(x, y)$ be replaced by a new variable z constrained by the linear McCormick envelope (Eq. App. 3.1 to Eq. App. 3.4).

Furthermore, one variable of $\mathcal{B}(x, y)$ may be discretized into smaller pieces and the McCormick relaxation is applied piecewise after introducing binary variables, which yields a MILP as formulated in § 3.3.2.1.2.

Appendix B

MILP of discontinuous piecewise linear functions

Let $f(x) = y$ a discontinuous piecewise linear function with N_{br} breakpoints defined over $N_{br} - 1$ intervals of a continuous domain $\mathcal{D}$ as in Eq. App. 3.9:

$$f(x) = y = \begin{cases} f_1(x) = a_1 \cdot x + b_1 & if \quad x_{P_1} \leq x \leq x_{P_2} \\ f_2(x) = a_2 \cdot x + b_2 & if \quad x_{P_2} \leq x \leq x_{P_3} \\ \vdots & \vdots \quad \vdots \\ f_k(x) = a_k \cdot x + b_k & if \quad x_{P_k} \leq x \leq x_{P_{k+1}} \\ \vdots & \vdots \quad \vdots \\ f_{N_{br}-1}(x) = a_{N_{br}-1} \cdot x + b_{N_{br}-1} & if \quad x_{P_{N_{br}-1}} \leq x \leq x_{P_{N_{br}}} \end{cases} \qquad \text{Eq. App. 3.9}$$

A generic plot of $f(x)$ is shown in Figure App. 3.2.

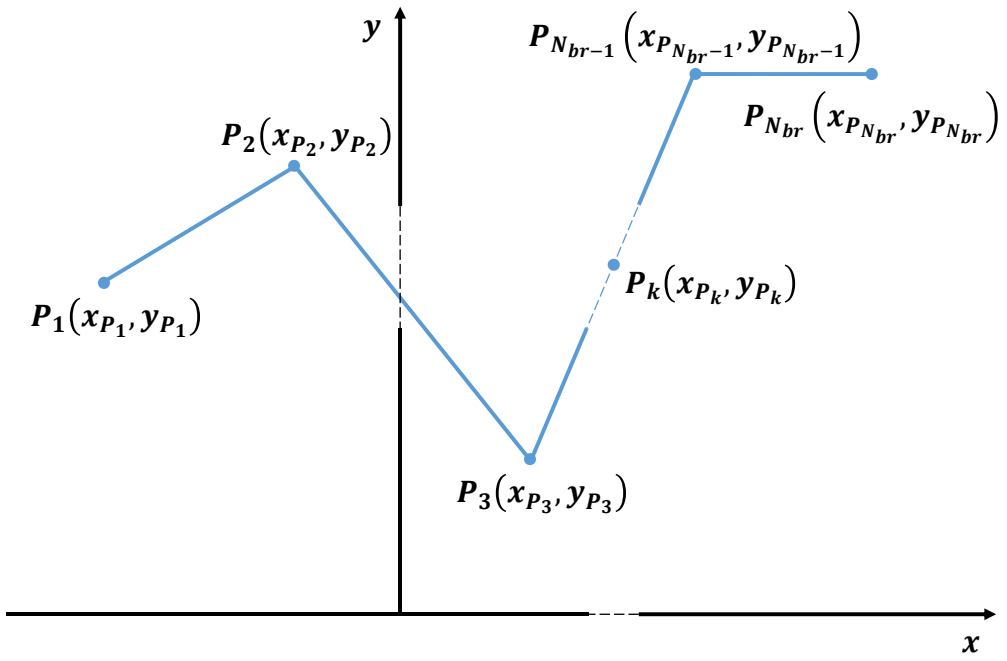

Figure App. 3.2 Generic graphical representation of a discontinuous piecewise linear function

$P_k(x_{P_k}, y_{P_k})$ and $P_{k+1}(x_{P_{k+1}}, y_{P_{k+1}})$ are breakpoints at the beginning and end of an interval of index k. We may write a_k and b_k in terms of x_{P_k}, y_{P_k}, $x_{P_{k+1}}$ and $y_{P_{k+1}}$ and substitute them, hence Eq. App. 3.10:

$$f_k(x) = \frac{y_{P_{k+1}} - y_{P_k}}{x_{P_{k+1}} - x_{P_k}} \cdot x + \frac{x_{P_{k+1}} \cdot y_{P_k} - x_{P_k} \cdot y_{P_{k+1}}}{x_{P_{k+1}} - x_{P_k}} \quad \text{Eq. App. 3.10}$$

$f(x)$ can be expressed in a MILP formulation by introducing $N_{br} - 1$ binary variables denoted $\alpha_{PWL}[k]$ in Eq. App. 3.11 subject to the constraint of Eq. App. 3.12. Interval of index k is said to be activated if $\alpha_{PWL}[k] = 1$; from Eq. App. 3.12 one and only one interval is activated.

$$f(x) = \sum_{k=1}^{N_{br}-1} \alpha_{PWL}[k] \cdot f_k(x) \quad \text{Eq. App. 3.11}$$

$$\sum_{k=1}^{N_{br}-1} \alpha_{PWL}[k] = 1 \quad \text{Eq. App. 3.12}$$

If a specific interval of index act is activated: $\alpha_{PWL}[act] = 1 \Longrightarrow f(x) = f_{act}(x)$; then x must fall in this activated interval. This is formulated through Eq. App. 3.13 and Eq. App. 3.14 where $\beta_{PWL}[k]$ is a continuous variable that determines the position x between x_{P_k} and $x_{P_{k+1}}$.

$$0 \leq \beta_{PWL}[k] \leq \alpha_{PWL}[k] \quad \text{Eq. App. 3.13}$$

$$x = \sum_{k=1}^{N_{br}-1} \alpha_{PWL}[k] \cdot x_{P_k} + \beta_{PWL}[k] \cdot \left(x_{P_{k+1}} - x_{P_k}\right) \quad \text{Eq. App. 3.14}$$

Substituting Eq. App. 3.10 and Eq. App. 3.14 in Eq. App. 3.11, we obtain Eq. App. 3.15:

$$f(x) = \sum_{k=1}^{N_{br}-1} \alpha_{PWL}[k] \cdot y_{P_i} + \beta_{PWL}[k] \cdot \left(y_{P_{k+1}} - y_{P_k}\right) \quad \text{Eq. App. 3.15}$$

Thus, the discontinuous function of Eq. App. 3.9 can be replaced by Eq. App. 3.12 to Eq. App. 3.15. This MILP formulation guarantees that for any x in $\mathcal{D}$, $f(x)$ lays on the correct line of Figure App. 3.2.

Bibliography

Alibabaei N., Fung A.S., Raahemifar K. - Development of Matlab-TRNSYS co-simulator for applying predictive strategy planning models on residential house HVAC system. *Energy Build.*, 2016, **128**, 81–98.

Al-Khayyal F.A., Falk J.E. - Jointly constrained biconvex programming. *Math. Oper. Res.*, 1983, **8** (2), 273–286.

Al-Sanea S.A., Zedan M.F., Al-Hussain S.N. - Effect of thermal mass on performance of insulated building walls and the concept of energy savings potential. *Appl. Energy*, 2012a, **89** (1), 430–442.

Al-Sanea S.A., Zedan M.F., Al-Hussain S.N. - Effect of thermal mass on performance of insulated building walls and the concept of energy savings potential. *Appl. Energy*, 2012b, **89** (1), 430–442.

Andrade-Cabrera C., Burke D., Turner W.J.N., Finn D.P. - Ensemble Calibration of lumped parameter retrofit building models using Particle Swarm Optimization. *Energy Build.*, 2017, **155**, 513–532.

Ansanay-Alex G. - An object-oriented architecture and simulation platform towards faster and portable SIMBAD simulations. In : SSB2010, 8th International Conference on System Simulation in Buildings. , 2010,.

Antonopoulos K.A., Koronaki E.P. - Effect of indoor mass on the time constant and thermal delay of buildings. *Int. J. Energy Res.*, 2000a, **24** (5), 391–402.

Antonopoulos K.A., Koronaki E.P. - Effect of indoor mass on the time constant and thermal delay of buildings. *Int. J. Energy Res.*, 2000b, **24** (5), 391–402.

Antoulas A.C., Sorensen D.C., Gugercin S. - A survey of model reduction methods for large scale systems. *Contemp. Math.*, 2000, 193–219.

Aoun N., Bavière R., Vallée M., Sandou G. - Development and assessment of a reduced-order building model designed for model predictive control of space-heating demand in district heating systems. In Wroclaw, Poland, 2019,.

Arrêté du 24 Mars 1982 modifié le 28 Octobre 1983 relatif à l'aération des logements 1983.

Arrêté du 30 avril 2013 relatif à des méthodes de calcul des caractéristiques thermiques et exigences de performance énergétique des bâtiments nouveaux 2013.

Arteconi A., Mugnini A., Polonara F. - Energy flexible buildings: A methodology for rating the flexibility performance of buildings with electric heating and cooling systems. *Appl. Energy*, 2019, **251**, 113387.

ASHRAE Standard: Ventilation for Acceptable Indoor Air Quality American Society of Heating, Refrigerating and Air-Conditioning Engineers, Incorporated, 1989.

Auliciems A., Szokolay S.V., Passive and Low Energy Architecture International, University of Queensland, Department of Achitecture - Thermal comfort. PLEA, Brisbane, 1997.

Bacher P., Madsen H. - Identifying suitable models for the heat dynamics of buildings. *Energy Build.*, 2011, **43** (7), 1511–1522.

Berthou T., Stabat P., Salvazet R., Marchio D. - Development and validation of a gray box model to predict thermal behavior of occupied office buildings. *Energy Build.*, 2014a, **74**, 91–100.

Berthou T., Stabat P., Salvazet R., Marchio D. - Development and validation of a gray box model to predict thermal behavior of occupied office buildings. *Energy Build.*, 2014b, **74**, 91–100.

Bianchini G., Casini M., Vicino A., Zarrilli D. - Demand-response in building heating systems: A Model Predictive Control approach. *Appl. Energy*, 2016, **168**, 159–170.

Blervaque H. - Règles de modélisation des systèmes énergétiques dans les bâtiments basse consommation. 2014,. Available at: https://pastel.archives-ouvertes.fr/tel-01139365/document [Accessed December 20, 2016].

Blum D.H., Arendt K., Rivalin L., Piette M.A., Wetter M., Veje C.T. - Practical factors of envelope model setup and their effects on the performance of model predictive control for building heating, ventilating, and air conditioning systems. *Appl. Energy*, 2019, **236**, 410–425.

Braun J.E. - Reducing energy costs and peak electrical demand through optimal control of building thermal storage. *ASHRAE Trans.*, 1990, **96** (2), 876–888.

Brun R., Reichert P., Künsch H.R. - Practical identifiability analysis of large environmental simulation models. *Water Resour. Res.*, 2001, **37** (4), 1015–1030.

Buffa S., Cozzini M., D'Antoni M., Baratieri M., Fedrizzi R. - 5th generation district heating and cooling systems: A review of existing cases in Europe. *Renew. Sustain. Energy Rev.*, 2019, **104**, 504–522.

Chen T.Y. - Application of adaptive predictive control to a floor heating system with a large thermal lag. *Energy Build.*, 2002, **34** (1), 45–51.

Chen C., Wang J., Heo Y., Kishore S. - MPC-based appliance scheduling for residential building energy management controller. *IEEE Trans. Smart Grid*, 2013, **4** (3), 1401–1410.

Costanzo G.T., Gehrke O., Bondy D.E.M., Sossan F., Bindner H., Parvizi J., Madsen H. - A coordination scheme for distributed model predictive control: Integration of flexible DERs. In : IEEE PES ISGT Europe 2013. IEEE, 2013, 1–5.

Crawley D.B., Lawrie L.K., Winkelmann F.C., Buhl W.F., Huang Y.J., Pedersen C.O., Strand R.K., Liesen R.J., Fisher D.E., Witte M.J., Glazer J. - EnergyPlus: creating a new-generation building energy simulation program. *Energy Build.*, 2001, **33** (4), 319–331.

Das S., Abraham A., Konar A. - Particle swarm optimization and differential evolution algorithms: technical analysis, applications and hybridization perspectives. In : Advances of computational intelligence in industrial systems. Springer, 2008, 1–38.

Dewson T., Day B., Irving A.D. - Least squares parameter estimation of a reduced order thermal model of an experimental building. *Spec. Issue Therm. Exp. Simpl. Build.*, 1993, **28** (2), 127–137.

Duffy M.J., Hiller M., Bradley D.E., Keilholz W., Thornton J.W. - TRNSYS-features and functionalitity for building simulation 2009 conference. In : 11th International IBPSA Conference-Building Simulation. , 2009, 1950–1954.

El Khoury Z., Riederer P., Couillaud N., Simon J., Raguin M. - A multizone building model for MATLAB/SIMULINK environment. In : IBPSA Conference, Montréal, Canada. , 2005,.

Elci M., Manrique Delgado B., Henning H.-M., Henze G.P., Herkel S. - Aggregation of residential buildings for thermal building simulations on an urban district scale. *Sustain. Cities Soc.*, 2018, **39**, 537–547.

Energietechnik GmbH T. - Multizone building modeling with Type56 and TRNBuild. *TRNSYS 17 TRaNsient Syst. Simul. Program*, 2010, **5**.

Fabrizio E., Monetti V. - Methodologies and advancements in the calibration of building energy models. *Energies*, 2015, **8** (4), 2548–2574.

FEDENE - Enquête nationale sur les réseaux de chaleur et de froid édition 2017 - Restitution des statistiques sur les données 2016. Fédération des Services Energie et Environnement, 2017. Available at: https://www.actu-environnement.com/media/pdf/news-29857-enquete-sncu-2017.pdf.

Fels M.F. - PRISM: an introduction. *Energy Build.*, 1986, **9** (1–2), 5–18.

Fernández M., Conde B., Eguía P., Granada E. - Parameter identification of a Round-Robin test box model using a deterministic and probabilistic methodology. *J. Build. Perform. Simul.*, 2018, **11** (6), 623–638.

Ferracuti F., Fonti A., Ciabattoni L., Pizzuti S., Arteconi A., Helsen L., Comodi G. - Data-driven models for short-term thermal behaviour prediction in real buildings. *Appl. Energy*, 2017, **204**, 1375–1387.

Ferrarini L., Mantovani G., Costanzo G.T. - A distributed model predictive control approach for the integration of flexible loads, storage and renewables. In , 2014, 1700–1705.

Firląg S., Zawada B. - Impacts of airflows, internal heat and moisture gains on accuracy of modeling energy consumption and indoor parameters in passive building. *Energy Build.*, 2013, **64**, 372–383.

Foteinaki K., Li R., Heller A., Rode C. - Heating system energy flexibility of low-energy residential buildings. *Energy Build.*, 2018a, **180**, 95–108.

Foteinaki K., Li R., Heller A., Rode C. - Heating system energy flexibility of low-energy residential buildings. *Energy Build.*, 2018b, **180**, 95–108.

Foucquier A., Robert S., Suard F., Stéphan L., Jay A. - State of the art in building modelling and energy performances prediction: A review. *Renew. Sustain. Energy Rev.*, 2013, **23**, 272–288.

Frederiksen S., Werner S. - District Heating and Cooling. Studentlitteratur AB, 2013.

Fritzson P., Engelson V. - Modelica—A unified object-oriented language for system modeling and simulation. In : European Conference on Object-Oriented Programming. Springer, 1998, 67–90.

FR_TABULA - Typology Approach for Building Stock Energy Assessment. 2015a,. Available at: http://episcope.eu/fileadmin/tabula/public/docs/brochure/FR_TABULA_TypologyBrochure_Pouget.pdf.

FR_TABULA - Typology Approach for Building Stock Energy Assessment. 2015b,. Available at: http://episcope.eu/fileadmin/tabula/public/docs/brochure/FR_TABULA_TypologyBrochure_Pouget.pdf.

Gaaloul S., Delinchant B., Wurtz F., Thiers S., Peuportier B. - Couplage d'un modèle thermique issu de COMFIE avec un chauffage régulé électriquement pour une simulation temporelle hybride à pas variable. In : IBPSA. Moret-sur-Loing, France, 2011,. Available at: https://hal.archives-ouvertes.fr/hal-00540361.

Gholamibozanjani G., Tarragona J., Gracia A. de, Fernández C., Cabeza L.F., Farid M.M. - Model predictive control strategy applied to different types of building for space heating. *Appl. Energy*, 2018, **231**, 959–971.

Giraud L. - Modélisation dynamique et gestion avancée de réseaux de chaleur. 2016,. Available at: http://www.theses.fr/s94851 [Accessed November 3, 2016].

Giraud L., Bavière R., Vallée M., Paulus C. - Presentation, validation and application of the DistrictHeating Modelica library. In : 11th International Modelica Conference. Versailles, 2015a,.

Giraud L., Bavière R., Vallée M., Paulus C. - Presentation, validation and application of the DistrictHeating Modelica library. In : 11th International Modelica Conference. Versailles, 2015b,.

Gouda M.M., Danaher S., Underwood C.P. - Low-order model for the simulation of a building and its heating system. *Build. Serv. Eng. Res. Technol.*, 2000, **21** (3), 199–208.

Gouda M.M., Danaher S., Underwood C.P. - Building thermal model reduction using nonlinear constrained optimization. *Build. Environ.*, 2002, **37** (12), 1255–1265.

Grötschel M., Lovász L., Schrijver A. - The ellipsoid method and its consequences in combinatorial optimization. *Combinatorica*, 1981, **1** (2), 169–197.

Guelpa E., Verda V. - Optimization of the Thermal Load Profile in District Heating Networks through "Virtual Storage" at Building Level. *Energy Procedia*, 2016, **101**, 798–805.

Halvgaard R. - Model Predictive Control for Smart Energy Systems. 2014,. Available at: http://orbit.dtu.dk/fedora/objects/orbit:129152/datastreams/file_ec7a995a-b7f4-4eaf-9880-4e3ebed9ed4b/content.

Halvgaard R., Poulsen N.K., Madsen H., Jørgensen J.B. - Economic Model Predictive Control for building climate control in a Smart Grid. In , 2012,. Available at: https://www.scopus.com/inward/record.uri?eid=2-s2.0-84860845015&doi=10.1109%2fISGT.2012.6175631&partnerID=40&md5=e877b9ad040f18c95e9f7c353276d13a.

Harb H., Boyanov N., Hernandez L., Streblow R., Müller D. - Development and validation of grey-box models for forecasting the thermal response of occupied buildings. *Energy Build.*, 2016, **117**, 199–207.

Harish V.S.K.V., Kumar A. - A review on modeling and simulation of building energy systems. *Renew. Sustain. Energy Rev.*, 2016, **56**, 1272–1292.

Henchoz S., Weber C., Maréchal F., Favrat D. - Performance and profitability perspectives of a CO2 based district energy network in Geneva's City Centre. *Energy*, 2015, **85**, 221–235.

Holøs S.B., Yang A., Lind M., Thunshelle K., Schild P., Mysen M. - VOC emission rates in newly built and renovated buildings, and the influence of ventilation – a review and meta-analysis. *Int. J. Vent.*, 2018, **0** (0), 1–14.

Hooke R., Jeeves T.A. - "Direct Search" Solution of Numerical and Statistical Problems. *J. ACM JACM*, 1961, **8** (2), 212–229.

Hu Q., Oldewurtel F., Balandat M., Vrettos E., Zhou D., Tomlin C.J. - Building model identification during regular operation - empirical results and challenges. In : 2016 American Control Conference (ACC). , 2016, 605–610.

Hu M., Xiao F., Jørgensen J.B., Li R. - Price-responsive model predictive control of floor heating systems for demand response using building thermal mass. *Appl. Therm. Eng.*, 2019a, **153**, 316–329.

Hu M., Xiao F., Jørgensen J.B., Li R. - Price-responsive model predictive control of floor heating systems for demand response using building thermal mass. *Appl. Therm. Eng.*, 2019b, **153**, 316–329.

Huang H., Chen L., Hu E. - A neural network-based multi-zone modelling approach for predictive control system design in commercial buildings. *Energy Build.*, 2015, **97**, 86–97.

Hudson G., Underwood C.P. - A simple building modelling procedure for MATLAB/SIMULINK. In : Proceedings of the International Building Performance and Simulation Conference, Kyoto Japan. , 1999, 777–783. Available at: http://www.inive.org/members_area/medias/pdf/Inive%5CIBPSA%5CUFSC806.pdf [Accessed August 2, 2017].

Husaunndee A., Lahrech R., Vaezi-Nejad H., Visier J.C. - SIMBAD: A simulation toolbox for the design and test of HVAC control systems. In : Proceedings of the 5th international IBPSA conference. International Building Performance Simulation Association (IBPSA) Prague …, 1997, 269–276.

Ionesi A., Jradi M., Thorsen J.E., Veje C.T. - Simulation of an Adaptive Heat Curve for Automatic optimization of District Heating Installation. In : International Conference of the International Building Performance Simulation AssociationConference of International Building Performance Simulation Association. , 2015, 2117–2124.

Johra H., Heiselberg P. - Influence of internal thermal mass on the indoor thermal dynamics and integration of phase change materials in furniture for building energy storage: A review. *Renew. Sustain. Energy Rev.*, 2017a, **69**, 19–32.

Johra H., Heiselberg P. - Influence of internal thermal mass on the indoor thermal dynamics and integration of phase change materials in furniture for building energy storage: A review. *Renew. Sustain. Energy Rev.*, 2017b, **69**, 19–32.

Johra H., Heiselberg P., Dréau J.L. - Influence of envelope, structural thermal mass and indoor content on the building heating energy flexibility. *Energy Build.*, 2019, **183**, 325–339.

Jordan U., Vajen K. - Influence Of The DHW Load Profile On The Fractional Energy Savings:: A Case Study Of A Solar Combi-System With TRNSYS Simulations. *Sol. Energy*, 2001, **69**, 197–208.

Jordan U., Vajen K. - DHWcalc: program to generate domestic hot water profiles with statistical means for user defined conditions. In : Proc. ISES Solar World Congress. Orlando (US), 2005,.

Jorissen F., Reynders G., Baetens R., Picard D., Saelens D., Helsen L. - Implementation and verification of the IDEAS building energy simulation library. *J. Build. Perform. Simul.*, 2018, **11** (6), 669–688.

Judkoff R., Neymark J. - International Energy Agency building energy simulation test (BESTEST) and diagnostic method. National Renewable Energy Lab., Golden, CO (US), 1995. Available at: https://www.osti.gov/biblio/90674-international-energy-agency-building-energy-simulation-test-bestest-diagnostic-method [Accessed June 6, 2019].

Kalai G. - Linear programming, the simplex algorithm and simple polytopes. *Math. Program.*, 1997, **79** (1–3), 217–233.

Kang G.-U., Chung B.-J., Kim H.-J. - Natural convection heat transfer on a vertical cylinder submerged in fluids having high Prandtl number. *Int. J. Heat Mass Transf.*, 2014, **79**, 4–11.

Kärkkäinen S., Sipilä K., Pirvola L., Esterinen J., Eriksson E., Soikkeli S., Nuutinen M., Aarnio H., Schmitt F., Eisgruber C. - Demand side management of district heating systems. 2003,. Available at: http://www.vtt.fi/inf/pdf/tiedotteet/2004/T2247.pdf.

Karmarkar N. - A New Polynomial-Time Algorithm for Linear Programming. *Combinatorica*, 1984, **4**, 373–395.

Kennedy J., Eberhart R. - Particle swarm optimization. In , 1995, 1942–1948. Available at: https://www.scopus.com/inward/record.uri?eid=2-s2.0-0029535737&partnerID=40&md5=e6bf04ae50f3268ae545d88ed91d1fc5.

Killian M., Zauner M., Kozek M. - Comprehensive smart home energy management system using mixed-integer quadratic-programming. *Appl. Energy*, 2018, **222**, 662–672.

Kim Y.-J., Park C.-S. - Stepwise deterministic and stochastic calibration of an energy simulation model for an existing building. *Energy Build.*, 2016, **133**, 455–468.

Kramer M., Jambagi A., Cheng V. - A model predictive control approach for demand side management of residential power to heat technologies. In : 2016 IEEE International Energy Conference (ENERGYCON). IEEE, 2016, 1–6.

Kramer R., van Schijndel J., Schellen H. - Simplified thermal and hygric building models: A literature review. *Front. Archit. Res.*, 2012, **1** (4), 318–325.

Kramer R., van Schijndel J., Schellen H. - Inverse modeling of simplified hygrothermal building models to predict and characterize indoor climates. *Build. Environ.*, 2013a, **68**, 87–99.

Kramer R., van Schijndel J., Schellen H. - Inverse modeling of simplified hygrothermal building models to predict and characterize indoor climates. *Build. Environ.*, 2013b, **68**, 87–99.

Lamoudi M.Y. - Distributed model predictive control for energy management in building. 2012,. Available at: https://tel.archives-ouvertes.fr/tel-00875593/document.

Land A.H., Doig A.G. - An automatic method for solving discrete programming problems. In : 50 Years of Integer Programming 1958-2008: From the Early Years to the State-of-the-Art. , 1960, 105–132. Available at: https://www.scopus.com/inward/record.uri?eid=2-s2.0-77955104238&doi=10.1007%2f978-3-540-68279-0_5&partnerID=40&md5=f2d764e617537fdaea313c920322b15d.

Lauster M., Teichmann J., Fuchs M., Streblow R., Mueller D. - Low order thermal network models for dynamic simulations of buildings on city district scale. *Build. Environ.*, 2014, **73**, 223–231.

Le Dréau J., Heiselberg P. - Energy flexibility of residential buildings using short term heat storage in the thermal mass. *Energy*, 2016a, **111**, 991–1002.

Le Dréau J., Heiselberg P. - Energy flexibility of residential buildings using short term heat storage in the thermal mass. *Energy*, 2016b, **111**, 991–1002.

Le Mounier A., Delinchant B., Ploix S. - Choix de structures de modèles pertinentes pour l'identification des systèmes de gestion d'énergique. In : IBPSA. Arras, 2014, G2Elab.

Lee J.H., Ricker N.L. - Extended Kalman filter based nonlinear model predictive control. *Ind. Eng. Chem. Res.*, 1994, **33** (6), 1530–1541.

Lehmann B., Gyalistras D., Gwerder M., Wirth K., Carl S. - Intermediate complexity model for model predictive control of integrated room automation. *Energy Build.*, 2013a, **58**, 250–262.

Lehmann B., Gyalistras D., Gwerder M., Wirth K., Carl S. - Intermediate complexity model for Model Predictive Control of Integrated Room Automation. *Energy Build.*, 2013b, **58**, 250–262.

Lerouge G. - Conformité RGPD et data privacy : le bâtiment aussi est concerné. 2019,. Available at: https://www.engie-vertuoz.fr/blog/conformite-rgpd-data-privacyt-tertiaire-batiment-connecte/#.

Leśko M., Bujalski W., Futyma K. - Operational optimization in district heating systems with the use of thermal energy storage. *Energy*, 2018, **165**, 902–915.

Li S., Joe J., Hu J., Karava P. - System identification and model-predictive control of office buildings with integrated photovoltaic-thermal collectors, radiant floor heating and active thermal storage. *Sol. Energy*, 2015, **113**, 139–157.

Li H., Wang S.J. - Load Management in District Heating Operation. *Clean Effic. Afford. Energy Sustain. Future 7th Int. Conf. Appl. Energy ICAE2015*, 2015, **75**, 1202–1207.

Li X., Wen J. - Review of building energy modeling for control and operation. *Renew. Sustain. Energy Rev.*, 2014, **37**, 517–537.

Liao Z., Dexter A.L. - An inferential model-based predictive control scheme for optimizing the operation of boilers in building space-heating systems. *IEEE Trans. Control Syst. Technol.*, 2009, **18** (5), 1092–1102.

Lin M.-H., Carlsson J.G., Ge D., Shi J., Tsai J.-F. - A review of piecewise linearization methods. *Math. Probl. Eng.*, 2013, **2013**.

Lin Y., Middelkoop T., Barooah P. - Issues in identification of control-oriented thermal models of zones in multi-zone buildings. In : 2012 IEEE 51st IEEE Conference on Decision and Control (CDC). , 2012, 6932–6937.

Liu L., Felgner F., Frey G. - Comparison of 4 numerical solvers for stiff and hybrid systems simulation. In : 2010 IEEE 15th Conference on Emerging Technologies & Factory Automation (ETFA 2010). IEEE, 2010, 1–8.

Liu X., Paritosh P., Awalgaonkar N.M., Bilionis I., Karava P. - Model predictive control under forecast uncertainty for optimal operation of buildings with integrated solar systems. *Sol. Energy*, 2018, **171**, 953–970.

Lund H., Duic N., Østergaard P.A., Mathiesen B.V. - Future district heating systems and technologies: On the role of smart energy systems and 4th generation district heating. *Energy*, 2018a, **165**, 614–619.

Lund H., Duic N., Østergaard P.A., Mathiesen B.V. - Future district heating systems and technologies: On the role of smart energy systems and 4th generation district heating. *Energy*, 2018b, **165**, 614–619.

Lund H., Möller B., Mathiesen B.V., Dyrelund A. - The role of district heating in future renewable energy systems. *Energy*, 2010, **35** (3), 1381–1390.

Lund H., Werner S., Wiltshire R., Svendsen S., Thorsen J.E., Hvelplund F., Mathiesen B.V. - 4th Generation District Heating (4GDH). *Energy*, 2014, **68**, 1–11.

Ma J., Qin J., Salsbury T., Xu P. - Demand reduction in building energy systems based on economic model predictive control. *Dyn. Control Optim. Energy Syst.*, 2012, **67** (1), 92–100.

Malisani P., Favre B., Thiers S., Peuportier B., Chaplais F., Petit N. - Investigating the ability of various buildings in handling load shiftings. In : 2011 IEEE Power Engineering and Automation Conference. , 2011, 393–397.

Mazhar A.R., Liu S., Shukla A. - A state of art review on the district heating systems. *Renew. Sustain. Energy Rev.*, 2018, **96**, 420–439.

McCormick G.P. - Computability of global solutions to factorable nonconvex programs: Part I—Convex underestimating problems. *Math. Program.*, 1976, **10** (1), 147–175.

McKinley T.L., Alleyne A.G. - Identification of building model parameters and loads using on-site data logs. *Proc. SimBuild*, 2008, **3** (1), 9–16.

Momoh J.A. - Smart grid design for efficient and flexible power networks operation and control. In , 2009,.

Morosan P.-D. - Commande prédictive distribuée. Approches appliquées à la régulation thermique des bâtiments. 2011,. Available at: https://tel.archives-ouvertes.fr/tel-00641311/document.

Müller D., Lauster M., Constantin A., Fuchs M., Remmen P. - AixLib-An open-source modelica library within the IEA-EBC annex 60 framework. In : Proc. BauSIM. , 2016, 3–9.

Münster M., Morthorst P.E., Larsen H.V., Bregnbæk L., Werling J., Lindboe H.H., Ravn H. - The role of district heating in the future Danish energy system. *Energy*, 2012, **48** (1), 47–55.

Mutani G., Giaccardi F., Martino M., Pastorelli M. - Modeling hourly profile of space heating energy consumption for residential buildings. In : 2017 IEEE International Telecommunications Energy Conference (IN^{TEL}EC). , 2017, 245–253.

Muthalib M., Nwankpa C. - Dynamic building model for demand response. In , 2014, 1171–1174.

Namerikawa T., Igari S. - Optimal energy management via MPC considering photovoltaic power uncertainty. In : 2016 IEEE international conference on smart grid communications (SmartGridComm). IEEE, 2016, 57–62.

Nytsch-Geusen C. - Modelica library BuildingSystems User guide. 2019,.

Oldewurtel F., Parisio A., Jones C.N., Gyalistras D., Gwerder M., Stauch V., Lehmann B., Morari M. - Use of model predictive control and weather forecasts for energy efficient building climate control. *Energy Build.*, 2012, **45**, 15–27.

Oldewurtel F., Parisio A., Jones C.N., Morari M., Gyalistras D., Gwerder M., Stauch V., Lehmann B., Wirth K. - Energy efficient building climate control using stochastic model predictive control and weather predictions. In : Proceedings of the 2010 American control conference. IEEE, 2010, 5100–5105.

Olsthoorn D., Haghighat F., Moreau A., Lacroix G. - Abilities and limitations of thermal mass activation for thermal comfort, peak shifting and shaving: A review. *Build. Environ.*, 2017, **118**, 113–127.

Padberg M., Rinaldi G. - Branch-and-cut algorithm for the resolution of large-scale symmetric traveling salesman problems. *SIAM Rev.*, 1991, **33** (1), 60–100.

Paiho S., Reda F. - Towards next generation district heating in Finland. *Renew. Sustain. Energy Rev.*, 2016, **65**, 915–924.

PAPAS I., Garcia - Rodriguez C., Estibals B., Ecrepont C., Alonso C. - ADREAM: Energy Consumption Optimization through Dynamic Energetic Simulations for an Intelligent Management of Energy. In : 2016 Intl IEEE Conferences Ubiquitous Intelligence & Computing, Advanced and Trusted Computing, Scalable Computing and Communications, Cloud and Big Data Computing, Internet of People, and Smart World Congress. Toulouse, France, 2016, PP.975-983.

Park H., Ruellan M., Bouvet A., Monmasson E., Bennacer R. - Thermal parameter identification of simplified building model with electric appliance. In : 11th International Conference on Electrical Power Quality and Utilisation. , 2011, 1–6.

Penman J.M. - Second order system identification in the thermal response of a working school. *Build. Environ.*, 1990, **25** (2), 105–110.

Peuportier B., Blanc I. - COMFIE: a software for passive solar design. In : 2nd International Conference, International Building Performance Simulation Association, IBPSA'91. Sophia Antipolis, France, 1991, 521–527. Available at: https://hal-mines-paristech.archives-ouvertes.fr/hal-00520421/document.

Plessis G., Kaemmerlen A., Lindsay A. - BuildSysPro: a Modelica library for modelling buildings and energy systems. In , 2014,.

Prívara S., Cigler J., Váňa Z., Oldewurtel F., Sagerschnig C., Žáčeková E. - Building modeling as a crucial part for building predictive control. *Energy Build.*, 2013a, **56**, 8–22.

Prívara S., Cigler J., Váňa Z., Oldewurtel F., Žáčeková E. - Use of partial least squares within the control relevant identification for buildings. *Control Eng. Pract.*, 2013b, **21** (1), 113–121.

Prívara S., Široký J., Ferkl L., Cigler J. - Model predictive control of a building heating system: The first experience. *Energy Build.*, 2011, **43** (2–3), 564–572.

Rabl A. - Parameter Estimation in Buildings: Methods for Dynamic Analysis of Measured Energy Use. *J. Sol. Energy Eng.*, 1988, **110** (1), 52–66.

Rabl A., Rialhe A. - Energy signature models for commercial buildings: test with measured data and interpretation. *Energy Build.*, 1992, **19** (2), 143–154.

Raftery P., Lee E., Webster T., Hoyt T., Bauman F. - Effects of furniture and contents on peak cooling load. *Energy Build.*, 2014, **85**, 445–457.

Reddy T.A. - Literature Review on Calibration of Building Energy Simulation Programs: Uses, Problems, Procedures, Uncertainty, and Tools. *ASHRAE Trans.*, 2006, **112** (1). Available at: http://search.ebscohost.com/login.aspx?direct=true&profile=ehost&scope=site&authtype=crawler&jrnl=00012505&AN=21489891&h=p8ojDgTz25mLEtPl4J%2F86zfAUGKoYzTVsDcvoE2LFrNnW0vox%2Bp0QW8edSwoCq%2BDwUzsmlj6wPJVrbTSmFK79g%3D%3D&crl=c [Accessed August 16, 2017].

Reynders G. - Quantifying the impact of building design on the potential of structural storage for active demand response in resi-dential buildings. 2015a,. Available at: https://lirias.kuleuven.be/handle/123456789/502579.

Reynders G. - Quantifying the impact of building design on the potential of structural storage for active demand response in resi-dential buildings. 2015b,. Available at: https://lirias.kuleuven.be/handle/123456789/502579 [Accessed March 21, 2017].

Reynders G., Amaral Lopes R., Marszal-Pomianowska A., Aelenei D., Martins J., Saelens D. - Energy flexible buildings: An evaluation of definitions and quantification methodologies applied to thermal storage. *Energy Build.*, 2018, **166**, 372–390.

Reynders G., Diriken J., Saelens D. - Quality of grey-box models and identified parameters as function of the accuracy of input and observation signals. *Energy Build.*, 2014a, **82**, 263–274.

Reynders G., Diriken J., Saelens D. - Quality of grey-box models and identified parameters as function of the accuracy of input and observation signals. *Energy Build.*, 2014b, **82**, 263–274.

Reynders G., Nuytten T., Saelens D. - Robustness of reduced-order models for prediction and simulation of the thermal behavior of dwellings. In : Proceedings of BS2013: 13th conference of international building performance simulation association, Chambéry, France. , 2013a,. Available at: http://www.ibpsa.org/proceedings/BS2013/p_1306.pdf.

Reynders G., Nuytten T., Saelens D. - Robustness of reduced-order models for prediction and simulation of the thermal behavior of dwellings. In : Proceedings of BS2013: 13th conference of international building performance simulation association, Chambéry, France. , 2013b,. Available at: http://www.ibpsa.org/proceedings/BS2013/p_1306.pdf [Accessed August 2, 2017].

Reynders G., Nuytten T., Saelens D. - Potential of structural thermal mass for demand-side management in dwellings. *Build. Environ.*, 2013c, **64**, 187–199.

Richardson I., Thomson M., Infield D. - A high-resolution domestic building occupancy model for energy demand simulations. *Energy Build.*, 2008a, **40** (8), 1560–1566.

Richardson I., Thomson M., Infield D. - A high-resolution domestic building occupancy model for energy demand simulations. *Energy Build.*, 2008b, **40** (8), 1560–1566.

Richardson I., Thomson M., Infield D., Clifford C. - Domestic electricity use: A high-resolution energy demand model. *Energy Build.*, 2010a, **42** (10), 1878–1887.

Richardson I., Thomson M., Infield D., Clifford C. - Domestic electricity use: A high-resolution energy demand model. *Energy Build.*, 2010b, **42** (10), 1878–1887.

Ríos-Moreno G.J., Trejo-Perea M., Castañeda-Miranda R., Hernández-Guzmán V.M., Herrera-Ruiz G. - Modelling temperature in intelligent buildings by means of autoregressive models. *Autom. Constr.*, 2007, **16** (5), 713–722.

Robillart M. - Etude de stratégies de gestion en temps réel pour des bâtiments énergétiquement performants. 2015a,. Available at: http://www.theses.fr/2015ENMP0042.

Robillart M. - Etude de stratégies de gestion en temps réel pour des bâtiments énergétiquement performants. 2015b,. Available at: http://www.theses.fr/2015ENMP0042 [Accessed January 19, 2017].

Rosen A. - Applying the lagrange method to solve problems of control constraints. *J. Appl. Mech. Trans. ASME*, 1999, **66** (4), 1013–1015.

Rossiter J.A. - Model-based predictive control: A practical approach. CRC Press, 2003.

Roubal J., Husek P., Stecha J. - Linearization: Students forget the operating point. *IEEE Trans. Educ.*, 2009, **53** (3), 413–418.

Rudolf A., Bayrleithner R. - A genetic algorithm for solving the unit commitment problem of a hydro-thermal power system. *IEEE Trans. Power Syst.*, 1999, **14** (4), 1460–1468.

Salomon T., Mikolasek R., Peuportier B. - Outil de simulation thermique du bâtiment, COMFIE. *Journ. Thématique SFT-IBPSA*, 2005,.

Saurav K., Chandan V. - Gray-box approach to thermal modelling of buildings for applications in district heating and cooling networks. 2017,.

Savran A. - Discrete state space modeling and control of nonlinear unknown systems. *ISA Trans.*, 2013, **52** (6), 795–806.

Scokaert P.O.M., Rawlings J.B. - Constrained linear quadratic regulation. *IEEE Trans. Autom. Control*, 1998, **43** (8), 1163–1169.

Shi Y., Eberhart R. - A modified particle swarm optimizer. In : 1998 IEEE international conference on evolutionary computation proceedings. IEEE world congress on computational intelligence (Cat. No. 98TH8360). IEEE, 1998, 69–73.

Stigter J.D., Beck M.B. - A new approach to the identification of model structure. *Environmetrics*, 1994, **5** (3), 315–333.

Touria G., Abdallah S., Abdelhamid H. - Analysis of the impact of internal loads on the behavior and electrical energy consumption of a building. In : Electrical and Information Technologies (ICEIT), 2015 International Conference on. IEEE, 2015, 275–280. Available at: http://ieeexplore.ieee.org/abstract/document/7162987/ [Accessed March 30, 2017].

Vallée M., Bavière R., Seguin V., Vuillerme V., Lamaison N., Descamps M., Aurousseau A. - An efficient co-simulation and control approach to tackle complex multi-domain energetic systems: concepts and applications of the PEGASE tool. In Wroclaw, Poland, 2019,.

Van Schijndel H., Zmeureanu R., Stathopoulos T. - Simulation of air infiltration through revolving doors. In : Eighth International IBPSA Conference, Eindhoven, Netherlands. , 2003,.

Verhoeven R., Willems E., Harcouët-Menou V., De Boever E., Hiddes L., Op't Veld P., Demollin E. - Minewater 2.0 project in Heerlen the Netherlands: transformation of a geothermal mine water pilot project into a full scale hybrid sustainable energy infrastructure for heating and cooling. *Energy Procedia*, 2014, **46**, 58–67.

Verrilli F., Srinivasan S., Gambino G., Canelli M., Himanka M., Del V., Sasso M., Glielmo L. - Model Predictive Control-based optimal operations of district heating system with thermal energy storage and flexible loads. 2016,.

Viot H., Sempey A., Mora L., Batsale J.-C. - Fast on-site measurement campaigns and simple building models identification for heating control. *Energy Procedia*, 2015, **78**, 812–817.

Vivian J., Zarrella A., Emmi G., De Carli M. - An evaluation of the suitability of lumped-capacitance models in calculating energy needs and thermal behaviour of buildings. *Energy Build.*, 2017a, **150**, 447–465.

Vivian J., Zarrella A., Emmi G., De Carli M. - An evaluation of the suitability of lumped-capacitance models in calculating energy needs and thermal behaviour of buildings. *Energy Build.*, 2017b, **150**, 447–465.

Von Rhein J., Henze G.P., Long N., Fu Y. - Development of a topology analysis tool for fifth-generation district heating and cooling networks. *Energy Convers. Manag.*, 2019, **196**, 705–716.

Vorger E., Schalbart P., Peuportier B. - Etude de l'influence des occupants sur la performance énergétique des logements par le biais d'une modélisation stochastique globale. In : Conférence Francophone de l'International Building Performance Simulation Association (IBPSA 2014). , 2014,.

Wang S., Xu X. - Simplified building model for transient thermal performance estimation using GA-based parameter identification. *Int. J. Therm. Sci.*, 2006, **45** (4), 419–432.

Werner S. - District heating and cooling in Sweden. *Energy*, 2017a, **126**, 419–429.

Werner S. - International review of district heating and cooling. *Energy*, 2017b, **137**, 617–631.

Werner S., Lund H., Vad Mathiesen B. - Progress and results from the 4DH research centre. In : The 14th International Symposium on District Heating and Cooling, Stockholm, Sweden, 7-9 September, 2014. Swedish District Heating Association, 2014, 302–307.

Wernstedt F., Davidsson P., Johansson C. - Demand Side Management in District Heating Systems. In : Proceedings of the 6th International Joint Conference on Autonomous Agents and Multiagent Systems. AAMAS '07, ACM, New York, NY, USA, 2007, 272:1–272:7. Available at: http://doi.acm.org/10.1145/1329125.1329454 [Accessed February 21, 2017].

Wetter M. - Co-Simulation of building energy and control systems with the Building Controls Virtual Test Bed. 2012,.

Wetter M. - GenOpt (R), Generic Optimization Program, User Manual, Version 3.1.1. Lawrence Berkeley National Laboratory: Berkeley, CA, USA, 2016. Available at: http://simulationresearch.lbl.gov/GO/.

Wetter M., Zuo W., Nouidui T.S. - Modeling of heat transfer in rooms in the modelica "buildings" library. In , 2011a, 1096–1103. Available at: https://miami.pure.elsevier.com/en/publications/modeling-of-heat-transfer-in-rooms-in-the-modelica-buildings-libr.

Wetter M., Zuo W., Nouidui T.S. - Modeling of heat transfer in rooms in the modelica "buildings" library. In : Proceedings of Building Simulation 2011: 12th Conference of International Building Performance Simulation Association. , 2011b, 1096–1103. Available at: https://miami.pure.elsevier.com/en/publications/modeling-of-heat-transfer-in-rooms-in-the-modelica-buildings-libr [Accessed January 21, 2019].

Wetter M., Zuo W., Nouidui T.S., Pang X. - Modelica Buildings library. *J. Build. Perform. Simul.*, 2014, **7** (4), 253–270.

Wicaksono D.S., Karimi I.A. - Piecewise MILP under-and overestimators for global optimization of bilinear programs. *AIChE J.*, 2008, **54** (4), 991–1008.

Wolisz H., Block P., Streblow R., Müller D. - Dynamic activation of structural thermal mass in a multi-zonal building with due regard to thermal comfort. In : 14th International Conference of the International Building Performance Simulation Association. Hyderabad, India. , 2015,.

Xu X., Wang S. - A simplified dynamic model for existing buildings using CTF and thermal network models. *Int. J. Therm. Sci.*, 2008, **47** (9), 1249–1262.

Ydstie B.E. - AUTO TUNING OF THE TIME HORIZON. In : Adaptive Systems in Control and Signal Processing 1986. eds. K.J. ÅSTRÖM et B. WITTENMARK. Pergamon, Oxford, 1987, 391–395. Available at: http://www.sciencedirect.com/science/article/pii/B9780080340852500705.

Zayane C. - Identification d'un modèle de comportement thermique de bâtiment à partir de sa courbe de charge. 2011,. Available at: https://pastel.archives-ouvertes.fr/pastel-00590810/ [Accessed December 20, 2016].

Zhang X., Schildbach G., Sturzenegger D., Morari M. - Scenario-based MPC for energy-efficient building climate control under weather and occupancy uncertainty. In : 2013 European Control Conference (ECC). IEEE, 2013, 1029–1034.

Titre : Modélisation et commande prédictive flexible de la demande en chauffage des bâtiments raccordés à des réseaux de chaleur

Mots clés : Réseaux de chauffage urbains, Modélisation de bâtiments, Commande prédictive, Identification paramétrique, Simulation thermique dynamique, Programmation linéaire mixte.

Résumé : La gestion de la demande en chauffage des bâtiments raccordés à des réseaux de chaleur s'effectue classiquement au moyen d'une courbe de chauffe : lorsque la température extérieure chute, la température de départ de l'eau alimentant le circuit de chauffage interne est relevée. Ce mode de contrôle, appelé régulation par loi d'eau, présente des atouts en termes de simplicité et de robustesse, mais ne tient pas compte de l'inertie thermique du bâtiment et ne permet donc pas une modulation de sa demande. La modulation de la demande en chauffage se définit comme l'action de contrôle consistant à modifier de manière stratégique les conditions de confort thermique dans le cadre d'une optimisation énergétique et/ou économique. Il s'agit d'une brique essentielle du contrôle flexible qui envisage le déplacement des charges et l'effacement des pics pour une meilleure efficacité de production favorisant la pénétration des énergies renouvelables et de récupération.

Ces travaux de thèse visent à développer une stratégie de contrôle prédictif et flexible de la demande en chauffage, applicable à grande échelle dans les réseaux de chaleur.

Tout d'abord, un simulateur thermique dynamique de bâtiment résidentiel, équipé de radiateurs hydrauliques connectés à une sous-station de réseau de chaleur, est développé. Il permet de définir plusieurs cas d'études de bâtiments représentatifs du parc résidentiel français et constitue l'environnement expérimental virtuel de nos travaux de recherche. Ensuite, une méthodologie permettant d'obtenir un modèle orienté-contrôle et d'ordre réduit de bâtiment avec son système de chauffage est proposée. Elle commence par la définition de la structure du modèle en se basant sur des connaissances physiques, puis consiste en l'identification des paramètres par optimisation méta-heuristique à l'aide des données générées par le simulateur. L'approche d'identification paramétrique évalue la possibilité de réaliser cette tâche en ne s'appuyant que sur des données disponibles au niveau de la sous-station, notamment en s'interdisant d'utiliser des mesures de température intérieure, données à caractère personnel dont l'exploitation en France, conformément au Règlement Général sur la Protection des Données (RGPD), est soumise à des conditions difficilement réalisables à grande échelle. Enfin, la stratégie de contrôle prédictif est implémentée. Elle permet la planification de la température de départ de l'eau de chauffage en fonction des prévisions météorologiques et des prix de l'énergie. Le contrôleur flexible s'appuie sur un problème d'optimisation linéaire sous contraintes, selon le principe de l'horizon fuyant. Il incorpore les équations linéarisées du modèle d'ordre réduit et calcule le compromis optimal entre coûts énergétiques et inconfort thermique, le degré de flexibilité de la demande en chauffage étant défini par l'intermédiaire de paramètres de réglage dédiés.

Title : Modelling and flexible predictive control of buildings space-heating demand in district heating systems

Keywords : District heating systems, Building modelling, Model predictive control, Parametric identification, Thermal dynamic simulation, Mixed-integer linear programming

Abstract : In District Heating Systems (DHSs), buildings Space-Heating (SH) demand management conventionally relies on a heating curve: when the outdoor temperature drops, the internal SH system supply water temperature is raised. This control mode, referred to as Weather-Compensation Control (WCC), offers widely recognized assets in terms of simplicity and robustness. However, WCC does not account for the building thermal inertia, and consequently, it does not allow modulation of its demand. SH demand modulation is the control action of strategically altering the indoor thermal comfort conditions within an energetic and/or economic optimization framework. It is a key measure in flexible demand control strategies, which seek loads shifting and peaks shaving to allow sustainable commitment of energy resources in favour of renewable power penetration and waste heat recovery.

The work presented in this thesis aims at developing a flexible Model Predictive Control (MPC) strategy for SH demand, applicable at large scale in DHSs.

Firstly, a thermal dynamic simulator of a residential building with a radiator SH circuit connected to a DHS substation is developed. It allows the definition of multiple case study buildings, well-representative of the french residential stock, and constitutes the virtual experimental environment for our research. Then, a methodology to obtain a control-oriented Reduced-Order Model (ROM) for the building and its SH system is proposed. It starts by defining the ROM structure based on physical knowledge, and proceeds to parameters identification by meta-heuristic optimization using data generated by the simulator. The parametric identification approach evaluates the possibility of carrying out this task by relying solely on data available at the substation level, refraining from using indoor temperature measurements, personal data whose exploitation in France, in accordance with the General Data Protection Regulation (GDPR), is subject to conditions that are difficult to achieve at large scale. Finally, MPC is implemented to schedule the SH supply water temperature as function of weather forecasts and energy price variations. The flexible controller is designed to solve a constrained linear optimization problem according to the receding horizon principle. It embeds the linearized ROM equations and computes the optimal trade-off between energy consumption costs and thermal discomfort, the degree of flexibility to modulate SH demand being defined through dedicated tuning parameters.